New developments of proazaphosphatranes : from organocatalysis to halogen bonding

Jian Yang

École Doctorale des Sciences Chimiques (ED250)

L'Institut des Sciences Moléculaires de Marseille (iSm2)

THÈSE DE DOCTORAT

pour obtenir le grade de

DOCTEUR de l'ÉCOLE CENTRALE de MARSEILLE

Discipline : Chimie

Nouveaux développements de la chimie des proazaphosphatranes : de l'organocatalyse à la liaison halogène

Par

Monsieur **YANG Jian**

Directeur de thèse : Pr. MARTINEZ Alexandre

Soutenue le 9 octobre 2018

devant le jury composé de :

Mme MICHELET Véronique, *Professeure de l'Université de Nice*	Rapporteur
M. DAVID Olivier, *Maître de Conférences de l'Université de Versailles*	Rapporteur
Mme METAY Estelle, *Maître de Conférences de l'Université de Lyon*	Examinateur
M. COQUEREL Yoann, *Directeur de recherche à l'Université d'Aix Marseille*	Examinateur
M. CHATELET Bastien, *Maître de Conférences de l' École Centrale de Marseille*	Membre invité
Mme DUFAUD Véronique, *Directrice de recherche à CPE Lyon*	Membre invité
M. HÉRAULT Damien, *Maître de Conférences de l' École Centrale de Marseille*	Co-encadrant
M. MARTINEZ Alexandre, *Professeur de l' École Centrale de Marseille*	Directeur de thèse

Acknowledgements

First of all, I would like to thank my PhD supervisor Pr. Alexandre Martinez for his supervision and direction. He is so knowledgeable in a wide range of disciplines that I benefit a lot every time when we discussed together. And meanwhile, he is such a nice and patient person. As the director of group, he gets along very well with everyone, but he never behaves like a boss, with whom you have to speak in a very gentle way, so it's always a pleasant talk with him. Despite his strong academic background, he is also a person who works so hard. All of this has impressed and inspired me a lot, that I will appreciate forever.

I would also like to thank Dr. Damien Herault, who is my co-supervisor. He is very knowledgeable and helpful, and I can always get useful suggestions from him when I encounter some problems in chemistry. Besides, he provided me with some technical support which facilitated my research a lot. He is also a very careful person, who could pick up some minor details, which leaves me very deep impression. I would also like to thank Dr. Bastien Chatelet, an associate professor of Centrale Marseille in our group. I appreciate so much that he taught me some basic skills of organic chemistry from the first day when I entered into the lab. He is very smart and has a solid background in chemistry. He is always helpful when I turned to him, that I really appreciate a lot.

Next, I would like to send my sincere thanks to Dr. Sabine Chevallier-Michaud for Mass; Dr. Roseline Rosas for liquid NMR; Dr. Fabio Ziarelli for solid NMR; Dr. Christophe Chendo and Valérie Monnier for HRMS; Dr. Michel Giorgi for single crystal X-ray diffraction; Dr. Nicolas Vanthuyne and Marion Jean for HPLC.

I would also like to thank jury members of my PhD defense: Mmm Véronique Michelet, professor of Nice University, M. Olivier David, associate professor of Versailles University, Mmm Estelle Metay, associate professor of Lyon University and M. Yoann Coquerel, research director of Aix-Marseille University for their examination and comments on my PhD work, that I appreciate so much.

I would also like to express my gratitude to Dr. Jean-Pierre Dutasta of ENS-Lyon, Pr. Vincent Robert at the University of Strasbourg, Dr. Véronique Dufaud at laboratory of C2P2, CPE Lyon for their help and insightful discussion for my papers.

I passed three years full of joy in Marseille which is definitely attributed to my friends and colleagues. They helped me so much especially in my life, and I spent very pleasant time with them. I want to express my sincere gratitude to you from the bottom of my heart: Hervé, Innocenzo, Rémy, Delphine, Didier, Alphonse, Laurent, Rui, Dawei, Hongguang, Qingqing, Magalie, Estelle, Xiaotong, Bohdan, Lingyu, Florian, Augustin, Gege, Yunlong, Marc, Romain, Qi, Guilhem, Xiaoxi, Dan, Wei, Bofei, Changshun ……

I would also like to address my gratitude to China Scholarship Council for financial support during my three years of PhD study in Marseille.

In the end, I would like to express my greatest gratitude to my parents and my younger brother for their unconditional love and support, which motivates me forward. No more words could express my gratitude, but I still want to say thank you, I love you!

List of abbreviations

Ac = acetyl

aq = aqueous

Ar = arylBINOL = binaphthol

Bn = benzyl

Boc = *t*-butoxycarbonyl

Bu = butyl; *i*-Bu = isobutyl; *t*-Bu = tertbutyl

cat. = catalyst

CTV = cyclotriveratrylene

d = doublet

DCM = dichloromethane

DMF = *N*, *N*-dimethylformamide

DMSO = dimethylsulfoxide

dr = diastereomeric excess

δ = chemical shift

ECD = Electronic circular dichroism

ee = enantiomeric excess

Et = ethyl

ESI = Electrospray ionization

h = hour

Hz = hertz

HPLC = High Performance Liquid Chromatography

HRMS = High Resolution Mass Spectroscopy

IR = infrared spectroscopy

J = coupling constant in hertz

m = multiplet

MAS = magic angel spinning

MBH = Morita-Baylis-Hillman

Me = methyl

NMR = Nuclear Magnetic Resonance spectroscopy

Ph = phenyl

ppm = parts per million

Pr = propyl; *i*-Pr = isopropyl

rt = room temperature

s = singlet

t = triplet

THF = tetrahydrofuran

TLC = thin film chromatography

TMS = trimethylsilyl

TON = turnover number

TOF = turnover frequency

tren = tris(2-aminoethyl)amine

Ts = *para*-toluenesulfonyl

Table of contents

General Introduction 8

Part I: Introduction 10

Chapter 1. Proazaphosphatranes: discovery, synthesis and applications 11

1.1 Introduction 12

1.2 Application of proazaphosphatranes in stoichiometric reactions 13

1.3 Application of proazaphosphatranes as organocatalysts 16

1.4 Application of proazaphosphatranes as ligands in metallic catalysis 20

1.5 Conclusions 22

Chapter 2. Covalent cages with inwardly directed reactive centers as confined organo- and metal-catalysts 23

2.1 Introduction 24

2.2 Confined metal-catalysts 25

2.3 Confined organocatalysts 36

2.4 Conclusions 41

Chapter 3. Halogen bonding: an emergent non-covalent interaction 42

3.1 Introduction 43

3.2 Halogen bonding in anion recognition 44

3.3 Halogen bonding in organocatalysis 51

3.4 Conclusions 54

Part II: New applications of proazaphosphatranes in catalysis 55

Chapter 4. Verkade's superbase as an organocatalyst for Strecker Reaction 56

4.1 Introduction 57

4.2 Results and discussion 62

4.2.1 Initial experiments 62

4.2.2 Optimization of reaction conditions 62

4.2.3 Scope of substrates 65

4.2.4 Mechanism study 66

4.3 Conclusions 67

Chapter 5. Endohedral functionalized cage as a tool to create Frustrated Lewis Pairs 68

5.1 Introduction 69

5.2 Results and discussion 78

5.2.1 Initial experiments 78
5.2.2 Scope of substrates 80
5.2.3 Mechanism study 83
5.2.4 MBH reaction in the presence of enantiopure *M*-74/*P*-74 and $TiCl_4$ 84
5.2.5 Synthesis of enantiopure encaged Verkade's superbase 85
5.2.6 Attempts to obtain enantiomeric excess for reactions in the presence of *M*-74/*P*-74 87
5.2.7 Synthesis of enantiopure BINOL-based hemicryptophanes 88
5.2.8 Assignment of the absolute configuration 90
5.3 Conclusions 91
Part III: Beyond proazaphosphatranes: haloazaphosphatrane - from organocatalysis to halogen bonding 93
Chapter 6 Halogenated azaphosphatrane: a new member of halogen-bond donor 94
6.1 Introduction 95
6.2 Results and discussion 100
6.2.1 Application of azaphosphatranes as hydrogen-bonding organocatalysts 100
6.2.2 Recognition properties 101
6.2.3 Halogen bonding in a cage 106
6.2.4 From halogen bonding to chalcogen bonding 108
6.3 Conclusions 109
General conclusions and perspectives 111
Experimental section 114
General information 115
Synthesis and characterization 116
NMR spectra 166
Mass spectra 188

General Introduction

Proazaphosphatranes have attracted considerable interests as versatile reagents in organic transformations because of their strong nonionic basicity and relatively weak nucleophilicity as well as bicyclic structure. This dissertation mainly deals with new developments of proazaphosphatranes, ranging from organocatalysis, frustrated Lewis pairs (FLPs) to halogen bonding.

In the first part of this dissertation, Part I comprises three chapters. Chapter 1 presents the discovery, synthesis and reported applications of proazaphosphatranes in stoichiometric reactions, organocatalysis as well as ligands in transition-metal catalysis. Some representative examples are selected to demonstrate the wide utility of proazaphosphatranes. Chapter 2 introduces the covalent cages-based confined metal-catalysts and organocatalysts. Different encaged molecules used as catalysts or ligands in organocatalysis and metal-catalysis will be discussed and compared with their model analogues without cavities. In Chapter 3, a brief introduction about halogen bonding will be presented including their applications in anion recognition and supramolecular catalysis.

Part II deals with new applications of proazaphosphatranes in catalysis, in which Chapter 4 demonstrated a highly efficient methodology for Strecker reaction of different substituted imines possessing various protecting groups including tosyl-, Bn-, and *N*-Boc with TMSCN in the presence of proazaphosphatranes. Besides, a mechanism involving a tetra-coordinated silicon complex is proposed and evidenced by ^{29}Si NMR. In Chapter 5, we have designed a FLP system, where the Lewis base partner (Verkade's superbase) is encapsulated in a hemicryptophane host which prevents the acid-base reaction with the Lewis acidic partner ($TiCl_4$) from taking place, thus providing an effective system for the MBH reaction where both partners can act in concert without neutralizing each other. Besides, four BINOL-based hemicryptophane diastereomers were synthesized, and their absolute configurations were assigned.

In the last part, in Chapter 6, we synthesized a phosphonium-based halogen-bond donor chloroazaphosphatrane which is applied in recognition of different halide anions, exhibiting preferred binding affinity for Cl^- over Br^- and I^-. Besides, encaged chloride, sulfide and selenide azaphosphatranes were synthesized.

Part I: Introduction

This thesis focuses on the new development of proazaphosphatranes – Verkade's superbases, which involves their novel applications in catalysis and their halogenated derivatives that are supposed to be a new member in halogen bonding domain, especially, the effect of confinement on their properties will be studied. Therefore, in this part, Chapter 1 will present the discovery, synthesis, and reported applications of proazaphosphatranes, Chapter 2 will introduce the covalent cage-based confined metal-catalysts and organocatalysts. Finally, in the Chapter 3, a brief introduction about halogen bonding will be presented from anion recognition to supramolecular catalysis.

Chapter 1. Proazaphosphatranes: discovery, synthesis and applications

1.1 Introduction

Proazaphosphatranes also known as Verkade's superbases, which were firstly discovered and synthesized by J. G. Verkade more than two decades ago, have attracted considerable interests.[1] Proazaphosphatranes have such a typical structure (Figure 1.1): the phosphorus atom is located in the middle of three bridgehead nitrogens linking to another axial nitrogen by adjacent ethylene groups, featuring a prolate cage framework.[2] The substituted groups on the bridgehead nitrogens could be the same or different. Surprisingly, in the conjugated analogues azaphosphatranes, it is the phosphorus atom that gets protonated not one of the nitrogens.[1,2] Besides, proazaphosphatranes were discovered to be extraordinarily strong nonionic bases with pKa value of about 32-34 for their protonated forms, which is believed to originate from their ability to undergo transannulation easily. [3] A large number of organic transformations from stoichiometric to catalytic reactions have been applied in the presence of proazaphosphatranes owing to the nature of strong basicity and relatively weak nucleophilicity.[4]

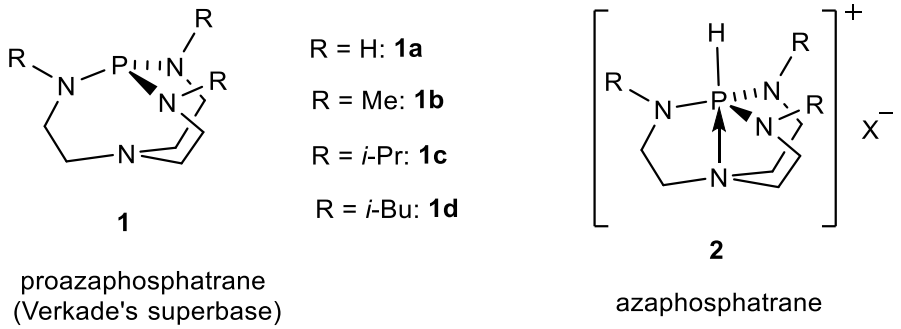

Figure 1.1 The structures of proazaphosphatranes and azaphosphatranes

[1] (a) Lensink, C.; Xi, S.-K.; Daniels, L. M.; Verkade, J. G. *J. Am. Chem. Soc*. **1989**, *111*, 3478–3479. (b) Laramay, M. A. H.; Verkade, J. G. *J. Am. Chem. Soc.* **1990**, *112*, 9421–9422. (c) Tang, J.-S.; Verkade, J. G. *J. Am. Chem. Soc.* 1993, 115, 1660–1664.
[2] (a) Verkade, J. G. *Top. Curr. Chem*. **2002**, *233*, 1–44. (b) Verkade, J. G. *Acc. Chem. Res*. **1993**, *26*, 483–489.
[3] Kisanga, P. B.; Verkade, J. G.; Schwesinger, R. *J. Org. Chem*. **2000**, *65*, 5431–5432.
[4] Verkade, J. G.; Kisanga, P. B. *Tetrahedron*, **2003**, *59*, 7819-7858.

1.2 Application of proazaphosphatranes in stoichiometric reactions

The synthesis of proazaphosphatranes follows such a general procedure[4]: the reaction of tris(2-ethylamino)amine ('tren') with aldehydes to give corresponding alkylated tetramine, which is then converted into protonated type azaphosphatrane **2**. Subsequently, **2** is deprotonated to produce a proazaphosphatrane of type **1** by strong ionic base, normally potassium *t*-butoxide (Figure 1.2).

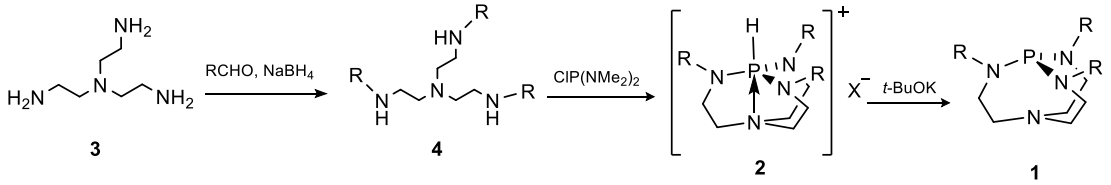

Figure 1.2 Typical procedure for synthesis of proazaphosphatranes

Proazaphosphatrane **1b** proves to be an efficient promoter for acylation of hindered alcohols giving desired products in high yields,[5] and only a very slight excess of the acid anhydride is required compared to other commonly used DMAP and tributylphosphine.[5] Moreover, **1b** could be easily recovered through deprotonation by *t*-BuOK. The excellent performance can be attributed to efficient delocalization of positive charge among the nitrogens in **1b**, making deprotonation of alcohol more easily by its anion, and further the acyl part becomes more attackable by RO^- (Figure 1.3).

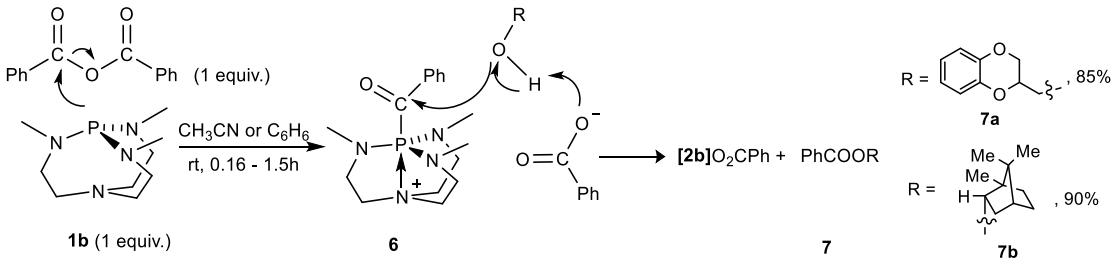

Figure 1.3 Acylation of hindered alcohols promoted by **1b**.

[5] D'Sa, B. A.; Verkade, J. G. *J. Org. Chem*. **1996**, *61*, 2963–2966.

Selective epoxidation is an important and challenging transformation in synthetic chemistry [6] especially when substrates bear sensitive functional groups. Proazaphosphatrane **1b** acts as a highly selective reagent which gives rises to epoxides with *trans*/*cis* ratio up to 99:1 when compared to its acyclic analogue triaminophosphine $P(NMe_2)_3$ (*trans*/*cis* ratios: 72/28-51/49) (Figure 1.4).[7] Besides, in the same conditions, the reactions in the presence of **1b** are faster (95% conversion) which could be attributed to the fact that **1b** is more nucleophilic than $P(NMe_2)_3$ (< 5% conversion).

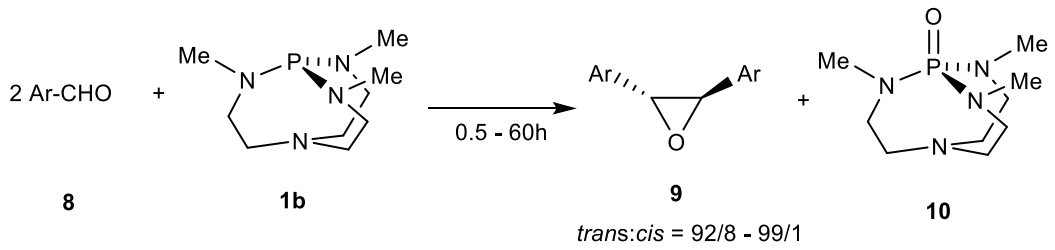

Figure 1.4 Epoxidation of aryl aldehydes with **1b**.

Oxazoles are important intermediates for preparing pharmaceutically valuable α-C-acyl amino acids, which are useful precursors in the preparation of β-hydroxy amino acids, like β-aryl serine, amino alcohols and sympathomimetic agents such as ephedrine and epinephrine.[8] However, long reaction times and a large excess of TEA or DBU are typically required. It is reported that in the presence of 1 equiv. of proazaphosphatrane **1b** (Figure 1.5), reactions of isocyanoacetates with acyl chlorides give oxazoles in nearly quantitative yields, which could further afford α-C-acyl amino acids through acid hydrolysis in high yields.[9] The resulted azaphosphatrane **2b** could be easily separated from reaction mixtures in high yield for regenerating **1b** by deprotonation with *t*-BuOK.[9]

[6] Sheldon, R. A. *Top. Curr. Chem*. **1993**, *164*, 23.
[7] Liu, X.; Verkade, J. G. *J. Org. Chem*. **2000**, *65*, 4560–4564.
[8] (a) Roush, W. R.; Murphy, M. *J. Org. Chem*. **1992**, *57*, 6622–6629. (b) Magnus, P.; Giles, M.; Bonnert, R.; Kim, C. S.; McQuire, L.; Merrit, A.; Vicker, N. *J. Am. Chem. Soc*. **1992**, *114*, 4403–4405.
[9] Tang, J.; Verkade, J. G. *J. Org. Chem*. **1994**, *59*, 7793–7802.

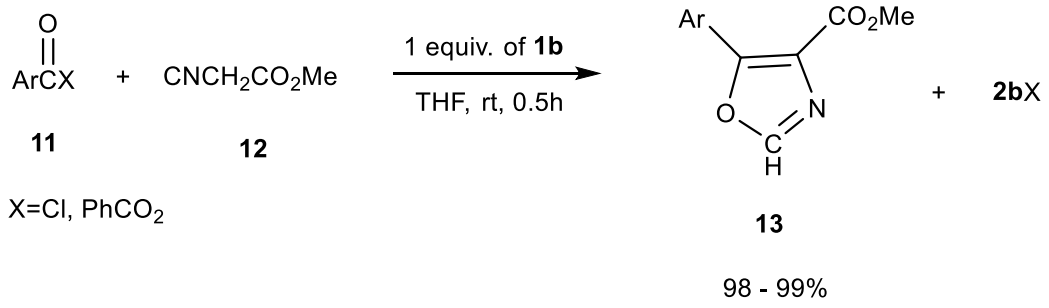

Figure 1.5 Preparation of oxazoles with **1b**.

With a stoichiometric amount of proazaphosphatrane **1b**, direct synthesis of *E*-α,β-unsaturated esters in excellent selectivity can be achieved by reacting ethyl acetate or methyl propionate with a variety of aromatic aldehydes (Figure 1.6).[10] This methodology is advantageous over most commonly used methods for preparing *E*-α,β-unsaturated esters such as the Wittig and the Wittig – Horner – Wadsworth, Peterson and Julia-Lythgoe olefinations, and the Perkin reaction, which present the following limitations: low selectivity for the *E* isomers, high temperatures and/or toxic reagents, low yields and requirements for preparing necessary intermediates.[11]

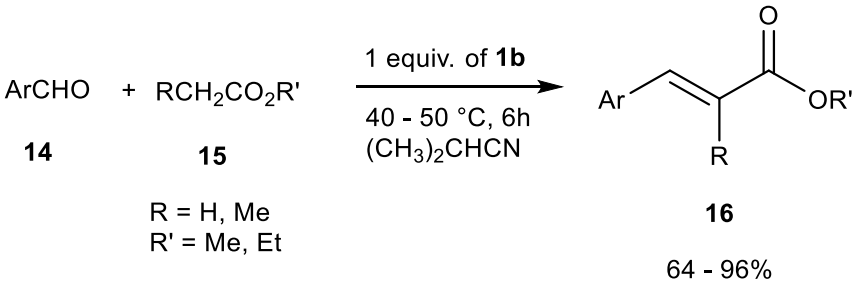

Figure 1.6 Direct synthesis of *E*-α, β-unsaturated esters promoted by **1b**.

As a strong nonionic superbase, **1b** is found to be an efficient reagent for deprotonating $[RCH_2PPh_3]X$ and $RCH_2P(O)(OEt)_2$ to their corresponding ylides under mild conditions for the Wittig and Wittig-Horner reactions to prepare alkenes in high yields

[10] Kisanga, P.; D'Sa, B.; Verkade, J. G. *Tetrahedron*, **2001**, *57*, 8047–8052.
[11] (a) Peterson, D. J. *J. Org. Chem*. **1968**, *33*, 780-784. (b) Bellassoued, M.; Majidi, A. *J. Org. Chem*. **1993**, *58*, 2517-2522. (c) Bellassoued, M.; Ozanne, N. *J. Org. Chem*. **1995**, *60*, 6582-6584. (d) Keck, G. E.; Savin, K. A.; Weglarz, M. A. *J. Org. Chem*. **1995**, *60*, 3194-3204. (e) Satoh, T.; Yamada, N.; Asano, T. *Tetrahedron Lett*. **1998**, *39*, 6935-6938.

(70-92%) with *E*/*Z* selectivities (up to 96:4 *E*/*Z* ratio) comparable to those reported with classical bases like NaH[12] (75% yield) (Figure 1.7).[13] Besides, proazaphosphatrane **1b** was also found to deprotonate sulfonium salts to produce ylides, which react readily with aromatic aldehydes to give oxiranes in generally high yields (70-96%).[14]

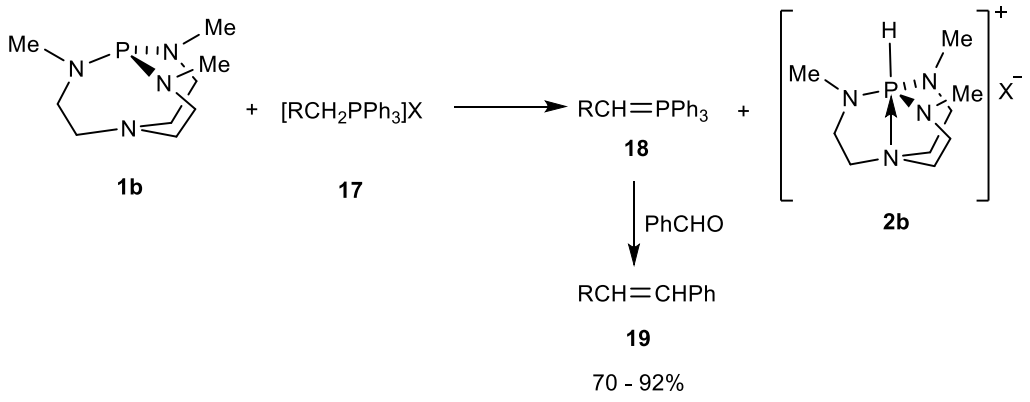

Figure 1.7 Synthesis of ylides in the presence of **1b** and subsequent reaction with aldehydes to give alkenes

1.3 Application of proazaphosphatranes as organocatalysts

Silylation of alcohols is one of most commonly used methods for protecting alcoholic OH groups in synthetic chemistry. *t*-Butyldimethylsilyl chloride (TBDMSCl) and *t*-butyldiphenylsilyl chloride (TBDPSCl) are the most popular silylation agents.[15] However, under conventional conditions such as TBDMSCl/ imidazole, 18-crown-6, Et_3N/TMG, Et_3N/DBU, DBU/potassium carbonate, *i*-Pr_2NEt, Et_3N/DMAP, the reactions of sterically hindered alcohols and phenols with TBDMSCl has been difficult to accomplish.[16] Nonionic superbase **1b** was reported to be a very effective catalyst for the preparation of TBDMS ethers of tertiary alcohols and hindered phenols in good yields (80-99%) under a nitrogen atmosphere in CH_3CN or in DMF (Figure 1.8).[17]

[12] A. G. M. Barrett, W. W. Doubleday, G. J. Tustin, *Tetrahedron*, **1996**, *52*, 15325.
[13] Wang, Z.; Verkade, J. G. *Heteroat. Chem*. **1998**, *9*, 687 – 689.
[14] Fei, X.-S.; Verkade, J. G. *Heteroat. Chem*. **1999**, *10*, 538 – 540.
[15] Corey, E. J.; Venkateswarlu, A. *J. Am. Chem. Soc*. **1972**, *94*, 6190-6191.
[16] (a) Aizpurua, J. M.; Palomo, C. *Tetrahedron Lett*. **1985**, *26*, 475-476. (b) Johnson, D. A.; Taubner, L. M. *Tetrahedron Lett*. **1996**, *37*, 605-608. (3) Barton, T. J.; Tully, C. R. *J. Org. Chem*. **1978**, *43*, 3649-3653. (4) Corey, E. J.; Cho, H.; Rucker, C.; Hua, D. H. *Tetrahedron Lett*. **1981**, *22*, 3455-3458.
[17] (a) D'Sa, B. A.; Verkade, J. G. *J. Am. Chem. Soc*. **1996**, *118*, 12832-12833. (b) D'Sa, B. A.; McLeod, D.; Verkade, J. G. *J. Org. Chem*. **1997**, *62*, 5057–5061.

Interestingly, an excellent selectivity of this methodology in protecting secondary alcohols in the presence of primary alcohols has been observed, which prefers to silylate secondary position rather than the primary one (Figure 1.9).[17]

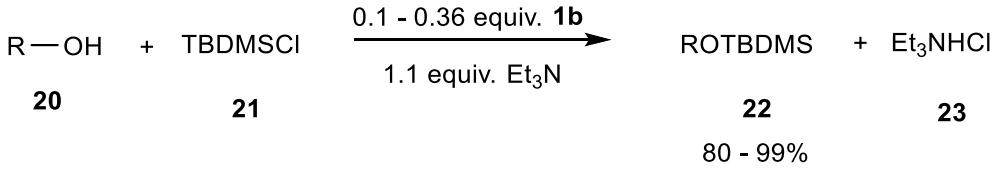

Figure 1.8 Silylation of alcohols in the presence of **1b**.

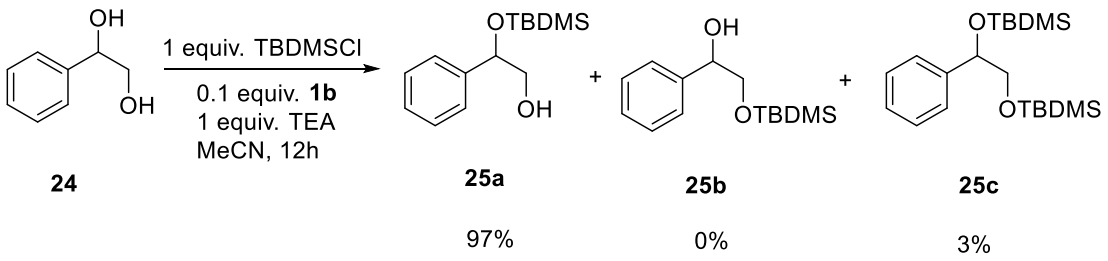

Figure 1.9 Silylation of phenyldiethanol in the presence of **1b**.

Transesterification is an important organic transformation, because an ester can be transformed into a more valuable one though this procedure.[18] Traditionally, strong acids and ionic bases are used as catalysts for this purpose.[19] Proazaphosphatrane **1b** is found to effectively catalyze the transesterification of esters with high selectivity and in excellent yields at room temperature in the presence of a catalytic amount of proazaphosphatrane **1b** (Figure 1.10).[20] This methodology has a large substrates tolerance ranging from aromatic esters to amino acid esters which are very useful protecting groups in peptide synthesis.

[18] Schuchardt, U.; Vargas, R. M.; Gelbard, G. J. Mol Cat. **1996**, *109*, 37-44.
[19] (a) Furlan, R. L. E.; Mata, E. G.; Mascaretti, O. A. *Tetrahedron Lett*. **1998**, *39*, 2257-2260. (b) Otera, J. *Chem. Rev*. **1993**, *93*, 1449-1470.
[20] Ilankumaran, P.; Verkade, J. G. *J. Org. Chem*. **1999**, *64*, 3086-3089.

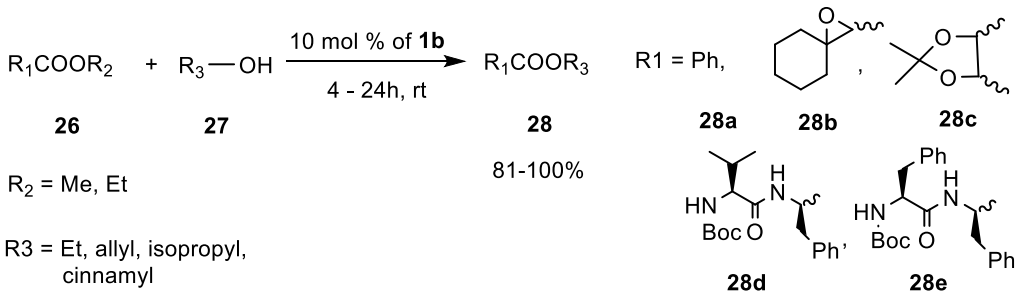

Figure 1.10 Transesterification in the presence of **1b**.

Allylation of aromatic aldehydes by the addition of allylsilanes to aldehydes is an important transformation in organic synthesis because of its importance in the formation of C-C bonds.[21] Extensive studies have been performed based on Lewis acid mediated reactions. Lewis base proazaphosphatrane **1c** was found to be effective to catalyze the reaction of allylsilanes with aldehydes at room temperature or 40 °C with 20 mol % catalyst loading (Figure 1.11).[22] Moderate yields were obtained, which suggested that an allylic anion is generated during the reaction, then reacts with the aldehyde to form the silyl ether product.[22]

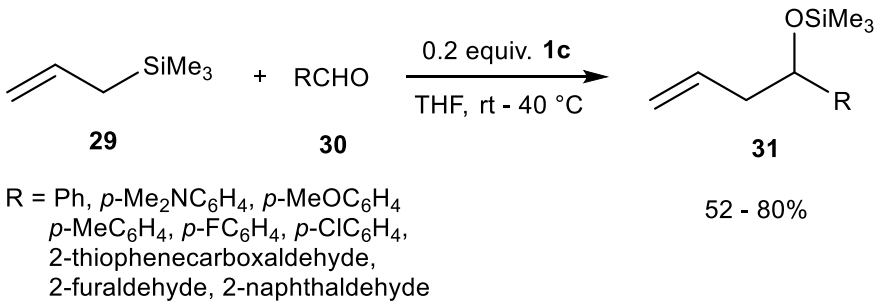

Figure 1.11 Allylation of aromatic aldehydes catalyzed by **1c**.

Species having acidic α-hydrogen atoms such as nitriles can be deprotonated by proazaphosphatranes to generate an equilibrium mixture of both the corresponding protonated base and the free base. The resulted carbanion can take part in a number of reactions relying on conditions such as temperature, solvent and other species available

[21] (a) Masse, C. E.; Panek, J. S. *Chem. Rev.* **1995**, *95*, 1293-1316. (b) Yamamoto, Y.; Asao, N. *Chem. Rev*. **1993**, *93*, 2207-2293.
[22] Wang, Z.; Kisanga, K.; Verkade, J. G. *J. Org. Chem*. **1999**, *64*, 6459-6461.

in the system.

Proazaphosphatrane **1b** was found to be a catalytic nonionic base for direct synthesis of α,*β*-unsaturated nitriles by the condensation of benzyl cyanide with a variety of functionalized aromatic and aliphatic aldehydes in excellent yields (Figure 1.12).[23] However, this methodology does not work for primary and secondary aliphatic aldehydes and ketones to produce the corresponding α,*β*-unsaturated nitriles with benzyl cyanide.[23] Proazaphosphatrane **1b** has advantages over traditional methods utilizing an alkali metal alkoxide or some other ionic base as a catalyst which lead to undesired side reactions such as self-condensation of the nitrile, aldol condensation of the carbonyl compound.[24]

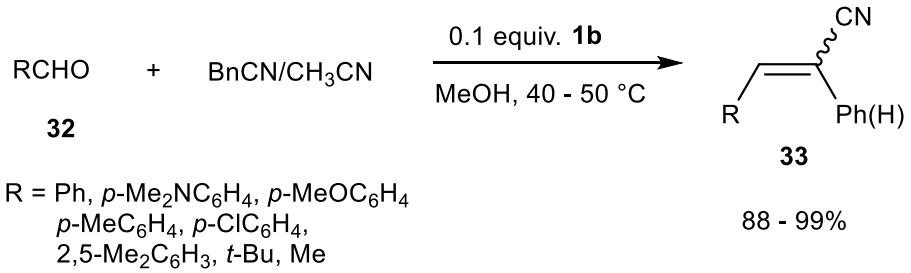

Figure 1.12 Direct synthesis of α,*β*-unsaturated nitriles promoted by **1b**.

β-Nitroalkanols are useful and significant building blocks in organic transformations, which act as the precursors of nitroalkenes, 2-amino alcohols, and α-nitro ketones. Conventional methods for preparing *β*-nitroalkanols comprise condensation of carbonyl compounds with a nitroalkane in the presence of an ionic base, which brings about a lot of disadvantages. For example, it suffers a base-catalyzed elimination of water, and often the work-up is tedious. The strong nonionic bases proazaphosphatranes **1b** and **1c** have been shown to be a superior promoter for nitroaldol reaction, giving rise to the corresponding *β*-nitroalkanols at room temperature in the presence of $MgSO_4$ in generally excellent yields.[25] A large variety of substrates are tolerated ranging from different substituted aldehydes and ketones (Figure 1.13).

[23] D'Sa,; Kisanga, P.; Verkade, J. G. *J. Org. Chem*. **1998**, *63*, 3961-3967.
[24] Ladhar, F.; Gharbi, E. *Synth. Commun*. **1991**, *21*, 413-417.
[25] Kisanga, P.; McLeod, D.; D'Sa, B.; Verkade, J. G. *J. Org. Chem.* **1999**, *64*, 3090-3094.

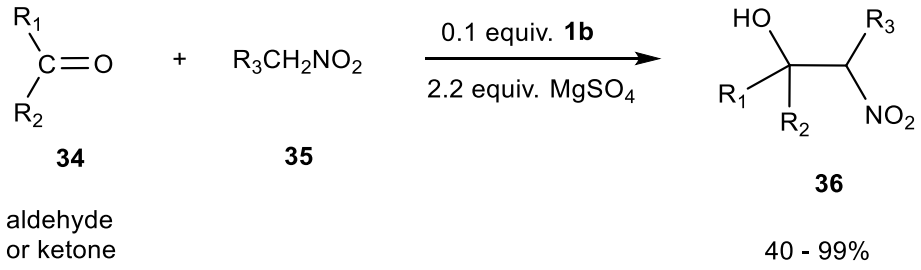

Figure 1.13 Synthesis of *β*-nitroalkanols in the presence of **1b**.

These are just several selected applications of proazaphosphatranes as organocatalysts in various organic transformations. Other examples such as deprotection of alcohols, synthesis of 3-substituted coumarins, oxa-Michael addition of alcohols have also been promoted successfully in the presence of proazaphosphatranes.[4]

1.4 Application of proazaphosphatranes as ligands in metallic catalysis

α-Aryl-substituted nitriles are important intermediates for synthesizing carboxylic acids, primary amines, aldehydes, esters, and biologically active compounds as well.[26] However, direct synthesis of α-aryl nitriles by arylation of nitriles has proved to be very difficult, not to mention much less reactive aryl chlorides.[27] An efficient catalyst system combining the commercially available proazaphosphatrane **1d** as a ligand with $Pd(OAc)_2$ in the presence of a base $NaN(SiMe_3)_2$ leads to successful coupling of a variety of nitriles with a broad range of aryl chlorides including electron-rich, electron-poor, electron-neutral, and sterically hindered examples in generally high yields (Figure 1.14).[28]

[26] Leader, H.; Smejkal, R. M.; Payne, C. S.; Padilla, F. N.; Doctor, B. P.; Gordon, R. K.; Chiang, P. K. *J. Med. Chem.* **1989**, *32*, 1522-1528.
[27] Stauffer, S. R.; Beare, N. A.; Stambuli, J. P.; Hartwig, J. F. *J. Am. Chem. Soc*. **2001**, *123*, 4641–4642. (b) N. A. Beare, J. F. Hartwig, *J. Org. Chem*. **2002**, *67*, 541–555.
[28] You, J.; Verkade, J. G. *Angew. Chem. Int. Ed*. **2003**, *42*, 5051-5053.

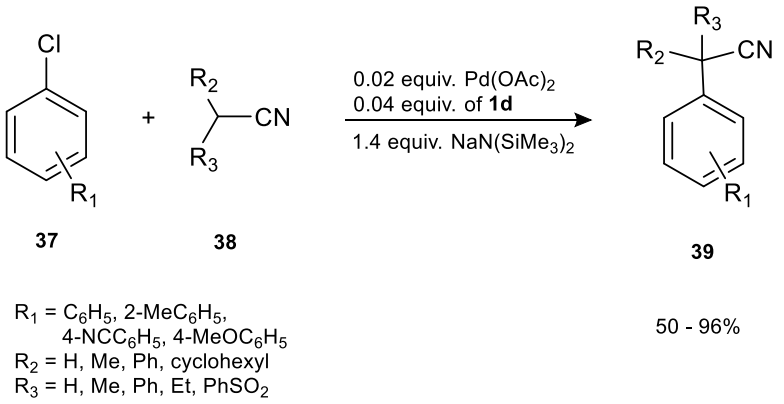

Figure 1.14 Arylation of nitriles promoted by **1d**/Pd(OAc)$_2$.

Besides, another catalytic system **1d**/Pd$_2$(dba)$_3$ (dba = dibenzylideneacetone) was found to be an efficient and general method for amination of aryl chlorides.[29] Different aryl chlorides substrates ranging from electron-poor to electron-rich ones can be coupled to a variety of amines. Good to excellent yields were observed (Figure 1.15). The authors attributed the effectiveness of ligand **1d** to the following facts that: (a) the possible transannulation of the bridgehead nitrogen lone pair to the phosphorus enriches the basicity of these proazaphosphatranes, and also the stability of reaction intermediates formed with them, thus enhancing the rate of oxidative addition step, and (b) steric hindrance stemming from the *iso*-butyl groups promotes the reductive elimination step.[29]

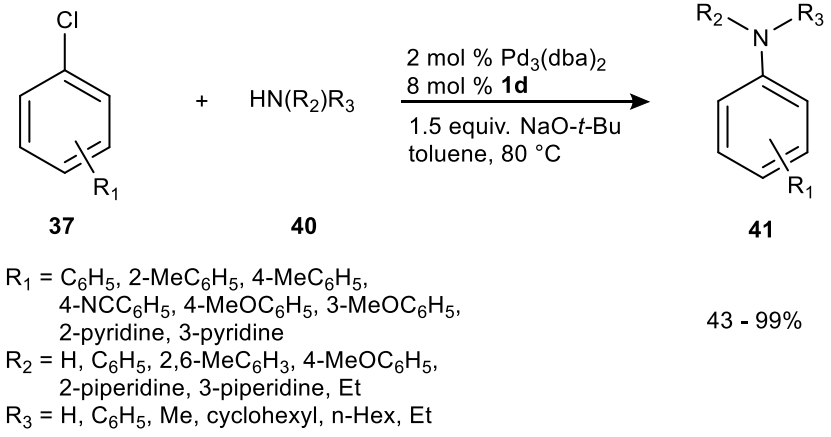

Figure 1.15 Amination of aryl chlorides promoted by **1d**/Pd$_3$(dba)$_2$.

[29] Urgaonkar, S.; Nagarajan, M.; Verkade, J. G. *Org. Lett*. **2003**, *5*, 815-818.

The Suzuki-Miyaura cross-coupling of halides with arylboronic acids to form C-C bonds is an important reaction in organic transformation for preparation of biaryls. Proazaphosphatrane **1d** has proved to be an excellent ligand for this reaction using aryl bromides and chlorides as substrates (Figure 1.16).[30] Compared to acyclic analogue triaminophosphine $P(NMe_2)_3$, the catalytic system **1d**/$Pd(OAc)_2$ is much more efficient and has a large tolerance for different substrates. For example, in the presence of **1d**/$Pd(OAc)_2$, the reaction of 2-chlorotoluene with phenylboronic acid gave the desired product in 92% yield, in contrast, no detectable product was observed with $P(NMe_2)_3$/$Pd(OAc)_2$ even after 36h.[30]

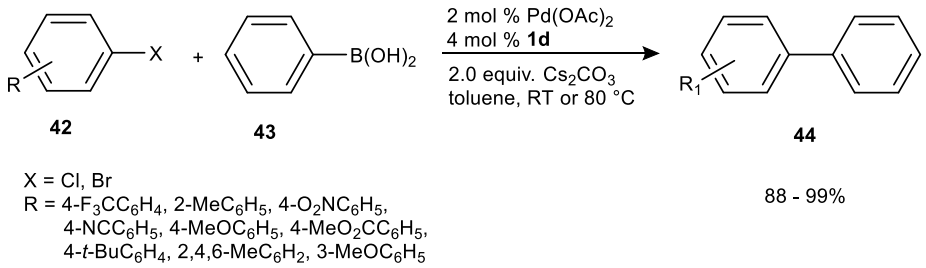

Figure 1.16 Suzuki cross-coupling promoted by **1d**/$Pd(OAc)_2$.

1.5 Conclusions

In the past two decades, proazaphosphatranes have been broadly explored in organic synthesis methodology as stoichiometric bases and as catalysts. However, it is still worth continuing to discover their new applications, tuning their activities by modifying substitution patterns, especially on the nitrogens adjacent to phosphorus. And also, their derivatives such as protonated azaphosphatranes analogues, oxidized or chalcogenated proazaphosphatranes may bring more novel catalytic applications. Besides, chiral proazaphosphatranes may yet prove fruitful in asymmetric synthesis, which will arouse considerable interest.

[30] Urgaonkar, S.; Nagarajan, M.; Verkade, J. G. *Tetrahedron Lett*. **2002**, *43*, 8921-8924.

Chapter 2. Covalent cages with inwardly directed reactive centers as confined organo- and metal-catalysts

2.1 Introduction

The complexity and remarkable tasks achieved by biological systems arouse an increasing interest. The non-covalent interactions and the resulting pre-organization account for the efficiency and selectivity of these systems. For instance, the folding of the protein chain in enzymes induce the formation of a well-defined cavity around the reactive center that can impose specific orientation and conformation of the incoming substrate, hence high catalytic activity and selectivity can be reached. Chemists have thus designed nano-reactors presenting a molecular cavity surrounding both the active site and the substrate, in order to mimic such efficient systems.[31] Nevertheless, endohedral functionalization is hard to achieve and has been rarely reported. Furthermore, such supramolecular catalysts often suffer from product inhibition: low turnover numbers are obtained when the product exhibits a high affinity for the cavity and remains in the confined space of the molecular cage, preventing any catalytic cycle.[32] Molecular receptors presenting a cavity just above a catalytic center, can fall into two main classes: covalent or self-assembled cages. These latter are obtained from smaller subcomponents, allowing the access to sophisticated structures in only few steps of synthesis. Following the pioneering work of M. Fujita, other remarkable examples of self-assembled cages have been reported by this group and those of K. N. Raymond, J. Rebeck, Jr., P. Ballester, J. N. Reek, P. J. Stang, M. Hardie and J. N. Nitschke, to only cite a few.[33] Here, only covalent cages presenting both endohedral functionalization of their inner cavity and activity as metal- or organocatalysts will be described in detail. The synthesis of such architectures and their use as catalysts are highly challenging and as a consequence only few examples have been reported to date. Recently, the groups of Ballester, Makita and Matt have described covalent cages bearing endohedral functionalization such as acidic pyrrole protons, cobalt or palladium

[31] (a) Rebek Jr, J. *Acc. Chem. Res*. **2009**, *42*, 1660-1668. (b) Lehn, J.-M. *Rep. Prog. Phy.* **2004**, *67*, 249-265. (c) Koblenz, T. S.; Wassenaar, J.; Reek, J. N. H. *Chem. Soc. Rev*. **2008**, *37*, 247-262. (d) Feiters, M. C.; Rowan, A. E.; Nolte, R. J. M. *Chem. Soc. Rev.* **2000**, *29*, 375-384. (e) Fiedler, D.; Leung, D. H.; Bergman, R. G.; Raymond, K. N. *Acc. Chem. Res*. **2005**, *38*, 349-358. (f) Murakami Y, Y.; Kikuchi J, J.; Hisaeda Y, Y.; Hayashida, O. *Chem Rev.* **1996**, *96*, 721-758. (g) Rebilly, J. N.; Colasson, B.; Bistri, O.; Over, D.; Reinaud, O. *Chem. Soc. Rev.* **2015**, *44*, 467-489. (h) Zhang, D.; Martinez, A.; Dutasta, J.-P. *Chem. Rev.* **2017**, *117*, 4900-4942.

[32] (a) Sanders, J. K. M. *Chem. Eur. J.* **1998**, *4*, 1378-1383. (b) Yoshizawa, M.; Tamura M, M.; Fujita, M. *Science* **2006**, *312*, 251-254. (c) Hooley, R. J. *Nat. Chem.* **2016**, *8*, 202-204.

[33] (a) Fujita, M.; Yazaki, J.; Ogura, K. *J. Am. Chem. Soc*., **1990**, *112*, 5645-5647. (b) Ueda, Y.; Ito, H.; Fujita, D.; Fujita, M. *J. Am. Chem. Soc*. **2017**, *139*, 6090-6093. (c) Ajami, D.; Rebek Jr, J. *Acc. Chem. Res*. **2013**, *46*, 990-999. (d) Galan, A.; Ballester, P. *Chem. Soc. Rev.* **2016**, *45*, 1720-1737. (e) Wang, Q. Q.; Gonell, S.; Leenders, S. H. A. M.; Dürr, M.; Ivanovic-Burmazovic, I.; Reek, J. N. H. *Nat. Chem.* **2016**, *8*, 225-230. (f) Henkelis, J. J.; Carruthers, C. J.; Chambers, S. E.; Clowes, R.; Cooper, A. I.; Fisher, J.; Hardie, M. J. *J. Am. Chem. Soc*. **2014**, *136*, 14393-14396. (g) Breiner, B.; Clegg, J. K.; Nitschke, J. R. *Chem. Sci.* **2011**, *2*, 51-56.

ions encapsulated in calix-pyrrole based cages, hemicryptophanes or cyclodextrines, respectively. However, the catalytic activity associated with these promising structures were not investigated, hence these systems will not be described herein.[34,35,36] Moreover, we will only focus on examples where the catalytic activity of the cage complex has been compared either with that of a model catalyst, which lacks cavity, or with another cage catalyst built from a ligand presenting similar stereoelectronic properties in the vicinity of the metal center. Covalent molecular structures encaging a metallic active site will be firstly presented, then organocatalysts confined in a molecular cavity will be described. Direct comparisons with the model catalysts, without cavity, will allow emphasizing the gains in activity and selectivity induced by the confinement of the catalytic center.

2.2 Confined metal-catalysts

Supramolecular systems combining a well-defined cavity with a metallic center are mainly based on resorcinarenes, cylclodextrins (CD), or calixarenes scaffolds. In most of these structures, the metal ion is located at the rim of the molecular cavity, and their remarkable binding properties allow for an increase of the concentration of the guest substrate near the active site, and good catalytic activities can be observed. However, true endohedral functionalization of a host molecule, i.e. a metal trapped in the heart of the cavity, is hard to achieve. Moreover, once such challenging structures are obtained, no catalytic activity is usually observed because of ligand degradations, under the reaction conditions, or product inhibitions.[37] As a consequence, very few true endohedral functionalized covalent cages and their applications as catalysts have been reported.

A Fe^{II} porphyrin complex **45** sandwiched by two cyclodextrins was reported in 1990, by Kuroda et al. (Figure 2.1).[38] This compound mimics the catalytic activity of

[34] Galán, A.; Escudero-Adán, E. C.; Ballester, P. *Chem. Sci*. **2017**, *8*, 7746-7750.
[35] Makita, Y.; Danno, T.; Ikeda, K.; Lee, H.-H.; Abe, T.; Sogawa, K.; Nomoto, A.; Fujiwara, S.-I; Ogawa, A. *Tetrahedron Lett.,* **2017**, *58*, 4507-4509.
[36] Sechet, D.; Kaya, Z.; Phan, T.-A.; Jouffroy, M.; Bentouhami, E.; Armspach, D.; Matt, D.; Toupet, L. *Chem. Commun*., **2017**, *53*, 11717-11720.
[37] Izzet, G.; Zeitouny, J.; Akdas-Killig, H.; Frapart, Y.; Ménage, S.; Douziech, B.; Jabin, I.; Y. Le Mest,; Reinaud, Olivia. *J. Am. Chem. Soc.* **2008**, *130*, 9514-9523.
[38] Kuroda, Y.; Hiroshige, T.; Ogoshi, H.; *J. Chem. Soc. Chem. Commun.* **1990**, *0*, 1594-1595**.**

cytochrome P-450 and acts as an efficient catalyst in the epoxidation of cyclohexene, whereas its model parent, which lacks cavity, displays no catalytic activity for this reaction (55% and less than 2% yields for **45** and **46**, respectively).

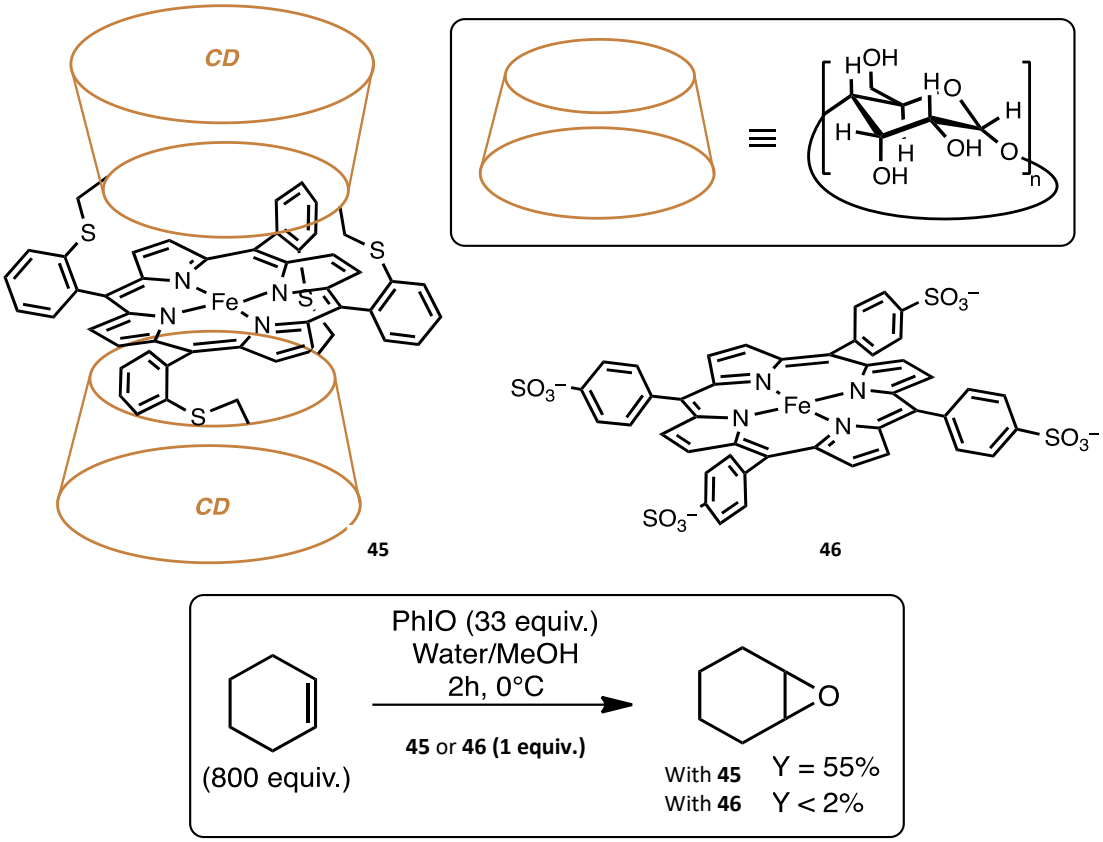

Figure 2.1 Cyclodextrin sandwiched Fe^{II} complex **45** and its model counterpart **46**. Their catalytic activities were compared using the epoxidation of cyclohexene as benchmark reaction.

The Mn^{III}-porphyrin rotaxane complex **47** was synthesized by the group of Nolte in order to mimic natural enzymes such as T4 DNA polymerases (Figure 2.2).[39] The TOF is doubled with the supramolecular system **47**, when compared to its model parent **48**.

[39] Coolen, H. A. K. C.; van Leeuwen, P. W. N. M.; Nolte, R. J. M. *Angew. Chem. Int. Ed.* **1992**, *31*, 905-907.

Progressive epoxidation of the polybutadiene thread as well as the endohedral formation of manganese-oxo intermediate was clearly evidenced by a thorough investigation.[40]

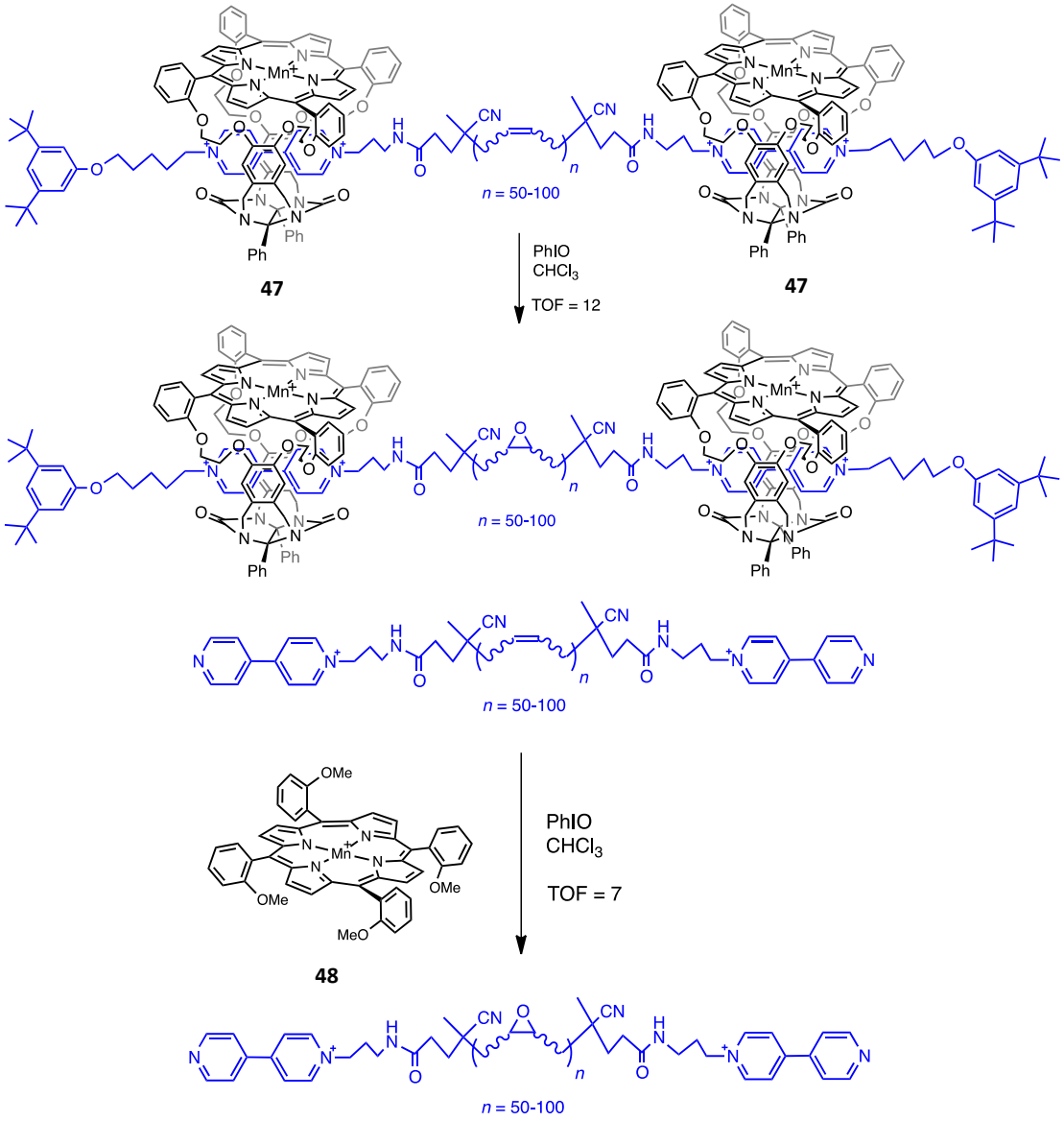

Figure 2.2 The bio-inspired Mn^{III}-porphyrin rotaxane **47** and its catalytic activity compared to that of **48**.

In 2002, the group of Rebek used the resorcin[4]arene-based cavitand **49**, presenting a palladium complex oriented inward the cavity, and tested it as catalyst in allylic

[40] (a) Thodarson, P.; Bijsterveld, E. J. A.; Rowan, A. E.; Nolte, R. J. M. *Nature*, **2003**, *424*, 915-918. (b) Deutman, A. B. C.; Monnereau, C.; Elemans, J. A. A. W.; Ercolani, G.; Nolte, R. J M.; Rowan, A. E. *Science*, **2008**, *322*, 1668-1671. (c) Deutman, A. B. C.; Cantekin, S.; Elemans, J. A. A. W.; Rowan, A. E.; Nolte, R. J. M. *J. Am. Chem. Soc.* **2014**, *136*, 9165-9172. (d) Thomassen, P. J.; Varghese, S.; Bijsterveld, E. J. A.; Thordarson, P.; Elemans, J. A. A. W.; Rowan, A. E.; Nolte, R. J. M. *Eur. J. Org. Chem.* **2015**, *23*, 5246-5253.

substitution reactions (Figure 2.3).[41] Whereas the model complex **50**, which lacks cavity, was unable to discriminate two different substrates, the encaged palladium complex was able to discriminate them efficiently, probably because the well-defined cavity can accommodate more easily a cyclohexyl group than a branched heptyl unit.

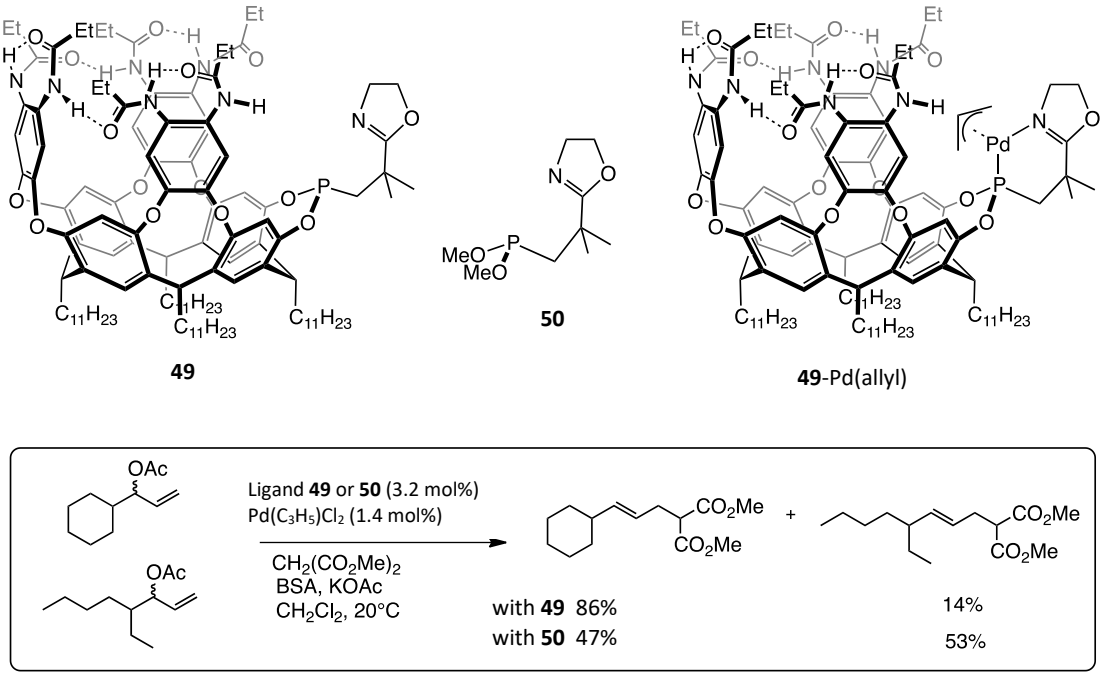

Figure 2.3 A resorcin[4]arene-based cavitand **49** and its model counterpart **50**. The catalytic activities of their palladium complexes have been compared using the allylic substitution as a benchmark reaction.

In 2017, Matt et al. reported the synthesis of a resorcinarene cavitand substituted with two *N*-anisyl-iminophosphoranyl moieties (Figure 2.4).[42] Hydrogenation of a 1:1 mixture of hex-1-ene and dec-1-ene using $[Rh(cod)_2]BF_4$ in the presence of **51** or **52** as catalyst led to a size-selective transformation of these α-olefins. Indeed, the model catalyst gave poor selectivity in favor of the hexane product, whereas the cavitand based catalyst provided much higher substrate selectivity, with a hexane/decane ratio of 5.4. The endohedral functionalization of the cavity of the ligand **51** by the rhodium metal could account for this improvement of the substrate discrimination.

[41] Gibson, C.; Rebek Jr, J. *Org Lett.* **2002**, *4*, 1887–1890.
[42] Chavangan, T.; Bauder, C.; Sémeril, D.; Matt D, D.; Toupet, L.; *Eur. J. Org. Chem.* 2017, 70–76.

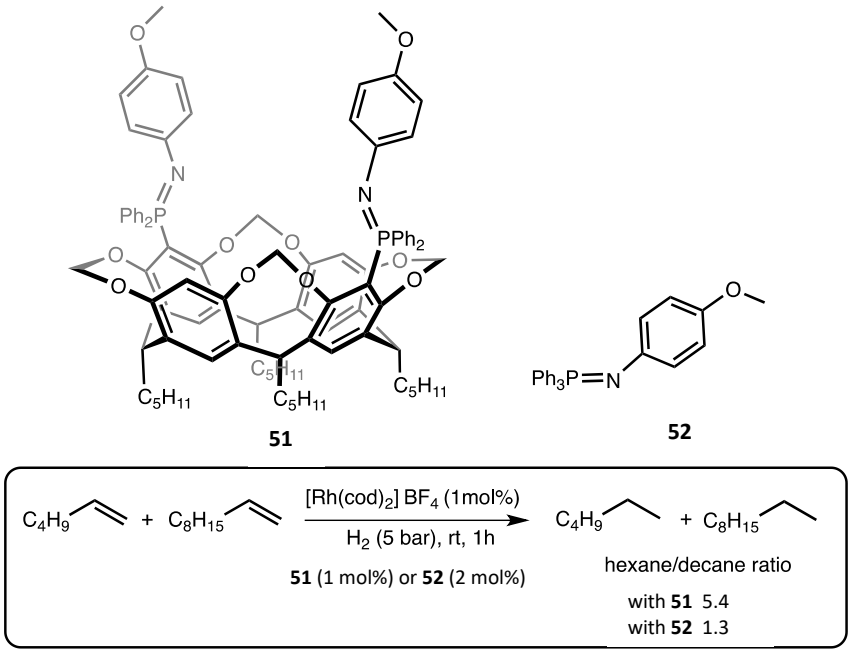

Figure 2.4 Cavitand **51** and its model counterpart **52** and their use in hydrogenation of alkenes.

The same group has described the synthesis of a molecular capsule **53** built with two resorcin[4]arene moieties linked by a meta-xylyl spacer and including two phosphane ligands complexing a "trans-$PtCl_2$" unit (Figure 2.5).[43] This cage complex was tested as catalyst in the hydroformylation of styrene in the presence of $SnCl_2$. The confinement turns out to have a beneficial effect on both activity and regioselectivity: (i) conversions of 55% and 40% are reached with the container **53** and the model catalyst **54**, respectively. This better catalytic activity of **53** was attributed to the formation, inside the cavity, of a hydrido intermediate with a distorted trigonal bipyramidal structure. (ii) The selectivity towards the branched aldehyde is also improved probably because of specific orientations and conformations of the intermediately formed Pt-alkyl units in the confined space of the molecular cavity.

[43] Chavagnan, T.; Sémeril, D.; Matt D, D.; Toupet, L. *Eur. J. Org. Chem.* **2017**, 313–323.

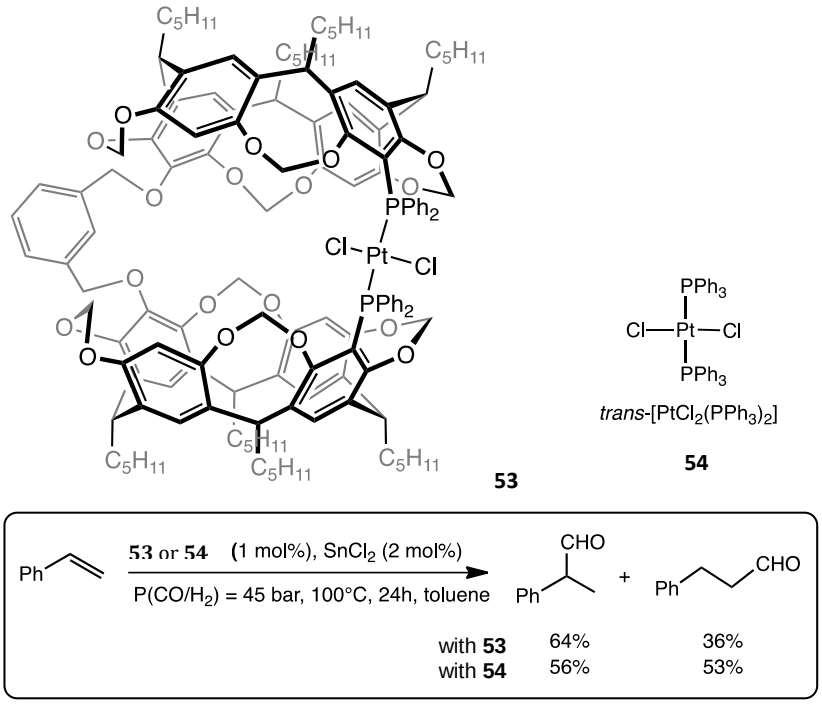

Figure 2.5 Capsule **53** and its model counterpart **54** and their used in hydroformylation of styrene.

Recently, the Sollougoub's group managed to obtain gold complexes of NHC-capped cyclodextrins (CD) (α-CD-AuCl **55** and β-CD-AuCl **56** complexes; Figure 2.6).[44] The encapsulation of the gold ion in the heart of the cavity was nicely demonstrated by a set of NMR and electrochemistry experiments. Besides the interesting enantioselectivities obtained (59% ee with Au(I)@**56**), the most striking point is the switch of ring-size selectivity when the cage is used as catalyst in the ring cyclisation of enynes: with the model catalyst **57** and the cage complex **55** the 5-membered ring product is the major one, whereas the 6-membered ring compound is favored with the confined gold catalyst **56**.

[44] Guitet, M.; Zhang, P.; Marcelo, F.; Tugny, C.; Jiménez-Barbero, J.; Buriez, O.; Amatore, C.; Mouriès-Mansuy, V.; Goddard, J.-P.; Fensterbank, L.; Zhang, Y.; Roland, S.; Ménand, M.; Sollogoub, M. *Angew. Chem. Int. Ed.* **2013**, *52*, 7213-7218.

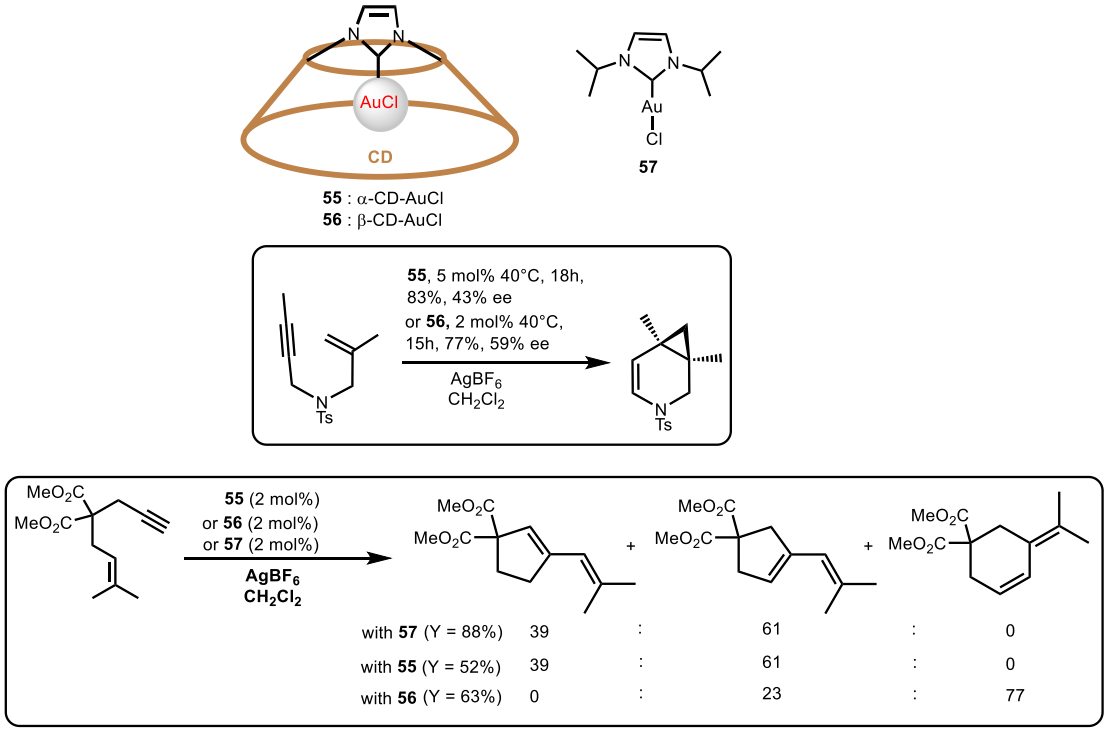

Figure 2.6 Cyclodextrins **55** and **56** functionalized with an endohedral gold-carbene complex and their use in cycloisomersization.

In 2017, the same group reported the two NHC-capped α- and β-cyclodextrins copper(I) complexes α-CD-CuCl **58** and β-CD-CuCl **59** (Figure **2.7**) with different cavity size.[45] The two complexes were compared to study the regioselectivity induced by the cyclodextrin (CD) cavity on the hydroboration of aromatic alkynes. Interestingly, sterically hindered ligand α-CD gives rise to linear products, while the larger β-CD derivative favors branched compounds. They demonstrated that the regioselectivity is governed by the difference of the shape of the catalysts. Besides the conventional "parallel" mechanism, they proposed in this study a new "orthogonal" mechanism, which is consistent with DFT calculations. Thus, changing the shape of the cavity induces a switch of both the mechanism and the regioselectivity of the reaction.

[45] Zhang, P.; Meijide Suárez, J.; Driant, T.; Derat, E.; Zhang, Y.; Ménand, M.; Roland, S.; Sollogoub, M. *Angew. Chem. Int. Ed.* **2017**, *56*, 10821.

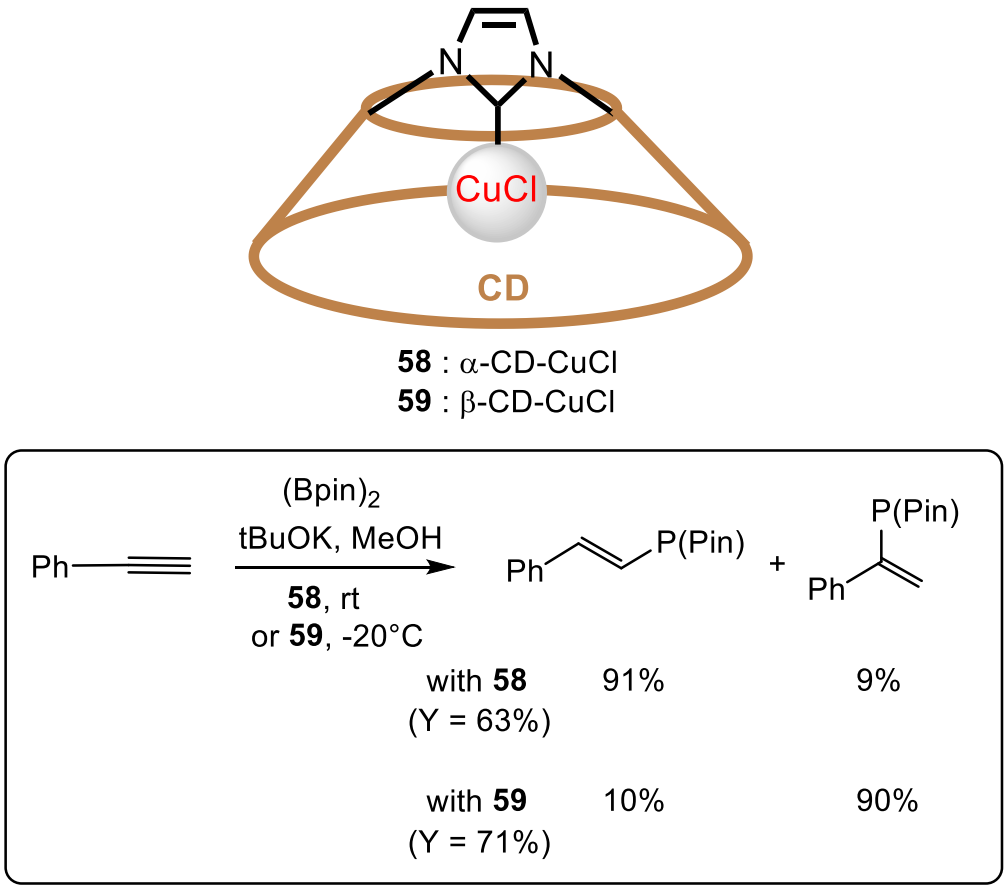

Figure 2.7 Cyclodextrins **58** and **59** functionalized with a copper carbene complex and their use in hydroboration.

In 2009, our group described the synthesis of a hemicryptophane host including an endohedral oxido-vanadium unit (compound **60**, Figure 2.8).[46] This supramolecular catalyst turned to be efficient and selective for the oxidation of sulfides into sulfoxides with yields up to 95%. When compared to the model complex **61**, which lacks cavity, the cage catalyst displayed rate constant up to six times higher, showing that the confinement of the oxido-vanadium site, improved the catalytic activity. Furthermore, a turnover number up to 180 was reached, highlighting that the hemicryptophane cage can be considered as a new class of supramolecular transition-metal based catalysts.

[46] Martinez, A.; Dutasta, J.-P. *J. Catal.* **2009**, *267*, 188-192.

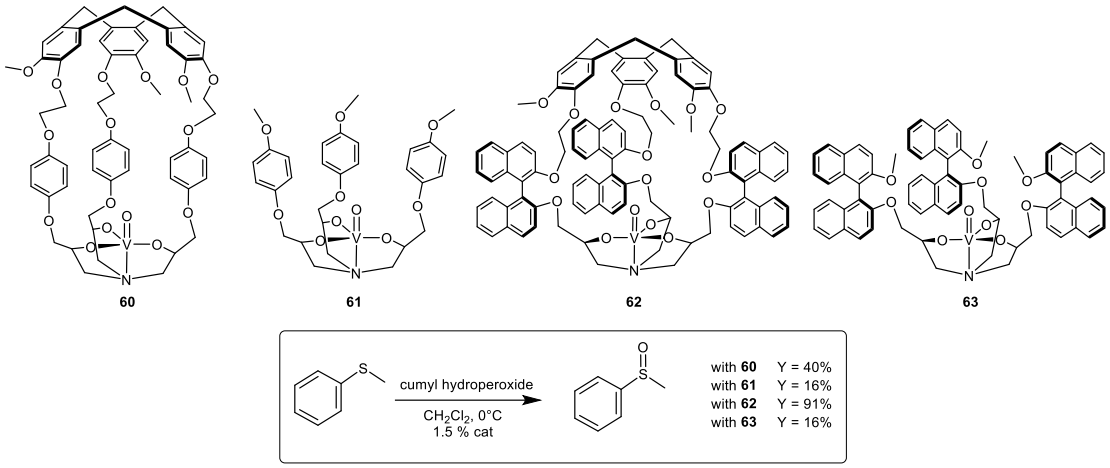

Figure 2.8 oxidovanadium@hemicryptophane hosts **60** and **62** and their model complexes **61** and **63** used as catalysts in the oxidation of thioanisol

More recently, a new set of hemicryptophane cages including an oxidovanadium site, was reported in order to further improve their catalytic performance in sulfoxidation reactions (Figure 2.8).[47] The binaphtol units introduced in the linkers of **62** were expected to isolate more efficiently the heart of the cavity from the bulk of the solvent and thus, should lead to an improved confinement effect. These new hemicryptophane complexes are indeed much more efficient than those previously reported. Reaction rates in the oxidation of thioanisole are 5-fold and 33-fold faster with the hemicryptophane catalysts **62** than with the cage **60** and the model **63**, respectively. Moreover, a TON of 10000 was reached with **62**, underlining the remarkable catalytic activity and stability of this supramolecular catalyst. The key role played by the cavity was evidenced by a competitive inhibition experiment using $Me_4N^+Pic^-$ as competitive guest. While its addition has no influence on the catalytic activity of the model complex, it dramatically affects the reaction rate of the cage catalyst, probably by preventing the access of the cavity to the substrate. Both Michaelis-Menten kinetic and substrate selection were also observed, showing an enzyme-like behavior of the cage catalyst.

Makita *et al.* have reported a zinc(II) complex trapped into the cavity of a hemicryptophane, and its use as a catalyst for the hydrolysis of methyl *para*-nitrophenyl

[47] Zhang, D.; Jamieson, K.; Guy, L.; Gao, G.; Dutasta, J.-P.; Martinez, A. *Chem. Sci.* **2017**, *8*, 789-794.

carbonate (MPC) (Figure 2.9).[48,49] The supramolecular catalyst turned out to be more efficient than the model since a k(**64**)/k(**65**) ratio up to 2.2 was measured. Based on DFT calculations, the cavity was proposed to avoid the inhibition by the solvent DMSO, which cannot coordinate to the Zn(II) inside the cage.

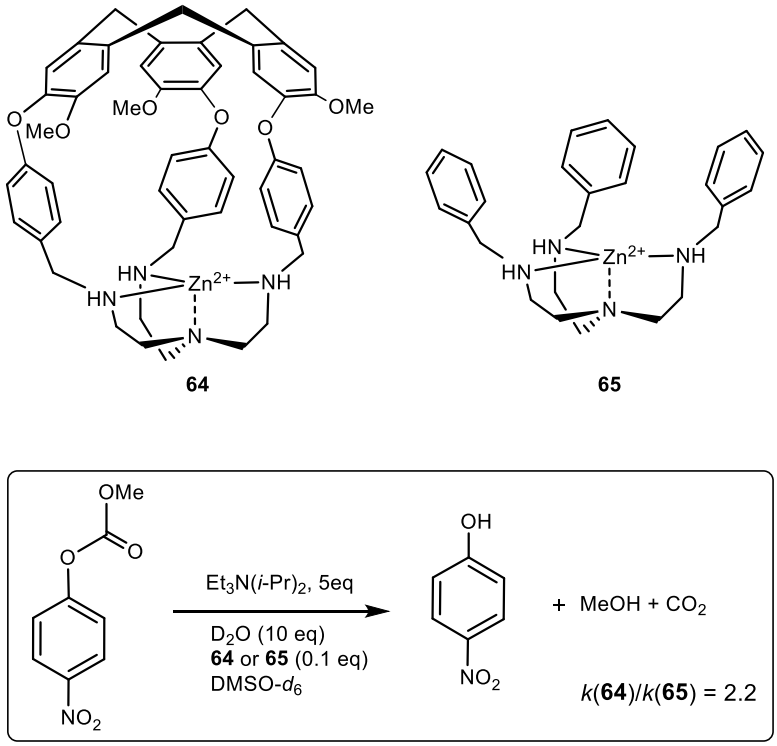

Figure 2.9 Zn@hemicryptophane supramolecular complex **64** and the model compound **65** tested as catalyst for the hydrolysis of methyl *para*-nitrophenyl carbonate.

Oxidation of unreactive C-H bonds, catalyzed by transition metal complexes, arouses a considerable interest as it can provide an easy and cheap access to valuable oxygenated products from alkanes of petroleum and natural gas. Among the supramolecular complexes presenting a well-defined cavity above the metallic site, mainly copper(II), very few examples display a catalytic activity in C-H oxidation of exogenous substrates. The Cu(II)@hemicryptophane complex **66** represents one of the rare supramolecular complexes capable of oxidation of cyclohexane under mild

[48] Makita, Y.; Sugimoto, K.; Furuyosho, K.; Ikeda, K.; Jujiwara, S.-I.; Shin-ike, T.; Ogawa, A. *Inorg. Chem.* **2010**, *49*, 7220-7222.
[49] Makita, Y.; Ikeda, K.; Sugimoto, K.; Fujita, T.; Danno, T.; Bobuatong, K.; Ehara, M.; Jujiwara, S.; Ogawa, A. *J. Organomet. Chem.* **2012**, *706*, 26-29.

conditions and using hydrogen peroxide as stoichiometric oxidant (Figure 2.10).[50,51] A direct comparison with the model compound **67** demonstrates that the cage structure protects the supramolecular catalyst from degradation, leading to yields two times higher. Moreover, the confined catalyst **66** was able to discriminate more efficiently cyclohexane from adamantane than the model **67**, probably because adamantane is too big to enter inside the cavity of **66**. This result opens up the way for a larger use of confined catalysts in C-H bond oxidation.

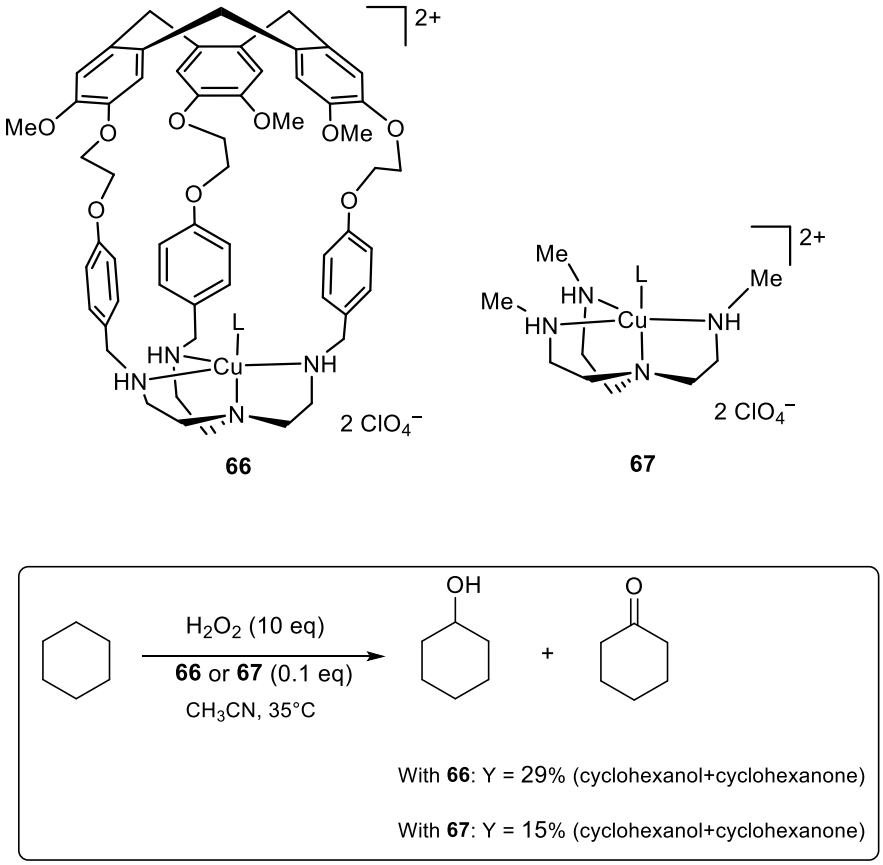

Figure 2.10 Cu(II)@hemicryptophane **66** caged catalyst and its model counterpart **67** used for the oxidation of cyclohexane to cyclohexanone and cyclohexanol (L = MeOH).

[50] Perraud, O.; Sorokin, A. B.; Dutasta, J.-P.; Martinez, A. *Chem. Commun*. **2013**, *49*, 1288-1290.
[51] Perraud, O.; Tommassino, J.-B.; Robert, V.; Albela, B.; Khrouz, L.; Bonneviot, L.; Dutasta, J.-P.; Martinez, A. *Dalton Trans.* **2013**, *42*, 1530-1535.

2.3 Confined organocatalysts

Supramolecular catalysts based on the confinement of organocatalysts into covalent molecular cages have been described. These nano-reactors present an endohedral functionalization of the inner space of their cavity without any metal in their catalytic site or in their framework. As in the previous section, only examples involving covalent cages including an organocatalytic center will be presented.

The group of Rebek Jr. reported the synthesis of cavitand **68**. The molecular cage, functionalized with a Kemp's triacid derivative, displays a carboxylic acid pointed inward a deep open-ended cavity (Figure 2.11).[52] The cavity imposes a specific folding of the substrate in the vicinity of the catalytic site, as a consequence a remarkable regioselectivity in the cyclization reaction of alcohol **69** into **70** was achieved when the cavitand **68** was used as catalyst. Furthermore, the rate constant is more than 50 times higher with the supramolecular catalyst than with its related model compound **71.** These remarkable confinement effects were attributed to the true endohedral functionalization of the molecular cage.

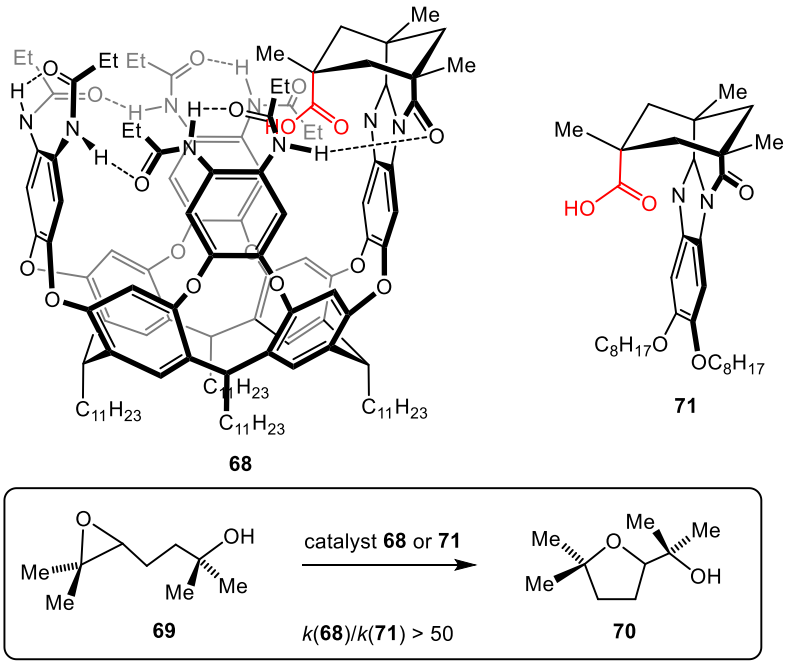

Figure 2.11 Cavitand **68** and its model counterpart **71** used as catalyst in the cyclization reaction of alcohol **69** into **70**.

[52] Shenoy, S. R.; Crisostomo, F. R. P.; Iwasawa, T.; Rebek Jr, J. *J. Am. Chem. Soc*. **2008**, *130*, 5658-5659.

Chen *et al.* synthesized two robust endohedral-functionalized organic cages *via* dynamic covalent chemistry, bearing three phenol hydroxyl groups inside the cavity (Figure 2.12, cage **72**).[53] Compared with the model catalyst **73** which lacks a cavity, the cage catalyst **72** demonstrated excellent catalytic activities in the Friedel-Craft reaction with a wide range of substrates. For instance, in the reaction of *trans*-β-nitrostyrene with 1-methylindole, a yield of 86% was obtained in the presence of cage catalyst **72**, while only 17% yield was obtained in the presence of model analogue **73**. Besides, the authors proposed that the reaction occurred inside the cavity: when steric bulky substrates were used as reactants very low yields were reached, indicating that the cage catalyst presents a remarkable substrate-size selectivity.

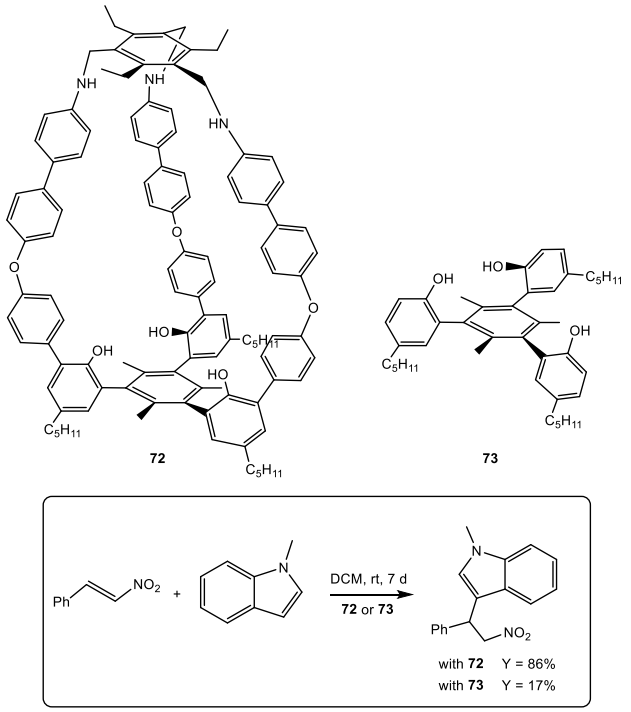

Figure 2.12 Cage **72** and model compound **73** used as catalysts in the Friedel-Craft reaction.

Proazaphosphatranes Verkade's superbases are very efficient basic or nucleophilic organocatalysts: when compared to most other organocatalysts, higher yields and better

[53] Chen, H.-Y.; Goubc, M.; Wanga, J.-B. *Chem. Commun*., **2017**, *53*, 3524-3526.

selectivities are reached while working under milder conditions, as described in Chapter 1.[54]

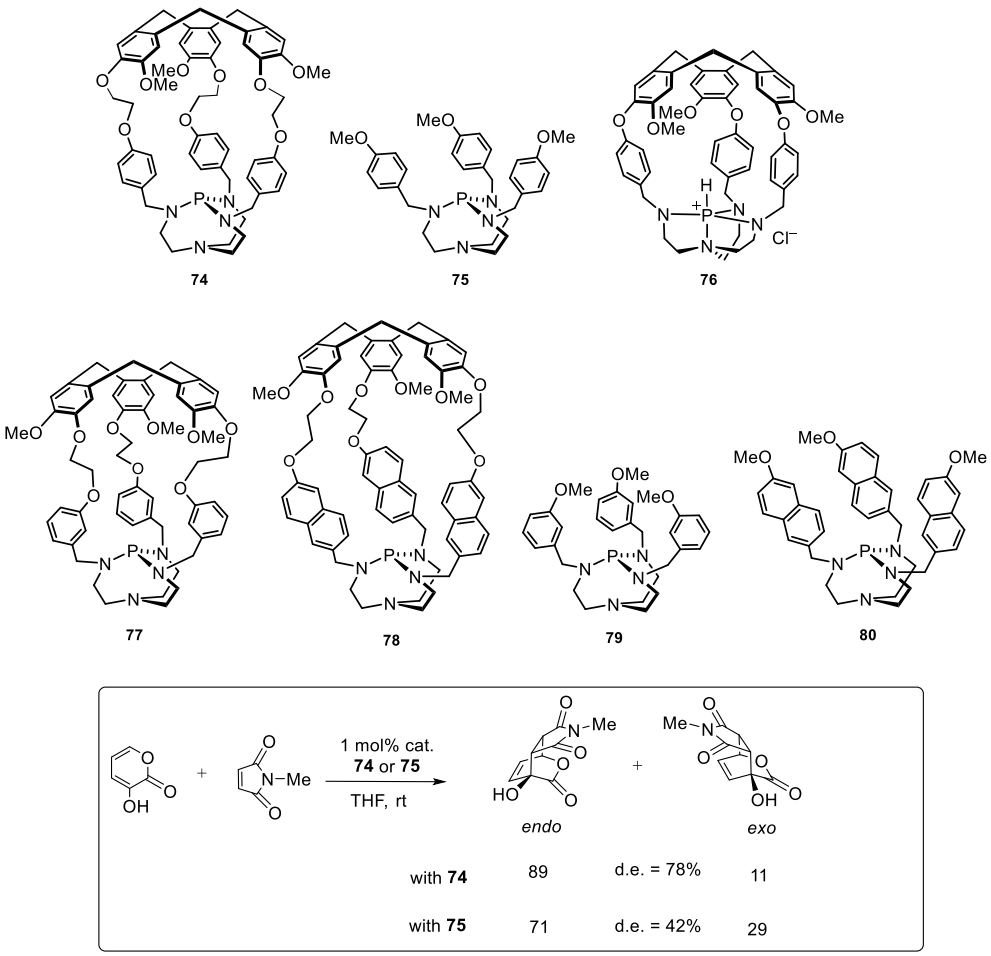

Figure 2.13 Structures of encapsulated superbases **74**, **77**, **78**, of the encaged azaphosphatrane **76** and their related model **75**, **79**, **80** and the compared selectivity of **74** and **75** when used as catalysts in a Diels-Alder reaction between 3-hydroxy-2-pyrone and *N*-methylmaleimide.

When the Verkade's superbase was encapsulated in a hemicryptophane host (compound **74**, Figure 2.13),[55] it was shown that the confinement both slightly increases the basicity of the proazaphosphatrane unit, and dramatically decreases the rate of proton transfer. Although the encaged Verkade's superbase **74** is seven times more basic than its model parent **75**, its protonation rate is one hundred times slower.

[54] For a review on Verkade's superbases, see: Kisanga, P. B.; Verkade, J. G. *Tetrahedron*, **2001**, *57*, 467-475.
[55] Dimitrov-Raytchev, P.; Martinez, A.; Gornitzka, H.; Dutasta, J.-P. *J. Am. Chem. Soc*. **2011**, *133*, 2157-2159.

Makita *et al.* reported the synthesis of the hemicryptophane **76** encaging an azaphosphatrane unit.[56] Due to the more rigid structure of this host, the endohedral proton was strongly shielded by the cage structure, hence the authors were unable to deprotonate the azaphosphatrane despite the various strongly basic conditions used.

In order to investigate the role of size and shape of the cavity on the rate and thermodynamic of the protons transfer, two new encaged proazaphosphatranes **77** and **78** were synthesized (Figure 2.13).[57] The confinement was found to strongly affect the pK_a values: the basicity of the Verkade's superbase is either dramatically improved or strongly decreased, depending on the cage structure. For instance, the basicity of the encaged superbase **77** is 30 times lower than that of its model parent **79** (K_a of 4.42 10^{-32} and 1.26 10^{-33}, respectively). This behavior is in sharp contrast with that of the encapsulated superbase **78,** which is more than 100 times more basic than the model counterpart **80**. The following general trend can be observed: an increase of cavity size (from **74** to **77** and **78)** is associated with a decrease of the rate of proton transfer, as a consequence, the rate of protonation of the highly basic species **78** is 500 000 times slower than that of its model counterpart. The X-ray molecular structures of the host compounds allow rationalizing this unexpected behavior: from **74** to **77** and **78**, the cavity becomes longer but also less wide and the naphthalene linkers of **78** prevent the access to the reactive center, making its protonation kinetically blocked. This underlines how the space available above the basic unit can affect the kinetics and thermodynamics of proton transfer.

The confined superbase **74** has been tested as organocatalyst in the base-catalyzed Diels-Alder reaction shown in Figure 2.13.[58] It displays a good catalytic activity, since a quantitative yield was obtained when anthrone and dimethylfumarate were used as substrates, whereas only 38% yield is reached with trimethylamine as catalyst. The direct comparison with the model superbase **75** shows that the rate of the reaction is twice slower with the cage catalyst **74**. The decrease of the reactivity is much less pronounced than that observed for proton transfer, rendering this system still efficient

[56] Makita, Y.; Furuyoshi, K.; Ikeda, K.; Fujita, T.; Fujiwara, S.; Ehara, M.; Ogawa, A. *Tetrahedron Lett.* **2011**, *52*, 4129-4131.
[57] Chatelet, B.; Gornitzka, H.; Dufaud, V.; Jeanneau, E.; Dutasta, J.-P.; Martinez, A. J. Am. Chem. Soc. 2013, 135, 18659-18664.
[58] Chatelet, B.; Dufaud, V.; Dutasta, J.-P.; Martinez, A. *J. Org. Chem*. **2014**, *79*, 8684–8688.

for organocatalysis. Moreover, it was found that the confinement improves the diastereomeric excess (d.e.) : d.e. of 78% and 42% (both in favor of the *endo* product) were obtained with the cage catalyst **74** and its corresponding model **75** in the reaction between 3-hydroxy-2-pyrone and *N*-methylmaleimide. The increase of the amount of *endo* product with the supramolecular superbase, is consistent with previous reports suggesting that catalysts presenting a deep and narrow cavity lead to an improvement of the *endo*/*exo* ratio, probably because the cavity above the reactive center favors the most compact geometry.[59,60] Thus, the confinement of organocatalyst in the tight space of a hemicryptophane cavity can improve the stereoselectivity of the targeted reaction.

Although Verkade's superbases have been widely used as organocatalyst or stoichiometric reactants in various reactions, their conjugated acid, the azaphosphatranes, have aroused little interest. However, these robust cations were recently reported to catalyze, under mild conditions (1 bar, 100°C), the conversion of CO_2 and epoxides into carbonates (Figure 2.14).[61] Azaphosphatranes encapsulated in a hemicryptophane host (compounds **81**-**84**) have been also tested as catalysts for this reaction. When compared to the model compounds **85**-**88**, (Figure 2.14)[62] the confined catalysts, except **83**, exhibit improved stability and reactivity, probably because the shielding of the aromatic wall of the cavity protects the active site, avoiding some degradations. As a consequence, TON up to 700 can be reached, making **81**, **82** and **84** efficient supramolecular catalysts. Due to their flexibility and the lability of the host-guest complex, the carbonated product is easily released from the cavity, and these hemicryptophane catalysts do not suffer from product inhibition, as often observed with supramolecular catalysts. As mentioned above, supramolecular catalyst **83** displays a specific behavior: its catalytic activity is much lower than that of its model counterpart **87**, whereas this latter presents an activity similar to the other model catalysts. The helical arrangement of the naphthalene linkers above the reactive center precludes its access to the substrates (as already observed for proton transfer), accounting for the observed low reactivity.

[59] Hatano, M.; Ishihara K, K. *Chem. Commun*. **2012**, *48*, 4273-4283.
[60] Hatano M, M.; Mizuno, T.; Izumiseki, A.; Usami, R.; Asai, T.; Akarura, M.; Ishihara, K. *Angew. Chem. Int. Ed*. **2011**, *50*, 12189-12192.
[61] Chatelet, B.; Joucla, L.; Dutasta, J.-P.; Martinez, A.; Szeto, K. C.; Dufaud. V. *J. Am. Chem. Soc*. **2013**, *135*, 5348-5351.
[62] Chatelet, B.; Joucla, L.; Dutasta, J.-P.; Martinez, A.; Dufaud. V. *Chem. Eur. J*. **2014**, *20*, 8571-8574.

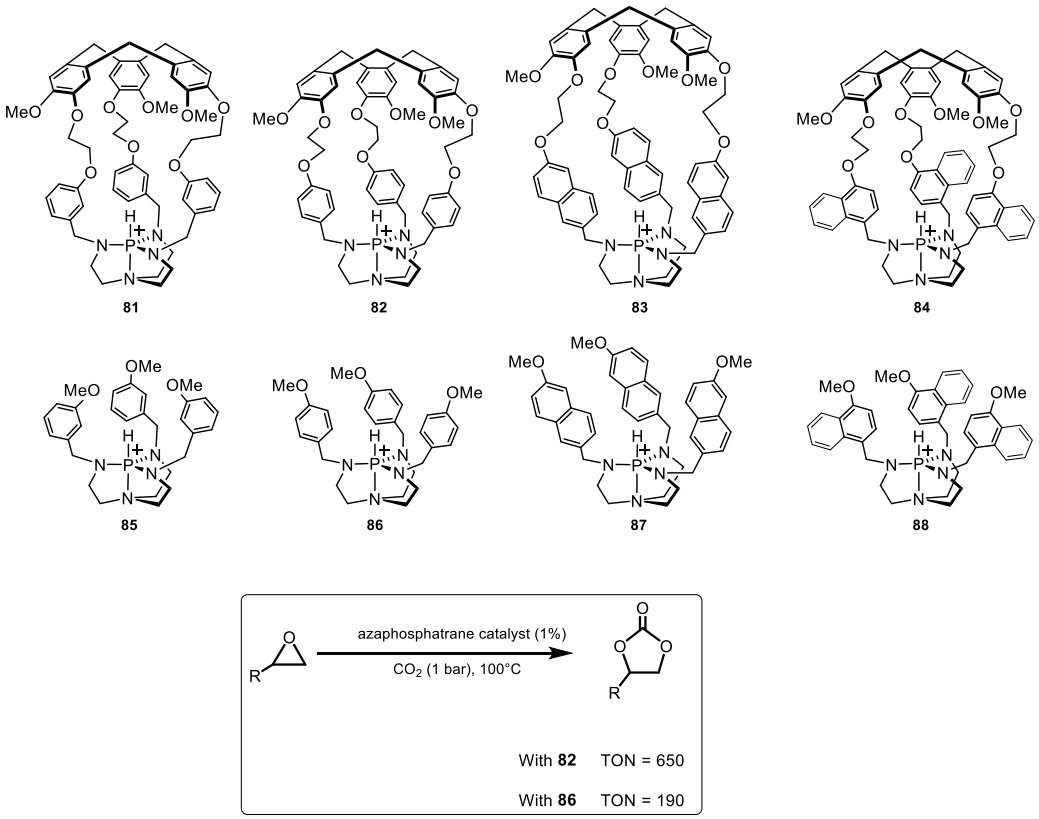

Figure 2.14 Structure of encaged azaphosphatranes, which differ by the size and shape of their cavity, and the corresponding model compounds used as catalysts for CO_2 conversion (chloride as counterion).

2.4 Conclusions

In summary, in this chapter covalent cages have been described including a reactive site oriented toward the molecular cavity. In each case, the catalytic activities of the resulting endohedral functionalized cages have been compared to those of the model catalysts lacking cavity. These comparisons highlight that an improvement on the reaction rate, stability of the catalyst, or selectivity of the reaction, can be induced by the confinement of the catalytic site. Although examples of host molecules presenting a well-defined cavity just above a reactive catalytic center, with catalytic activities directly compared to model catalysts, remain to some extend under-explored, we believe that this field of research will arise a blossoming interest, given the high potentiality of such an approach.

Chapter 3. Halogen bonding: an emergent non-covalent interaction

3.1 Introduction

Supramolecular chemistry is "the chemistry of molecular assemblies and of the intermolecular bond".[63] According to this definition, the task of supramolecular chemistry is to study the non-covalent intermolecular interactions. Typically, non-covalent intermolecular interactions include hydrogen-bonding (HB), electrostatic, dispersion, cation–, anion– and π–π interactions, solvophobic and hydrophobic effects. When considering a supramolecular system, it is vital to consider the interplay of all of these interactions and effects relating both to the host and guest as well as their surroundings.[64] Hydrogen bonding interactions have been widely known and extensively studied in a variety of areas such as organocatalysis and anion recognition. As defined by IUPAC, halogen bonding (XB) is an attractive non-covalent interaction between an electrophilic region associated with a halogen atom and a nucleophilic region associated with a Lewis base,[65] which, however, has been less exploited. The nature of halogen bond origins from the anisotropic distribution of electron density around a covalently bonded halogen atom. Typically, in an XB interaction, the interatomic distance between X and the corresponding nucleophilic atom from Lewis base tends to be shortened and less than the sum of the van der Waals radii. Consequently, the covalent bond R–X lengthens compared to the unbonded one. Another remarkable characteristic of XB is linearity, the interbonded angle is close to 180°. The halogen bond is regarded as an analogue to the more well-known hydrogen bond with respect to the comparable binding strengths and directionality, and has recently aroused considerable interest as a useful alternative non-covalent interaction with immense application in the field of anion recognition and organocatalysis,[66] Extensive studies about halogen bonding have been carried out in crystal engineering and theoretical calculations for a long time.[67] Halogen bonging-based application in solution phase including anion recognition and organocatalysis has been still largely unexplored. Similar to hydrogen bonding, electronic property of moieties bonded to

[63] Lehn, J. -M. *Proc. Nat. Acad. Sci. USA*, **2002**, *99*, 4763–4768.
[64] Steed, J. W.; Atwood, J. L. *Supramolecular chemistry*. **2013**. John Wiley & Sons
[65] Desiraju, G. R.; Ho, P. S.; Kloo, L.; Legon, A. C.; Marquardt, R.; Metrangolo, P.; Politzer, P.; Resnati, G.; Rissanen, K. *Pure Appl. Chem*. **2013**, *85*, 1711−1713.
[66] (a) Cavallo, G.; Metrangolo, P.; Milani, R.; Pilati, T.; Priimagi, A.; Resnati, G.; Terraneo, G. *Chem. Rev*. **2016**, *116*, 2478−2601. (b) Brown, A.; Beer, P. D. *Chem. Commun.* **2016**, *52*, 8645-8658.
[67] (a) Bent, H. A. *Chem. Rev*. **1968**, *68*, 587–648.; (b) Murray-Rust, P.; Motherwell, W. D. S. *J. Am. Chem. Soc*. **1979**, *101*, 4374–4376.; (c) Ramasubbu, N.; Parthasarathy, R.; Murray-Rust, P. *J. Am. Chem. Soc*. **1986**, 108, 4308–4314.; (d) Kolář, M. H.; Hobza, P. *Chem. Rev*. **2016**, *116*, 5155–5187.

halogen atom is of enormous importance to the strength of the halogen bond, and also the steric environment surrounding the halogen bond plays a key role in application. The electronic property of halogen-bonded moieties could be reasonably modified by organic synthesis based on specific requirements, thus making halogen bonding a powerful tool in non-covalent interaction based applications.

3.2 Halogen bonding in anion recognition

The field of non-covalent anion coordination chemistry may be traced back to the pioneering work on the cation-binding behavior of dibenzo[18]crown-6 by Charles Pedersen in 1967 which revealed the beginning of modern supramolecular chemistry. Franz P. Schmidtchen and Jean-Marie Lehn established fundamental developments in non-covalent anion coordination with the synthesis of several hosts of crucial conceptual importance.[68] Anion complexation became a popular topic since the late 1980s as a new generation of chemists began to address this relatively unconquered frontier. Cation coordination chemistry has been well developed. On the contrary, the coordination chemistry of anions received little attention which could be attributed to the factor that anions have a lower charge to radius ration, which leads to less effective electrostatic binding interactions.[66] Besides, intrinsic sensitivity to pH values makes it more challenging for anion recognition.[66] Despite this, the importance of anion coordination chemistry should not be ignored. Anions are ubiquitous throughout biological systems and in nature world. There have been a number of research concerning anion recognition and sensing.[66,69] Different receptors for various anions have been developed. A series of non-covalent interactions are utilized independently or concertedly for anion recognition including electrostatic interactions, hydrogen bonding, the hydrophobic effect, etc. As an emergent non-covalent interaction, halogen bonding is expected to occur when relatively electron-poor halogen-containing moieties interact with naturally electro-rich anions.[69] Some representative examples will be selected to demonstrate the validity of halogen binding in anion recognition.

[68] (a) Schmidtchen, F. P.; Berger, M. *Chem. Rev.* **1997**, *97*, 1609–1646. (b) Lehn, J.-M. *Acc. Chem. Res.* **1978**, *11*, 49–57.
[69] Gilday, L. C.; Robinson, S. W.; Barendt, T. A.; Langton, M. J.; Mullaney, B. R.; Beer, P. D. *Chem. Rev*. **2015**, *115*, 7118-7195.

Haloperfluoroarene-based halogen bond backbones are commonly used in the design of XB donors. This is because the electron-withdrawing ability of fluorine atoms could enhance the electronic deficiency of XB, and thus increasing the interaction towards anions. The XB interactions directing anion recognition processes in solution was first demonstrated by Resnati and co-workers.[70]

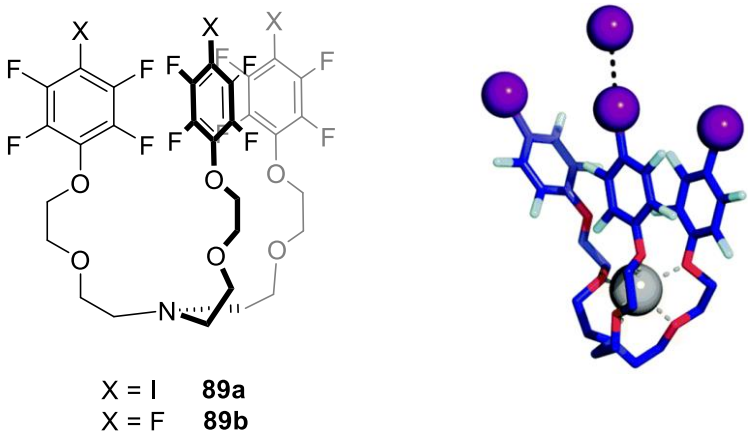

Figure 3.1 Chemical structure of Resnati's heteroditopic halogen-bonding receptor **89a** (left), and solid state structure of the [NaI(**89a**)] complex (right).

The authors designed and synthesized a heteroditopic iodo-perfluoroaromatic tripodal receptor (**89a**, Figure 3.1) comprising a well-established motif for cation binding and a motif for XB-based anion recognition. Solid state characterization of the [NaI(**89a**)] complex confirmed simultaneous binding of I^- and Na^+ by **89a**. Solution NMR experiments indicated that **89a** has a higher binding affinity for Na^+ than the monotopic receptor **89b** (K_a = 2.6 ×10^5 M^{-1}; K_b = 1.3 × 10^4 M^{-1}), which evidenced the enhanced effect of XB-mediated anion binding on the cation complexation. Mass spectrometry competition experiments revealed a preferential selectivity of **89a** for I^- in the presence of Br^- and Cl^- anions. These results proved that **89a** acted as a specific XB receptor for effectively selective anion recognition processes, which provides a strategy for designing novel XB-based anion recognition receptors.

Another tridentate iodoperfluoroarene derivative **90a** reported by Taylor and co-workers was demonstrated to act as a multidentate halogen bonding receptor to achieve

[70] Mele, A.; Metrangolo, P.; Neukirch, H.; Pilati, T.; Resnati, G. *J. Am. Chem. Soc*., **2005**, *127*, 14972–14973.

a higher affinity binding for Cl^- than Br^- and I^- anions (Figure 3.2).[71] Electron-withdrawing carboxyl groups were introduced to promote halogen-bond donor ability. Calculation results suggested geometrical feasibility of multipoint binding from halides of **90a**. A 1:1 stoichiometric binding mode was confirmed by the Job plots and electrospray ionization mass spectrometry (ESI-MS). The binding data evidenced significant effect of "the chelate cooperativity": the tridentate receptor **90a** has a higher association constant for Cl^- than that of the bidentate receptor **90b** ($K_{2a} = 1.9 \times 10^4$ M^{-1}; $K_{2b} = 1.8 \times 10^3$ M^{-1}). A modified receptor **90c** was prepared with two iodine substituents replaced by fluorine. Negligible affinity for chloride by **90c** ($K_{2c} < 10$ M^{-1}) suggested that halogen bonding is responsible for the observed binding rather than anion-π interactions.

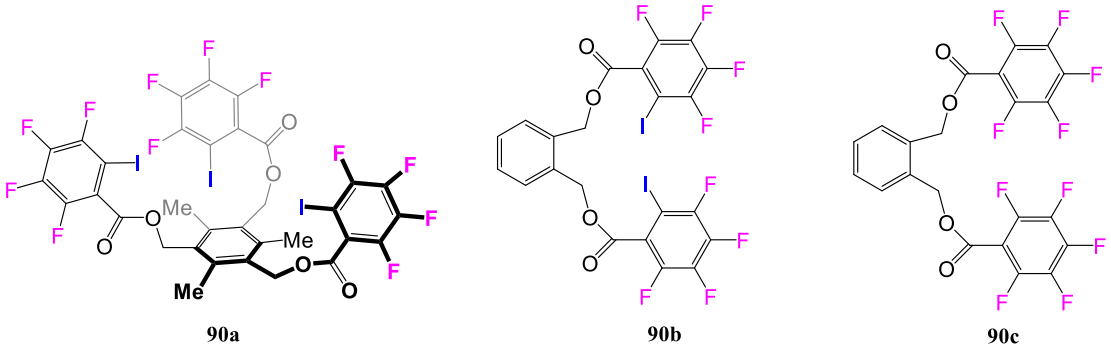

Figure 3.2 Structures of haloperfluoroarene-based XB anion receptors (**90a** and **90b**) and control receptor **90c**.

The two haloperfluoroarene-based XB anion receptors discussed above are both neutral receptors, of which the interaction strength strongly depends on the electronic properties of the organic backbones. Another general strategy to boost binding affinities is the use of positively charged receptors which benefit from charge assistance. Halopyridinium, haloimidazolium or halotriazolium moieties-based XB anion recognition receptors have been extensively studied and this strategy has proved to be successful.[66]

[71] Sarwar, M. G.; Dragisic, B.; Sagoo, S.; Taylor M. S., *Angew. Chem., Int. Ed.*, **2010**, *49*, 1674–1677.

Beer and coworkers reported a series of macrocyclic charge-assisted haloimidazolium receptors. The *syn* atropisomer **91a** demonstrated an evident selectivity for Br^- among the halide anions (K_a = 889 M^{-1}, Figure 3.3).[72] Protoimidazolium-functionalised HB analogue **91b** was compared under the same conditions, showing much weaker binding affinity for bromide (K_b = 130 M^{-1}). Besides, no chemical shift changes in the ^1H NMR spectrum of the receptor *anti* bromoimidazoliophane **91c** upon addition of halide ions illustrated that the steric effect and preorganized behavior of host **91a** contributed to a pronounced selectivity.

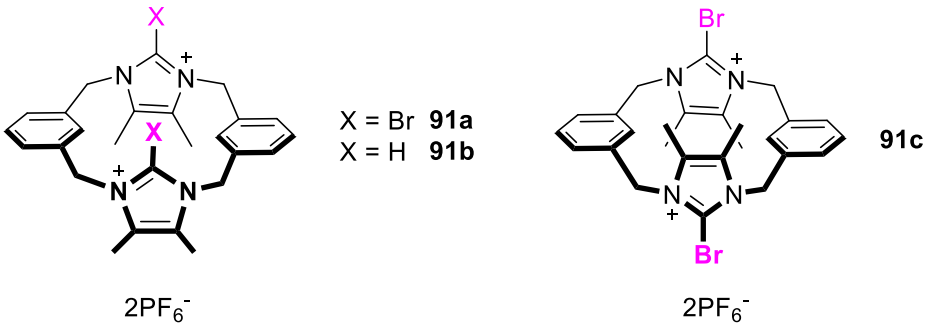

Figure 3.3. Structures of haloimidazolium receptors **91a** (*syn*), **91c** (*anti*) and protic analogue **91b**.

Subsequently the same group synthesized a new series of fluorescent halogen bonding (XB) macrocyclic halo-imidazolium receptors by replacing the xylyl spacer with an extended naphthalene motif. This results in remarkably stronger affinities for I^- by receptor **92a** (K_a = 9.55 ×10^5 M^{-1}) and for Br^- by receptor **92b** (K_b = 6.31 × 10^5 M^{-1}), respectively, as demonstrated through ^1H NMR and fluorescence spectroscopic titration experiments in a competitive CD_3OD/D_2O (9:1) aqueous solvent mixture (Figure 3.4).[73] Both the protic- and chloro- imidazoliophane receptors **92d** and **92c** showed ineffective complexation under the same conditions. Computational DFT and molecular dynamics simulations confirmed the formation of complexes between receptors and anions through a cooperative way.

[72] Caballero, A.; White, N. G.; Beer, P. D. *Angew. Chem., Int. Ed.*, **2011**, *50*, 1845–1848.
[73] Zapata, F.; Caballero, A.; White, N. G.; Claridge, T. D. W.; Costa, P. J.; Fe ´lix, V.; Beer, P. D. *J. Am. Chem. Soc.*, **2012**, *134*, 11533–11541.

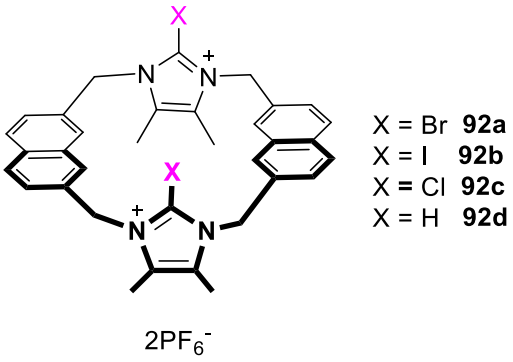

Figure 3.4 Structures of haloperfluoroarene-based XB anion receptors

The first example of enantioselective anion recognition using XB interactions has been demonstrated by Beer and coworkers. They synthesized a novel dicationic XB chiral receptor that contains the (*S*)-1,1'-bi-2-naphthol (BINOL) backbone and iodotriazolium motif (Figure 3.5).[74] They also prepared the HB analogue for comparison. In all chiral anions pairs investigated, the XB receptor **93a** exhibited remarkably higher binding affinities than HB analogue **93b** did, more than one order of magnitude enhancement in association constant values were observed in all cases.

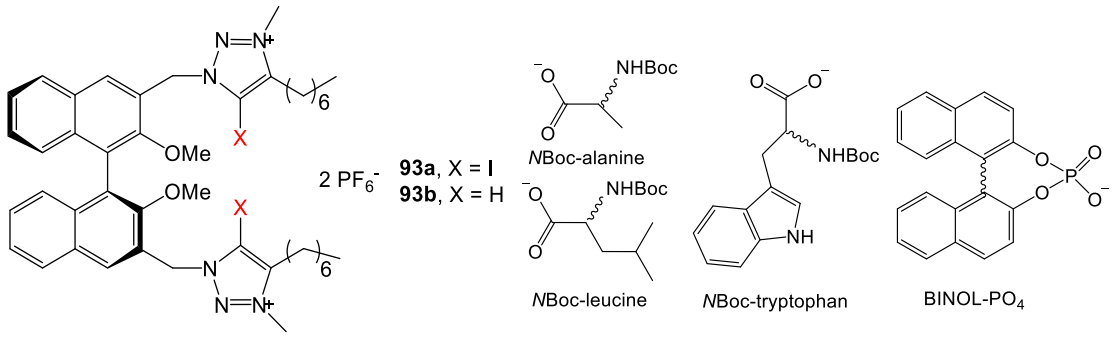

Figure 3.5 Structures of the (*S*)-BINOL receptors **93a**, **93b**, and the chiral anions investigated.

In addition, XB receptor **93a** proved to be able to recognize a range of chiral amino acid carboxylate or BINOL-phosphate anions with enhanced enantioselectivities compared to the HB analogue **93b**, which showed almost no enantiodiscrimination

[74] Lim, J. Y., Marques, I., Ferreira, L., Félix, V., Beer, P. D. *Chem. Commun*. **2016**, *52*, 5527-5530.

capabilities for all of the chiral anion investigated. Besides, molecular dynamics (MD) simulations and DFT calculations were performed to demonstrate that the strict linearity of XB and host–guest steric interactions attributed to the enhanced chiral recognition behavior observed experimentally.

Mechanically interlocked molecular architectures such as rotaxanes and catenanes are a fascinating member of host systems for sensing charged guest species as well as for prototypical molecular switches and shuttles. In 2010, Beer and coworkers demonstrated the first XB interlocked host system through the bromide anion-templated synthesis strategy (Figure 3.6).[75] This rotaxane contained a bidentate HB donor motif and iodotriazolium XB donor group converging towards a central binding cavity.

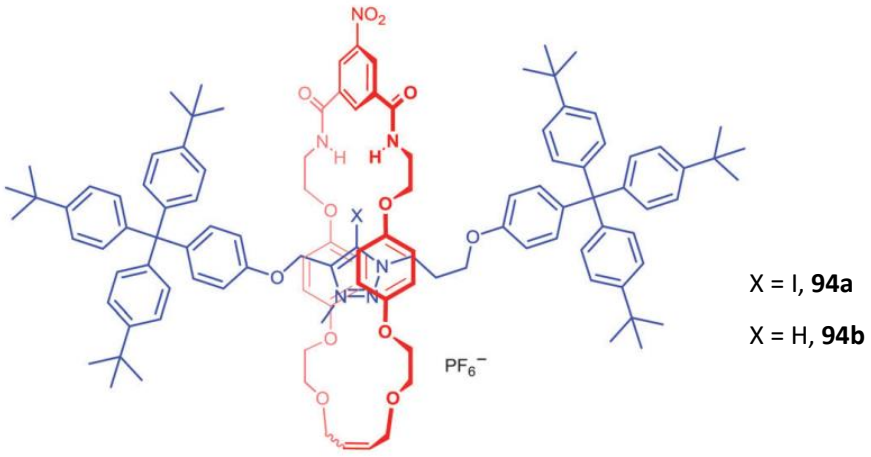

Figure 3.6 Structures of rotaxanes receptors **94a** and **94b**.

The resulted XB rotaxane receptor **94a** demonstrated a significantly enhanced binding affinity compared to the HB rotaxane analogue **94b**. Among halide anions studied, **94a** showed stronger binding affinity for I^- (K_a = 2228 M^{-1}) over Br^- (K_a = 1251 M^{-1}) and Cl^- (K_a = 457 M^{-1}) in a competitive aqueous solvent mixture ($CDCl_3$: CD_3OD : D_2O 45 : 45 : 10). The authors attributed the selectivity preference for the larger halide anion to the accessibility of the binding site to larger anions and weaker competition for the more lipophilic halide by the aqueous solvent medium.

[75] Kilah, N. L; Wise, M. D.; Serpell, C. J.; Thompson, A. L.; White, N. G.; Christensen, K. E.; Beer, P. D. *J. Am. Chem. Soc.*, **2010**, *132*, 11893–11895.

Subsequently, Beer's group prepared the first all halogen-bonding symmetrical 2-bromoimidazolium homo[2]catenane **95** by bromide anion templation (Figure 3.7).[76] Fluorescence titration experiments were carried out to investigate anion recognition properties of the XB catenane **95**. Addition of Cl^- and Br^- to catenane **95** caused significant changes in the intensity of the emission band with a binding constant value of $Ka = 3.71 \times 10^6\ M^{-1}$ for Cl^- and $Ka = 1.48 \times 10^5\ M^{-1}$ for Br^-, respectively. By contrast, addition of F^-, I^-, AcO^-, $H_2PO_4^-$, NO_3^-, and HCO_3^- to a solution of the catenane **95** induced negligible spectral response, which probably suggested the precise preorganized interlocked cavity of catenane **95** for binding Cl^- and Br^- and that convergent XB bromoimidazolium–halide interactions played dominant roles in the recognition process.

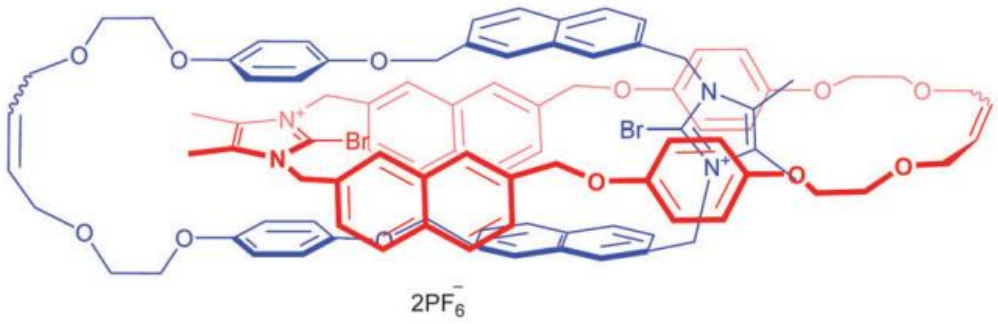

Figure **3.7** Structure bromoimidazolium homo[2]catenane **95**.

Although halogen bonding has been known for decades, its application has been still largely unexplored. Recent advances in anion recognition by XB-based receptors strongly suggested XB-based host molecules are able to compete and even outperform HB analogues, especially in halide anions recognition. Anions recognition in competitive aqueous solution has been developed, paving the way to the practical applications concerning our daily life such as selective detection, removal and transportation of negatively charged species of interest. In the light of fascinating results obtained up to now, much more effort would be put into halogen bonding anion recognition, and the potential could be fully exploited in this area.

[76] Caballero, A.; Zapata, F.; White, N. G.; Costa, P. J.; Fe ´lix, V.; Beer, P. D. *Angew. Chem., Int. Ed.*, **2012**, *51*, 1876–1880.

3.3 Halogen bonding in organocatalysis

As well known, noncovalent hydrogen bonding has been largely explored and firmly established as a tool in a wide range of organic transformations. Impressive performance like relatively mild reaction conditions, outstanding enantioselectivities has been observed in the presence of well-tailored hydrogen bonding donors.[77] Given the similarities shared by hydrogen and halogen bonding, it is rational to expect halogen bonding to be a promising candidate to act as a noncovalent interaction in organocatalysis, though few examples reported so far involving halogen bonding interaction.

In 2015, Huber and coworkers reported the first case of a halide-abstraction-type reaction of 1-chloro-isochroman with a silyl enol ether in the presence of catalytic amount of preorganized halogen-bond donor **96** (Figure 3.8).[78] The inhibition of the catalyst was avoided in this reaction by the formation of stable silylchloride (TBSCl) between the liberated chloride and silyl compound. Comparisons with monodentate variants and neutral halogen-bond donors highlighted the potency of bidentate halobenzimidazolium halogen-bond donor **9**6. The authors also argued that there is limit to the strength of halogen bonding, since the decomposition of compound **96** was detected in the presence of chloride at room temperature.

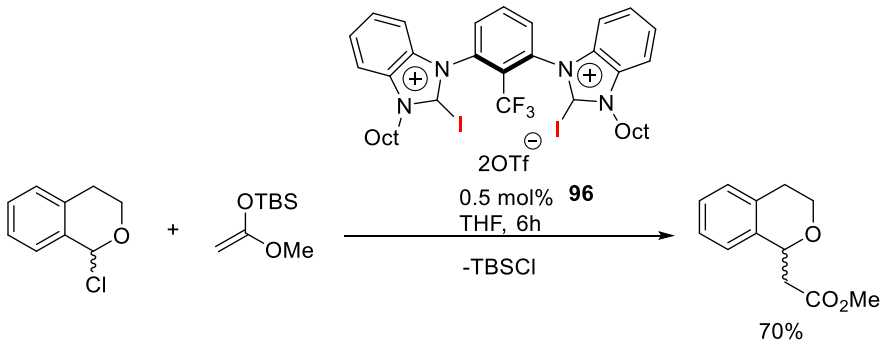

Figure 3.8 Reaction of 1-chloro-isochroman with a silyl enol ether catalyzed by preorganized XB donor **96**.

[77] (a) Doyle, A. G.; Jacobsen, E. N. *Chem. Rev.* **2007**, *107*, 5713 – 5743; (b) Zhang, Z. G.; Schreiner, P. R. *Chem. Soc. Rev*. **2009**, *38*, 1187 –1198.
[78] Jungbauer, S. H.; Huber, S. M. *J. Am. Chem. Soc*., **2015**, *137*, 12110.

Subsequently, the same group prepared benzimidazolium-based halogen bond donor **97** with the same cation of **96** and a less coordinating $BArF_4^-$ as counterion (Figure 3.9).[79] The resulted halogen bond donor **97** was used as a catalyst in a Michael addition reaction. Systematic comparisons with its variants including non-halogenated compounds and imidazolium-based analogues strongly suggested that the halogen bonding interaction played a dominant role in activating Michel addition acceptor.

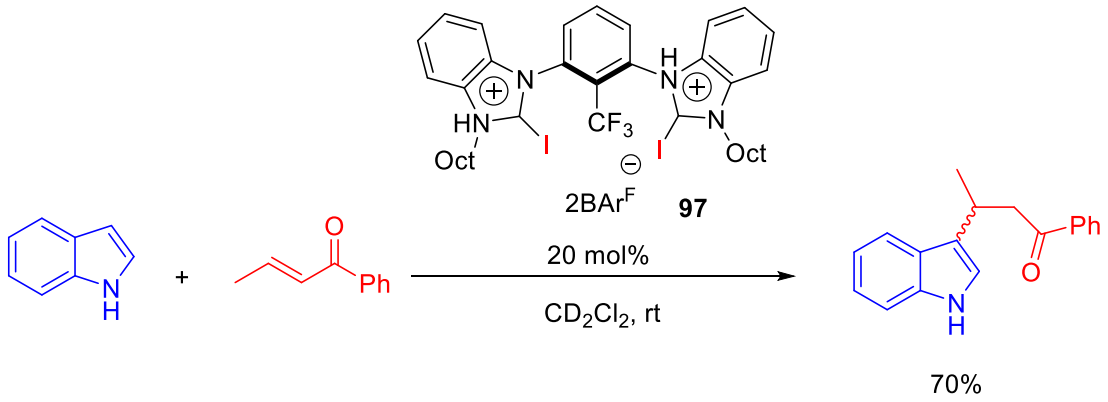

Figure 3.9 Michael addition benchmark reaction catalyzed by halogen bonding donor catalyst **97**.

Takemoto and coworkers successfully applied halogen bond donors like neutral electrophilic iodine(I) species *N*-iodosuccinimide (NIS) and *N*-iodosaccharin (NISac) as activators to promote semipinacol rearrangement in good yields under mild conditions with good functional group tolerance (Figure 3.10).[80] In the proposed mechanism, C-X bond of compound **98** was cleaved through halogen bonding interaction, generating carbocation intermediate, which underwent rearrangement and gave final product **100**. At the same time, the liberated halide (Br^-, Cl^-) cleaved N-I bond of NIS or NISac to form interhalogen compound, and also a Si-N bond was formed. Evidently, the halogen bond donor **98** was consumed completely in the end, and therefore a stoichiometric amount of activators **98** were needed. Besides, computational studies were performed indicating that charge transfer from bromine atom of **98** to iodine atom of NIS or NISac was supposed to be the driving force for the rearrangement of **98**.

[79] Gliese, J. P.; Jungbauer, S. H.; Huber, S. M. *Chem. Commun.* **2017**, *53*, 12052-12055.
[80] Tsuji, N.; Kobayashi, Y.; Takemoto, Y. *Chem. Commun*. **2014**, *50*, 13691–13694.

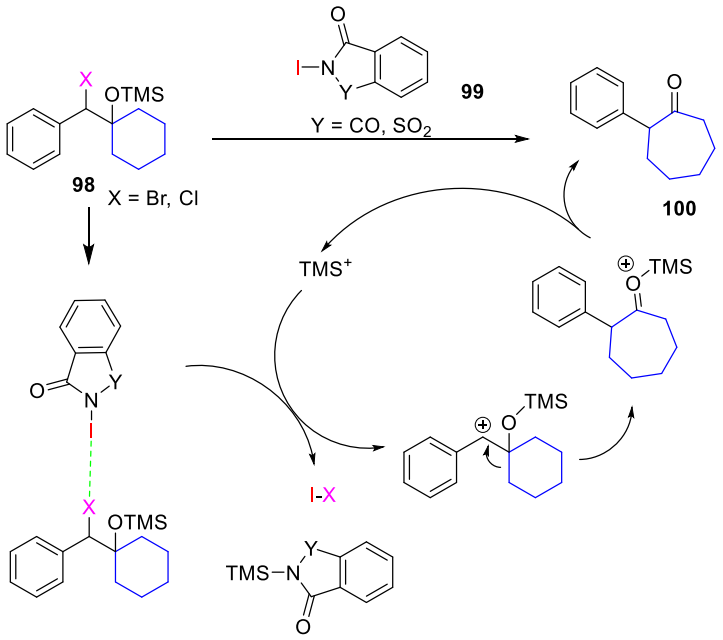

Figure 3.10 Proposed pathway for the semipinacol rearrangement promoted by halogen bond donors NIS or NISac.

Very recently, Kuwano and Arai et al. reported a quinidine-based chiral organic base catalyst **101** with halogen-bonding-donor functionality for asymmetric Mannich reaction between malononitrile and *N*-Boc imines with excellent enantioselectivities (Figure 3.11).[81] The protonated analogue was also applied in the same reaction for comparison, resulting in a much lower yield and selectivity than that of **101**. Besides, NMR studies showed stronger interaction between XB donor **101** and substrates than that of protic analogue, indicating a cooperative catalytic role of the halogen-bonding with the amine base.

[81] Kuwano, S.; Suzuki, T.; Hosaka, Y.; Arai, T. *Chem. Commun*. **2018**, *54*, 3847-3850.

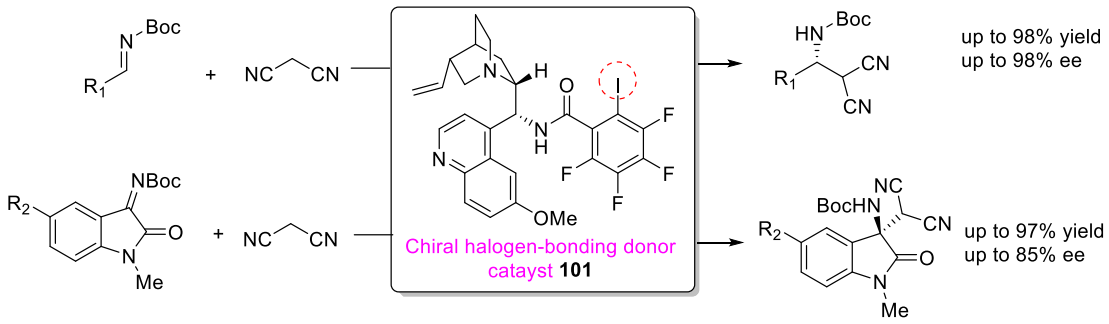

Figure 3.11 Asymmetric Mannich reaction catalyzed by a quinidine-based chiral halogen bond donor organic base catalyst **101**.

Halogen bonding interactions used for organocatalysis are still limited for the moment compared to hydrogen bonding interactions applied in a variety of organic transformations. But from increasing published results, XB-related research is growing rapidly. It can be anticipated that more applications will be achieved in the area of organocatalysis by halogen bonding.

3.4 Conclusions

As an emerging intermolecular interaction, the utilization of halogen bonding interactions in solution phase applications is still in its infancy. Inspired by hydrogen bonding, some strategies related to HBs have been performed to exploit and optimize XB-based applications in solution. Considering the many expressive examples of halogen-bonding-involved recognition and catalysis, more fascinating results in enantioselective catalysis and recognition can be expected.

Part II: New applications of proazaphosphatranes in catalysis

Proazaphosphatranes, as described in Chapter 1, have a large variety of applications in organic transformations acting as either nonionic bases or organocatalysts. Strong basicity and relatively weak nucleophilicity make proazaphosphatranes versatile reagents. Easy transannulation of bicyclic structure of proazaphosphatranes, which could stabilize the intermediates during reaction processes, also accounts for their remarkable performance. On the other hand, tailored cage molecules have proved to have significant effects on catalytic activities in terms of selectivity and efficiency just as described in Chapter 2. Encaged proazaphosphatranes in confined hemicryptophane structures have demonstrated manifest effects on proton transfer and on diastereoselectivities. Inspired by these attracting results, we continued to put our efforts into discovering new applications of proazaphosphatranes. In the following two chapters, Chapter 4 will demonstrate proazaphosphatrane -Verkade's superbase- as an organocatalyst for Strecker reaction, and subsequently a FLP (frustrated Lewis pair) system for MBH reaction (Morita–Baylis–Hillman reaction), where encaged proazaphosphatrane acts as Lewis base and $TiCl_4$ as Lewis acid, will be presented in Chapter 5.

Chapter 4. Verkade's superbase as an organocatalyst for Strecker Reaction

4.1 Introduction

Proazaphosphatranes, also known as Verkade's superbases, were first described by J. G. Verkade in 1989.[1] In contrast to iminophosphine -phosphazenes- bases, the Verkade's superbases protonate on the phosphorus atom: upon this proton transfer, the apical nitrogen links to the positive phosphorus creating a highly stable azaphosphatrane structure (Figure 4.1).[4] The remarkable stability of this conjugate acid renders the Verkade's superbase highly basic (pKa = 32),[3] one of the most basic nonionic base reported so far.

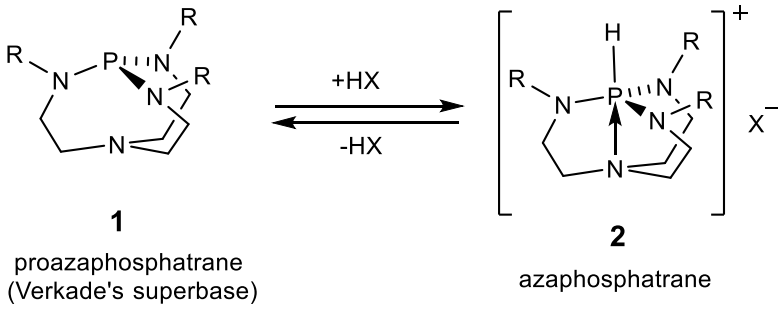

Figure 4.1 The structures of proazaphosphatrane and azaphosphatrane.

Proazaphosphatranes have therefore attracted considerable interests as highly efficient basic and nucleophilic catalysts to promote a large number of reactions, such as trimerization of isocyanates,[82] acylation of alcohols,[5] dehydrohalogenations of alkyl halides,[83] silylation of alcohols,[17] the Henry reaction,[84] transesterification of esters,[20] and additions of trimethylsilyl cyanide to aldehydes and ketones.[85] The reaction conditions are generally milder with the Verkade's superbase than with other organocatalysts: lower temperatures and shorter reaction times are usually used and the reactions are often more selective.[4] Besides this remarkable activity as organocatalyst, new aspects of the chemistry of Verkade's superbases have recently been developed, i.e. they were found to act as highly donor ligand for transition metal complexes,[86] leading to very active organometallic catalysts, for Suzuki-Miyaura cross-coupling

[82] Tang, J.-S.; Verkade, J. G. *Angew. Chem., Int. Ed. Engl*. **1993**, *32*, 896–898.
[83] Arumugam, S.; Verkade, J. G. *J. Org. Chem*. **1997**, *62*, 4827–4828.
[84] Kisanga, P. B.; Verkade, J. G. *J. Org. Chem*. **1999**, *64*, 4298-4303.
[85] Wang, Z.; Fetterly, B.; Verkade, J. G. *J. Organomet. Chem*. **2002**, *646*, 161–166.
[86] (a) Thammavongsy, Z.; Khosrowabadi Kotyk, J. F.; Tsay, C.; Yang, J. Y. *Inorg. Chem.* **2015**, *54*, 11505-11510; (b) Thammavongsy, Z.; Kha, I. M.; Ziller, J. W.; Yang, J. Y. *Dalton Trans.* **2016**, *45*, 9853-9859; (c) Chatelet, B.; Nava, P.; Clavier, H.; Martinez, A. *Eur. J. Inorg. Chem*. **2017**, *37*, 4311–4316.

reactions, [87] or Buchwald−Hartwig amination reactions of aryl chlorides. [88] Proazaphosphatranes have also been confined in molecular cages or mesoporous silica leading to unexpected behavior and reactivity.[55,57,89]

Recently, proazaphosphatranes turned out to be remarkable catalysts for the reductive functionalization of CO_2 into methyl amines, in the presence of hydroborane (Figure 4.2).[89]

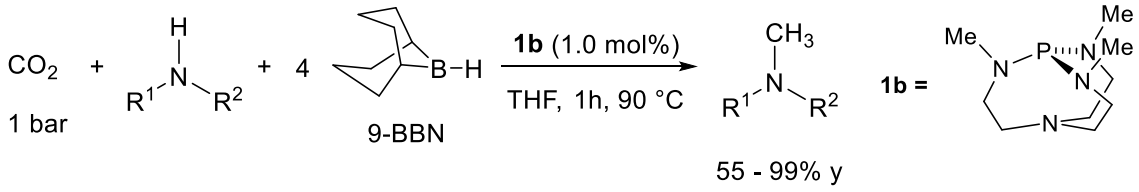

Figure 4.2 Catalytic methylation of secondary amines with CO_2 and 9-BBN in the presence of **1b**.

Moreover, Krempner et al. demonstrated that Verkade's super-bases can be used to create intermolecular frustrated Lewis pairs (FLP) when associated to a weak boron-containing Lewis acid.[90] These "inverse" FLPs were able to cleave dihydrogen leading to efficient hydrogenation catalysts. The same group also reported the interactions and coordination properties of Verkade's superbase with strong Lewis acids by reaction of proazaphosphatrane with various gallium-, boron- aluminium-containing Lewis acids.[91]

Although these recent developments bring new insight into the potentiality of such structure for new applications, the classical use of the Verkade's superbases as organocatalysts remains attractive because of their high performance in term of activity and selectivity.[4] Among the base-catalyzed transformations, the Strecker reaction is an appealing target reaction since it leads to the synthesis of α-aminonitriles which are important and versatile building blocks in organic synthesis as well as in biologically

[87] Kingston, J. V.; Verkade, J. G. *J. Org. Chem*. **2007**, *72*, 2816–2822.
[88] Urgaonkar, S.; Xu, J. H.; Verkade, J. G. *J. Org. Chem*. **2003**, *68*, 8416–8423.
[89] Blondiaux, E.; Pouessel, J.; T, Cantat. *Angew. Chem., Int. Ed*. **2014**, *53*, 12186–12190.
[90] Mummadi, S.; Unruh, D. K.; Zhao, J.; Li, S.; Krempner, C. *J. Am. Chem. Soc.* **2016**, *138*, 3286–3289.
[91] Mummadi, S.; Kenefake, D.; Diaz, R.; Unruh, D. K.; Krempner, C. *Inorg. Chem*. **2017**, *56*, 10748–10759.

active products.[92] Consequently, numerous catalysts have been developed to perform this reaction.[93] One can cite the use of 10% of InI_3 as a catalyst to catalyze three-component Strecker reaction in water, giving a range of cynide products (Figure 4.3).[94] Other Lewis acids such as $BiCl_3$,[95] $RuCl_3$,[96] $Yb(OTf)_3$,[97] $Sc(OTf)_3$,[98] and $Cu(OTf)_2$[99] are also reported to catalyze this kind of reaction.

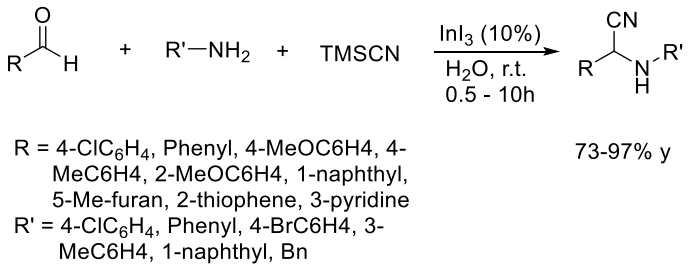

Figure 4.3 Three-component Strecker reaction in the presence of InI_3.

Generally, in those reactions, the aqueous workup is tedious and a large amount of toxic metal waste is generated inevitably. A few organocatalysts have also been reported to catalyze Strecker type reactions. N-heterocyclic carbenes were shown to catalyze the addition of trimethylsilyl cyanide to imines with excellent yields in the presence of 5 mol% catalyst loading at 0 °C, but substrates were limited to tosyl protected imines, and, in most cases, long reaction times were needed (5-6 hours) (Figure 4.4).[100]

[92] (a) Feldman, P. L.; Brackeen, M. F. *J. Org. Chem*. **1990**, *55*, 4207–4209; (b) Feldman, P. L.; James, M. K.; Brackeen, M. F.; Bilotta, J. M.; Schuster, S. V.; Lahey, A. P.; Lutz, M. W.; Johnson, M. R.; Leighton, M. J. *J. Med. Chem*. **1991**, *34*, 2202–2208; (c) Walz, A. J.; Hsu, F. L. *Tetrahedron Lett*. **2014**, *55*, 501–502; d) Zhang, F. G.; Zhu, X. Y.; Li, S.; Nie, J.; Ma, J. A. *Chem. Commun*. **2012**, *48*, 11552–11554; (e) Sadhukhan, A.; Saravanan, S.; Khan, N. U. H.; Kureshy, R. I.; Abdi, S. H.; Bajaj, SH. C. *J. Org. Chem.* **2012**, *77*, 7076–7080; (f) Bolm, C.; Mocci, R.; Schumacher, C.; Turberg, M.; Puccetti, F.; Hernandez, J. G. *Angew. Chem. Int. Ed.* **2018**, *57*, 2423 –2426.
[93] For reviews, see: (a) Gröger, H. *Chem. Rev*. **2003**, *103*, 2795–2828; (b) Wang, J.; Liu, X.; Feng, X. *Chem. Rev*. **2011**, *111*, 6947–6983; (c) Yet, L. *Angew. Chem., Int. Ed*. **2001**, *40*, 875-877; (d) Merino, P.; Marqués-López, E.; Tejero, T.; Herrera, R. P. *Tetrahedron*. **2009**, *65*, 1219–1234; (e) Kouznetsov, V. V.; Galvis, C. E. P. *Tetrahedron*. **2018**, *74*, 773-810.
[94] Shen, Z. L.; Ji, S. J.; Loh, T. P. *Tetrahedron*. **2008**, *64*, 8159–8163.
[95] De, S. K.; Gibbs, R. A. *Tetrahedron Lett*. **2004**, *45*, 7407–7408.
[96] De, S. K. *Synth. Commun*. **2005**, *35*, 653-656.
[97] Kobayashi, S.; Ishitani, H.; Ueno, M. *Synlett*. **1997**, 115–116.
[98] Kobayashi, S.; Busujima, T. *Chem. Commun*. **1998**, 981–982.
[99] Paraskar, A. S.; Sudalai, A. *Tetrahedron Lett*. **2006**, *47*, 5759–5762.
[100] (a) Fukuda, Y.; Maeda, Y.; Kondo, K.; Aoyama, T. *Synthesis*. **2006**, *12*, 1937–1939; (b) Fukuda, Y.; Kondo, K.; Aoyama, T. Synthesis. **2006**, *16*, 2649–2652.

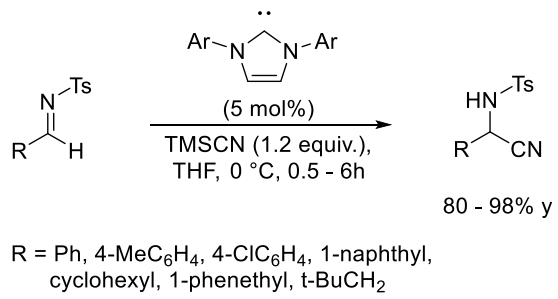

Figure 4.4 N-heterocyclic carbenes catalyzed Strecker reaction.

Heydari et al. showed that guanidine hydrochloride could act as catalyst for Strecker type reactions using aliphatic, aromatic, heterocyclic conjugated aldehydes, and primary, secondary amines as substrates.[101] However, only moderate activity could be achieved with TON around 33 at 40 °C in 1 hour (Figure 4.5).

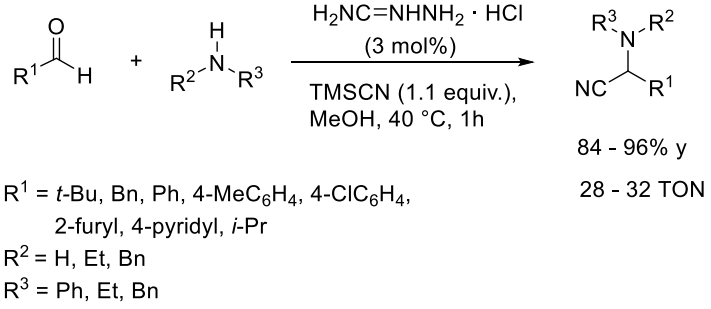

Figure 4.5 Guanidine hydrochloride catalyzed Strecker reaction.

Thiourea also performed well as catalyst with moderate to high yields in the presence of 5 mol% catalyst loading at 0 °C, using primary amines and a range of aldehydes as substrates, in the presence of acyl cyanides as cyanide source. However, extended reaction times were required (1.5-2 days) for the reaction to proceed (Figure 4.6).[102]

[101] Heydari, A.; Arefi, A.; Khaksar, S.; Shiroodi, R. K. *J. Mol. Catal. A: Chem*. **2007**, *271*, 142-144.
[102] Pan, S. C.; List, B. *Synlett*. **2007**, *2*, 318–320.

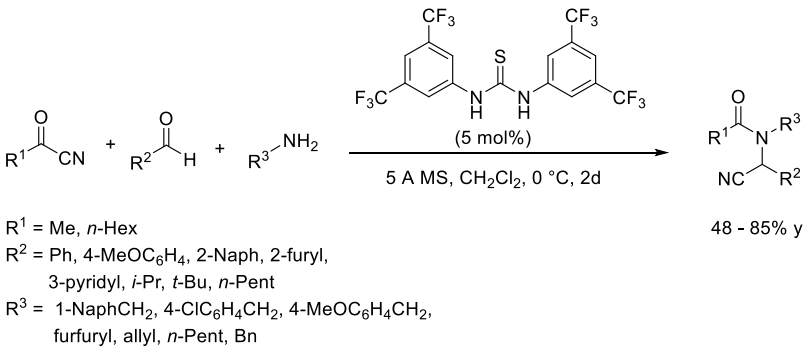

Figure 4.6 Thiourea catalyzed Strecker reaction of amines aldehydes and acyl cyanides.

Although significant progress has been made, these methodologies are far from ideal from a sustainability viewpoint and greener organocatalysts able to function under milder reaction conditions while exhibiting high turnover numbers (TONs) and initial turnover frequencies (TOFs) still need to be developed.

In this chapter, differently substituted proazaphosphatranes **1b**-**1e** (Figure 4.7) were used as catalysts for the Strecker reaction using Ts-, *N*-Boc-, and Bn- protected imines as substrates and TMSCN as cyanide source. These catalysts proved to be highly efficient under very mild reaction conditions providing at 0°C high TOFs around 10^5 h^{-1} and TONs up to 10^4. Besides, a mechanism is proposed for the cyanation of imines catalyzed by proazaphosphatrane.

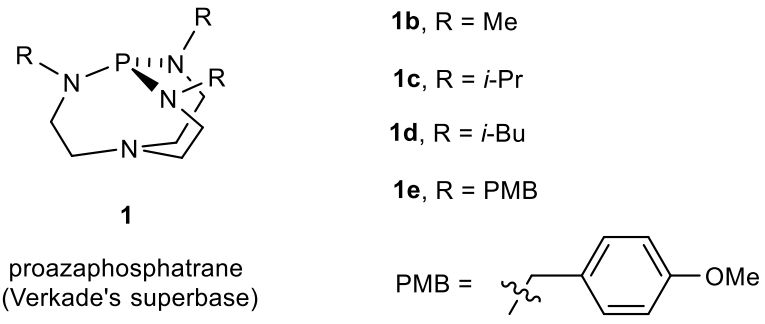

Figure 4.7 Proazaphosphatranes **1b** – **1e** used in this study.

4.2 Results and discussion

4.2.1 Initial experiments

The cyanation of imines was first investigated in the presence of proazaphosphatrane **1e** as catalyst using the addition of TMSCN (1.5 equiv) to *N*-Tosyl-benzaldimine (1.0 equiv) as a benchmark reaction (Table 4.1). We were pleased to observe that, in the presence of 1 mol% of proazaphosphatrane **1e** in 20 minutes and at 0°C, more than 99% yield was reached (entry 1, Table 4.1), and even in a very short reaction time (2 minutes), yield as high as 97% could be achieved (entry 2, Table 4.1), highlighting the high efficiency of the Verkade's superbase as organocatalyst for this reaction. In addition, **1e** proved to be very selective leading to α-aminonitriles as the sole products, in line with the results previously reported by J. G. Verkade for other transformations.[84,85]

4.2.2 Optimization of reaction conditions

Motivated by these results, we then decided to decrease the catalyst loading to explore further the performance scope of **1e**: with 0.1 mol% loading, 83% and 99% yields were obtained in 2 and 20 minutes respectively (entries 3 and 4 respectively, Table 4.1). Decreasing further the amount of **1e** to 0.01 mol% produced a 31% yield in only 2 minutes which corresponds to a TOF of 9.3 10^4 h^{-1}, a remarkable activity value for an organocatalyst for the Strecker reaction (entry 6, Table 4.1). Prolonging the reaction time at this very low catalyst loading resulted in additional activity improvement with yield attaining 58% in 20 minutes and up to 99% after 12 hours, affording a total TON around 10^4 (entries 5 and 7, Table 4.1). It is noteworthy that no reaction occurred without catalyst (entry 8, Table 4.1), even after 12 hours, and that Et_3N failed to catalyze this reaction when used in the same reaction conditions (entry 9, Table 4.1). Thus, it appears that the Verkade's superbase is a powerful catalyst for the Strecker reaction displaying remarkable initial TOF and TON under mild conditions, underlining both its high catalytic activity and stability. It is worth mentioning that J. G. Verkade demonstrated in a previous report that an azaphosphatrane nitrate salt could catalyze the three-component Strecker reaction, however 20% mol of catalyst loading and long

reaction times ranging from 15 to 35 hours were needed.[103]

Table 4.1 Optimization of catalyst loading and reaction time for proazaphosphatrane **1e** catalyzed cyanation of imines.[a]

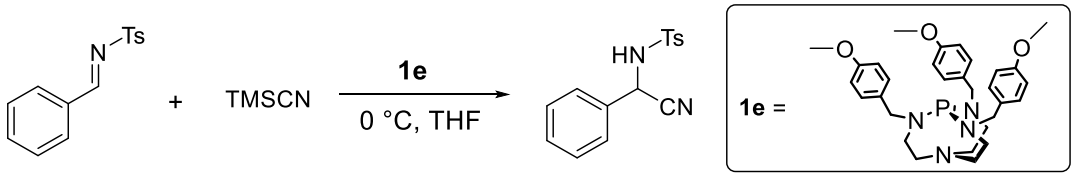

Entry	**1e** (mol%)	Time	Yield (%)[b]
1	1	20 min	>99
2	1	2 min	97
3	0.1	20 min	99
4	0.1	2 min	83
5	0.01	20 min	58
6	0.01	2 min	31
7	0.01	12 h	99
8	-	12 h	<1
9	Et_3N[c]	20 min	<1

[a] Reaction conditions: *N*-Tosyl-benzaldimine (0.5 mmol), TMSCN (0.75 mmol), 1.5 mL THF, under argon, then 3 mL H_2O. [b] Yields were determined by ^1H NMR. [c] 0.1 mol % Et_3N used without **1e**.

We then chose to use the following reaction conditions to further screen the reaction parameters and catalyst structural pattern: 0.1 mol% of catalyst loading at 0°C for 20 minutes, as they allow for the reaction to proceed in high yield and in relatively short reaction timeframe. We first examined the influence of the solvent on catalytic performance. As shown from Table 4.2, high conversion levels were achieved in all the cases with yields of 93% for DCM and up to 99% for both THF and toluene (entries 1, 2, and 3, Table 4.2). The influence of the stereoelectronic properties and basicity of the

[103] Fetterly, B. M.; Jana, N. K.; Verkade, J. G. *Tetrahedron*. **2006**, *62*, 440–456.

proazaphosphatranes **1b**-**1e** on catalytic activity was then investigated using THF as solvent (Table 4.2). In the presence of 0.1 mol% catalyst within 20 minutes, all four proazaphosphatranes displayed excellent catalytic activity with yields approaching 100% (entries 3, 4, 5 and 6, Table 4.2). In order to further discriminate catalytic activity among the proazaphosphatranes **1b**-**1e**, a lower catalyst loading of 0.001 mol% was used within the same reaction period. The results indicated that catalytic activity was correlated to the basicity of proazaphosphatranes: stronger basicity resulted in higher yield (entries 3-6, Table 4.2). Indeed, the catalytic activity follows the same trend (**1e** < **1b** < **1d** < **1c**) as the basicity order of proazaphosphatranes (**1e** < **1b** < **1d** < **1c**).

Table 4.2 Influence of solvent and stereoelectronic properties of proazaphosphatranes on catalytic activity.[a]

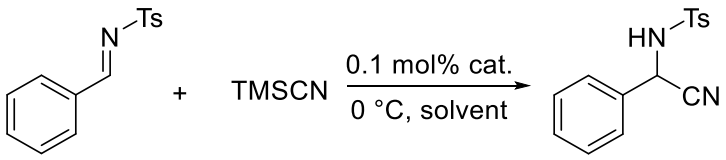

Entry	Catalyst	Solvent	pKa[b]	Yield(%)[c]
1	**1e**	DCM	32.14	93
2	**1e**	Toluene	32.14	99
3	**1e**	THF	32.14	99 (15)[d]
4	**1d**	THF	33.53	99 (22)[d]
5	**1c**	THF	33.63	99 (28)[d]
6	**1b**	THF	32.90	99 (17)[d]

[a] Reaction conditions: *N*-Tosyl-benzaldimine (0.5 mmol), TMSCN (0.75 mmol), 0.1 mol% catalyst, 1.5 mL solvent, under argon，20 min, then 3 mL H_2O; [b] pKa values of conjugate acids of proazaphosphatrane bases in acetonitrile;[55, 104] [c] Yields were determined by ^{1}H NMR. [d] 0.001 mol% catalyst was used for 2 hours.

[104] Chintareddy, V. R.; Wadhwa, K.; Verkade, J. G. *J. Org. Chem*. **2009**, *74*, 8118–8132.

4.2.3 Scope of substrates

Table 4.3 Substrate scope of proazaphosphatrane **1e**-catalyzed cyanation of imines[a]

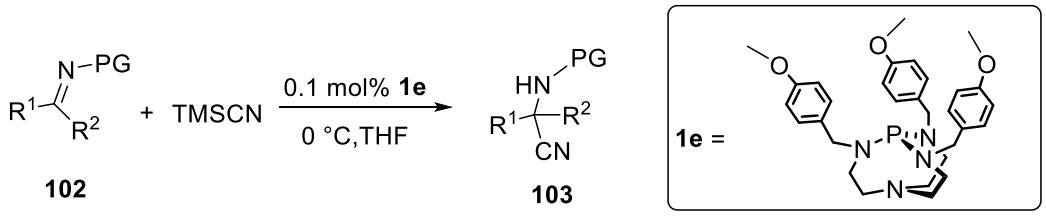

102 103

Entry	Imine	R^1	R^2	PG	Product	Yield(%)[b]
1	**102a**	Ph	H	Tosyl	**103a**	quant.
2	**102b**	*p*-MeC_6H_4	H	Tosyl	**103b**	quant.
3	**102c**	*p*-$MeOC_6H_4$	H	Tosyl	**103c**	quant.
4	**102d**	*p*-CNC_6H_4	H	Tosyl	**103d**	quant.
5	**102e**	2-naphthyl	H	Tosyl	**103e**	quant.
6	**102f**	*t*-Bu	H	Tosyl	**103f**	85
7	**102g**	Ph	H	*N*-Boc	**103g**	94
8	**102h**	Ph	H	Bn	**103h**	92
9	**102i**	2-furan	H	Tosyl	**103i**	95[c]
10	**102j**	Ph	CH_3	Tosyl	**103j**	93[c,d]

[a] Reaction conditions: imines (0.5 mmol), TMSCN (0.75 mmol), 0.1 mol% **1e**, 1.5 mL THF, 20 min, under argon, then 3 mL H_2O; [b] Isolated yields are given; [c] 2 mol% of catalyst was used; [d] The reaction was performed for 2h.

With optimized conditions in hand, we then studied the scope of substrates for the cyanation of imines on representative examples. Tosyl-protected imines bearing phenyl groups differently substituted were first explored (entries 1-4, Table 4.3), for which nearly quantitative isolated yields were obtained. In addition to aromatic substituents, aliphatic analogue **102f** also proceeded well with 85% yield (entry 6, Table 4.3). Furthermore, *N*-Boc and Bn- protected imines were tested in our system. Remarkably, excellent yields of 94% and 92% of corresponding products were reached, respectively (entries 7 and 8, Table 4.3). Clearly, different protecting groups are compatible with our

methodology, which provides an attractive alternative for some specific low-reactive imines. Another key advantage is the use of TMSCN as cyanide source, which is more convenient and safer than typical cyanide salts such as NaCN, KCN or extremely toxic ones like HCN. Cyanation of an imine bearing a heterocyclic furan group was also successfully achieved in high yield (95 %) after 2 hours (entry 9, Table 4.3). Using ketimine **102j** as substrate also provides the expected product **103j** in 93% yield (entry 10, Table 4.3).

4.2.4 Mechanism study

A possible reaction mechanism is depicted in scheme **4.1**. The first step is the activation of TMSCN by attack of the superbase to form a tetra-coordinated silicon complex **A** which was confirmed by solid-state CP MAS ^{29}Si NMR: the appearance of a new signal was observed at 7.8 ppm by mixing 1 equiv. of TMSCN with 1 equiv. of **1e**, in addition to the resonance at −12.0 ppm for TMSCN, in agreement with the literature data (Figures S12-13 in experimental section).[85] Then, the nucleophilic anion CN^- attacks the imine substrate affording the key intermediate ion pair **B**. Cleavage of the Si-P bond leads to the regeneration of the catalyst **1e** and the concomitant release of the TMS-protected amine product **C** which is subsequently hydrolyzed to give the desired amine product **D**.[105]

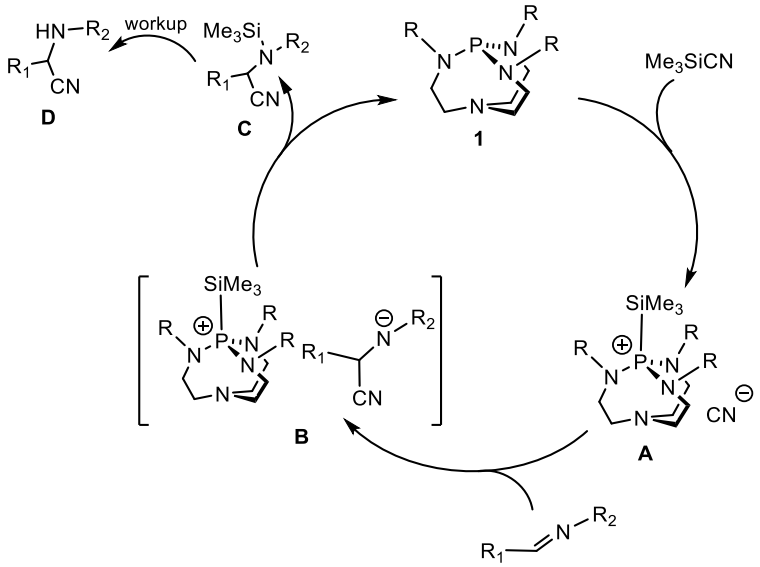

Scheme 4.1 Proposed mechanism for the cyanation of imines catalyzed by proazaphosphatrane.

[105] Wadhwa, K.; Chintareddy, V. R.; Verkade, J. G. *J. Org. Chem*. **2009**, *74*, 6681–6690.

In order to shed light on the nature of the high efficiency of proazaphosphatranes, we carried out a control experiment using *N*-tosyl-benzaldimine and TMSCN as substrates in the presence of 20 mol% of HMPT at 0 °C in THF for 24 h (Scheme **4.2**). Only 23% yield was reached, which can be compared to the quantitative yield obtained with 0.1 mol% of proazaphosphatrane **1e** in only 20 minutes (entry 1, Table **4.3**). As can be seen, HMPT and **1e** have similar structure except for the bridgehead nitrogen in **1e**, the transannulation between bridgehead nitrogen and phosphorus enhanced the basicity and nucleophilicity of the phosphorus atom in **1e**, which makes it more reactive for activation of TMSCN in agreement with other reported proazaphosphatrane-catalyzed transformations.[85,105]

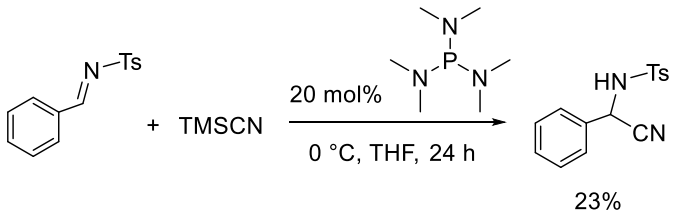

Scheme 4.2 Cyanation of imine in the presence of HMPT

4.3 Conclusions

In summary, we have presented a mild, convenient and highly efficient methodology for the synthesis of α-aminonitriles using proazaphosphatranes **1b**-**1e** as catalysts. In general, our method tolerates a variety of substrates, ranging from aromatic, heteroaromatic to aliphatic imines with different protecting groups including tosyl-, Bn-, and *N*-Boc. Excellent to quantitative yields were reached and, compared to other systems, only low catalyst loading and short reaction times were required for the reaction to proceed efficiently. A remarkable initial turnover frequency (TOF), close to 10^5 h^{-1}, was achieved, associated with an excellent selectivity since no side reactions were observed. A reaction mechanism was proposed and the key role played by the apical nitrogen in the proazaphosphatrane structure was demonstrated. The very low catalyst loading, safer cyanide source and excellent yield and selectivity make **1b**-**1e** outstanding among the best organocatalysts for the Strecker reaction.

Chapter 5. Endohedral functionalized cage as a tool to create Frustrated Lewis Pairs

5.1 Introduction

Molecules possessing a cavity are of great interest,[106] since they can be used to stabilize reactive species,[107] or to build nanoreactors presenting a confined catalytic site.[108] For instance, Raymond et al. reported a self-assembly supramolecular cage which could stabilize the reactive cationic species $[Me_2C(OH)PEt_3]^+$ (Figure 5.1).[108c] The encapsulation behaviors were confirmed by ^{31}P NMR, ^1H NMR as well as electrospray mass spectra. This stabilization by encapsulation in the tetrahedron cluster $[Ga_4L_6]^{12-}$ **104** makes the guest cation $[Me_2C(OH)PEt_3]^+$ remain stable in D_2O for several hours, and in CD_3OD for at least one day.

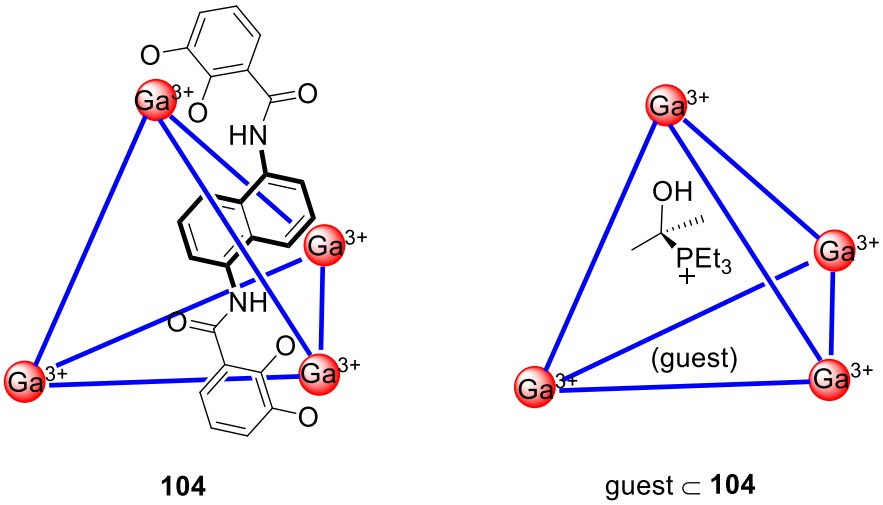

Figure 5.1 Schemetic presentation of the $[Ga_4L_6]^{12-}$ **104** (left), and encapsulated guest inside the cavity guest ⊂ **104** (right).

Another self-assembly tetrahedron container molecule **105** was found able to stabilize air-sensative white phosphorus P_4 within the hydrophobic hollows. Interestingly, the resulted complex P_4 ⊂ **105** was soluble in water, and the encapsulated P_4 could be easily

---

[106] Cram, D. J.; Tanner, M. E. *Angew. Chem, Int. Ed.* **1991**, *30*, 1024-1027.

[107] (a) Warmuth, R.; Marvel, M. A. *Angew. Chem. Int. Ed.* **2000**, *39*, 1117-1119; (b)) Fujita, M.; Oguro, D.; Miyazawa, M.; Oka, H.; Yamaguchi, K.; Ogura, K. *Nature*, **1995**, *378*, 469-471; (c) Ziegler, M.; Brumaghim, J. L.; Raymond, K. N. *Angew. Chem., Int. Ed.* **2000**, *39*, 4119-4121; (d) Mal, P.; Breiner, B.; Rissanen, K.; Nitschke, J. R. *Science,* **2009**, *324*, 1697-1699.

[108] (a) Raynal, M.; Ballester, P.; Vidal-Ferran, A.; Van Leeuwen, P. W. *Chem. Soc. Rev.* **2014**, *43*, 1734-1787; (b) Brown, C. J.; Toste, F. D.; Bergman, R. G.; Raymond, K. N. *Chem. Rev.* **2015**, *115*, 3012; (c) Leenders, S. H.; Gramage-Doria, R.; De Bruin, B.; Reek, J. N. *Chem. Soc. Rev*. **2015**, *44*, 433-448; (d) Breiner, B.; Clegg, J. K.; Nitschke, J. R. *Chem. Sci*. **2011**, *2*, 51-56; (e) Ueda, Y.; Ito, H.; Fujita, D.; Fujita, M. *J. Am. Chem. Soc.* **2017**, *139*, 6090-6093; (f) Ajami, D.; Rebek Jr, J. *Acc. Chem. Res.* **2013,** *46*, 990-999; (g) Pochorovski, I.; Diederich, F. *Acc. Chem. Res*., **2014**, *47*, 2096-2105; (h) Kim, D. S.; Sessler, J. L. *Chem. Soc. Rev*., **2015**, *44*, 532-546.

extracted into benzene without disrupting the cage (Figure 5.2).[108d]

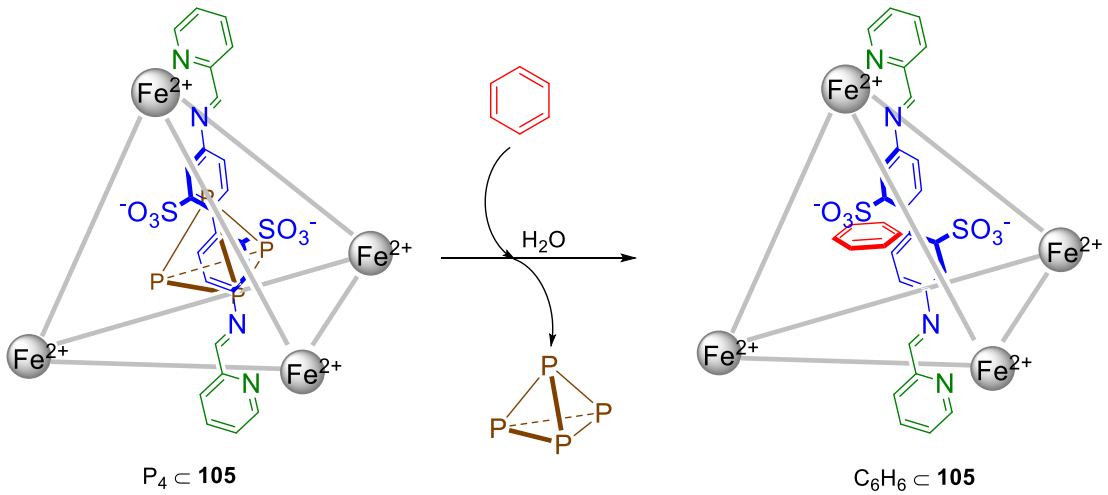

Figure 5.2 Schemetic presentation of conversion from $P_4 \subset$ **105** to $C_6H_6 \subset$ **105**.

In addition to stabilizing the reactive species, cage molecules also serve as vehicles to act as catalysts carriers for catalytic reactions. In 2017, the group of Fujita reported two permeable self-assembled molecular containers for catalyst isolation enabling two-step cascade reactions (Figure 5.3).[108e] Generally, the catalyst **106a** and MacMillan's catalyst **106b** are not compatible with each other when free in solution. However, when **106a** and **106b** were encapsulated separately within the cavity of an $M_{12}L_{24}$-type molecular capsule, the resulted supramolecular catalyst **107a** could smoothly oxidize substrate **108a** into corresponding aldehyde **108b** followed by stereoselective Diels-Alder cascade reaction achieved in the presence of **107b** in one-pot. The capsule successfully prevented **106a** and **106b** from reacting with each other, and made them cooperatively catalyze the two-step cascade reactions mentioned above.

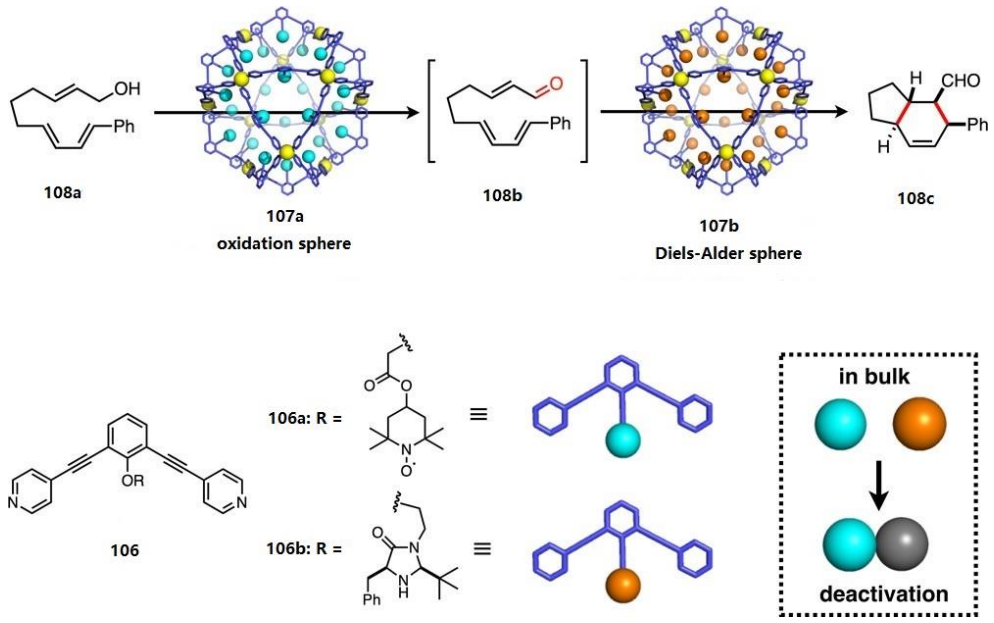

Figure 5.3 Schemetic presentation of cascade reactions in the presence of **107a** and **107b**.

In 2016, Hunter, Williams and Ward et al. reported a water-soluble M_8L_{12} coordination cage **109** which acted like enzyme to catalyze Kemp elimination reaction of benzisoxazole with hydroxide to form 2-cyanophenolate inside the hollow cavities (Figure 5.4).[109] The rate acceleration of the reaction is excellent with the value of k_{cat}/k_{uncat} up to 2×10^5. The authors attributed this remarkable catalytic activity to the encapsulation of benzisoxazole in the hydrophobic cavity and accumulated high concentration of desolvated hydroxide ions around the bound guest.

[109] Cullen, W.; Misuraca, M.C.; Hunter, C. A.; Williams, N. H.; Ward, M. D. *Nat Chem*, **2016**, *8*, 231–236.

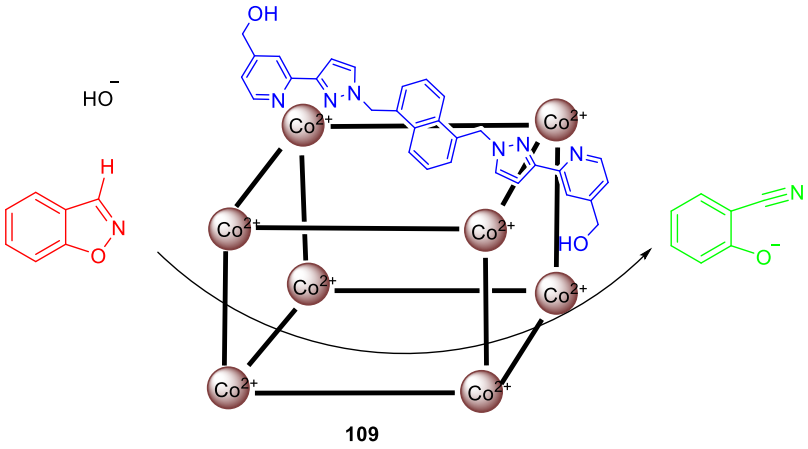

Figure 5.4 Kemp elimination reaction of benzisoxazole with hydroxide to form 2-cyanophenolate catalyzed by M_8L_{12} coordination cage **109**.

However, endohedral functionalization of the inner cavity of a molecular capsule is far from trivial, and host molecules presenting true endohedral functionalization of their inner space have been rarely reported and even more seldom used as supramolecular catalyst. [110] The Martinez's group recently reported the synthesis of the hemicryptophane host **74** incorporating a Verkade's superbase (Figure 5.5), for which they observed a strong increase of the thermodynamic basicity and a drop in the rate of proton transfer: **74** is seven times more basic than its counterpart **1e** without cavity, but its protonation rate is one hundred times slower. [1b,3,4,31h,55,57]

[110] (a) Thordarson, P.; Bijsterveld, E. J.; Rowan, A. E.; Nolte, R. J. *Nature* **2003**, *424*, 915-918; (b) Zhang, P.; Meijide Suarez, J.; Driant, T.; Derat, E.; Zhang, Y.; Ménand, M.; Roland, S.; Sollogoub, M. *Angew. Chem. Int. Ed.* **2017**, *56*, 10821-10825; (c) Makita, Y.; Sugimoto, K.; Furuyoshi, K.; Ikeda, K.; Fujiwara, S.I.; Shin-ike, T.; Ogawa, A. *Inorg. Chem.* **2010**, *49,* 7220-7222; (d) Shenoy, S. R.; Pinacho Crisóstomo, F. R.; Iwasawa, T.; Rebek Jr, J. *J. Am Chem Soc*. **2008**, *130*, 5658-5659; (e) Futagoishi, T.; Murata, M.; Wakamiya, A.; Murata, Y. *Chem. Commun.* **2017**, *53*, 1712-1714; (f) Galán, A.; Escudero-Adán, E. C.; Ballester, P. *Chem. Sci.* **2017**, *8*, 7746-7750; (g) Sechet, D.; Kaya, Z.; Phan, T.A.; Jouffroy, M.; Bentouhami, E.; Armspach, D.; Matt, D.; Toupet, L. *Chem. Commun*. **2017**, *53*, 11717-11720.

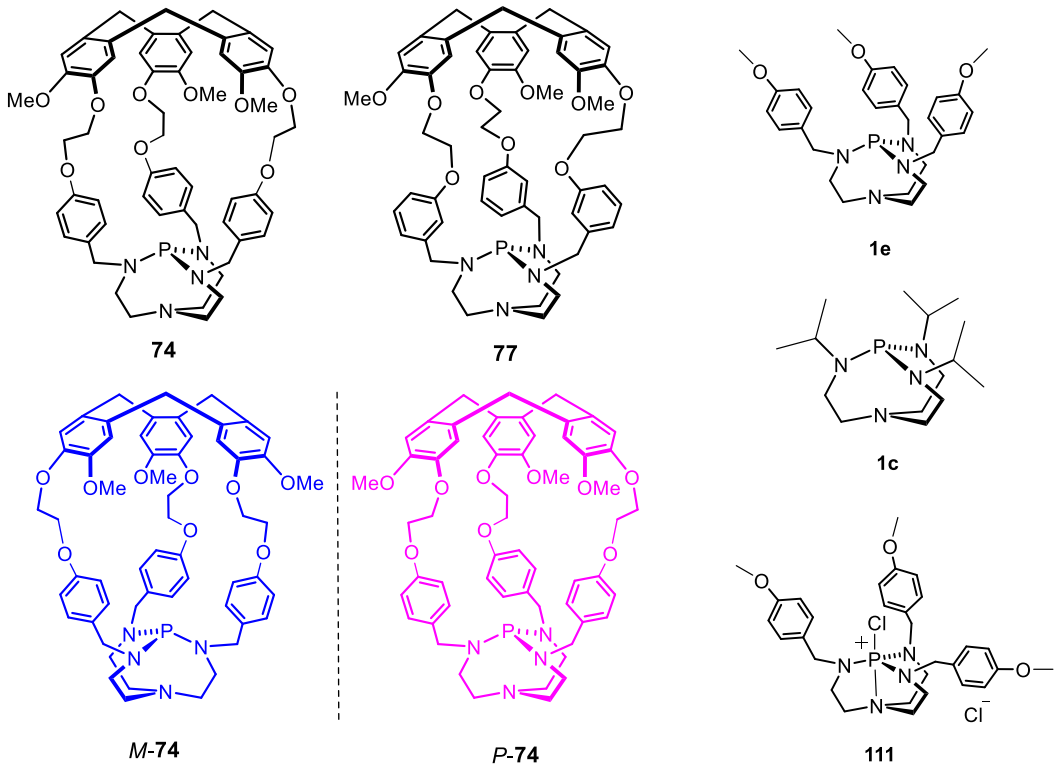

Figure 5.5 Structures of superbases **1e**, **1c**, **74**, **77**, enantiomers *M*-**74**/*P*-**74** and chlorinated azaphosphatrane **111**.

The X-ray crystal structure of the related Verkade's superbase-hemicryptophane **77** (Figure 5.6) showed an acetonitrile solvent molecule trapped inside the molecular cavity. Its acidic protons were located in the upper part of the cavity, far from the basic phosphorus, accounting for the low kinetic rate of proton transfer.[57] This system could be viewed as a Frustrated Brønsted Pair: the specific orientation of the acid partner inside the cavity prevents the acid-base reaction to occur between the entrapped basic phosphorus and the encaged acidic solvent molecule.

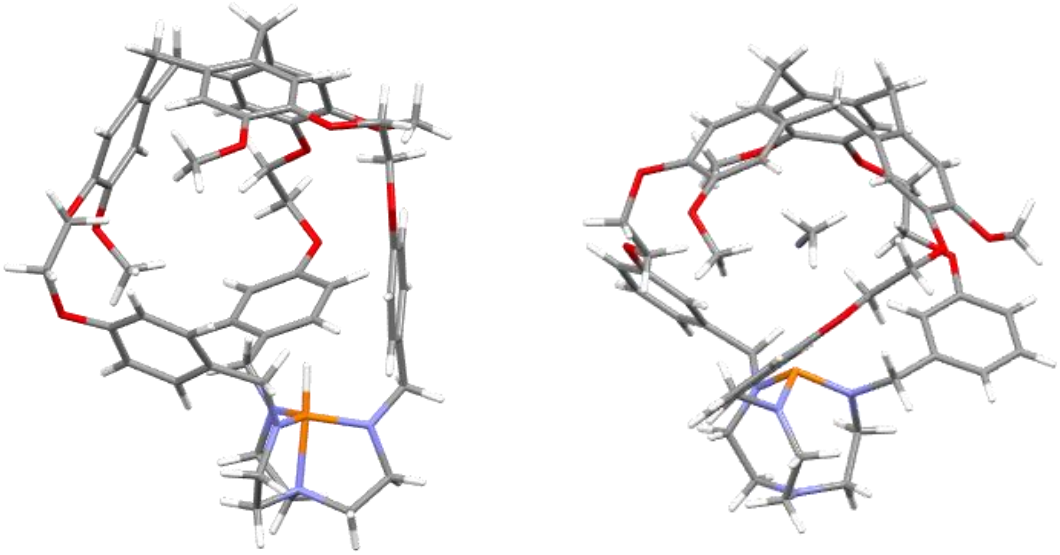

74-H^+ $CH_3CN \subset$ **77**

Figure 5.6 X-ray crystal structures of **74**-H^+ and $CH_3CN \subset$ **77**.

We thus decided to investigate whether it could be possible to take advantage of this lack of reactivity inside the cavity and extend this behavior to FLP systems within a cage. FLPs, which are systems made of a Lewis base prevented to react with an acidic Lewis counterpart (Figure 5.7), are of great interest since they can activate small molecules like H_2 or CO_2, and lead to new and original reactive systems for catalysis.[111]

[111] For reviews on FLPs: (a) Stephan, D. W. *Acc. Chem. Res.* **2015**, *48*, 306-316; (b) Stephan, D. W.; Erker, G. *Angew. Chem. Int. Ed.* **2015**, *54*, 6400-6441; (c) Stephan, D. W. *J. Am. Chem. Soc.* **2015**, *137*, 10018-10032; (d) Stephan, D. W.; G. Erker, *Angew. Chem., Int. Ed.* **2010**, *49*, 46-76; (e) Stephan, D. W. *Science* **2016**, *354*, 6317.

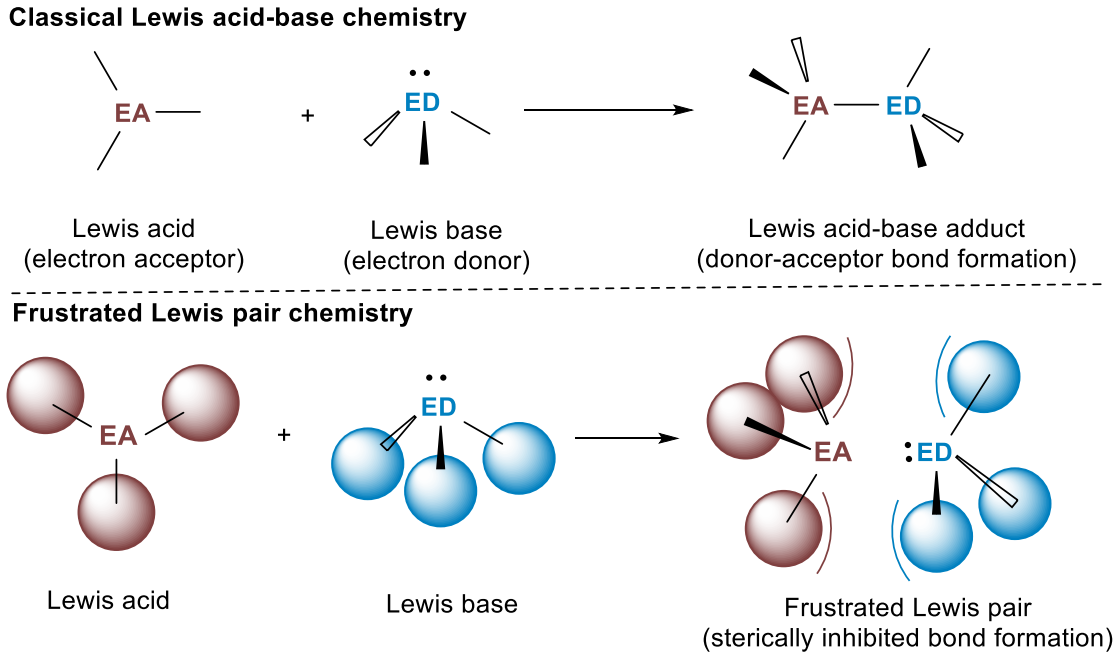

Figure 5.7 Comparison between Lewis acid-base adduct and Frustrated Lewis pair.

D. W. Stephan has done pioneering work in the area of FLPs.[112] Stephan and co-workers reported the first example of metal-free intramolecular FLP system consisted of a phosphonium-borate species, which could undergo reversible liberation and addition of H_2 by heating and exposing under 1 atmosphere of H_2 at 25 °C (Figure 5.8).[112] Interestingly, the phosphine-borane species with orange color reacted smoothly with H_2, generating colorless phosphonium-borate species.

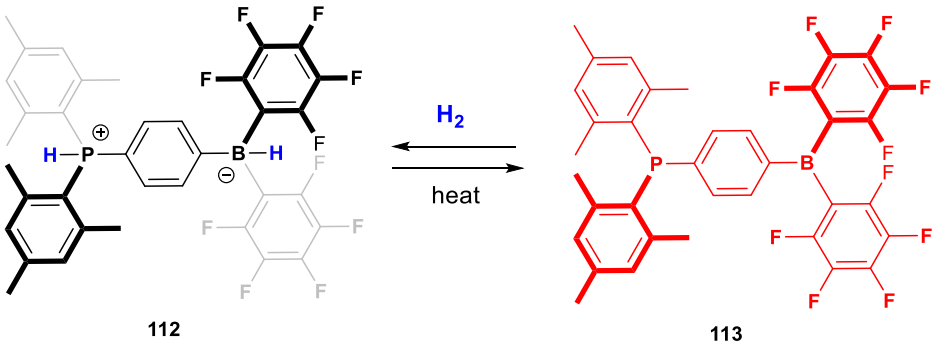

Figure 5.8 Reversible activation of H_2 by the intramolecular FLP.

[112] Welch, G. C.; San Juan, R. R.; Masuda, J. D.; Stephan, D. W. *Science* **2006**, *314*, 1124-1126.

In 2009, Grimme, Stephan and Erker et al. reported a intermolecular FLP system, made up of $B(C_6F_5)_3$ as Lewis acid part and P*t*Bu$_3$ as Lewis base counterpart (Figure 5.9).[113] This FLP could readily react with CO_2 to form stable carbonic acid derivative **114**. Remarkably, this derivative underwent loss of CO_2 to regenerate the starting materials at 80 °C under vacuum. The authors claimed that the formation of thermodynamically favored **114** indicated that this FLP system could act as CO_2 carrier for controlled uptake and release of carbon dioxide.

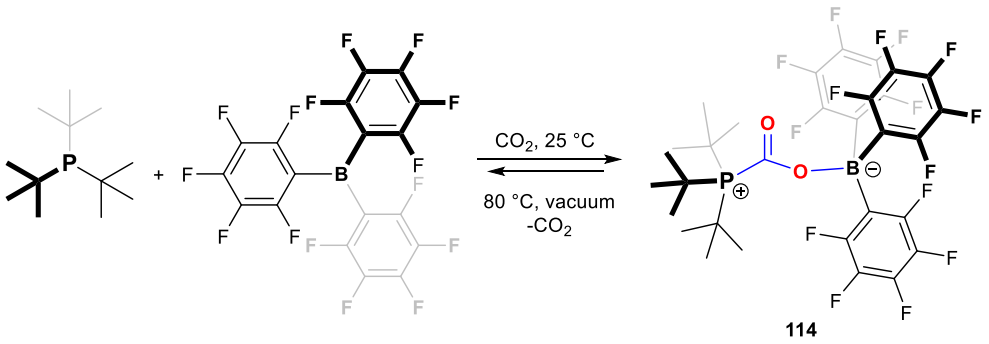

Figure 5.9 Reversible carbon dioxide binding by the intermolecular FLP.

Evidently, as illustrated above, the cage molecules have significant impact on catalysis in terms of activity and selectivity. And on the other hand, FLPs appeared as a novel system which have led to a variety of new reactions through unprecedented ways. We turned our attention to the Morita Baylis Hillman (MBH) reaction since the methylene-hydroxy-carbonyl derivatives obtained by this atom-economical reaction are key intermediates and valuable building blocks in the synthesis of complex natural products and bio-active compounds.[114] This reaction is usually catalyzed in the presence of a nucleophilic base, such as amines, or phosphines, that can be combined with a transition metal complex to increase the reaction rate.[115] J. G. Verkade reported previously that proazaphosphatrane sulfides efficiently catalyzed the MBH reaction in the presence of $TiCl_4$ whereas the sulfur-free superbases failed, probably because of phosphorus-titanium interactions (Figure 5.10).[116] This highlights that the right balance between the

[113] Mömming, C. M.; Otten, E.; Kehr, G.; Fröhlich, R.; Grimme, S.; Stephan, D. W.; Erker, G. *Angew. Chem. Int. Ed*. **2009**, *48*, 6643–6646.
[114] Bhowmik, S.; Batra, S. *Curr. Org. Chem.* **2014**, *18*, 3078-3119.
[115] Wei, Y.; Shi, M. *Chem. Rev.* **2013**, *113*, 6659-6690.
[116] You, J.; Xu, J.; Verkade, J. G. *Angew. Chem. Int. Ed.* **2003**, *42*, 5054-5056.

Lewis acidic and basic properties of the two partners is necessary in order to avoid the formation of Lewis acid-base adducts and hence, allow the dual activation of both the enone and the aldehyde (Figure 5.11).

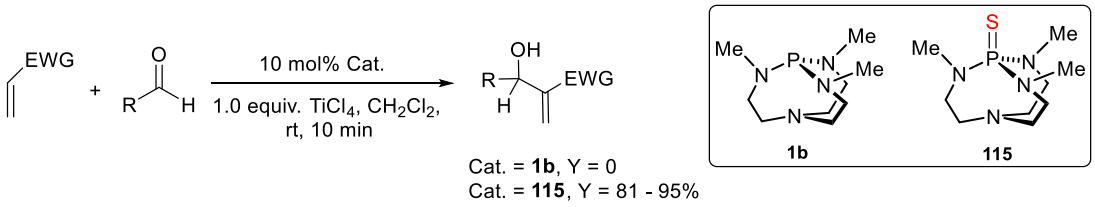

Figure 5.10 The MBH reaction in the presence of **1b** and **115**, respectively.

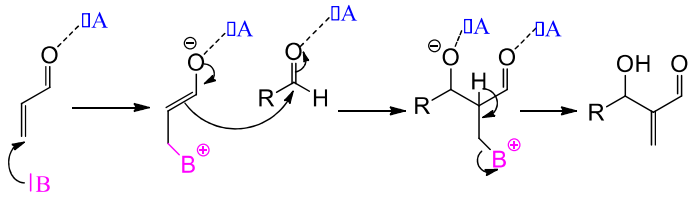

Figure 5.11 Mechanism of the Morita Baylis Hillman reaction.

In this chapter, we wanted to investigate organocatalysis with FLP and that we thought that protection of the superbase within a hemicryptophane structure could prevent the interaction of the base with $TiCl_4$. To do so, we designed a FLP system for MBH reaction, where the frustrated behavior relates to the confinement of the Lewis base partner in a supramolecular cage structure. Compared to other reported approaches, this strategy proved successful, since the model superbases, even with bulky substituents, either failed to catalyze this reaction or displayed much lower catalytic activity. The key role of the cavity was also evidenced by control and inhibition experiments, DFT calculations and substrate selections.

5.2 Results and discussion

5.2.1 Initial experiments

We first tested the reaction between *p*-chlorobenzaldehyde (1 equivalent) and cyclopentenone (3 equivalents) with 10 mol % of model superbase **1e** as catalyst and one equivalent of $TiCl_4$ relative to the aldehyde, in dichloromethane (DCM) at room temperature. A very low yield, similar to that obtained without superbase, was achieved, showing that the model superbase **1e** displays no catalytic activity under our reaction conditions, as previously reported by J. G. Verkade *et al*. (Table 5.1, entries 1 and 2).[117] ^{31}P NMR experiments were performed to investigate if a phosphorus-titanium interaction could be responsible for this lack of reactivity (Figures S14-S18 in experimental section). Mixing the model superbase **1e** with $TiCl_4$ led to the disappearance of the signal of the free superbase **1e** at +126.7 ppm and to the appearance of two new peaks (Figures S17-S18 in experimental section): the first one at –11.9 ppm corresponds to the protonated azaphosphatrane conjugated acid **1b**–H^+ arising from the traces of HCl present in $TiCl_4$, and the second signal at –20.9 ppm is consistent with the formation of the chlorinated azaphosphatrane **111** (Figure 5.6), which was further confirmed by ^1H NMR and mass spectroscopy (Figures S19 and S57 respectively in experimental section). [117] Besides, **111** was isolated and fully characterized (see experimental section). Thus, the Lewis acid/base partners interact and then react to give **111** lacking any nucleophilic properties (Scheme S19). The proazaphosphatrane **1c** bearing three isopropyl groups (Figure 5.5) was recently reported by the group of Krempner to act in combination with bulky boranes as reversed FLP system for hydrogen activation (Figure 5.12).[91,92]

[117] Liu, X. D.; Verkade, J. G. *Inorg. Chem.* **1998**, *37*, 5189-5197.

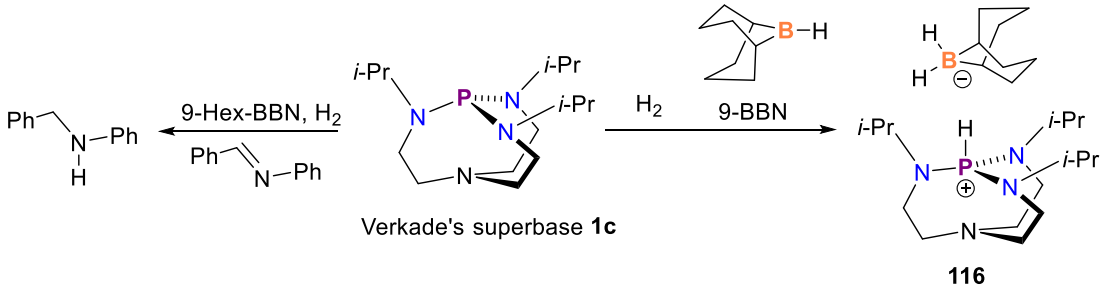

Figure 5.12 Formation of FLP and hydrogenation of *N*-benzylidenaniline in the presence of **116**.

We thus hypothesized that the titanium-phosphorus interaction might be also precluded with this bulky superbase, restoring some catalytic activity. We were pleased to observe that **1c** associated with $TiCl_4$ is able to catalyze this MBH reaction. However, the improvement of the yield is moderate (Table 5.1, entry 3, 17% yield), underlining that the extensive steric shielding of the central phosphorus donor by the surrounding isopropyl groups probably only partially isolates these two Lewis acid-base partners. In order to promote more efficiently this FLP behavior, we decided to carry out the MBH reaction using the encapsulated superbase **74** as catalyst under the above conditions. As shown in Table 5.1 (entry 4), the association of **74** with $TiCl_4$ led to the formation of the MBH product with 48% yield after only 10 minutes of reaction. This demonstrates that the confined Lewis base, in combination with titanium tetrachloride, acts as an efficient catalyst for this reaction. Control experiments were carried out using the protonated encaged azaphosphatrane **74**-H^+•Cl^- in the presence of $TiCl_4$, and the superbases **74** and **1e** alone: no catalytic activities were observed in these cases (entries 5-7, Table 5.1). All these results are consistent with our preliminary studies related to proton transfer,[55,57] and suggest that the confined superbase behaves as a FLP and active catalytic system, when associated with $TiCl_4$, whereas the catalytic activity is totally shut down in the case of the model superbase **1e**.

Table 5.1 The Morita Baylis Hillman reaction catalyzed by different systems.

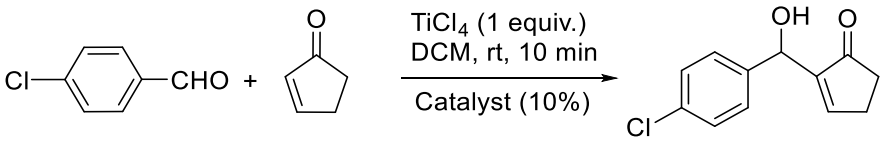

Entry	Catalyst	Yield (%)
1	-	7
2	**1e**	9
3	**1c**	17
4	**74**	48
5	**74**-H^+ Cl^-	8
6	**74**[a]	ND
7	**1e**[a]	ND

Reaction conditions: Aldehyde (0.25 mmol), cyclopentenone (0.75 mmol), catalyst (0.025 mmol), $TiCl_4$ (0.25 mmol), DCM (1.5 mL). [a] Reactions without $TiCl_4$. ND = not detected.

The FLP behavior of the **74**/$TiCl_4$ catalytic system was further assessed by ^{31}P NMR and mass spectrometry (Figures S20-24 and S58 respectively). Mixing equimolar amounts of **74** and $TiCl_4$ did not lead to the formation of any detectable P-Cl adducts (expected around -21 ppm in the ^{31}P NMR spectrum, Figures S23-24), suggesting that the interaction and the subsequent reaction between the two Lewis acid/base partners, are prevented. Thus, these experiments suggest the formation of a FLP between the encaged superbase **74** and $TiCl_4$ where both the nucleophilicity and the Lewis acidity of the two partners are preserved.

5.2.2 Scope of substrates

The applicability of this FLP catalyst system was then investigated using two cyclic enones and three differently substituted aldehydes. The catalysis conditions were slightly modified as we observed that using a solution of $TiCl_4$ in DCM instead of pure $TiCl_4$ strongly improved the yields of the reaction: a yield of 75% is reached for the

reaction *p*-chlorobenzaldehyde and cyclopentenone with the **74**/$TiCl_4$ catalytic system (against 48% in our previous conditions), whereas the **1e**/TiCl4 catalytic system provides the same yield as the solution of $TiCl_4$ alone (15% in each case). The lower amount of HCl present in the solution of $TiCl_4$ in DCM, when compared to pure $TiCl_4$, could account this experimental result. The results are displayed in Table 5.2 along with those of **1e** and blank control experiments. While the model **1e** failed to catalyze these reactions, giving yields similar to those obtained with $TiCl_4$ alone, the encapsulated superbase **74** showed in all the cases enhanced activity (Table 5.2). To compare more accurately the catalytic activity of the two systems, the improvement of the rate constant of the reaction in the presence of a superbase (**74** or **1e**) with respect to that with $TiCl_4$ alone was calculated ($(k_{cat} - k_{TiCl4})/k_{TiCl4}*100$; Table 5.2).

Whereas with the model catalyst **1e**, no or very little catalytic activity was observed (the improvement of the rate constants ranges from 0% to 25%), the use of the cage catalyst **74** always led to an improvement of the catalytic activity by a factor of 170% to 700% (Table 5.2). Thus, in each case, the confinement of Verkade's superbase switches its catalytic activity from values close to 0% to a true synergistic effect with $TiCl_4$ (up to 700%, entry 6, Table 5.2). The lower gain in activity was obtained for the reaction between cyclohexenone and *p*-nitrobenzaldehyde (170%, entry 12, Table 5.2), probably because, under these conditions, $TiCl_4$ can perform this reaction alone (entry 10, Table 5.2). Even with the less reactive electron-rich *p*-tolualdehyde and cyclopentenone as substrates, the reaction rate is improved by a factor of 300% in the presence of **74** (entry 15, Table 5.2), whereas the model **1e** displays no catalytic activity whatsoever (0%, entry 14, table 5.2). The highest gain in catalytic activity was achieved with *p*-chlorobenzaldehyde and cylohexenone or cyclopentanone, the reaction rate being enhanced by more than 700% and 400% when the catalyst **74** was present (entries 6 and 3 respectively, Table 5.2), against 0% and 25% with the model superbase **1e**.

Table 5.2 Comparison of the catalytic activity of **74** and **1e** with various substrates.

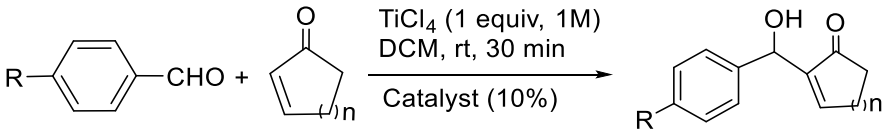

Entry	R	n	Catalyst	Yield (%)[b]	Improvement of the reaction rate (%)[a]
1	Cl	1	-	15	-
2	Cl	1	**1e**	14	0
3	Cl	1	**74**	75	400
4	Cl	2	-	8	-
5	Cl	2	**1e**	10	25
6	Cl	2	**74**	63	700
7	NO_2	1	-	10	-
8	NO_2	1	**1e**	10	0
9	NO_2	1	**74**	55	450
10	NO_2	2	-	30	-
11	NO_2	2	**1e**	28	0
12	NO_2	2	**74**	81	170
13	CH_3	1	-	11	-
14	CH_3	1	**1e**	11	0
15	CH_3	1	**74**	44	300
16	CH_3	2	-	12	-
17	CH_3	2	**1e**	10	0
18	CH_3	2	**74**	48	300
19	Cl	1	Et_3N	18	20
20	Cl	1	**74**[c]	20	33

Reaction conditions: Aldehyde (0.3 mmol), enone (0.9 mmol), catalyst (0.03 mmol, 10 mol%), $TiCl_4$ (0.3 mmol, 1M in DCM), DCM (1.0 mL). [a] Defined as $(k_{cat}-k_{TiCl4})/k_{TiCl4}*100$. [b] Isolated yields are given. [c] The reaction was performed in the presence of Me_4N^+ picrate salt (1 equiv. relative to **74**).

5.2.3 Mechanism study

A series of experiments was then undertaken to demonstrate that the reaction does occur in the confined space of the cage catalyst. First, to rule out the possible contribution of the apical nitrogen in **74** for some of the catalytic activity observed, the reaction between *p*-chlorobenzaldehyde and cyclopentenone was performed with Et_3N instead of the caged catalyst **74**. As shown from Table 5.2 (compare entries 3 and 19), a dramatic decrease in activity was observed with the improvement of the reaction rate dropping from 400% to 20% and a yield close to that obtained with $TiCl_4$ alone (entry 1, Table 5.2). This suggests that the apical nitrogen of the encaged Verkade's superbase **74** does not take part, at least to a significant extent, in the catalytic process. Our second concern was to assess if the inner space of the cavity was large enough to accommodate the intermediates of the MBH reaction. The minimized structures obtained by DFT calculations (Scheme S20), showed that both intermediates can be formed inside the molecular cavity. One can see that the most bulky intermediate is partially encapsulated, as previously observed in solution and in the solid state with hemicryptophane complexes of acetylcholine or sugars.[31h,118]

Further evidences of the crucial role of the endohedral phosphorus site on the reactivity were obtained from inhibition and substrate selection experiments. In the first case, like in enzymatic reactions, the idea was to introduce a suitable nonreactive molecule in the cage. The Me_4N^+ cation is well complexed by hemicryptophane cages because of the cation-π interactions between the aromatic rings of the CTV unit and the ammonium guest.[31h] The catalytic reaction between 4-chlorobenzaldehyde and cyclopentenone was thus carried out in the presence of tetramethyl ammonium picrate (1 equivalent relative to catalyst **74**). Under these conditions, the yield dropped to 20%, similar to that obtained without superbase, shutting down the improvement of the reaction rate from 400% to 33% (entries 6 and 20, Table 5.2). The presence of the ammonium cation inside the cage prevents the access of the substrates to the phosphorus active site, hence blocking the reaction. In a second experiment, the bulky enone substrate, 6,6'-diphenyl-2-cyclohexen-1-one, was synthesized (Scheme S9 in experimental section) and reacted with 4-chlorobenzaldehyde in the presence of **74**. In this case no MBH product could

[118] Makita, Y.; Katayama, N.; Lee, H. H.; Abe, T.; Sogawa, K.; Nomoto, A.; Fujiwara, S. I.; Ogawa, A. *Tetrahedron Lett*. **2016**, *57*, 5112-5115.

be detected, probably because this bulky compound cannot enter in the cavity of **74** (Figure 5.13). This substrate size-dependent behavior, mimicking that of enzymes, brings new evidence that the reaction likely takes place inside the molecular cage.

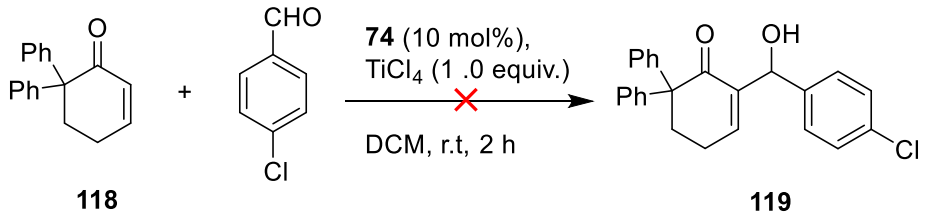

118 **119**

Figure 5.13 Size-dependent behavior of 6,6'-diphenyl-2-cyclohexen-1-one **118** and *p*-chlorobenzaldehyde in the presence of **74** and $TiCl_4$.

As demonstrated above, Verkade's superbase encaged in a supramolecular hemicryptophane has been successfully applied to constructing a FLP system with $TiCl_4$ as Lewis acid counterpart for MBH reaction with much more higher yields than that in the presence of model superbase without a cavity. The evidences for catalytic reaction taking place inside the cavity were supported by size-dependent reaction as well as DFT calculations.

5.2.4 MBH reaction in the presence of enantiopure *M*-74/*P*-74 and $TiCl_4$

Inspired by these fascinating results and the facts that highly confined enantiopure molecular cages have been widely applied in enantioselective recognition and catalysis. Especially, as supramolecular hosts, hemicryptophanes consisting of a cyclotribenzylene (or cyclotriveratrylene CTV) unit with another different C3-symmetrical moiety, have attracted considerable interests for enantioselective recognition of chiral guests,[31h] we wondered if the enantiopure version of encaged Verkade's superbase in a hemicryptophane structure with a chiral CTV unit could lead to asymmetric synthesis of MBH products in this FLP system. Consequently, we synthesized the corresponding enantiopure encaged superbase *M*-**74**/*P*-**74**, and then applied it in the MBH reaction (Figure 5.14). Unfortunately, no enantioselectivity was observed under our conditions. Probably, the confinement of enantiopure cavity is not sufficient for chiral induction to products.

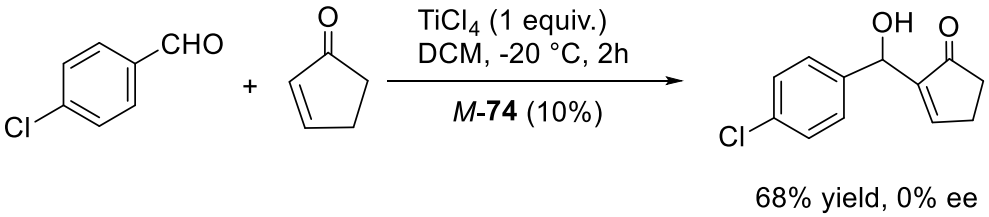

Figure 5.14 Reaction of *p*-chlorobenzaldehyde and cyclopentenone in the presence of enantiopure *M*-**74** and $TiCl_4$.

5.2.5 Synthesis of enantiopure encaged Verkade's superbase

Although Verkade's superbases have been applied in a wide range of organic transformations with high efficiencies, no asymmetric synthesis has ever been achieved in the presence of very few examples of enantiopure Verkade's superbases.[119] If we take a close look at these enantiopure Verkade's superbases, it can be found that the chiral moieties on the catalysts are far away from the catalytic sites, which could be the reason for unsuccessful enantioselectivities.

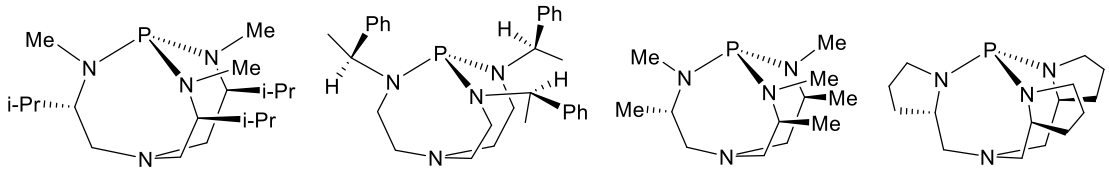

Figure 5.15 Few reported examples of enantiopure Verkade's superbases.

Enantiopure hemicryptophanes have been widely reported for enantioselective recognition of chiral guests, encapsulation of Verkade's superbases in a chiral hemicryptophane is supposed to result in asymmetric synthesis in some reactions. The synthesis of enantiopure encaged Verkade's superbases *M*-**74**/*P*-**74** refers to the procedure for preparing racemic encaged Verkade's superbase **74**, using chiral CTV unit instead of racemic one. Enantiopure CTV *M*-**125**/*P*-**125** reacted with 4-

[119] (a) Cernerud, M.; Adolfsson, H.; Moberg, C. *Tetrahedron: Asymmetry*. **1997**, *8*, 2655–2662. (b) Liu, X.; Ilankumaran, P.; Guzei, I. A.; Verkade, J. G. *J. Org. Chem*. **2000**, *65*, 701–706. (c) Ishihara, K.; Karumi, Y.; Kondo, S.; Yamamoto, H. *J. Org. Chem*. **1998**, *63*, 5692–5695.

hydroxybenzaldehyde in the presence of cesium carbonate to give enantiopure CTV derivative *M*-SI-**4**/*P*-SI-**4** which then reacted with tris(2-aminoethyl)amine (tren) following reduction by sodium borohydride to afford enantiopure hemicryptophane *M*-SI-**5**/*P*-SI-**5**. Subsequently, enantiopure hemicryptophane *M*-SI-**5**/*P*-SI-**5** reacted with $ClP(NMe_2)_2$ overnight to give corresponding enantiopure encaged azaphosphatrane *M*-**74**-H^+/*P*-74-H^+, which was deprotonated in the presence of *t*-BuOK to give rise to final enantiopure encaged Verkade's superbase *M*-**74**/*P*-**74**.

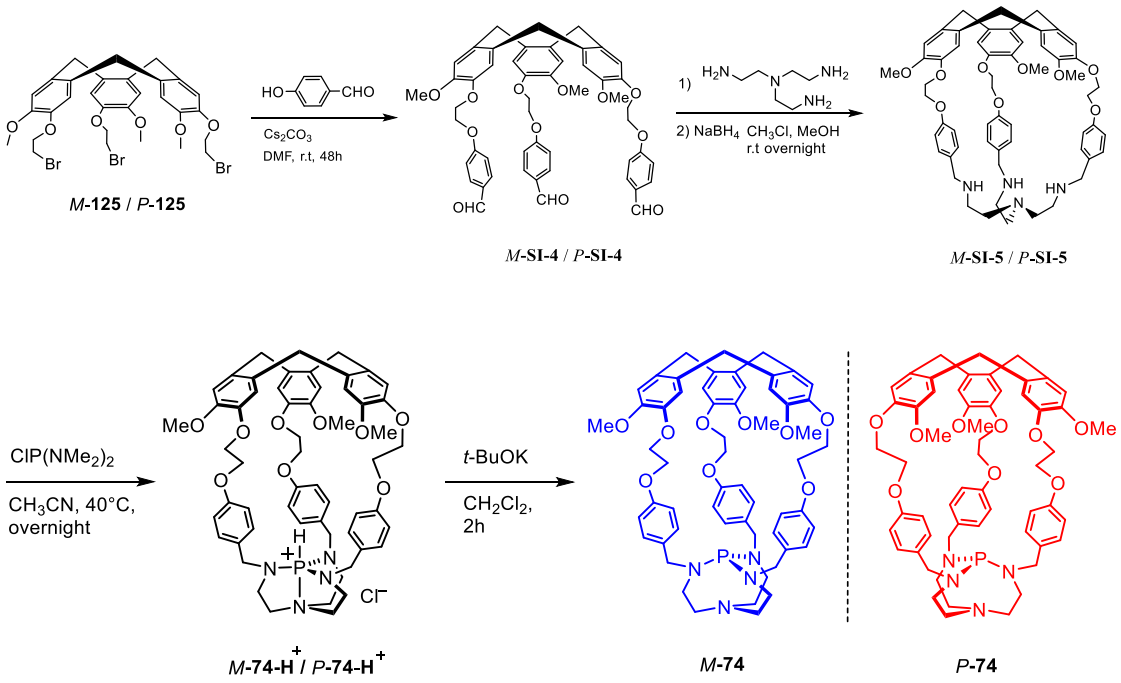

Figure 5.16 Synthetic procedure for preparation of enantiopure encaged *M*-**74**/*P*-**74**.

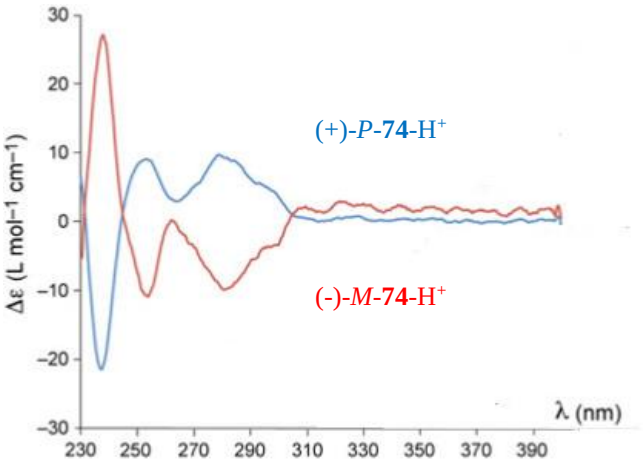

Figure 5.17 ECD spectra (CH_2Cl_2, 298 K) of two enantiopure *P*-**74**-H^+/*M*-**74**-H^+.

5.2.6 Attempts to obtain enantiomeric excess for reactions in the presence of *M*-74/*P*-74

With enantiopure version of proazaphosphatrane *M*-**74**/*P*-**74** in hand, in addition to MBH reaction, we attempted other two reactions 1) Diels Alder reaction, 2) Strecker reaction, and 3) acylation of racemic mixture of alcohol[5] in the presence of chiral *M*-**74**/*P*-**74**. The two tested reactions proceeded smoothly, however, disappointingly, no ee was observed under our conditions for both of them.

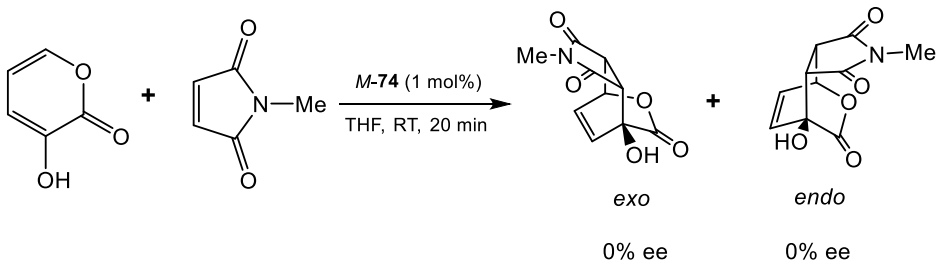

Figure 5.18 Asymmetric Diels Alder reaction in the presence of *M*-**74**.

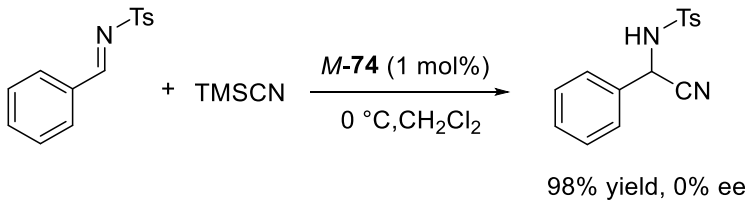

Figure 5.19 Asymmetric Strecker reaction in the presence of *M*-**74**.

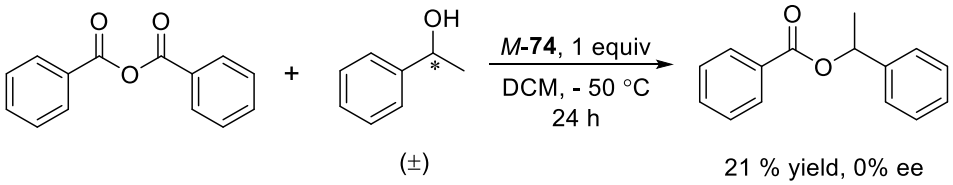

Figure 5.20 Kinetic resolution of racemic alcohol in the presence of *M*-**74**.

5.2.7 Synthesis of enantiopure BINOL-based hemicryptophanes

In order to further enhance the confinement of the cavity, a chiral BINOL linker was introduced to replace the benzene linker. Thus two chiral scaffolds are present in one hemicryptophane structure. The synthetic procedure for enantiopure hemicryptophanes is depicted in Figure 5.21. One of the precursors enantiopure *S*-**122** was prepared based on a reported procedure.[120] The intermolecular dehydration of racemic 1,1'-binaphthol (BINOL) (±)-**120** in the presence of *p*-TsOH under reflux in toluene gave rise to dinaphthofuran **121**, which then reacted with lithium pieces for 24 h. Subsequently, the mixture was cooled to -78 °C, in which several drops of DMF was added. The reaction mixture was stirred for 2 h, then allowed to room temperature and kept stirring overnight. The reaction was then quenched by HCl (3 mol/L) to give racemic compound (±)-**122** which was separated by chiral HPLC to produce enantiopure *S*-**122** and *R*-**122**. Another important intermediate enantiopure CTV unit *P*-**125**/*M*-**125** was synthesized following a reported protocol.[121] The first step started from the reaction of vanillyl alcohol **123** and 1,2-dibromoethane with potassium carbonate as base to give

[120] Areephong, J.; Ruangsupapichart, N.; Thongpanchang, T. *Tetrahedron Lett*. **2004**, *45*, 3067-3070.
[121] Chatelet, B.; Payet, E.; Perraud, O.; Dimitrov-Raytchev, P.; Chapellet, L.-L.; Dufaud, V.; Martinez, A.; Dutasta, J.-P. *Org. Lett*. **2011**, *13*, 3706-3709.

brominated compound **124**, which subsequently underwent cyclization to give racemic CTV **125**, enantiomers *M*-**125** and *P*-**125** were obtained by chiral HPLC separation. The reaction of enantiopure *P*-**125** with enantiopure *S*-**122** afforded *P*-*S*,*S*,*S*-**126**, which then reacted with tris(2-aminoethyl)amine (tren) followed by reduction of $NaBH_4$ to give the final enantiopure hemicryptophane *P*-*S*,*S*,*S*-**127**. The other three stereoisomers *M*-*S*,*S*,*S*-**127**, *M*-*R*,*R*,*R*-**127,** and *P*-*R*,*R*,*R*-**127** were synthesized in a similar procedure.

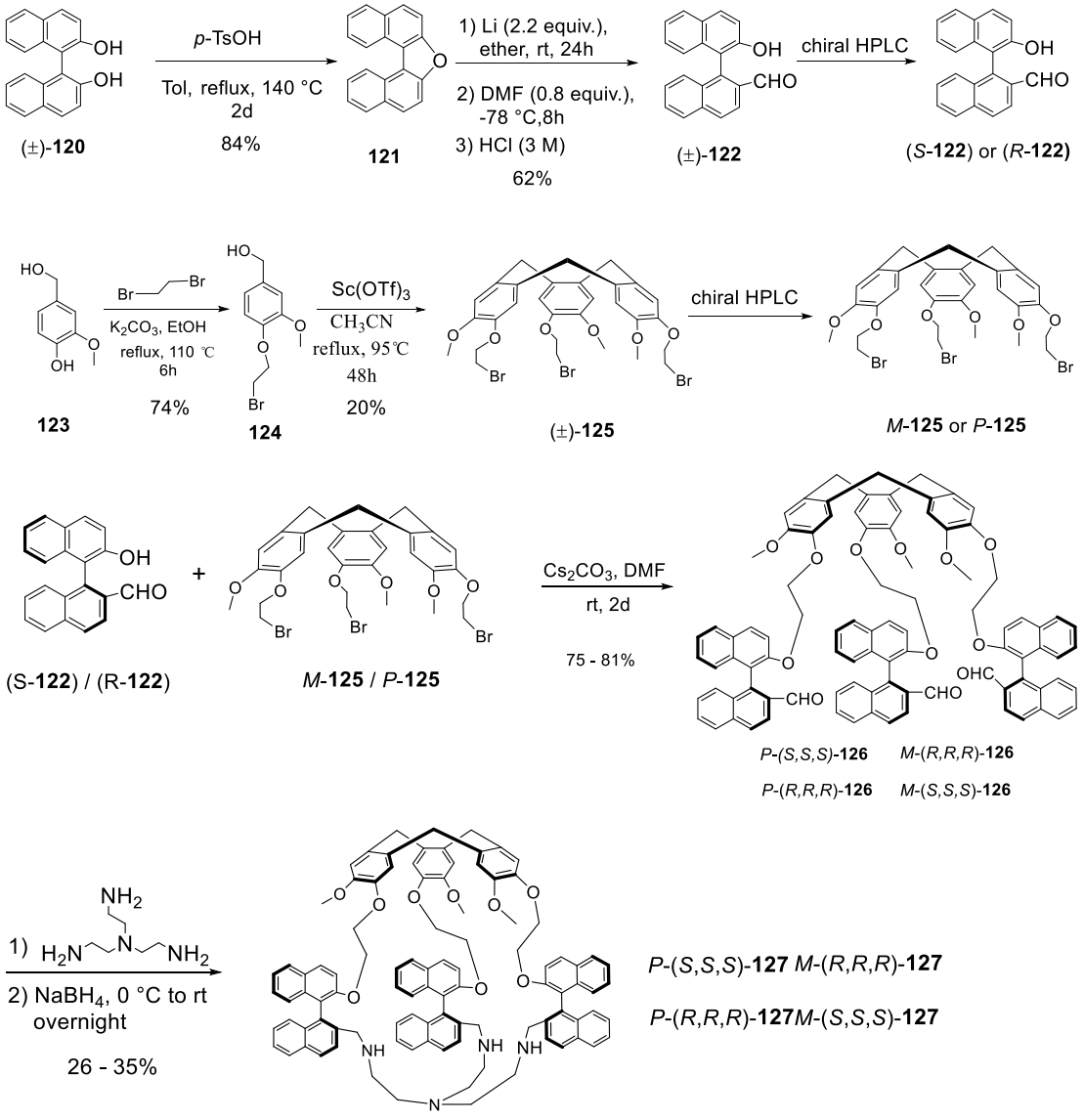

Figure 5.21 Synthetic route for preparation of four hemicryptophanes.

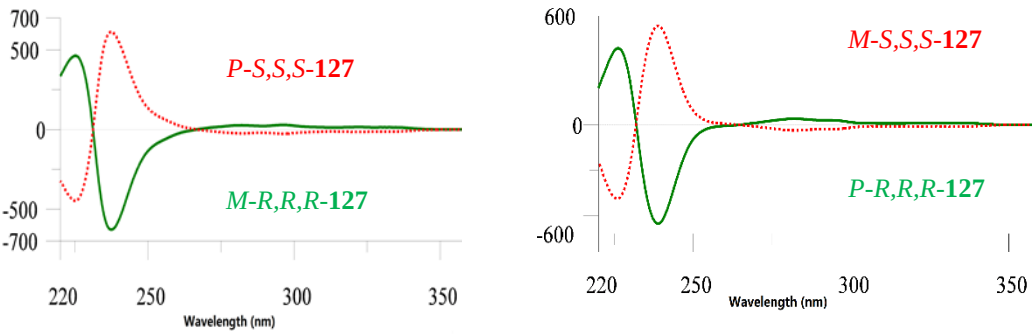

Figure 5.22 ECD spectra (CH_2Cl_2, 298 K) of four enantiopure hemicryptophanes *M*-*S*,*S*,*S*-**127**/*P*-*R*,*R*,*R*-**127**, *P*-*S*,*S*,*S*-**127**/*M*-*R*,*R*,*R*-**127**.

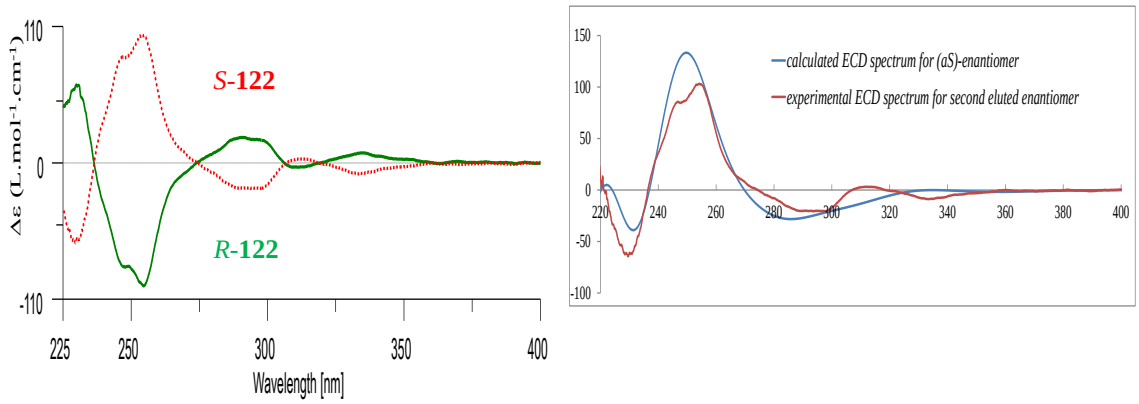

Figure 5.23 ECD spectra of *R*-**122**/*S*-**122** and comparison with calculated spectra.

5.2.8 Assignment of the absolute configuration

In order to determine the absolute configuration of four diastereomers *M*-*S*,*S*,*S*-**127**/*P*-*R*,*R*,*R*-**127**, *P*-*S*,*S*,*S*-**127**/*M*-*R*,*R*,*R*-**127,** we first turned our attention on the assignment of the absolute configuration of BINOL derivatives *S*-**122**/*R*-**122**. Electronic circular dichroism (ECD) spectra of the enantiomers *S*-**122**/*R*-**122** were recorded, as depicted in Figure 5.23. Absolute configuration *S*-**122**/*R*-**122** was determined by comparison of calculated and experimental optical rotation. Optical rotation calculations have been carried out at 589.3 nm by DFT at SMD(CH_2Cl_2)/B3LYP/6-311G(d,p) level for the two populated conformers. Calculated $[\alpha]_D^{25}$ for (*S*)-enantiomer was +18, which is consistent with experimental value ($[\alpha]_D^{25}$ = +22) for the second eluted enantiomer. We

can thus determine that the absolute configuration of the second eluted enantiomer is *S*-**122**. The ECD spectra of four hemicryptophane diastereomers were recorded in CH_2Cl_2 at 298 K (Figure 5.22). The absolute configuration of enantiopure CTV derivatives is usually assigned by ECD with a characteristic transition pattern of the ^1L_A located at around 240 nm. If an enantiopure CTV derivative has two characteristic sequent negative-positive signals from high to lower energies, a *P*-configuration is assigned, otherwise a *M*-configuration. The two pairs of enantiomers displayed perfect mirror image to each other (Figure 5.22). And ECD spectra of four diastereomers exhibited one of the main excitation patterns centered at 239 nm simultaneously. However, it is found that, the characteristic signal of CTV was strongly overlapped with intense signal from binaphthol moiety. Therefore we decided to use enantiopure CTV for the synthesis of BINOL-based hemicryptophanes, and then compared their ECD spectra with those of reported structures with CTV units and BINOL scaffolds,[122] thus the absolute configuration of four hemicryptophane diastereomers was successfully assigned (Figure 5.22).

5.3 Conclusions

In summary, in this Chapter we have designed a FLP system, where the Lewis base partner is encapsulated in a cage structure. The confinement of the Verkade's superbase in the cavity of a hemicryptophane host prevents the acid-base reaction with the Lewis acidic partner ($TiCl_4$) to take place, thus providing an effective system for the MBH reaction where both partners can act in concert without neutralizing each other. A direct comparison with model even bulky superbases, emphasizes the potentiality of such an approach. The key role of the cavity has been highlighted by a set of experiments, bringing evidence that the reaction does occur in the confined space of the molecular cavity. The encapsulation of the Verkade's superbase turns its catalytic activity on, allowing some cooperativity with titanium chloride to activate more efficiently the substrate and/or reaction intermediates. Besides, the enantiopure *M*-**74**/*P*-**74** were synthesized and used in this system for MBH reaction instead of racemic **74**, although no enantioselectivity was observed as well as for Diels Alder reaction and Strecker

[122] Lefevre, S.; Héloin, A.; Pitrat, D.; Mulatier, J. C.; Vanthuyne, N.; Jean, M.; Dutasta, J. -P.; Guy, L.; Martinez, A. *J. Org. Chem*. **2016**, *81*, 3199−3205.

reaction, the strategy provided a nice possibility for asymmetric catalysis in a chiral confined molecular cage. In the end, four novel enantiopure hemicryptophanes bearing chiral CTV units and BINOL scaffolds were synthesized, and their absolute configuration was determined. The chiral BINOL-based hemicryptophanes will be applied for enantioselective recognition of chiral guests of great interest. These ligands also open up the door for the synthesis of an encaged Verkade's superbase in a "highly" chiral environment, expected to provide the first Verkade's superbase efficient in enantioselective catalysis.

Part III: Beyond proazaphosphatranes: haloazaphosphatrane - from organocatalysis to halogen bonding

As described before, proazaphosphatranes have been extensively studied as organocatalysts in a wide range of organic transformations. And meanwhile, their protonated analogue azaphosphatranes have also been successfully applied in some halogen-bonding catalyzed reactions, where azaphosphatranes acted as halogen-bond donors, though limited. In this part, we turned our interest in their halogenated derivative haloazaphosphatranes, which could be treated as halogen-bond donors in anion recognition.

Chapter 6 Halogenated azaphosphatrane: a new member of halogen-bond donor

6.1 Introduction

Supramolecular interactions play key roles in living biological systems from membrane transfer to DNA structure.[64] Inspired by nature, chemists have categorized supramolecular interactions as following non-covalent interactions including ion-ion interactions, ion-dipole interactions, dipole-dipole interactions, hydrogen bonding, cation-π interactions, anion-π interactions, π-π interactions and Van der Waals Forces etc.[64] Halogen bonding (XB), an emergent non-covalent interaction that can be comparable to the well-known hydrogen bonding in terms of strength, has aroused considerable attraction because of potential applications in a variety of areas. Halogen-bonding interaction occurs when electron density transfers from a halogen-bond acceptor (electron donor) to a halogen-bond donor (electron acceptor), as depicted in Figure 6.1. The anisotropic charge distribution of polarized halogen bonded to highly electron-withdrawing moieties could account for this intermolecular electron density transfer.[66]

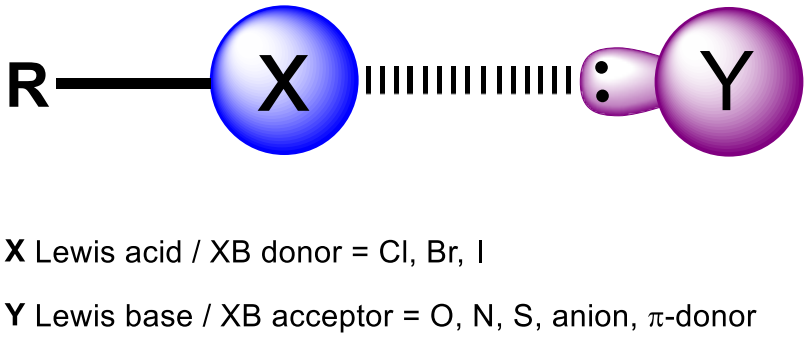

Figure 6.1 Schematic presentation of halogen bonding.

Different types of halogen bonds have been developed including cationic and neutral halogen-bond donors.[123] One strategy to tune the strength of halogen bonds is varying halogen atoms and modifying the moiety covalently bonded to the halogen, and thus halogen-bond donor ability is well modified by adjusting the electronic properties of the motif surrounding the halogen atom. Cationic halogen-bond donors have been largely employed in anion recognition because of their intrinsic attraction to anions.

[123] Tepper, R.; Schubert, U. S. *Angew. Chem., Int. Ed*., **2018**, *57*, 6004-6016.

In general, imidazolium, triazolium, pyridinium are motifs frequently used in the design of halogen-bond donors, because these charged nitrogen heterocycles could strongly polarize the covalently bound halogens.[66]

In 2010, the group of Beer reported the interpenetrative assembly of a pseudorotaxane by using imidazolium-based halogen bond anion as a template, which consists of a bromo-functionalized imidazolium threading component **129** and an isophthalamide macrocycle **128** (Figure 6.2).[124] The possibility of improved π-π stacking induced formation of the pseudorotaxane was ruled out, because the hexafluorophosphate salt **129**-PF_6 showed no interaction with the macrocycle. Besides, further evidences for formation of interpenetrative pseudorotaxane **129** ⊂ **128** in the solution phase mediated by halogen-bond anion template were confirmed by ^{1}H ROESY NMR spectroscopy, molecular dynamics and density functional theory calculations.

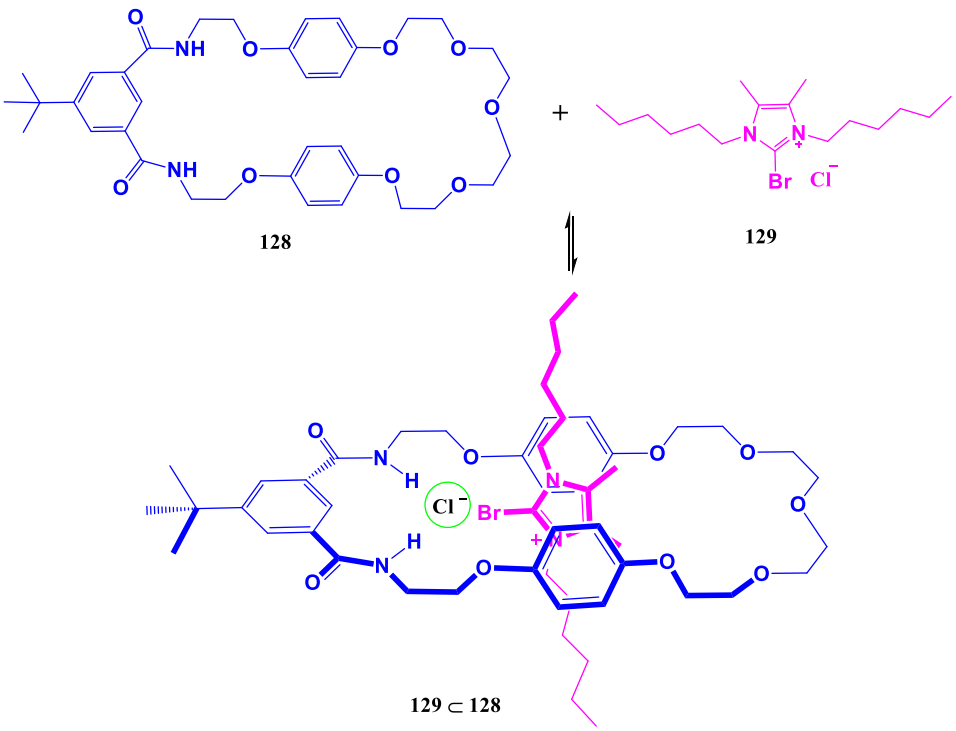

Figure 6.2 Halogen bonding promoted anion-templated penetration of **129** through macrocycle **128**.

[124] Serpell, C. J.; Kilah, N. L.; Costa, P. J.; Félix, V.; Beer, P. D. *Angew. Chem., Int. Ed*., **2010**, *49*, 5322-5326.

In addition to charged nitrogen heterocycles-based halogen-bond donors, metal complexes are also introduced as a backbone to halogen-bond subunit to enhance binding affinities and selectivities. Ghosh et al. reported a bis-heteroleptic Ru(II) complex with a triazole-backboned XB donor (Figure 6.3).[125] UV/Vis titration experiments revealed that complex **130** displayed selective phosphate recognition, and also higher association constant, lower limit of detection, and greater change in lifetime in the presence of phosphates were observed for complex **130**, compared with its hydrogen-bonding analogue complex **131**. The authors attributed the enhanced performance to significant amplification of Ru(II)-centered metal-to-ligand charge transfer (MLCT).

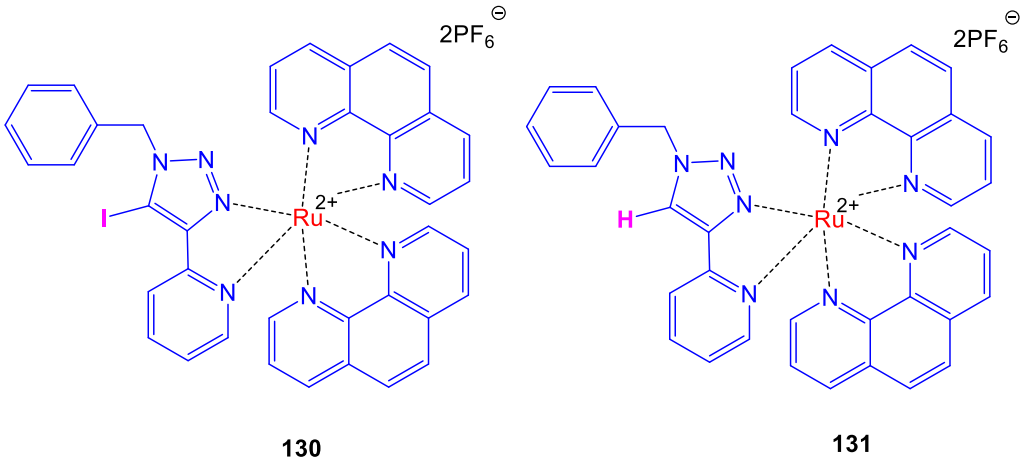

Figure 6.3 Triazole-backboned halogen-bond donor attached to a bis-heteroleptic Ru(II) complex **130** and its hydrogen-bond analogue **131**.

Different from cationic halogen-bond donors, of which the binding affinity is largely dependent on the benefits of charge assistance, the electronic properties of organic backbones strongly impact the interaction strength of neutral XB donors. Generally, in order to obtain high binding affinity, exceedingly electron-withdrawing moieties iodoperfluoroarenes are frequently introduced in the design of neutral halogen-bond donors.

[125] Chowdhury, B.; Sinha, S.; Ghosh, P. *Chem. Eur. J.* **2016**, *22*, 18051 – 18059.

Recently, the group of Beer synthesized a series of neutral XB rotaxanes containing two, three and four XB-donor iodotriazole components, showing strong and selective halide anion binding in wet organic solvent mixtures ($(CD_3)_2CO$:D_2O 98:2, 298 K, Figure 6.4).[126] Interestingly, the halide binding affinity and selectivity could be well controlled by varying the position and the number of XB donor iodotriazole moieties within the interlocked macrocycles, the highest halide binding affinity was observed in the presence of the rotaxane containing the largest number of XB donor moieties. Besides, it was found that the anion binding affinity by these neutral XB rotaxanes was significantly sensitive to solvent polarity, for example, dramatic reduction in binding affinity was observed for chloride when 2% of D_2O was added (from K_a = 4384 to 116 M^{-1} in $(CD_3)_2CO$).

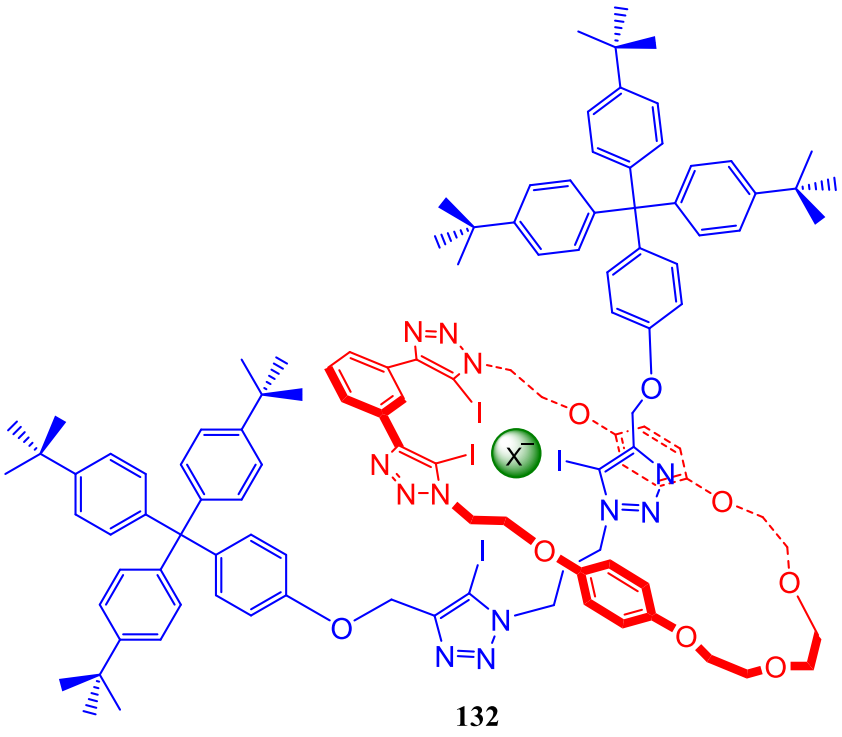

132

K_a (Cl^{-1}) = 496 M^{-1}
K_a (Br^{-1}) = 1200 M^{-1}
$(CD_3)_2CO$:D_2O 98:2, 298 K

Figure 6.4 Selective halide binding in the presence of neutral XB-based rotaxane **132** containing four iodotriazole moieties.

[126] Lim, J. Y.; Bunchuay, T.; Beer, P. D. *Chem. Eur. J.* **2017**, *23*, 4700 – 4707.

Neutral halogen-bond donors have also been found capable of catalyzing organic transformations. In 2016, Sugita et al. reported the use of pentafluorophenyl iodoalkyne as a halogen bond donor catalyst in the reaction of thioamides with 2-aminophenol to give corresponding products benzoxazoles (Figure 6.5).[127] This study demonstrated the advantages of neutral XB donor catalysts over cationic ones, including better solubility in organic solvents, higher stability under elevated temperatures. Control experiments were performed by using non-iodinated alkynes as catalysts to give the products with yields similar to that observed in the absence catalysts, which further confirmed the XB-mediated activation of substrate.

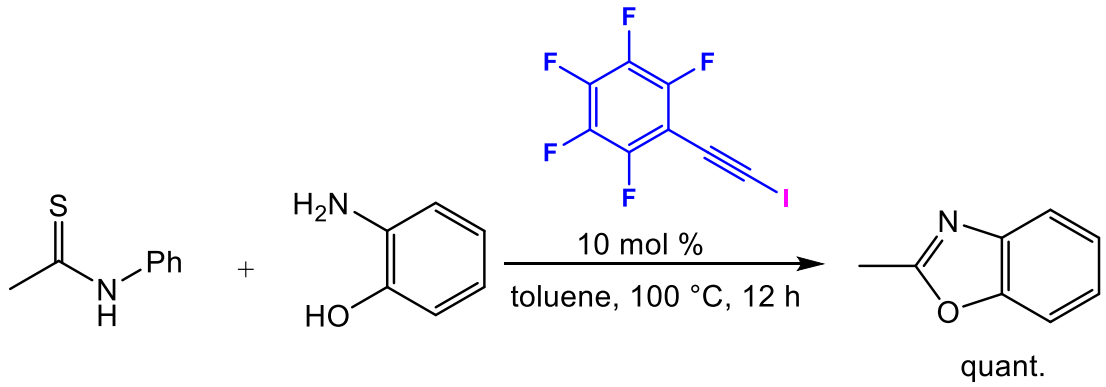

Figure 6.5 Iodoalkyne-based XB-mediated catalytic reaction of thioamide with 2-aminophenol.

Although a variety of halogen-bond donors have been developed, witnessing some fascinating results, the reported XB species are limited to *N*-heterocyclic backbones to date. Therefore, it is of high demand to develop new halogen-bond donors to complement the existing library in the domain of halogen bonding. In this chapter, a phosphonium-based halogen-bond donor chloroazaphosphatrane **111** was synthesized and ^{1}H NMR titration experiments were carried out to study the recognition selectivity for halide anions. Besides, encaged chloroazaphosphatrane, sulfide and selenide proazaphosphatranes were also synthesized.

[127] Matsuzawa, A.; Takeuchi, S.; Sugita, K. *Chem. Asian J.* **2016**, *11*, 2863-2866.

6.2 Results and discussion

6.2.1 Application of azaphosphatranes as hydrogen-bonding organocatalysts

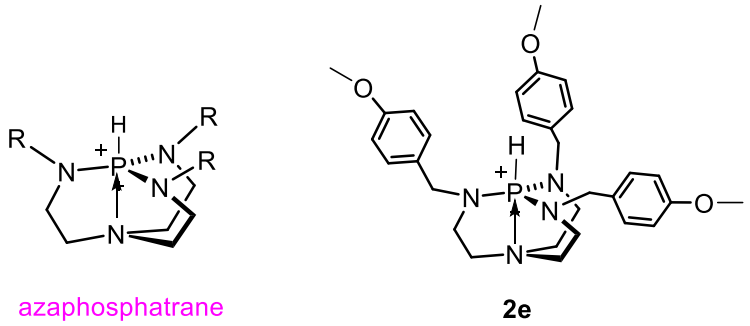

Figure 6.6 The structure of azaphosphatrane.

Our interest in haloazaphosphatranes as XB donors stems from the protonated analogue proazaphosphatranes, which have been utilized as hydrogen-bonding organocatalysts for some organic transformations. For example, previously, our group has applied azaphosphatranes as organocatalysts for CO_2 conversion to cyclic carbonates in the presence of epoxides under mild conditions, exhibiting high stability and productivity (Figure 6.7).[61] Importantly, the catalytic activities of azaphosphatranes could be well tuned by varying the substitution patterns on the catalysts. Reaction mechanism involved the activation of the epoxide by hydrogen bonding formed between P-H^+ of the azaphosphatrane and cyclic oxygen of the epoxide. Besides, a series of endohedral-functionalized azaphosphatranes in hemicryptophane hosts were prepared to study cage effect on CO_2 conversion compared with their model analogues without cavity. The results indicated that caged azaphosphatranes could indeed improve the catalytic activity by preventing the degradation of catalysts protected inside the cavity.[62]

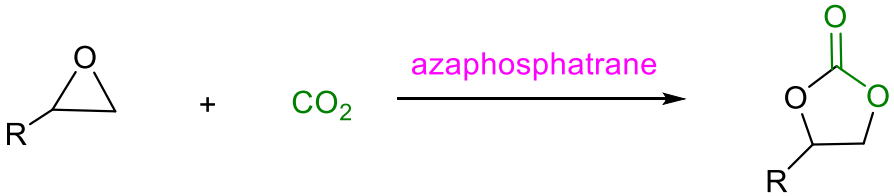

Figure 6.7 Azaphosphatrane catalyzed cyclic carbonate synthesis from CO_2 and epoxides.

Another application of azaphosphatrane as hydrogen-bond donor catalyst was catalytic ring-opening polymerization of lactide (Figure 6.8). [128] In the presence of azaphosphatranes, the polymerization process could be controlled to obtain polylactides in narrow dispersity under mild conditions.

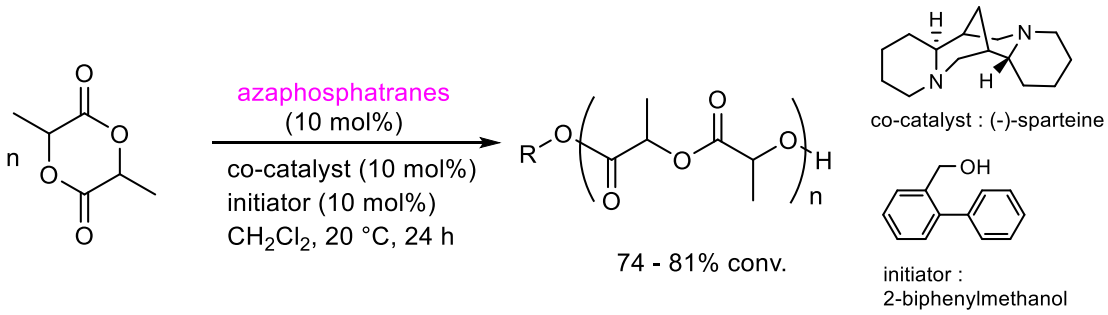

Figure 6.8 Azaphosphatranes catalyzed ring-opening polymerization of lactide in the presence of co-catalyst.

6.2.2 Recognition properties

Given the fact that halogen bonding and hydrogen bonding share a lot of similarities in terms of the nature and the strength for both noncovalent interactions.[65,66] We turned our attention to the possible use of haloazaphosphatranes as halogen-bond donors.

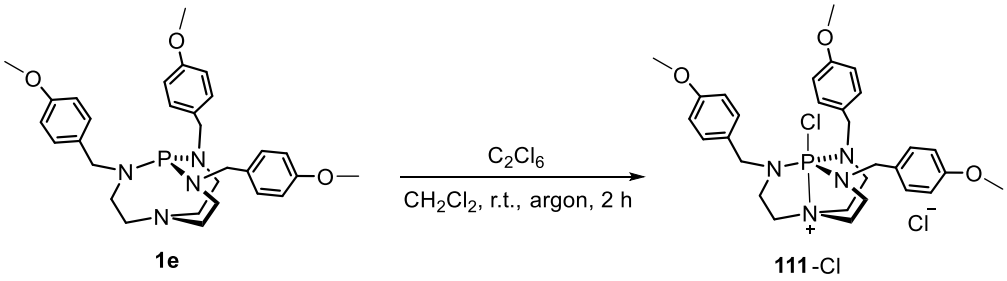

Figure 6.9 Synthesis of chloroazaphosphatrane **111**.

Initially, we synthesized chloroazaphosphatrane **111** according to a reported procedure of J. G. Verkade by reacting proazaphosphatrane **1e** with hexachloroethane in dichloromethane (Figure 6.9).[117] The first attempt to investigate chloroazaphosphatrane as halogen-bond donor was carried out by mixing an equimolar amount of

[128] Zhang, D.; Jardel, D.; Peruch, F.; Calin, N.; Dufaud, V.; Dutasta, J. P.; Martinez, A.; Bibal, B. *Eur. J. Org. Chem.* **2016**, *8*, 1619–1624.

chloroazaphosphatrane and elemental iodine in deuterated chloroform. Interestingly, both ^{31}P NMR and ^{1}H NMR studies indicated that significant chemical shifts were observed when iodine was added to the solution of chloroazaphosphatrane.

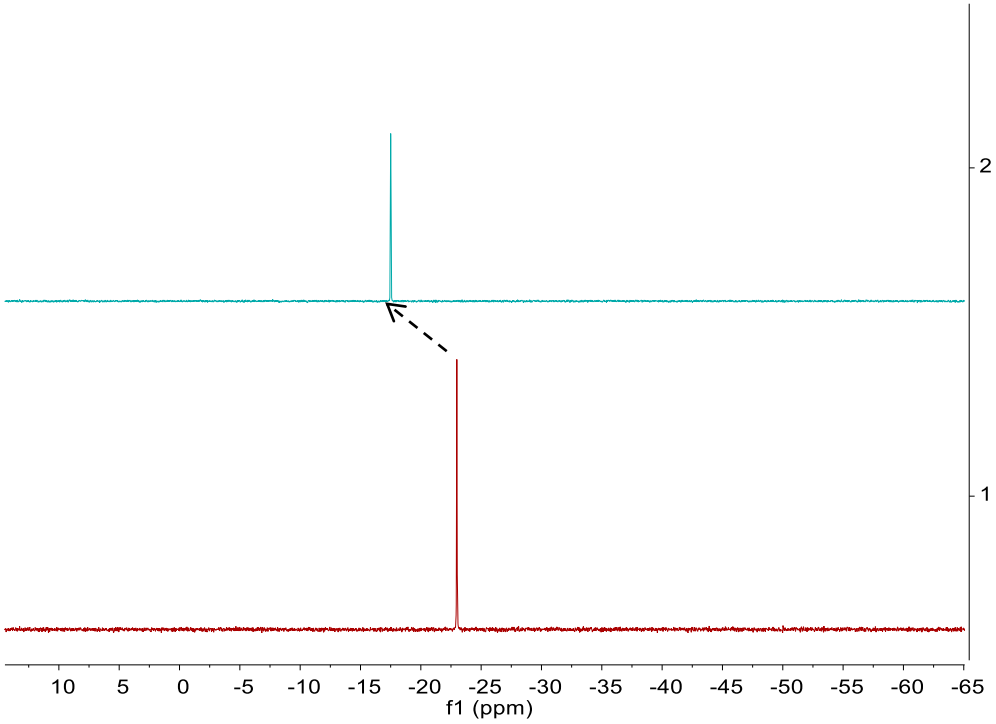

Figure 6.10 ^{31}P NMR (162 MHz, $CDCl_3$, 273K) spectra of 1) **111**-Cl, and 2) **111**-Cl + I_2.

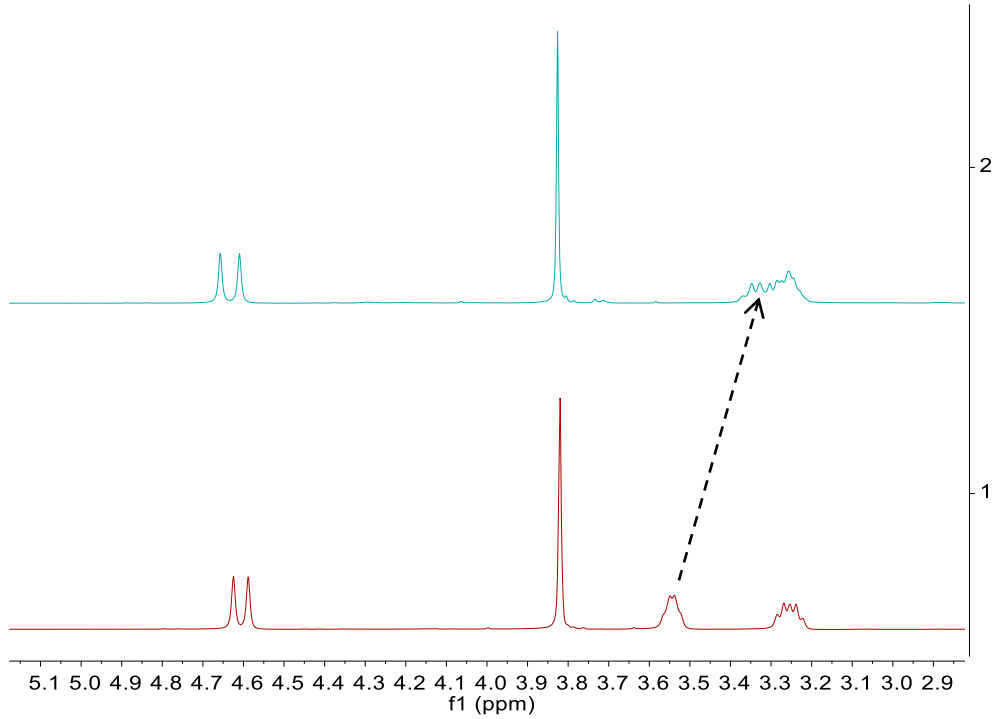

Figure 6.11 ^{1}H NMR (400 MHz, $CDCl_3$, 273K) spectra of 1) **111**-Cl, and 2) **111**-Cl + I_2.

However, it was still not clear whether halogen-bonding interaction occurred just based on the observed shifts. Because elemental iodine is supposed to interact with counter anion Cl^- to from species like I-I-Cl^-. Therefore, the observed chemical shifts could probably be induced by exchanging counter anion Cl^- with I-I-Cl^- rather than halogen bonding.

We then exchanged counter anion Cl^- with a non-coordinated anion PF_6^- readily by precipitating corresponding **111**-PF_6 from aqueous solution, and indeed negligible chemical shifts were detected in the presence of chloroazaphosphatrane with PF_6^- and elemental iodine, which might be attributed to poor polarizability of molecular I_2.

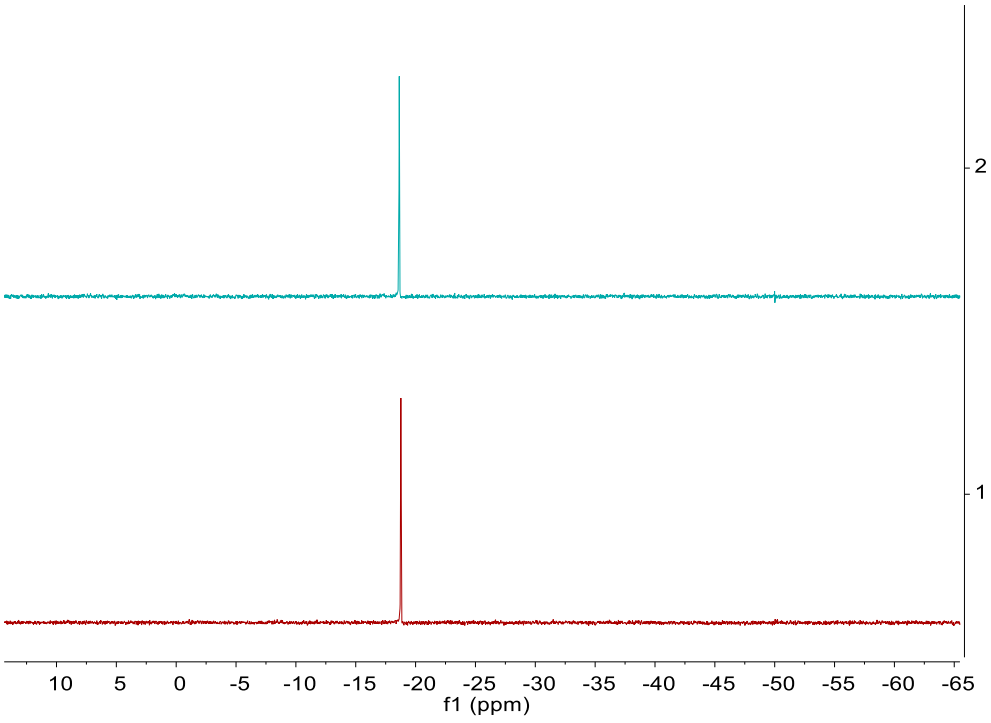

Figure 6.12 ^{31}P NMR (162 MHz, $CDCl_3$, 273K) spectra of 1) **111**-PF_6, and 2) **111**-PF_6 + I_2.

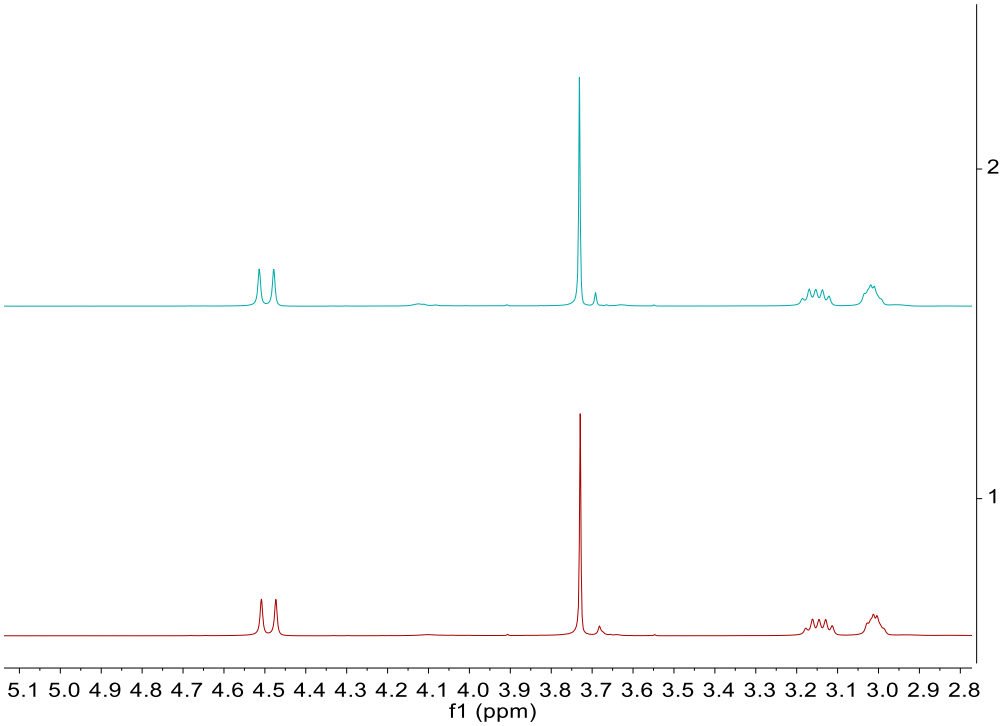

Figure 6.13 ^{1}H NMR (400 MHz, $CDCl_3$, 273K) spectra of 1) **111**-PF_6, and 2) **111**-PF_6 + I_2.

Anion recognition is an area that has been extensively studied by halogen bonding.[66b] Subsequently, we performed ^{1}H NMR titration experiments to study recognition properties of **111**-PF_6. Complexation behavior with halides were studied by ^{1}H NMR titrations in CD_3CN at 273K. Only one set of signals was detected for all titrations, indicating that the recognition process is fast on NMR timescale. A downfield shift was observed for proton of methylene adjacent to the apical nitrogen as a solution of guest was added into a solution of **111**-PF_6, indicating interaction between the halide and chloroazaphosphatrane host. In contrast, the protonated analogue azaphosphatrane with PF_6^- as counter anion was also tested as host in titration with halides, almost no detectable shifts were observed. Complexation induced shifts of **111**-PF_6 were measured and plotted as a function of the guest/host ratio. Binding constants were determined by Bindfit program after fitting the titration curves with a 1:1 host/guest stoichiometric complexation.[129]

[129] Thordarson, P. *Chem. Soc. Rev*., **2011**, *40*, 1305-1323.

Table 6.1 Binding constants K_a (M^{-1}) for 1:1 complexes formed between different halides and host **111**-PF_6 or **2e**-PF_6.[a]

Anion[b]	Host	K_a (M^{-1})
Cl^-	**111**-PF_6	66
	2e-PF_6	n.d[c]
Br^-	**111**-PF_6	23
	2e-PF_6	n.d[c]
I^-	**111**-PF_6	15
	2e-PF_6	n.d[c]

[a] K_a was determined by fitting ^1H NMR titration curves (CD_3CN, 500 MHz, 298 K) on the methylene adjacent to the apical nitrogen with the Bindfit program.[129] Estimated error < 10%. [b] Anions used as tetrabutylammonium (TBA) salts. [c] No complexation detected.

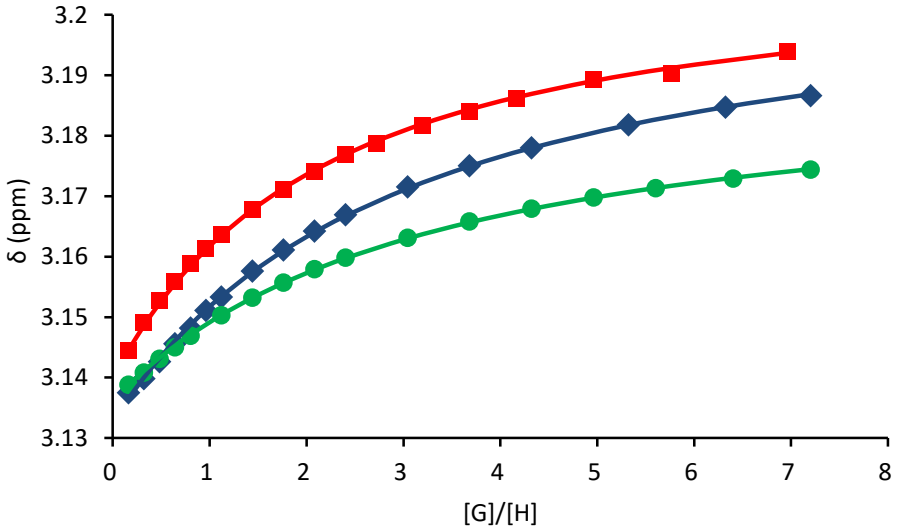

Figure 6.14 Titration curves of **111**-PF_6 with Cl^- (red dot), Br^- (blue dot) and I^- (green dot), respectively. Solid lines are fitted by Bindfit program.[129]

As can be seen in Figure 6.14, the titration curves perfectly matched the fitted lines. From the binding constants obtained by titrations in Table 6.1, **111**-PF_6 was able to selectively recognize Cl^- over Br^- and I^- in CD_3CN, with a binding affinity order ($Cl^- > Br^- > I^-$), which is consistent with charge density of the anion ($Cl^- > Br^- > I^-$) as reported in literatures.[130] On the contrary, no complexation was detected in the presence of the protonated analogue **2e**-PF_6, which further confirmed halogen-bonding interaction P-Cl···Cl between the halide and chloroazaphosphatrane **111**-PF_6 rather than simple electrostatic interactions induced by counter anion exchange from the TBA salts. However, it is worth mentioning that the affinity strength was weak of **111**-PF_6 with halides compared to reported halogen-bonding interaction. Actually, the observed weak complexation between **111**-PF_6 and halides was expected, because chlorine is regarded as a halogen with poor polarizability, and charge could not effectively transfer from halogen-bond acceptors to chlorine-based halogen-bond donors. In fact, according to the procedure reported by J. G. Verkade,[131] we have attempted to synthesize the iodoazaphosphatrane without success, unfortunately.

6.2.3 Halogen bonding in a cage

As described in chapter 2, cage molecules could cause significant and unexpected effect on recognition and catalytic properties. Previously, our group has studied effect of confinement on proton transfer and on catalytic activities of proazaphosphatranes.[57] We thus continued our effort to encage chloroazaphosphatrane in a confined hemicryptophane supramolecular structure. The encaged chloroazaphosphatrane was readily prepared by reacting encaged proazaphosphatrane with hexachloroethane.

[130] (a) Cametti, M.; Raatikainen, K.; Metrangolo, P.; Pilati, T.; Terraneo, G.; Resnati, G. *Org. Biomol. Chem.,* **2012**, *10*, 1329–1333. (b) Gilday, L. C.; White, N. G.; Beer, P. D. *Dalton Trans.*, **2013**, *42*, 15766-15773.
[131] Kingston, J. V.; Verkade, J. G. *J. Org. Chem.* **2007**, *72*, 2816-2822.

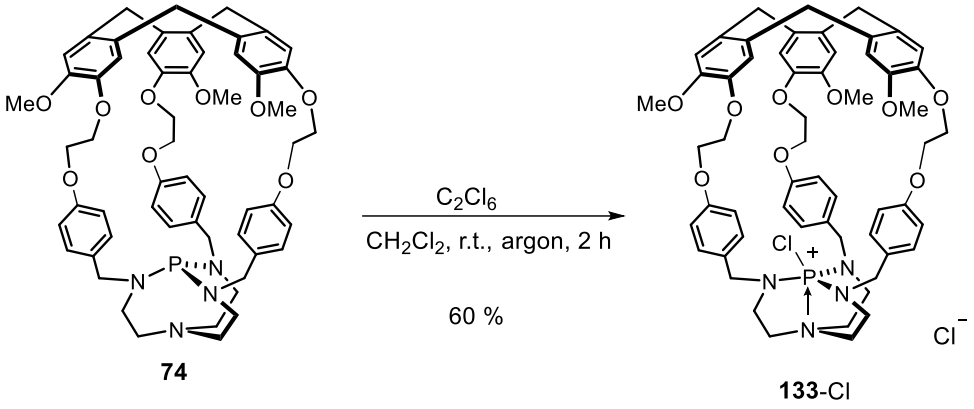

Figure 6.15 Synthesis of encaged chloroazaphosphatrane **133**·Cl.

Fascinatingly, single crystals of **133**·Cl suitable for X-Ray diffraction analysis were obtained by slow evaporation from a concentrated solution in $CHCl_3$. The structure of **133**·Cl displayed a C_3 symmetric characteristic (Figure 6.16). Surprisingly, a chloroform molecular was trapped inside the cavity, the crystal structure of $CHCl_3 \subset$ **133**·Cl showed that the distance (Cl···Cl 3.48 Å) measured between two chlorines was slightly shorter than the sum of van der Waals distance of two Cl atoms (Cl···Cl 3.64 Å), between which the interaction was probably halogen-bonding interaction, considering the neutral chloroform can be regarded as an extremely weak Lewis base as halogen-bond acceptor in this case to some extent. In contrast, in the structure of $CH_2Cl_2 \subset$ **74**-$H^+ \cdot Cl^-$.[55] the encapsulated dichloromethane was encaged through C-H ··· π interactions (Figure 6.16). The different interactions observed above underlined that the mode of interaction could be varied by changing functionalization.

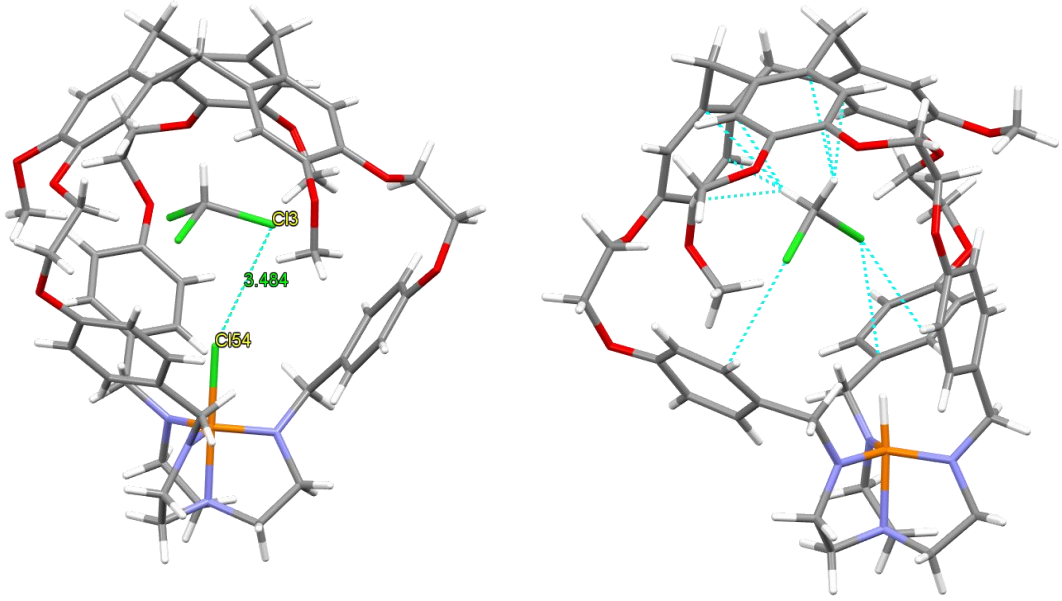

Figure 6.16 Crystal structures of $CHCl_3 \subset$ **133**·Cl (left) and $CH_2Cl_2 \subset$ **74**-H^+·Cl^- (right). Solvent molecules are omitted for clarity. Dashed lines represent short contacts.

As we have observed halogen-bonding interaction between chloroazaphosphatrane and halides, we were fascinated to explore the effect of confinement on halogen bonding. However, the preparation of corresponding encaged chloroazaphosphatrane with PF_6^- as counter anion seemed unsuccessful, as ^1H, ^{31}P NMR and mass spectra failed to detect it.

6.2.4 From halogen bonding to chalcogen bonding

Chalcogen bonding is another type of noncovalent interaction, in which a covalently bonded electrophilic chalcogen atom serves as an electron acceptor and interacts with a nucleophilic species acting as an electron donor.[132] Chalcogen bonding is much similar to halogen bonding in terms of the nature of bonding, both of which could be attributed to the anisotropic distribution of electron density around a covalently bonded chalcogen or halogen atom. Chalcogen bonding has been used in the area of crystal

[132] Mahmudov, K. T.; Kopylovich, M. N.; da Silva, M. F. C. G.; Pombeiro, A. J. *Dalton Trans.*, **2017**, *46*, 10121-10138.

engineering, synthesis and catalysis, which is very limited though.[132] As an extension study of halogen bonding, we synthesized encaged sulfide and selenide proazaphosphatranes in order to compare their properties with the chlorinated analogue in recognition and catalysis, etc.

The procedure for synthesizing encaged sulfide and selenide proazaphosphatranes referred to a reported procedure by J. G. Verkade.[133] The reaction of encaged proazaphosphatrane with elemental sulfur and selenium afforded corresponding encaged sulfide and selenide proazaphosphatranes, respectively.

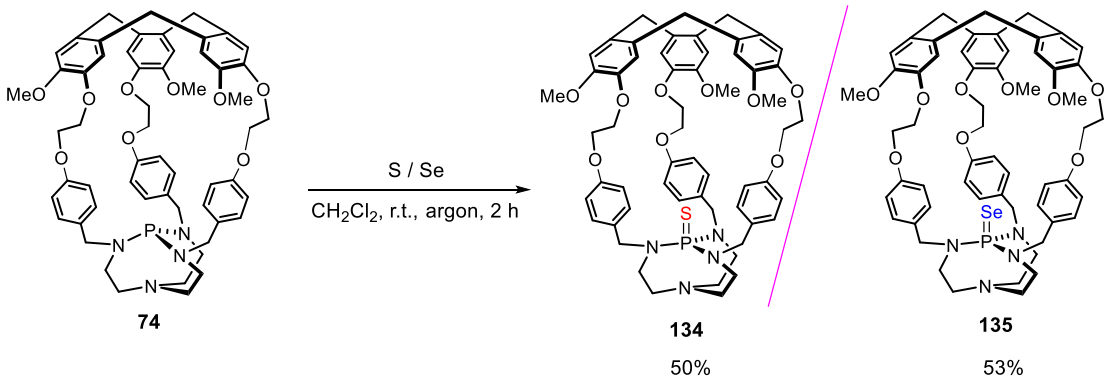

Figure 6.17 Synthesis of encaged sulfide and selenide proazaphosphatranes **134** and **135**.

6.3 Conclusions

In this chapter, we synthesized a Verkade's superbase derivative phosphonium chloroazaphosphatrane which acted as a halogen-bond donor in the recognition of different halides. Titration experiment results indicated that the binding affinity order was in line with charge density of the anion ($Cl^- > Br^- > I^-$), though complexation was rather weak. The phosphonium-based structure was for the first time studied as halogen-bond donor, which can serve as a new backbone in the development of designing and constructing halogen bonding. Besides, in the crystal structure of the inclusion complex comprising an encaged chloroazaphosphatrane and a chloroform

[133] Schmidt, H.; Lensink, C.; Xi, S. K.; Verkade, J. G. *Z. Anorg. Allg. Chem*. **1989**, *578*, 75-80.

inside, the shortened distance P-Cl···Cl indicated weak halogen-bonding interaction between two chlorines. In the end, encaged sulfide and selenide proazaphosphatranes were synthesized and will be applied in recognition and catalysis.

General conclusions and perspectives

The objective of this thesis is multiple: 1) exploring new reactions in the presence of proazaphosphatranes, broadening their applications in catalysis; 2) synthesizing chiral encaged proazaphosphatranes for asymmetric transformations; 3) synthesizing new chiral hemicryptophanes; 4) synthesizing the derivatives of proazaphosphatranes of interest and exploring their possible applications.

In this thesis, we have first of all established a mild, convenient and highly efficient methodology for the synthesis of α-aminonitriles in the presence of proazaphosphatranes. Differently substituted substrates with various protecting groups are tolerated. Besides, we found that the catalytic activity of proazaphosphatranes is consistent with their basicity, i.e. higher basicity leads to a better yield. In the end, a possible mechanism is proposed involving a four-coordinated silicon intermediate which is detected by ^{29}Si NMR.

Subsequently, the encaged proazaphosphatrane as a Lewis base in a hemicryptophane structure was used to construct a FLP system with $TiCl_4$ being Lewis acid counterpart, which was successfully applied in MBH reaction. Direct comparison with model analogue without a cavity evidenced that the confinement of encaged proazaphosphatrane prevented acidic-basic interaction between proazaphosphatrane and $TiCl_4$, thus their catalytic activities were conserved, further activated substrates in a cooperative way. The result demonstrates a clever strategy for constructing FLP in a supramolecular cage

Given the high efficiency and a lack of asymmetric synthesis in the presence of proazaphosphatranes in organic transformations, chiral encaged proazaphosphatranes were synthesized and tested as catalysts in Diels-Alder reaction, Strecker reaction and MBH reaction, however, no enantioselectivity was observed, probably, the steric hindrance was not enough for chiral induction to products. Subsequently, in order to acquire a more steric environment, BINOL linkers were introduced instead of phenyl connectors to obtain enantiopure BINOL-based hemicryptophanes with highly steric hindrance, which are promising in selective recognition of guests with higher enantioselectivity.

In the last part, chloroazaphosphatrane, as derivative of proazaphosphatranes, was applied in the recognition of halide anions by halogen bonding, showing selective sensing for chloride despite weak complexation strength. Phosphonium-based haloazaphosphatrane emerges as a new member of halogen-bond donors, providing a new scaffold for designing halogen-bond donor. It can be anticipated that, it would be

of great interest to compare recognition and catalytic property with their encaged analogues, taking the confinement effect into consideration. In addition, halogen-bonding affinity could be tuned by varying electronic properties of phosphonium-based scaffolds to meet specific requirements in recognition and catalysis. In the end, encaged selenide azaphosphatranes were synthesized and characterized, which could be regarded as chalcogen-bond donors, direct comparison of their properties with their uncapped analogues would bring about a lot of new insights into supramolecular chemistry.

Experimental section

General information

All commercial reagents and starting materials were used directly as received without further purification, unless otherwise noted. All dry solvents were purified prior to use through standard procedures or obtained from a solvent drying system (MB-SPS-800). All the reactions were carried out under an atmosphere of argon, unless otherwise noted. Flash column chromatography was performed using silica gel 60 (230-400 mesh). Thin-layer chromatography was per-formed on aluminum-coated plates with silica gel 60 F_{254} and was visualized with a UV lamp or by staining with potassium permanganate. ^{1}H NMR spectra were recorded at either 300 or 400 MHz on BRUKER Avance III nanobay spectrometers. ^{13}C NMR spectra were recorded at either 101 or 126 MHz and reported in ppm relative to $CDCl_3$ (δ = 77.4 ppm), unless otherwise noted. Single Pulse Magic Angle Spinning (SP MAS) ^{29}Si Solid State NMR spectra were obtained with a Bruker Avance 400 MHz WB spectrometer at the ^{29}Si resonance frequency of 79.5 MHz. Chemical shifts were referenced to tetramethyl silane, whose resonance was set to 0 ppm. High-resolution mass spectra (HRMS) were performed at Spectropole Analysis Service of Aix Marseille University. Infrared spectra were performed on FT-IR Brucker Alpha Platinum ATR.

Synthesis and characterization

Procedure for preparation of proazaphosphatrane 1e

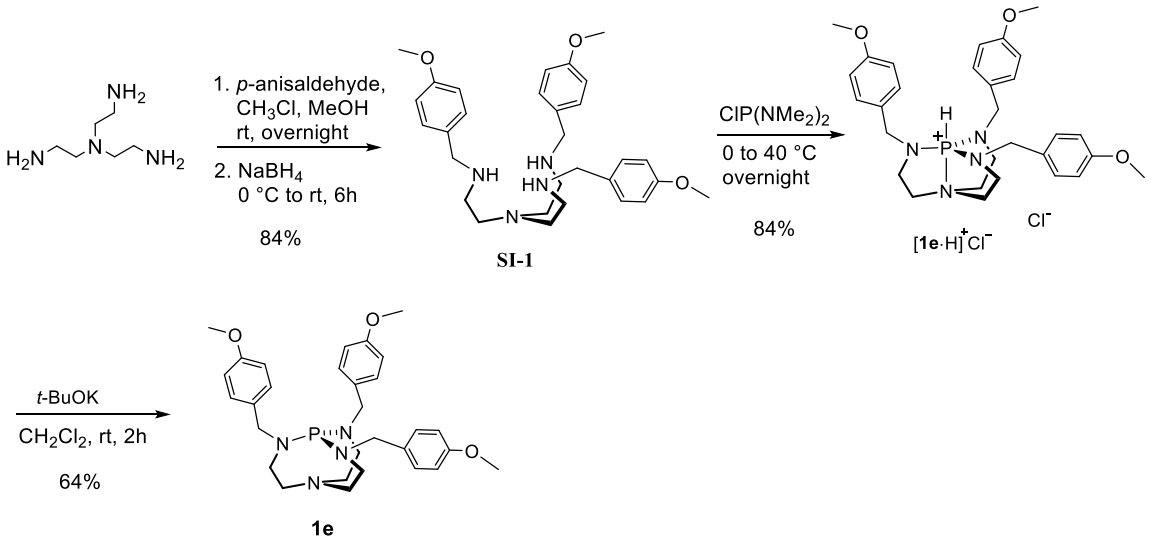

Scheme S1. Synthetic route for preparation of **1e**.

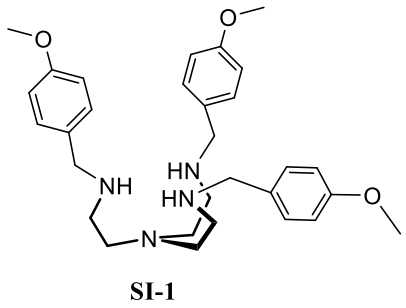

Compound tris(4-methoxybenzyl)tren **SI-1** was prepared following a known procedure with modification.[55] To a flame dried round bottom flask was added tris(2-aminoethyl)amine (tren) (1.46 g, 10 mmol), *p*-anisaldehyde (4.08 g, 30 mmol) and MeOH (100 mL), the reaction was stirred at room temperature for 6 h, then the reaction was allowed to cool at 0 °C, $NaBH_4$ (2.3 g, 60 mmol) was added slowly over a period of one hour, then the reaction was allowed to warm to room temperature and stirred for another 2 h. When reaction finished, solvent was removed. The remaining mixture was added 100 mL of H_2O and extracted by $CHCl_3$ (3 ×100 mL), Organic phase was collected, dried over anhydrous Na_2SO_4, filtered, and concentrated under vacuum to give crude product, which was then purified on silica gel by flash chromatography (CH_2Cl_2/MeOH/Et_3N, 15/2/0.1) to obtain pure tris(4-methoxybenzyl)tren **SI-1** as a yellow oil (4.3 g, 84%). **^{1}H NMR** (300 MHz, $CDCl_3$) δ 7.16 (d, *J* = 8.43 Hz, 6H), 6.84 (d, *J* = 8.43 Hz, 6H), 3.76 (s, 9H), 3.69 (s, 6H,) 2.68 (t, *J* = 5.83 Hz, 6H), 2.59 (t, *J* = 5.83 Hz, 6H); **^{13}C NMR** (300 MHz, $CDCl_3$ δ 158.57, 132.58, 129.27, 113.79, 55.24, 54.36, 53.42, 47.08. These data are consistent with literature.[55]

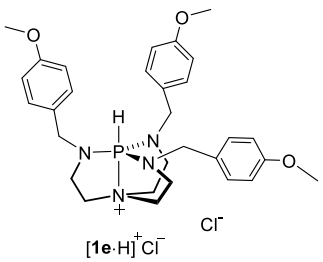

[1e·H]$^{+}$Cl^{-} was prepared from a reported literature with modification.[55] In an ice-bath cooled round bottom flask equipped with a stirring bar, bis(dimethylamino)chlorophosphine (1.76 mL, 11.38 mmol) was dissolved in dry acetonitrile (20 mL), and a solution of tris(4-methoxybenzyl)tren (4.82 g, 9.48 mmol) in acetonitrile (10 mL) was added dropwise. The reaction mixture was stirred at 0 °C under an argon atmosphere for 30 minutes. And then the reaction was heated to 40 °C and stirred overnight. The solvent was removed under reduced pressure to give the crude product, which was purified on silica gel by column chromatography (CH_2Cl_2/MeOH/, 15/1) to obtain pure [**1e**·H]$^{+}$Cl^{-} as a white powder (4.54 g; 84 % yield). ^{1}H NMR (300 MHz, $CDCl_3$) δ 7.06 (d, J = 8.6 Hz, 6H), 6.85 (d, J = 8.6 Hz, 6H), 5.78 (d, $^{1}J_{P\text{-}H}$ = 495.7 Hz, 1H), 4.07 (d, J = 17.1 Hz, 6H), 3.79 (s, 9H), 3.64 – 3.49 (m, 6H), 3.15 – 2.97 (m, 6H). ^{13}C NMR (75 MHz, $CDCl_3$) δ 159.32, 129.06, 128.64, 114.38, 55.34, 50.82, 47.03, 39.20. ^{31}P NMR (121 MHz, $CDCl_3$) δ -12.48. These data are consistent with literature.[55]

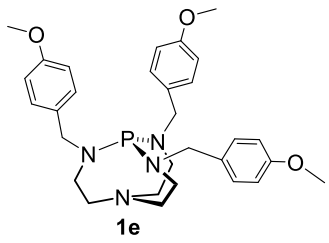

1e was prepared form a reported literature with modification.[55] [**1e**·H]$^{+}$Cl^{-} (200 mg; 0.35 mmol) was placed in a flame-dried Schlenk flask and dissolved in dry DCM (2mL). Then, *t*-BuOK (84 mg, 0.75 mmol) was added and the mixture was stirred vigorously for two hours under argon. The solvent was evaporated with a vacuum pump and toluene (4 mL) was added. The mixture was stirred for an additional 0.5 h and then the suspension was let to settle and filtered under argon on a fritted glass. The filtrate was placed in a Schlenk tube and the solvent was removed under vacuum to give pure **1e** as a yellow oil (120 mg; 64% yield). ^{1}H NMR (400 MHz, Toluene-d_8) δ 7.33 (d, J = 8.4 Hz, 6H), 6.84 (d, J = 8.4 Hz, 6H), 4.20 (d, J = 9.3 Hz, 6H), 3.42 (s, 9H), 2.86 – 2.76 (m, 6H), 2.76 – 2.65 (m, 6H); ^{13}C NMR (75 MHz, Toluene-d_8) δ 158.92, 137.39, 137.09, 133.30, 54.35, 52.65, 51.04, 45.15; ^{31}P NMR (162 MHz, Toluene-d_8) δ 126.63. These data are consistent with literature.[55]

General procedure for preparation of *N*-tosylaldimines 102a-102e.

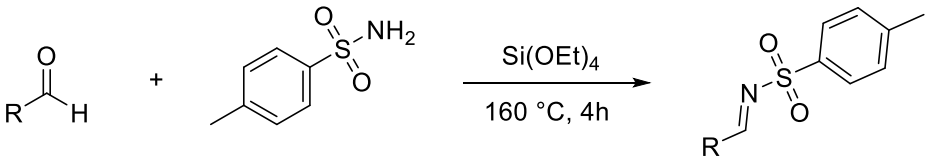

Scheme **S2**. Preparation of starting materials *N*-tosylaldimines **102a-102e**.

***N*-tosylaldimines 102a-102e** were prepared readily from the corresponding aldehyde and *p*-toluenesulfonamide according to the literatures.[134] The aldehyde (10 mmol), $TsNH_2$ (10 mmol) and $Si(OEt)_4$ (2.4 mL) were combined in a flask equipped with a still head and heated at 160 °C for 4 hours, during which time EtOH was collected in the receiving flask. After cooling, the reaction mixture was added Et_2O (80 mL) to give the precipitate, which was filtered and washed with Et_2O. The crude product was then recrystallized (EtOAc/hexane) for purification.

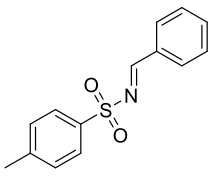

102a

***N*-benzylidene-4-methylbenzenesulfonamide (102a)**.[134] ^{1}H NMR (300 MHz, $CDCl_3$) δ 9.03 (s, 1H), 7.97 – 7.85 (m, 4H), 7.65 – 7.57 (m, 1H), 7.48 (t, *J* = 7.6 Hz, 2H), 7.34 (d, *J* = 8.1 Hz, 2H), 2.44 (s, 3H); ^{13}C NMR (75 MHz, $CDCl_3$) δ 170.07, 144.55, 135.25, 134.87, 132.45, 131.27, 129.78, 129.12, 128.09, 21.62.

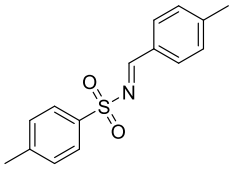

102b

4-methyl-*N*-(4-methylbenzylidene)benzenesulfonamide (102b).[134] ^{1}H NMR (300 MHz, $CDCl_3$) δ 8.99 (s, 1H), 7.88 (d, *J* = 8.3 Hz, 2H), 7.81 (d, *J* = 8.1 Hz, 2H), 7.33 (d, *J* = 8.1 Hz, 2H), 7.28 (d, *J* = 8.0 Hz, 2H), 2.43 (s, 6H); ^{13}C NMR (75 MHz, $CDCl_3$) δ 169.92, 146.34, 144.38, 135.50, 131.40, 129.91, 129.73, 128.01, 126.47, 21.96, 21.61.

[134]. Love, B. E.; Raje, P. S.; Williams II, T. C. *Synlett.* **1994**, *7*, 493-494.

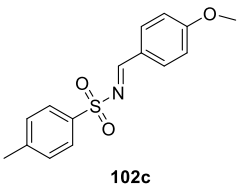

102c

***N*-(4-methoxybenzylidene)-4-methylbenzenesulfonamide (102c)**.[134] ^{1}H NMR (300 MHz, $CDCl_3$) δ 8.93 (s, 1H), 7.91 – 7.84 (m, 4H), 7.32 (d, *J* = 8.1 Hz, 2H), 6.96 (d, *J* = 8.8 Hz, 2H), 3.87 (s, 3H), 2.42 (s, 3H); ^{13}C NMR (75 MHz, $CDCl_3$) δ 169.16, 165.28, 144.20, 135.83, 133.68, 129.69, 127.88, 125.27, 114.68, 55.66, 21.59.

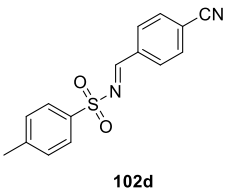

102d

***N*-(4-cyanobenzylidene)-4-methylbenzenesulfonamide (102d)**.[134] ^{1}H NMR (300 MHz, $CDCl_3$) δ 9.05 (s, 1H), 8.03 (d, *J* = 8.4 Hz, 2H), 7.89 (d, *J* = 8.3 Hz, 2H), 7.77 (d, *J* = 8.3 Hz, 2H), 7.37 (d, *J* = 8.1 Hz, 2H), 2.45 (s, 3H); ^{13}C NMR (75 MHz, $CDCl_3$) δ 167.72, 145.21, 135.96, 134.34, 132.74, 131.25, 129.96, 128.33, 117.68, 117.57, 77.44, 77.01, 76.59, 21.68.

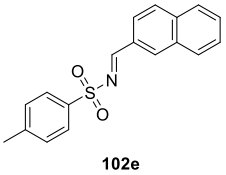

102e

4-methyl-N-(naphthalen-2-ylmethylene)benzenesulfon- amide (102e).[134] ^{1}H NMR (300 MHz, $CDCl_3$) δ 9.17 (s, 1H), 8.33 (s, 1H), 8.03 (dd, *J* = 8.6, 1.7 Hz, 1H), 7.99 – 7.85 (m, 5H), 7.69 – 7.53 (m, 2H), 7.36 (d, *J* = 8.1 Hz, 2H), 2.44 (s, 3H); ^{13}C NMR (75 MHz, $CDCl_3$) δ 170.00, 144.53, 136.54, 136.01, 135.37, 132.66, 130.16, 129.80, 129.48, 129.43, 129.16, 128.12, 128.05, 127.23, 124.16, 21.63.

General procedure for preparation of *N*-tosylaldimines 102f and 102i.

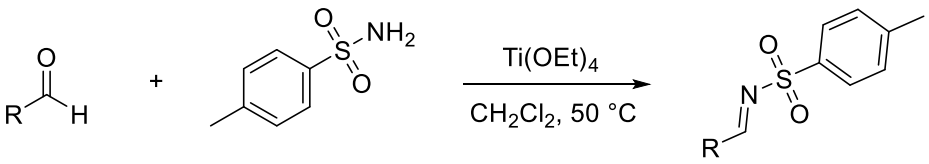

Scheme **S3**. Preparation of starting materials *N*-tosylaldimines **102f** and **102i**.

N-tosylaldimines **102f** and **102i** were prepared readily from the corresponding aldehyde and *p*-toluenesulfonamide according to the literatures.[135] In a 250 mL round-bottom flask was added 5 mmol of $TsNH_2$, aldehyde (5 mmol), and 5.24 mL (25 mmol) of titanium-(IV) ethoxide in 80 mL of dry CH_2Cl_2, the reaction was reflux at 50 °C under

[135] Jiang, B.; Meng, F. F.; Liang, Q. J.; Xu, Y. H.; Loh, T. P. *Org. Lett*. **2017**, *19*, 914-917.

argon atmosphere. The reaction was monitored by TLC, and when the conversion completed, the reaction mixture was quenched at 0 °C by addition of H_2O (40 mL). The turbid solution was filtered through Celite, and the filtered cake was washed with CH_2Cl_2 (2 × 40 mL). The phases were separated, and the aqueous phase was extracted with CH_2Cl_2 (2 × 50 mL). The combined organic portions were dried over anhydrous Na_2SO_4 and concentrated to give the corresponding *N*-tosylaldimine. The crude product was then recrystallized (EtOAc/hexane) for purification.

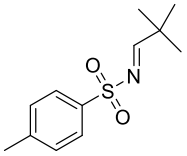

102f

***N*-(2,2-dimethylpropylidene)-4-methylbenzenesulfonamide (102f)**.[135] ^{1}H NMR (300 MHz, $CDCl_3$) δ 8.45 (s, 1H), 7.80 (d, *J* = 8.3 Hz, 2H), 7.33 (d, *J* = 8.0 Hz, 2H), 2.44 (s, 3H), 1.14 (s, 9H).

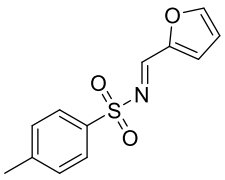

102i

***N*-(furan-2-ylmethylene)-4-methylbenzenesulfonamide (102i)**.[135] ^{1}H NMR (300 MHz, $CDCl_3$) δ 8.81 (s, 1H), 7.87 (d, *J* = 8.3 Hz, 2H), 7.76 – 7.70 (m, 1H), 7.38 – 7.28 (m, 3H), 6.64 (dd, *J* = 3.7, 1.7 Hz, 1H), 2.42 (s, 3H). ^{13}C NMR (75 MHz, $CDCl_3$) δ 155.66, 149.67, 149.18, 144.51, 135.31, 129.77, 128.05, 124.39, 113.66, 21.61.

Procedure for preparation of *p*-tolylsulfonylimine (102j).

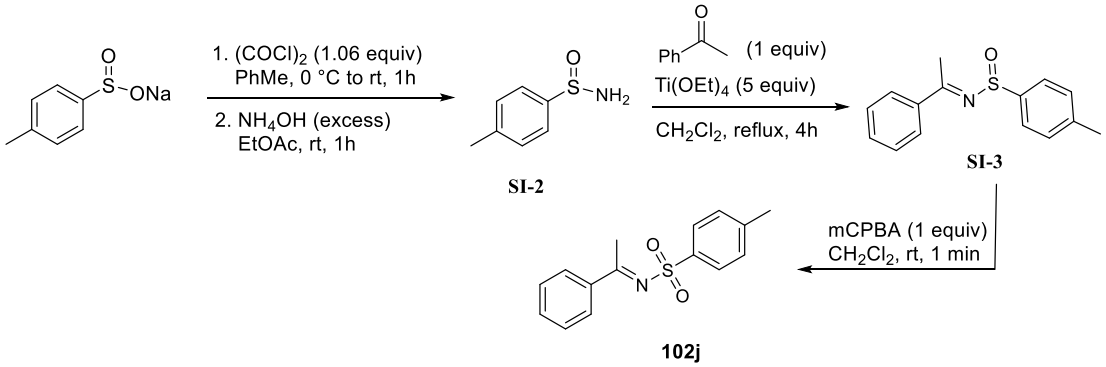

Scheme **S4**. Synthetic route for preparation of starting material **102j**.

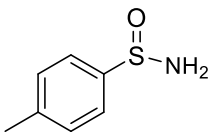

SI-2

***p*-toluenesulfonamide (SI-2)** was prepared according to a reported procedure.[136] To a 250 mL flame-dried round-bottom flask equipped with a stirring bar was added sodium *p*-toluenesulfinate (3.60 g, 20.0 mmol). Anhydrous toluene (50 mL) was added and the solution was set at 0 °C. Oxalyl chloride (1.80 mL, 21.2 mmol) was added dropwise. Then the reaction mixture was warmed to room temperature and let stir for one hour. A biphasic mixture of NH_4OH (20 mL) and EtOAc (30 mL) was added to the reaction mixture, and let stir for one hour open to air. The reaction mixture was diluted with EtOAc (30 mL) and the aqueous layer was extracted with EtOAc (2 x 60 mL). The combined organic layers were washed with brine, dried over Na_2SO_4, and concentrated in vacuo to yield the title compound. The crude product was then recrystallized (EtOAc/hexane) for purification. ^{1}H NMR (300 MHz, $CDCl_3$) δ 7.57 (d, J = 8.2 Hz, 2H), 7.25 (d, J = 8.0 Hz, 2H), 4.63 (s, 2H), 2.37 (s, 3H). ^{13}C NMR (75 MHz, $CDCl_3$) δ 143.57, 141.27, 129.50, 125.42, 21.28.

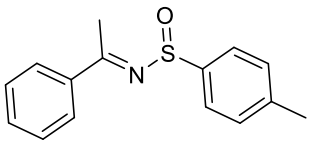

SI-3

***p*-tolylsulfinimine (SI-3)** was prepared according to a reported procedure.[137] In a 250 mL three-neck round-bottom flask equipped with a condenser, septum, argon inlet, and magnetic stirring bar were charged with racemic *p*-toluenesulfonamide **(SI-2)** 800 mg (5.20 mmol), acetophenone (26 mmol) in 100 mL of CH_2Cl_2, and $Ti(OEt)_4$ (20.8 mmol). The solution was heated under reflux at 50 °C and monitored by TLC. When the reaction completed, 10 mL of MeOH and some drops of $NaHCO_3$ were added, until full precipitation of the titanium salts. Then it was filtered through Celite, washed with EtOAc. The organic layer was dried over anhydrous Na_2SO_4, and concentrated to give the crude product, which was purified on silica gel by chromatography (petroleum ether/EtOAc: 10/1) to obtain *p*-tolylsulfinimine (**SI-3**). ^{1}H NMR (300 MHz, $CDCl_3$) δ 7.91 (d, J = 7.1 Hz, 2H), 7.77 (d, J = 8.1 Hz, 2H), 7.54 – 7.39 (m, 3H), 7.35 (d, J = 8.0 Hz, 2H), 2.81 (s, 3H), 2.43 (s, 3H). ^{13}C NMR (75 MHz, $CDCl_3$) δ 173.98, 143.42, 141.81, 138.18, 131.84, 129.83, 128.44, 127.50, 125.22, 21.44, 20.21.

[136] Erickson, L.W.; Lucas, E. L.; Tollefson, E. J.; Jarvo, E. R. *J. Am. Chem. Soc*. **2016**, *138*, 14006–14011.
[137] Garcia Ruano, J. L.; Alemán, J.; Belen Cid, M.; Parra, A. *Org. Lett*. **2005**, 7, 179–182.

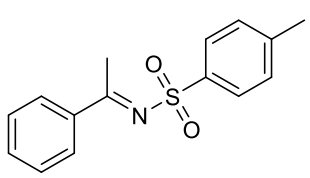

102j

***p*-Tolylsulfonylimine (102j)** was prepared according to a reported procedure.[137] To a solution of the sulfinylimine **SI-3** (1 mmol) in CH_2Cl_2 (10 mL) *m*-CPBA (1 mmol) was added at room temperature in one portion under open air. When the reaction was completed (less than 1 minute), the reaction was diluted with 5 mL of CH_2Cl_2, washed with 3x15 mL of saturated solution of $NaHCO_3$. Finally, the organic layer was dried over anhydrous Na_2SO_4 and the solvent evaporated, obtaining crude *p*-tolylsulfonylimine **102j**. The crude product was then recrystallized (EtOAc/hexane) for purification. ^{1}H NMR (300 MHz, $CDCl_3$) δ 7.99 – 7.86 (m, 4H), 7.59 – 7.48 (m, 1H), 7.47 – 7.30 (m, 4H), 2.99 (s, 3H), 2.45 (s, 3H). ^{13}C NMR (75 MHz, $CDCl_3$) δ 179.79, 143.49, 138.77, 137.63, 133.11, 129.44, 128.60, 128.26, 127.09, 21.56, 21.12.

General procedure for proazaphosphatrane-catalyzed cyanation of imines

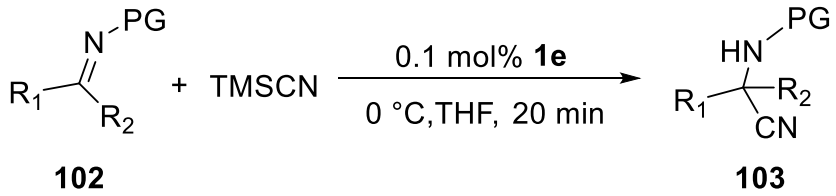

102 **103**

Scheme S5. Cyanation of imines catalyzed by proazaphosphatrane **1e**.

To a solution of proazaphosphatrane (0.1% mmol) and TMSCN (94 μL, 0.75 mmol) in THF (1.5 mL) was added imine (0.5 mmol) under an atmosphere of argon. The mixture was stirred at 0 °C for 20 minutes, upon completion monitored by TLC, 3 mL of H_2O were added and the mixture was stirred for another 30 minutes. The reaction mixture was then extracted with ethyl acetate (3 × 50 mL). The combined organic phase was collected, dried over anhydrous Na_2SO_4, filtered, and concentrated under vacuum. The crude product was purified on silica gel by flash column chromatography using petroleum ether and ethyl acetate (10: 1) as eluent to give products **103a** – **103j**.

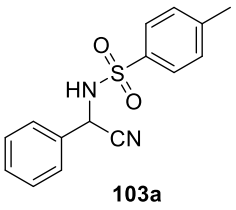

103a

***N*-(cyano(phenyl)methyl)-4-methylbenzenesulfonamide (103a).**[138] Obtained as white solid, 143 mg (quant.). ^{1}H NMR (400 MHz, $CDCl_3$) δ 7.81 (d, *J* = 7.8 Hz, 2H), 7.50 – 7.39 (m, 5H), 7.37 (d, *J* = 7.8 Hz, 2H), 5.48 (s, 1H), 5.12 (s, 1H), 2.46 (s, 3H); ^{13}C NMR (101 MHz, $CDCl_3$) δ 144.7, 136.1, 132.1, 130.1, 129.9, 129.4, 127.3, 127.1, 116.3, 48.2, 21.7. HRMS (ESI-TOF) *m*/*z*: calcd for $C_{15}H_{18}N_3O_2S^+$ $[M+NH_4]^+$, 304.1114; found 304.1112.

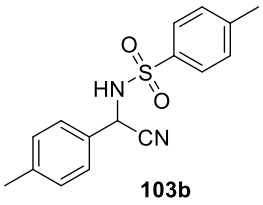

103b

***N*-(cyano(*p*-tolyl)methyl)-4-methylbenzenesulfonamide (103b)**.[138] Obtained as white solid, 151 mg (quant.) ^{1}H NMR (400 MHz, $CDCl_3$) δ 7.82 (d, *J* = 8.3 Hz, 2H), 7.37 (d, *J* = 8.0 Hz, 2H), 7.32 (d, *J* = 8.1 Hz, 2H), 7.21 (d, *J* = 8.0 Hz, 2H), 5.44 (d, *J* = 8.8 Hz, 1H), 4.93 (d, *J* = 8.8 Hz, 1H), 2.46 (s, 3H), 2.36 (s, 3H); ^{13}C NMR (101 MHz, $CDCl_3$) δ 144.68, 140.12, 136.11, 130.05, 129.15, 127.36, 126.99, 116.39, 48.04, 21.66, 21.16. HRMS (ESI-TOF) *m*/*z*: calcd for $C_{16}H_{20}N_3O_2S^+$ $[M+NH_4]^+$, 318.1271; found 318.1272.

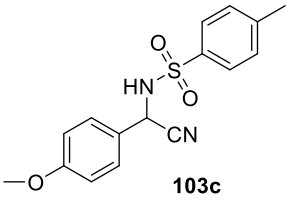

103c

***N*-(cyano(4-methoxyphenyl)methyl)-4-methylbenzenesulfonamide (103c)**.[138] Obtained as white solid, 158 mg (quant.). ^{1}H NMR (400 MHz, $CDCl_3$) δ 7.81 (d, *J* = 7.1 Hz, 2H), 7.46 – 7.28 (m, 4H), 6.90 (d, *J* = 7.4 Hz, 2H), 5.42 (d, *J* = 8.5 Hz, 1H), 5.00 (d, *J* = 8.2 Hz, 1H), 3.81 (s, 3H), 2.46 (s, 3H); ^{13}C NMR (101 MHz, $CDCl_3$) δ 160.72, 144.66, 136.12, 130.04, 128.54, 127.35, 124.03, 116.47, 114.74, 55.44, 47.78, 21.66. HRMS (ESI-TOF) *m*/*z*: calcd for $C_{16}H_{20}N_3O_3S^+$ $[M+NH_4]^+$, 334.1220; found 334.1221.

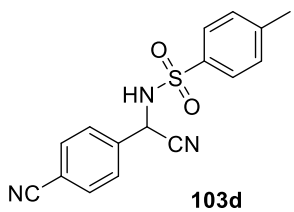

103d

***N*-(cyano(4-cyanophenyl)methyl)-4-methylbenzenesulfonamide (103d)**.[138] Obtained as white solid, 156 mg (quant.). ^{1}H NMR (400 MHz, $CDCl_3$) δ 7.75 (d, *J* = 7.5 Hz, 2H), 7.69 – 7.50 (m, 4H), 7.34 (d, *J* = 7.1 Hz, 2H), 5.95 (d, *J* = 9.3 Hz, 1H), 5.50 (d, *J* = 9.4 Hz, 1H), 2.45 (s, 3H); ^{13}C NMR (101 MHz, $CDCl_3$) δ 145.12, 137.14, 135.65, 133.02, 130.19, 127.95, 127.24, 117.76, 115.47,

[138] Kadam, S. T.; Thirupathi, P.; Kim, S. S. *Synthesis*. **2011**, *6*, 919–923.

113.73, 47.75, 21.69. HRMS (ESI-TOF) *m*/*z*: calcd for $C_{16}H_{13}N_3O_2SNa^+$ $[M+Na]^+$, 334.0621; found 334.0621.

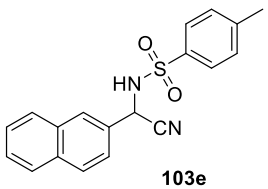

103e

***N*-(cyano(naphthalen-2-yl)methyl)-4-methylbenzenesulfonamide (103e)**.[139] Obtained as white solid, 170 mg (quant.). ^{1}H NMR (400 MHz, $CDCl_3$) δ 7.97 – 7.78 (m, 6H), 7.56 (d, *J* = 4.5 Hz, 2H), 7.47 (d, *J* = 8.7 Hz, 1H), 7.36 (d, *J* = 8.0 Hz, 2H), 5.65 (d, *J* = 8.8 Hz, 1H), 5.12 (d, *J* = 9.1 Hz, 1H), 2.45 (s, 3H); ^{13}C NMR (101 MHz, $CDCl_3$) δ 144.77, 136.08, 133.54, 132.87, 130.08, 129.70, 129.18, 128.24, 127.78, 127.49, 127.37, 127.17, 126.66, 123.91, 116.26, 48.47, 21.66. HRMS (ESI-TOF) *m*/*z*: calcd for $C_{19}H_{20}N_3O_2S^+$ $[M+NH_4]^+$, 354.1271; found 354.1270.

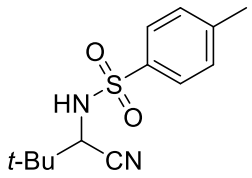

103f

***N*-(1-cyano-2,2-dimethylpropyl)-4-methylbenzenesulfonamide (103f)**.[140] Obtained as white solid, 133 mg (85%). ^{1}H NMR (400 MHz, $CDCl_3$) δ 7.79 (d, *J* = 8.1 Hz, 2H), 7.35 (d, *J* = 7.8 Hz, 2H), 5.68 (d, *J* = 10.2 Hz, 1H), 3.88 (d, *J* = 10.3 Hz, 1H), 2.43 (s, 3H), 1.04 (s, 9H); ^{13}C NMR (101 MHz, $CDCl_3$) δ 144.49, 136.02, 130.04, 127.23, 116.68, 54.69, 35.30, 25.66, 21.63. HRMS (ESI-TOF) *m*/*z*: calcd for $C_{13}H_{22}N_3O_2S^+$ $[M+NH_4]^+$, 284.1427; found 284.1422.

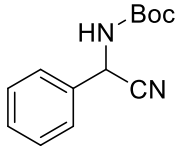

103g

***tert*-butyl (cyano(phenyl)methyl)carbamate (103g)**.[100a] Obtained as white solid, 110 mg (94%). ^{1}H NMR (400 MHz, $CDCl_3$) δ 7.60 – 7.30 (m, 5H), 5.80 (s, 1H), 5.16 (s, 1H), 1.48 (s, 9H); 13C NMR (101 MHz, CDCl3) δ 154.17, 133.49, 129.50, 129.32, 126.89, 117.74, 81.60, 46.13, 28.24. HRMS (ESI-TOF) *m*/*z*: calcd for $C_{13}H_{16}N_2O_2Na^+$ $[M+Na]^+$, 255.1104; found 255.1104.

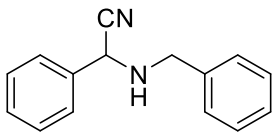

103h

2-(benzylamino)-2-phenylacetonitrile (103h).[140] Obtained as yellow oil, 102 mg (92%). ^{1}H NMR (400 MHz, $CDCl_3$) δ 7.66 – 7.28 (m, 10H), 4.77 (s, 1H), 4.08 (d, *J* = 13.1 Hz, 1H), 3.97 (d, *J* = 13.0 Hz, 1H), 1.89 (s, 1H); 13C NMR (101 MHz, CDCl3)

[139] Wang, J.; Hu, X.; Jiang, J.; Gou, S.; Huang, X.; Liu, X.; Feng, X. *Angew. Chem*. **2007**, *119*, 8620 –8622.
[140] Noor-ul, H. K.; Agrawal, S.; Kureshy, R. I.; Abdi, S. H.; Singh, S.; Suresh, E.; Jasra, R.V. *Tetrahedron Lett*. **2008**, *49*, 640–644

δ 138.17, 134.81, 129.05, 128.99, 128.67, 128.44, 127.67, 127.33, 118.78, 53.49, 51.29. HRMS (ESI-TOF) *m*/*z*: calcd for $C_{15}H_{15}N_2^+$ $[M+H]^+$, 223.1230; found 223.1228.

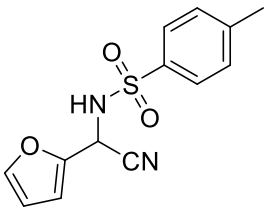

103i

***N*-(cyano(furan-2-yl)methyl)-4-methylbenzenesulfonamide (103i)**.[140] Obtained as colorless solid, 131mg (95%) ^{1}H NMR (400 MHz, $CDCl_3$) δ 7.76 (d, *J* = 8.1 Hz, 2H), 7.39 – 7.35 (m, 1H), 7.32 (d, *J* = 8.1 Hz, 2H), 6.45 (d, *J* = 3.2 Hz, 1H), 6.33 (t, *J* = 2.5 Hz, 1H), 5.71 (d, *J* = 8.9 Hz, 1H), 5.52 (d, *J* = 9.0 Hz, 1H), 2.43 (s, 3H). ^{13}C NMR (75 MHz, $CDCl_3$) δ 144.63, 144.43, 144.14, 136.09, 129.97, 127.25, 114.68, 110.97, 110.36, 42.26, 21.60. HRMS (ESI-TOF) *m*/*z*: calcd for $C_{13}H_{16}N_3O_3S^+$ $[M+NH_4]^+$, 294.0907; found 294.0907.

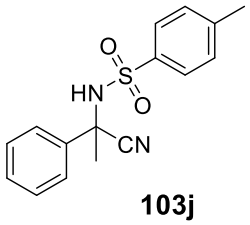

103j

***N*-(1-cyano-1-phenylethyl)-4-methylbenzenesulfonamide (103j)**.[141] Obtained as colorless solid, 139mg (93%) ^{1}H NMR (400 MHz, $CDCl_3$) δ 7.61 (d, *J* = 8.0 Hz, 2H), 7.48 (d, *J* = 7.2 Hz, 2H), 7.38 – 7.28 (m, 3H), 7.26 – 7.18 (m, 2H), 5.40 (s, 1H), 2.42 (s, 3H), 1.94 (s, 3H). ^{13}C NMR (75 MHz, $CDCl_3$) δ 144.05, 137.38, 137.19, 129.56, 129.24, 128.90, 127.47, 125.58, 118.94, 56.62, 30.17, 21.55. HRMS (ESI-TOF) *m*/*z*: calcd for $C_{16}H_{20}N_3O_2S^+$ $[M+NH_4]^+$, 318.1271; found 318.1271.

[141] Huang, X.; Huang, J.; Wen, Y.; Feng, X. *Adv. Synth. Catal*. **2006**, *348*, 2579-2584.

Procedure for preparation of proazaphosphatrane 74

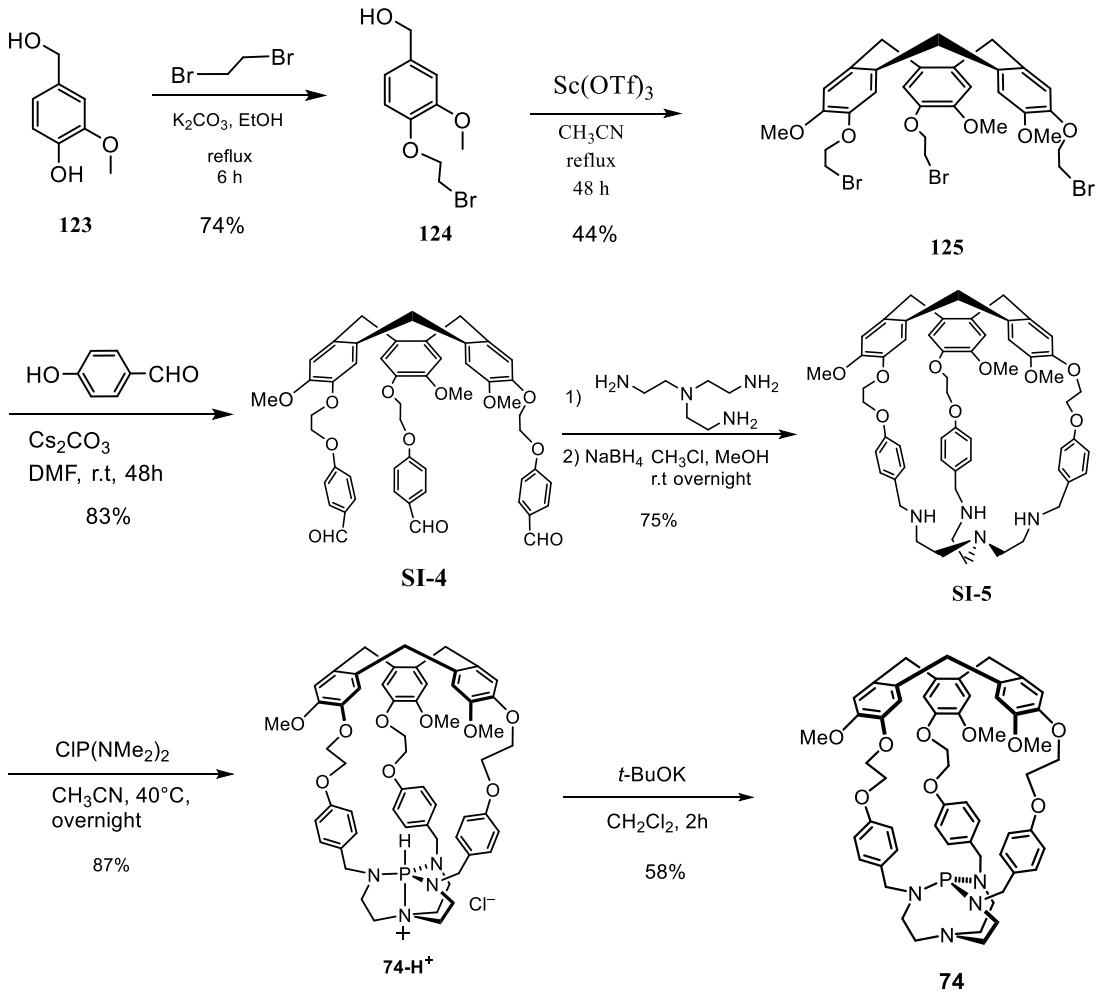

Scheme **S6**. Synthetic route for preparation of proazaphosphatrane **74**.

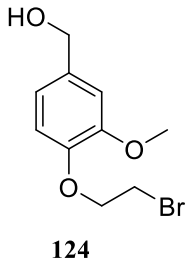

124

(4-(2-bromoethoxy)-3-methoxyphenyl)methanol (**124**) was prepared according to a known procedure.[142] To a flame-dried 1000 mL round-bottomed flask was added vanillyl alcohol (45.0 g), 1,2-dibromoethane (100.0 mL), potassium (45.0 g) and ethanol (200 mL) as solvent. The mixture was stirred and refluxed for 6 h. When the reaction finished, and cooled to room temperature, the volatile solvent was evaporated, then 300 mL of EtOAc and 200 mL of deionized water were added and stirred overnight. The mixture was filtered and was washed by EtOAc (100 mL) and water (100 mL), the liquid phase was collected and extracted by EtOAc (3 × 100 mL).

[142] Raytchev, P. D.; Perraud, O.; Aronica, C.; Martinez, A.; Dutasta, J. P. *J. Org. Chem.*, **2010**, *75*, 2099–2102.

The combined organic phases were gathered and dried over anhydrous Na_2SO_4, filtered, and concentrated under vacuum to give crude product as yellow oil, to which was added diisopropyl ether (300 mL). Two layers appeared, the heavier oil stayed at the bottom. The upper colorless phase was transferred carefully to another 500 mL flask, and concentrated to give pure product **124** as white solid (56.4 g, 74%). **^{1}H NMR** (300 MHz, $CDCl_3$) δ 6.94 (s, 1H), 6.91 – 6.83 (m, 2H), 4.61 (s, 2H), 4.31 (t, *J* = 6.7 Hz, 2H), 3.87 (s, 3H), 3.64 (t, *J* = 6.7 Hz, 2H); **^{13}C NMR** (75 MHz, $CDCl_3$) δ 150.09, 146.99, 135.29, 119.40, 115.07, 111.39, 69.50, 65.12, 56.03, 28.90. These data are consistent with literature.[142]

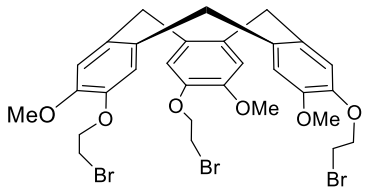

125

Cyclotriveratrylene (CTV) **125** was prepared following a reported literature.[223] To a flame-dried 250 mL round-bottom flask was added **124** (10.0 g), $Sc(OTf)_3$ (0.8 g) and CH_3CN (100 mL), the reaction mixture was refluxed at 95 °C for 48 h. When reaction completed, solvent was evaporated, the remaining mixture was added H_2O (100 mL), and extracted by CH_2Cl_2 (3 × 100 mL), The combined organic phases were collected, dried over anhydrous Na_2SO_4, filtered, and concentrated under vacuum to give crude product, which was purified on silica gel by flash chromatography (pure CH_2Cl_2) to give the title compound **125** as a white solid (4.2 g, 44%). **^{1}H NMR** (300 MHz, $CDCl_3$) δ 6.93 (s, 3H), 6.85 (s, 3H), 4.73 (d, *J* = 13.7 Hz, 3H), 4.29 (t, *J* = 6.7 Hz, 6H), 3.85 (s, 9H), 3.62 – 3.50 (m, 9H); **^{13}C NMR** (75 MHz, $CDCl_3$) δ 149.04, 145.98, 133.86, 131.83, 117.95, 113.99, 69.97, 56.25, 36.40, 29.19. These data are consistent with literature.[142]

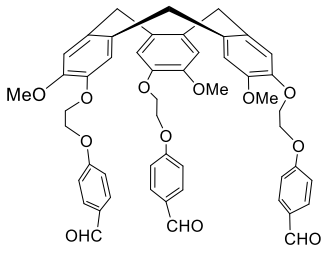

SI-4

Compound **SI-4** was prepared following a reported procedure.[121] To a flame-dried 100 mL round-bottomed flask was added **125** (730 mg, 1.0 mmol, 1.0 equiv), 4-hydroxybenzaldehyde (366 mg, 3.0 mmol, 3.0 equiv), cesium carbonate (1.3 g, 4.0 mmol, 4.0 equiv) and DMF (40 mL), the reaction mixture was stirred for 48 h at room temperature. When reaction completed, the solvent was evaporated, 50 mL of H_2O was added, the mixture was extracted by EtOAc (3 × 50 mL). The combined organic phases were collected, dried over anhydrous Na_2SO_4, filtered, and concentrated under vacuum to give crude product, which was purified by recrystallization (EtOAc and petroleum

ether) to give the title compound **SI-4** as a light yellow solid (710 mg, 83%). **^{1}H NMR** (400 MHz, $CDCl_3$) δ 9.95 (s, 3H), 7.87 (d, *J* = 8.6 Hz, 6H), 7.05-6.96 (m, 9H), 6.89 (s, 3H), 4.82 (d, *J* = 13.9 Hz, 3H), 4.34–4.45 (m, 12H), 3.84 (s, 9H), 3.62 (d, *J* = 13.9 Hz, 3H); **^{13}C NMR** (101 MH, $CDCl_3$) δ 190.5, 163.4, 148.8, 146.2, 133.9, 132.1, 131.4, 130.6, 117.3, 113.2, 114.5, 68.2, 67.7, 56.3, 36.8. These data are consistent with literature.[121]

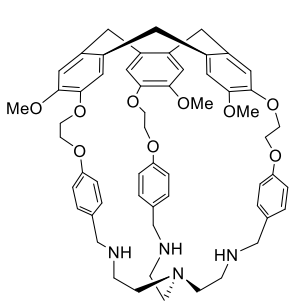

SI-5

Hemicryptophane **SI-5** was prepared following a reported procedure.[121] To a flame-dried 1000 mL round-bottom flask equipped with a constant pressure funnel was added **SI-4** (853 mg, 1.0 mmol, 1.0 equiv), MeOH (250 mL) and $CHCl_3$ (250 mL), and a solution of tris(2-aminoethyl)amine (tren) (146 mg, 1.0 mmol, 1.0 equiv) in MeOH (100 mL) $CHCl_3$ (100 mL) was added drop-wise. The reaction was stirred overnight at room temperature, and then was cooled by an ice bath followed by addition of $NaBH_4$ (1.14 g, 30 mmol, 30 equiv). The reaction was stirred for 2h and then solvent was evaporated. The remaining mixture was added 100 mL of H_2O and extracted by $CHCl_3$ (3 ×100 mL), The combined organic phases were collected, dried over anhydrous Na_2SO_4, filtered, and concentrated under vacuum to give crude product, which was purified on silica gel by flash chromatography (CH_2Cl_2/MeOH/Et_3N; 90/10/2) to give the title compound **SI-5** as a white solid (713 mg, 75%). **^{1}H NMR** (400 MHz, $CDCl_3$) δ 7.02 (s, 3H), 6.78 (s, 3H), 6.75 (d, *J* = 8.3 Hz, 6H), 6.38 (d, *J* = 8.3 Hz, 6H), 4.72 (d, *J* = 13.7 Hz, 3H), 4.52 – 4.38 (m, 3H), 4.35 – 4.26 (m, 3H), 4.18 – 4.06 (m, 6H), 3.58 (s, 9H), 3.52 (d, *J* = 13.7 Hz, 3H), 3.42 (d, *J* = 13.5 Hz, 3H), 3.34 (d, *J* = 13.5 Hz, 3H), 2.41–2.32 (m, 12H); **^{13}C NMR** (101 MH, $CDCl_3$) δ 157.8, 148.9, 146.4, 133.6, 132.2, 132.4, 128.7, 116.8, 115.2, 114.1, 68.4, 67.5, 56.3, 55.7, 52.2, 47.7, 36.8. These data are consistent with literature.[121]

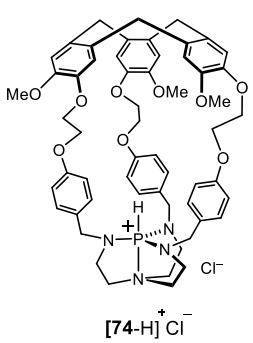

[74-H]$^{+}$ Cl^{-}

Azaphosphatrane **[74**·H]$^{+}$Cl^{-} was prepared following a reported procedure with modification.[55] In an ice-bath cooled round-bottom flask, bis(dimethylamino)chlorophosphine (0.154 mL, 1.0 mmol, 1.0 equiv) was dissolved in acetonitrile (6 mL), which was then added a solution of hemicryptophane (952 mg, 1 mmol, 1.0 equiv) in acetonitrile (15 mL) drop-wise. The reaction mixture was vigorously stirred at 0°C for 0.5 h. The mixture was then heated to 40 °C overnight. The solvent was then removed under vacuum and the residue was eluted on silica gel by a flash chromatography (CH_2Cl_2/MeOH; 15/2) to give pure azaphosphatrane [**74**·H]$^{+}$Cl^{-} as a white solid (884 mg, 87%). **^{1}H NMR** (400 MHz, $CDCl_3$) δ 7.32 (s, 3H), 6.97 (s, 3H), 6.15 (d, J = 8.27 Hz, 6H), 6.01 (d, J = 8.27 Hz), 4.82-4.93 (m, 3H), 4.89 (d, J = 13.6 Hz, 3H), 4.45 (d, $^{1}J_{P\text{-}H}$ = 491 Hz, 1H, P-H), 4.42-4.19 (m, 9H), 3.87-3.74 (m, 3H), 3.64 (d, J = 13.5 Hz, 3H), 3.57 (s, 9H), 3.36 – 3.47 (m, 3H), 3.31-3.17 (m, 9H), 2.68 - 2.76 (m, 3H); **^{13}C NMR** (400 MHz, $CDCl_3$) δ 158.27, 147.20, 146.45, 132.03, 131.71, 131.31, 129.01, 114.95, 114.61, 112.74, 70.23, 65.65, 55.12, 50.38, 47.63, 42.54, 36.80; **^{31}P NMR** (121 MHz, $CDCl_3$) δ -31.98. These data are consistent with literature.[55]

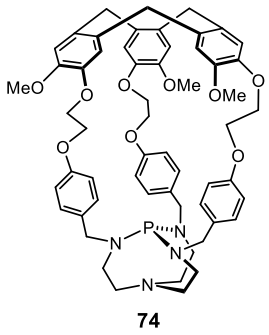

74

Proazaphosphatrane **74** was prepared according to a known procedure.[55] Under an atmosphere of argon, in a flame-dried Schlenk flask, azaphosphatrane (350 mg, 0.35 mmol, 1.0 equiv) was dissolved in dried CH_2Cl_2 (2 mL), *t*-BuOK (98 mg, 0.875 mmol, 2.5 equiv) was added, and the reaction mixture was stirred at room temperature for 2 h. Then the solvent was removed under vacuum, and toluene (5 mL) was added. The reaction mixture was stirred for another 0.5 h, and then the suspension was filtered under argon through a two-necked fritted glass funnel, thus the filtrate was transferred to another Schlenk tube and the solvent was removed under vacuum to give pure proazaphosphatrane **74** as a white solid (200 mg, 58%). **^{1}H NMR** (300 MHz, Toluene-d_8) δ 7.31 (s, 3H), 7.04 (d, J = 6.6 Hz, 6H), 6.91 (s, 3H), 6.73 (d, J = 8.5 Hz, 6H), 4.80 (d, J = 13.6 Hz, 3H), 4.27 – 4.11 (m, 12H), 4.10 – 3.93 (m, 6H), 3.84 – 3.71 (m, 3H), 3.69 (s, 9H), 3.60 (d, J = 13.2 Hz, 3H), 3.15 – 2.99 (m, 3H), 2.99 – 2.90 (m, 6H), 2.88 – 2.74 (m, 3H); **^{31}P NMR** (121 MHz, Toluene-d_8) δ 121.29; **^{13}C NMR** (400 MHz, $CDCl_3$) δ 157.35, 149.68, 147.27, 134.13, 133.57, 132.03, 128.56, 118.57, 115.13,

114.82, 68.78, 67.26, 54.83, 54.41, 52.42, 48.83, 36.15. These data are consistent with literature.[55]

Procedure for preparation of enantiopure *M*-74/*P*-74

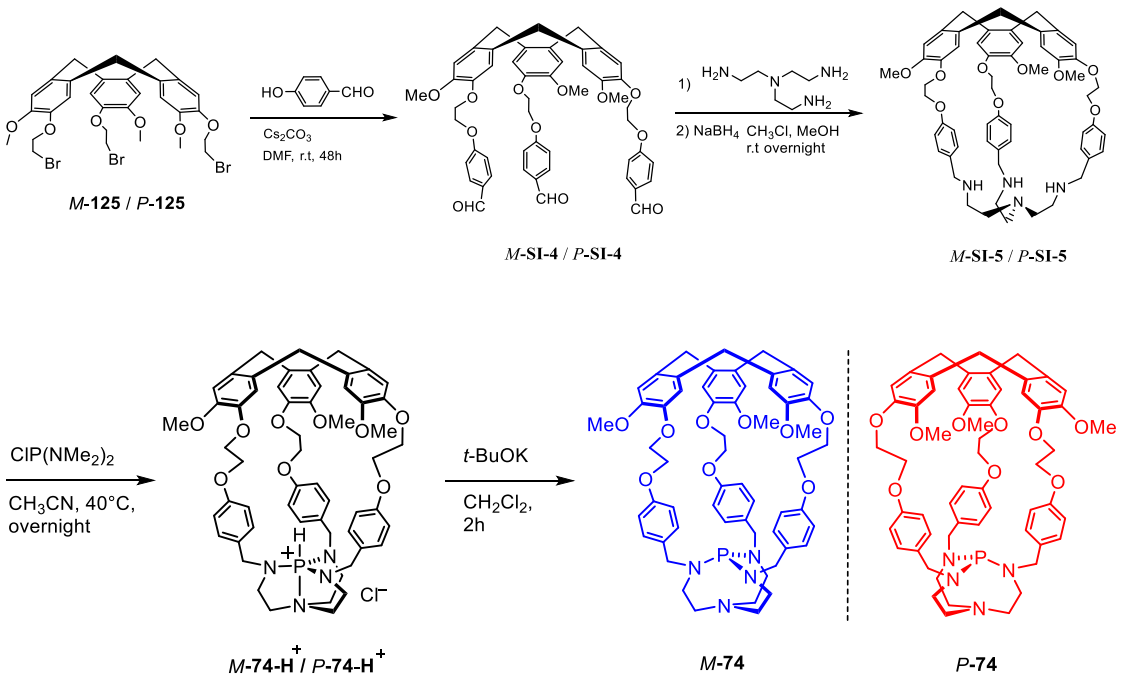

Scheme S7. Synthetic route for preparation of enantiopure *M*-**74**/*P*-**74**.

The procedure for preparation of enantiopure *M*-**74**/*P*-**74** is similar to that of preparation of racemic **74** as described before, just using enantiopure CTV *M*-**125**/*P*-**125** instead of racemic **125**. The spectra data are exact the same as their racemic ones.

General procedure for MBH reaction of cycloenones with aldehydes.

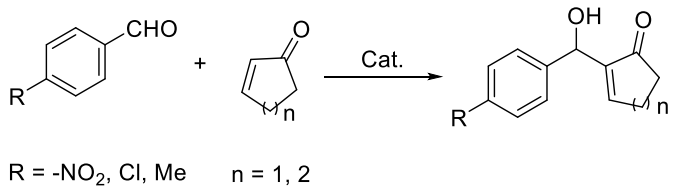

Scheme S8. The MBH reaction of cycloenones with aldehydes in the presence of different catalytic system.

In an oven-dried 5 mL Schlenk tube was introduced a solution of aldehyde (0.3 mmol, 1.0 equiv.), enone (0.9 mmol, 3.0 equiv.), and catalyst (0.03 mmol, 0.1 equiv.) in anhydrous dichloromethane (DCM) (1.0 mL), which was followed by addition of $TiCl_4$ solution in DCM (1 M) (0.3 mmol, 1.0 equiv.) under an argon atmosphere at room temperature. The mixture was stirred for 30 min and then it was quenched with saturated aqueous $NaHCO_3$ solution (3.0 mL), and kept stirring for 30 min. Then, the inorganic precipitate was filtered through Celite. The organic phase was dried over Na_2SO_4, filtered and evaporated under vacuum to give the crude products, which were isolated on silica gel by flash column chromatography using petroleum ether and ethyl acetate (8: 1) as eluent to give products **117a** –**117f**.[143]

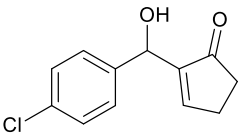

117a

2-((4-chlorophenyl)(hydroxy)methyl)cyclopent-2-en-1-one (117a): ^{1}H NMR (400 MHz, $CDCl_3$) δ 7.23 (s, 4H), 7.22-7.19 (m, 1H), 5.43 (s, 1H), 3.62 (s, 1H), 2.53-2.49 (m, 2H), 2.37-2.34 (m, 2H); ^{13}C NMR (101 MHz, $CDCl_3$) δ 209.46, 159.50, 147.46, 139.92, 133.52, 128.60, 127.75, 69.09, 35.22, 26.70. HRMS (ESI-TOF) *m/z* Calcd for $C_{12}H_{11}ClO_2Na^+$ $[M+Na]^+$ 245.0340, found 245.0342. These data are consistent with literature.[143]

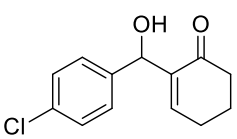

117b

2-((4-chlorophenyl)(hydroxy)methyl)cyclohex-2-en-1-one (117b): ^{1}H NMR (300 MHz, $CDCl_3$) δ 7.27 (s, 4H), 6.81-6.68 (m, 1H), 5.49 (s, 1H), 3.55 (s, br 1H), 2.51-2.30 (m, 4H), 2.01-1,92 (m,

[143] Shi, M., Xu, Y.M., Zhao, G.L. and Wu, X.F. *Eur. J. Org. Chem*. **2002**, *21*, 3666-3679.

2H); ^{13}C NMR (75 MHz, $CDCl_3$) δ 200.14, 147.35, 140.82, 140.42, 133.14, 128.40, 127.84, 71.72, 38.49, 25.74, 22.46. HRMS (ESI-TOF) *m/z* Calcd for $C_{13}H_{13}ClO_2Na^+$ $[M+Na]^+$ 259.0496, found 259.0496. These data are consistent with literature.[143]

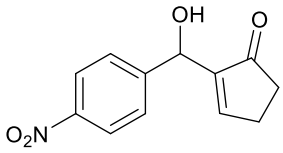

117c

2-(hydroxy(4-nitrophenyl)methyl)cyclopent-2-en-1-one (117c): ^{1}H NMR (300 MHz, $CDCl_3$) δ 8.19 (d, *J* = 8.8 Hz, 2H), 7.57 (d, *J* = 8.6 Hz, 2H), 7.29-7.31 (m, 1H), 5.66 (d, *J* = 2.9 Hz, 1H), 3.65 (d, *J* = 4.4 Hz, 1H), 2.60-2.65 (m, 2H), 2.49 – 2.45 (m, 2H); ^{13}C NMR (75 MHz, $CDCl_3$) δ 209.16, 159.71, 148.51, 147.51, 146.71, 127.08, 123.70, 69.02, 35.13, 26.82. HRMS (ESI-TOF) *m/z* Calcd for $C_{12}H_{11}NO_4Na^+$ $[M+Na]^+$ 256.0580, found 256.0580. These data are consistent with literature.[143]

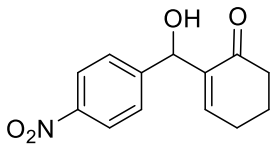

117d

4-(hydroxy(6-oxocyclohex-1-en-1-yl)methyl)phenyl nitrate (117d): ^{1}H NMR (300 MHz, $CDCl_3$) δ 8.19-8.04 (m, 2H), 7.58-7.43 (m, 2H), 6.89-6.79 (m, 1H), 5.58 (d, *J* = 5.3 Hz, 1H), 3.70 (d, *J* = 5.6 Hz, 1H), 2.43-2.37 (m, 4H), 2.01-1.92 (m, 2H); ^{13}C NMR (75 MHz, $CDCl_3$) δ 199.87, 149.61, 148.12, 147.16, 140.27, 127.15, 123.43, 71.53, 38.38, 25.78, 22.37. HRMS (ESI-TOF) *m/z* Calcd for $C_{13}H_{13}NO_4Na^+$ $[M+Na]^+$ 270.0737, found 270.0734. These data are consistent with literature.[143]

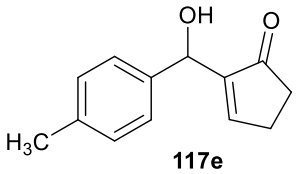

117e

2-(hydroxy(p-tolyl)methyl)cyclopent-2-en-1-one (117e): ^{1}H NMR (300 MHz, $CDCl_3$) δ 7.36-7.34 (m, 1H), 7.27 (d, *J* = 8.1 Hz, 2H), 7.15 (d, *J* = 8.0 Hz, 2H), 5.50 (s, 1H), 3.82 (s, br 1H), 2.59-2.55 (m, 2H), 2.42-2.39 (m, 2H), 2.35 (s, 3H); ^{13}C NMR (75 MHz, $CDCl_3$) δ 209.35, 159.23, 148.09, 138.73, 137.33, 129.08, 126.32, 69.37, 35.25, 26.62, 21.12. HRMS (ESI-TOF) *m/z* Calcd for $C_{13}H_{14}O_2Na^+$ $[M+Na]^+$ 225.0886, found 225.0887. These data are consistent with literature.[143]

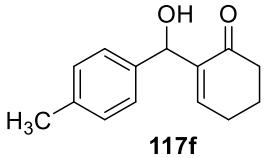

117f

2-(hydroxy(p-tolyl)methyl)cyclohex-2-en-1-one (117f): ^{1}H NMR (300 MHz, $CDCl_3$) δ 7.27 (d, *J* = 8.1 Hz, 2H), 7.18 (d, *J* = 8.0 Hz, 2H), 6.79 (t, *J* = 4.1 Hz, 1H), 5.56 (s, 1H), 3.64 (s, br 1H), 2.52 – 2.38 (m, 4H), 2.37 (s, 3H), 2.12 – 1.93 (m, 2H); ^{13}C NMR (75 MHz, $CDCl_3$) δ 200.32, 147.06, 141.18, 138.79, 137.08, 128.98, 126.39, 72.34, 38.59, 25.75, 22.53, 21.09. HRMS (ESI-TOF) *m/z* Calcd for $C_{14}H_{16}O_2Na^+$

[M+Na]$^+$ 239.1043, found 239.1041. These data are consistent with literature.[143]

Synthesis of 6,6-diphenyl-2-cyclohexen-1-one 118

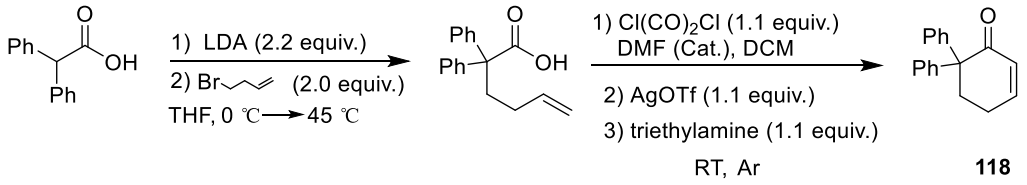

Scheme S9. Synthetic route for preparation of 6,6-diphenyl-2-cyclohexen-1-one **118**

The synthesis of **118** referred to a described procedure and was obtained as a white solid (610 mg, 87%).[144] ^{1}H NMR (300 MHz, $CDCl_3$) δ 7.39 – 7.25 (m, 6H), 7.23 – 7.04 (m, 4H), 6.82 (dt, *J* = 10.0, 4.1 Hz, 1H), 6.22 (dt, *J* = 10.0, 2.2 Hz, 1H), 2.77 (t, *J* = 5.7 Hz, 2H), 2.33 (dq, *J* = 7.8, 3.6, 2.9 Hz, 2H). These data are consistent with those described in the literature.[144]

Stoichiometric reactions of superbase 1e and 74 with $TiCl_4$.

To a solution of superbase (0.1 mmol) in dry DCM (2 mL) was added dropwise one equivalent of $TiCl_4$ (0.1 mmol) under an argon atmosphere. The reaction mixture was stirred at room temperature for 20 minutes. Then, the solvent was removed under vacuum. The residue was directly analyzed by NMR and mass spectroscopy.

[144] Barczak, N. T.; Jarvo, E. R. *Chem. Eur. J.* **2011**, *17*, 12912-12916.

Synthesis of 111.

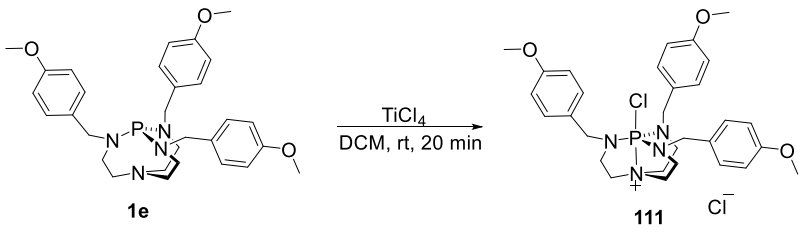

Scheme S10. Synthesis of chlorinated azaphosphatrane **111**.

To a solution of superbase **1e** (0.5 mmol, 267 mg) in dry DCM (5 mL) was added dropwise one equivalent of $TiCl_4$ (0.5 mmol, 55 μL) under argon atmosphere. The reaction mixture was stirred at room temperature for 20 minutes which was then quenched with saturated aqueous $NaHCO_3$ (6.0 mL). The inorganic precipitate was filtered through Celite. The solution was extracted by DCM (3 × 20 mL), combiend organic phases were collected and dried over anhydrous Na_2SO_4 and concentrated under vacuum to give the crude product, which was purified on silica gel by column chromatography on silica gel (DCM/methanol 20:1). **111** was isolated as white solid,yield 139 mg (23%). ^{1}H NMR (400 MHz, $CDCl_3$) δ 7.21 (d, J = 8.2 Hz, 6H), 6.85 (d, J = 8.7 Hz, 6H), 4.59 (d, J = 14.6 Hz, 6H), 3.80 (s, 9H), 3.53 (q, J = 6.0 Hz, 6H), 3.24 (dt, J = 13.1, 6.7 Hz, 6H); ^{31}P NMR (162 MHz, $CDCl_3$) δ -22.98; ^{13}C NMR (101 MHz, $CDCl_3$) δ 159.40, 129.16, 128.64 (d, J = 4.6 Hz), 114.23, 55.33, 54.82 (d, J = 4.0 Hz), 44.26 (d, J = 9.6 Hz), 43.82 (d, J = 9.4 Hz). HRMS (ESI-TOF) m/z Calcd for $C_{30}H_{39}ClN_4O_3P^+$ $[M\text{-}Cl]^+$ 569.2443, found 569.2443.

Reaction of 6,6-diphenyl-2-cyclohexen-1-one with *p*-chlorobenzaldehyde.

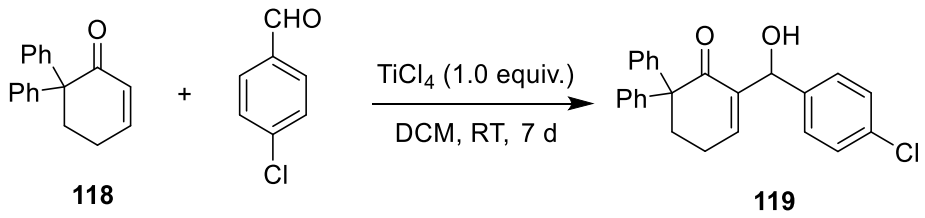

Scheme S11. Reaction of 6,6-diphenyl-2-cyclohexen-1-one with *p*-chlorobenzaldehyde in the presence of $TiCl_4$.

To a solution of 6,6-diphenyl-2-cyclohexen-1-one **118** (372 mg, 1.5 mmol, 3.0 equiv.) and *p*-chlorobenzaldehyde (70 mg, 0.5 mmol, 1.0 equiv.), was added $TiCl_4$ (50 µL, 0.5 mmol, 1.0 equiv.) in freshly distilled DCM (2 mL) under argon atmosphere at room temperature. The reaction was allowed to stir for 7 days, and then quenched by saturated $NaHCO_3$ solution (5 mL). Then, the inorganic precipitate was filtered through Celite. The organic phase was extracted by DCM (3×100 mL), collected and dried over Na_2SO_4, filtered and evaporated under vacuum to give the crude product, which was then purified on silica gel by flash chromatography on silica gel (Rf: 0.10, (5:1 Petroleum Ether / AcOEt)), to afford final MBH product **119** as a white solid: 10 mg, 5%. **^{1}H NMR** ($CDCl_3$, 400 MHz) δ 7.32 – 7.26 (m, 4H), 7.24 (m, 6H), 7.03 – 6.83 (m, 4H), 6.76 – 6.62 (m, 1H), 5.58 (d, *J* = 5.7 Hz, 1H), 3.46 (d, *J* = 6.0 Hz, 1H), 2.79 (t, *J* = 5.7 Hz, 2H), 2.46 – 2.27 (m, 2H).; **^{13}C NMR** ($CDCl_3$, 101 MHz) δ 201.18, 145.53, 141.03, 140.98, 140.70, 140.06, 133.21, 128.32, 128.31, 128.26, 128.13, 128.00, 127.05, 72.95, 59.32, 34.43, 24.06; IR (thin film, cm^{-1}) 3456, 3058, 3030, 2926, 1665, 1491, 1445, 1225; HRMS (ESI-TOF) m/z Calcd for $C_{25}H_{21}O_2ClNH_4$ $(M+NH_4)^+$ 406.1568, found 406.1568.

Procedure for preparation of enantiopure hemicryptophanes *M*-*S*,*S*,*S*-127/*P*-*R*,*R*,*R*-127, *P*-*S*,*S*,*S*-127/*M*-*R*,*R*,*R*-127.

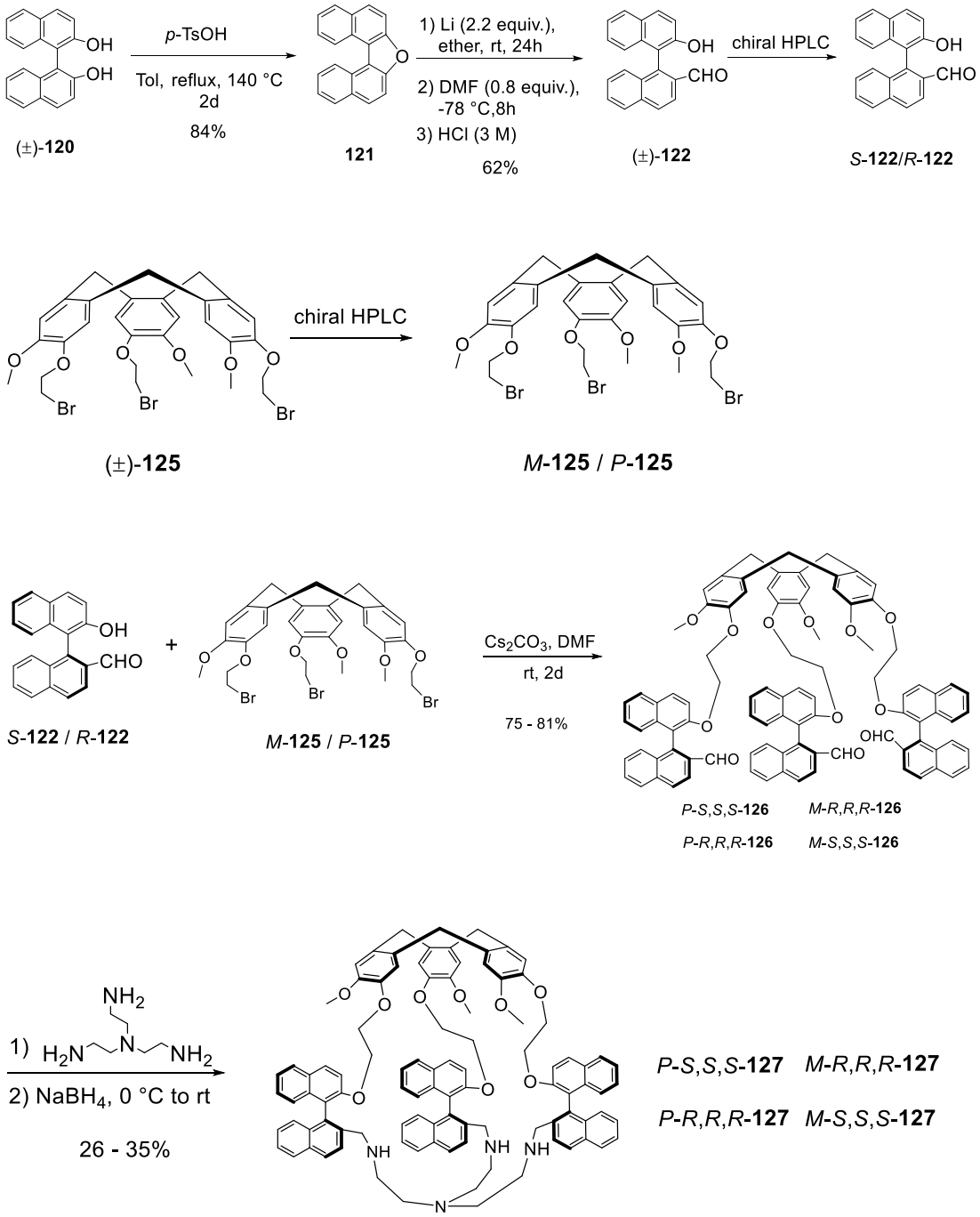

Scheme S12. Synthetic route for preparation of enantiopure hemicryptophanes *M*-*S*,*S*,*S*-**127**/*P*-*R*,*R*,*R*-**127**, *P*-*S*,*S*,*S*-**127**/*M*-*R*,*R*,*R*-**127**.

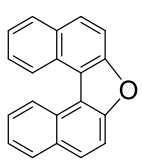

121

Dinaphthofuran **121** was prepared following a reported procedure.[145] To a flame-dried round bottom 500 mL flask was added 1,1'-binaphthol (BINOL) (5.7 g, 20 mmol, 1.0 equiv), *p*-TsOH (3.4 g, 20 mmol, 1.0 equiv) and toluene (250 mL). The reaction was refluxed at 140 °C for two days. When the reaction completed, solvent was removed to give crude product which was purified on silica gel by flash column chromatography (petroleum ether 100%) to afford pure product **121** as a white solid (4.5 g, 84%). **^{1}H NMR** (300 MHz, $CDCl_3$) δ 9.17 (d, *J* = 8.5 Hz, 2H), 8.08 (d, *J* = 7.9 Hz, 2H), 7.96 (d, *J* = 8.9 Hz, 2H), 7.84 (d, *J* = 8.9 Hz, 2H), 7.79 – 7.72 (m, 2H), 7.65 – 7.54 (m, 2H). **^{13}C NMR** (75 MHz, $CDCl_3$) δ 154.37, 131.25, 129.48, 128.65, 128.32, 126.18, 125.63, 124.39, 119.44, 112.72. These data are consistent with those described in the literature.[145]

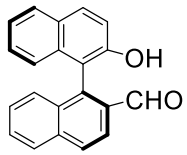

***R*-122**

R*-122** was prepared according to a reported procedure with modification.[146] To a flame-dried round bottom 250 mL flask was added dinaphthofuran **121** (1.34 g, 5 mmol, 1.0 equiv), Li pieces (0.80 g, 11 mmol, 2.2 equiv), dry Et_2O (50 mL), and dry toluene (15 mL). The reaction mixture was stirred for 24 h at room temperature. Then the reaction was allowed to -78 °C, and DMF (0.3 g, 4 mmol, 0.8 equiv) was added. The reaction mixture was stirred at this temperature for 2 h, and then allowed to warm up to room temperature and stirred overnight. HCl (30 mL, 3mol/L) was added at 0 °C to the reaction mixture. The organic phase was collected and washed with HCl (3 mol/L, 3 × 20 mL), dried over anhydrous Na_2SO_4, filtered and concentrated to give crude product which was purified on silica gel by flash chromatography (EtOAc/petroleum ether, 1/10) to afford pure racemic **122** as a white solid (0.92 g, 62%). Enantiopure ***R*-122**/S*-122** were obtained after chiral HPLC. NMR data for ***R*-122**: **^{1}H NMR** (300 MHz, $CDCl_3$) δ 9.65 (s, 1H), 8.16 (d, *J* = 8.6 Hz, 1H), 8.05 (d, *J* = 8.6 Hz, 1H), 7.97 (d, *J* = 8.7 Hz, 2H), 7.90 (d, *J* = 8.1 Hz, 1H), 7.68 – 7.57 (m, 1H), 7.46 (d, *J* = 8.3 Hz, 1H), 7.42 – 7.30 (m, 3H), 7.29 – 7.21 (m, 1H), 6.95 (d, *J* = 8.4 Hz, 1H), 5.16 (s, 1H). **^{13}C NMR** (75 MHz, $CDCl_3$) δ 192.39, 151.79, 139.05, 136.71, 134.52, 133.19, 132.66, 130.99, 129.65, 129.44, 128.83, 128.57, 128.20, 127.66, 127.38, 126.86, 124.66, 123.89, 122.63, 117.55, 113.69. These data are consistent with those described in the

[145] Shuklov, I. A.; Dubrovina, N. V.; Jiao, H.; Spannenberg, A.; Börner, A. *Eur. J. Org. Chem*. **2010**, *9*, 1669-1680.
[146] Xie, X.; Ding, L.; Ni, G.; Zhang, Z.; Gao, J. *Chin. J. Chem*. **2010**, *28*, 1630-1634.

literature.[146] $[\alpha]_D^{25}$ for ***R*-122**: −23 (CH_2Cl_2, c = 0.18), $[\alpha]_D^{25}$ for ***S*-122**: +22 (CH_2Cl_2, c = 0.20).

The ^1H and ^{13}C NMR spectra of ***S*-122** are exactly the same as that of ***R*-122**, as they are enantiomers.

Analytical chiral HPLC separation for compound 122

The sample is dissolved in dichloromethane, injected on the chiral column, and detected with an UV detector at 254 nm, and a circular dichroism detector at 254 nm.

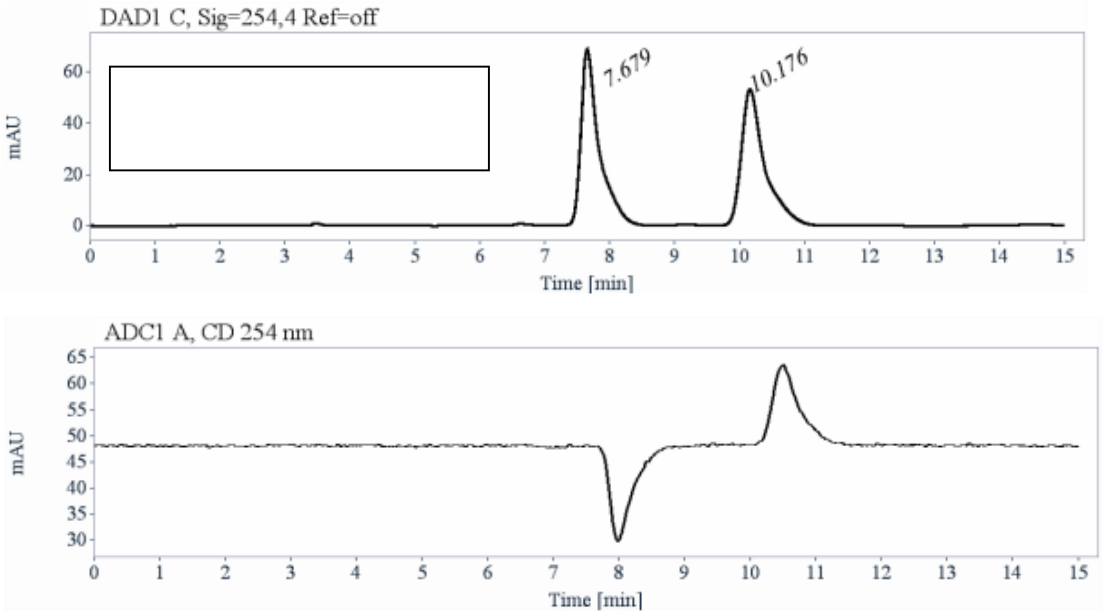

Figure S1. Analytical chiral HPLC analysis for racemic **122**: UV and CD spectra recorded in CH_2Cl_2.

Semi-preparative separation for compound 122:

• Sample preparation: About 810 mg of compound **122** are dissolved in 8 mL of a mixture of hexane / iPrOH / dichloromethane (38/2/60).

• Chromatographic conditions: Chiralpak IC (250 x 10 mm), hexane / iPrOH / dichloromethane (85/5/10) as mobile phase, flow-rate = 5 mL/min, UV detection at 280 nm.

• Injections (stacked): 80 times 100 µL, every 13.4 minutes.

• First fraction: 337 mg of the first major eluted enantiomer with ee > 99.5%.

• Second fraction: 341.7 mg of the second major eluted enantiomer with ee > 99.5%.

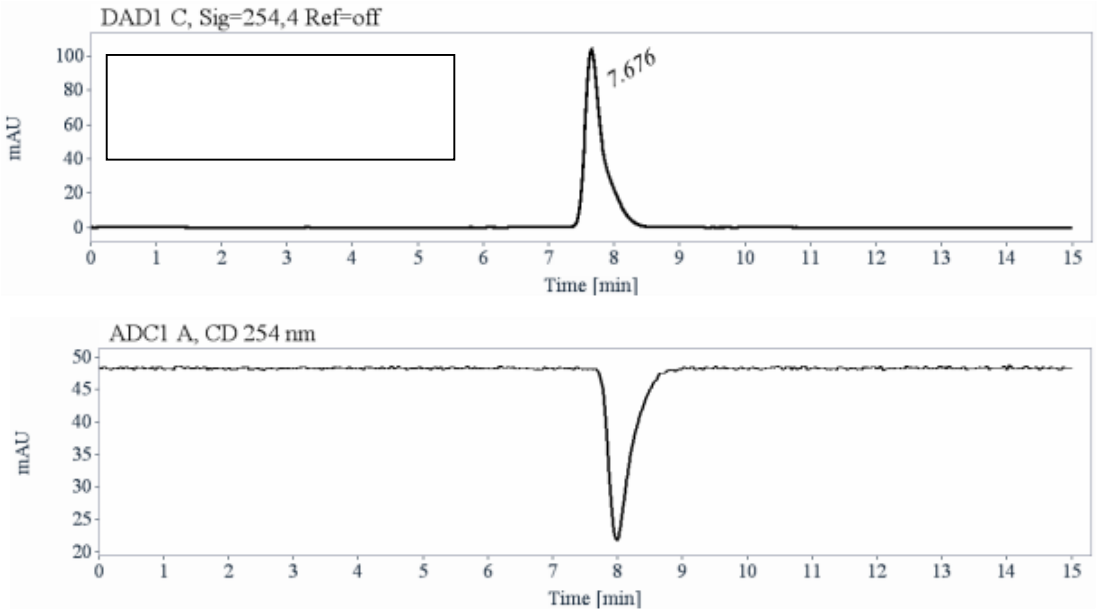

Figure S2. Chromatograms of the first eluted enantiomer.

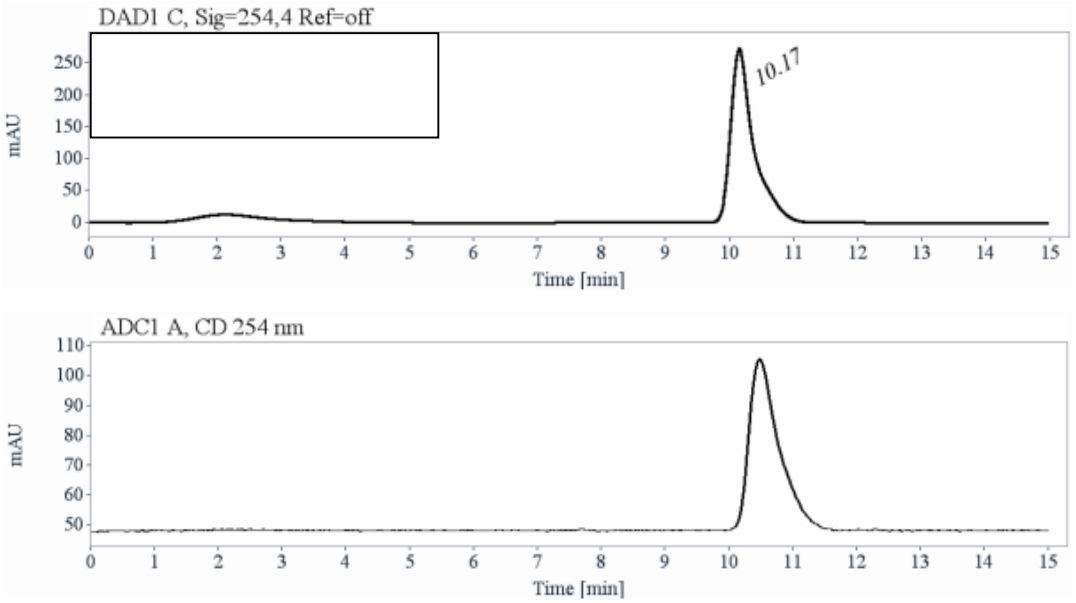

Figure S3. Chromatograms of the second eluted enantiomer of **122**.

Optical rotations for *R*-122 and *S*-122

Optical rotations were measured on a Jasco P-2000 polarimeter with a sodium lamp (589 nm), a halogen lamp (578, 546 and 436 nm), in a 10 cm cell, thermostated at 25°C with a Peltier controlled cell holder.

λ (nm)	***R*-122** first eluted on Chiralpak IC $[\alpha]_\lambda^{25}$ (CH_2Cl_2, c = 0.18)	***S*-122** second eluted on Chiralpak IC $[\alpha]_\lambda^{25}$ (CH_2Cl_2, c = 0.20)
589	- 23	+ 22
578	- 22	+ 22
546	- 19	+ 19
436	+ 69	- 70

Electronic Circular Dichroism for *R*-122/*S*-122

ECD and UV spectra were measured on a JASCO J-815 spectrometer equipped with a JASCO Peltier cell holder PTC-423 to maintain the temperature at 25.0 ± 0.2°C. A CD quartz cell of 1 mm of optical pathlength was used. The CD spectrometer was purged with nitrogen before recording each spectrum, which was baseline subtracted.

The baseline was always measured for the same solvent and in the same cell as the samples. The spectra are presented without smoothing and further data processing.

First eluted enantiomer (***R*-122**): green solid line, concentration = 0.229 mmol·L^{-1} in dichloromethane.

Second eluted enantiomer (***S*-122**): red dotted line, concentration = 0.224 mmol·L^{-1} in dichloromethane.

Acquisition parameters: 0.1 nm as intervals, scanning speed 50 nm/min, band width 1 nm, and 3 accumulations per sample.

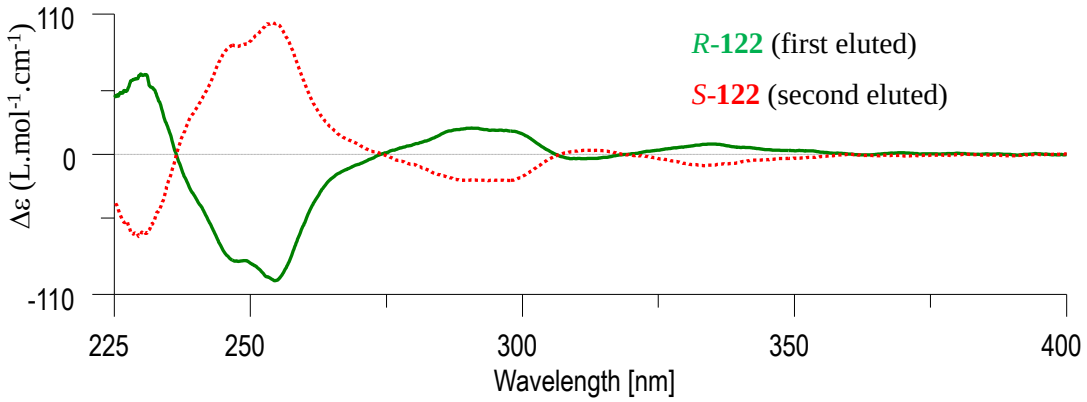

Figure S4. ECD spectra of enantiomers ***R*-122/*S*-122** in CH_2Cl_2.

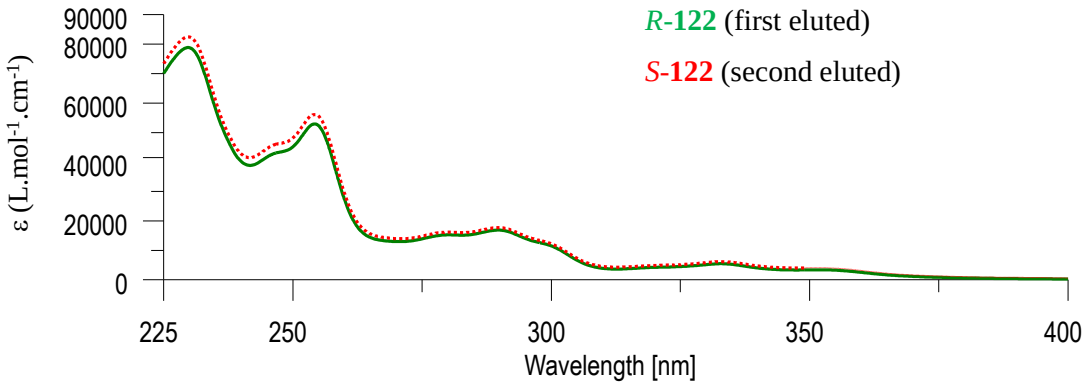

Figure S5. UV spectra of enantiomers ***R*-122/*S*-122** in CH_2Cl_2.

Absolute configuration determination for (±)-122 by comparison of calculated and experimental ECD spectra

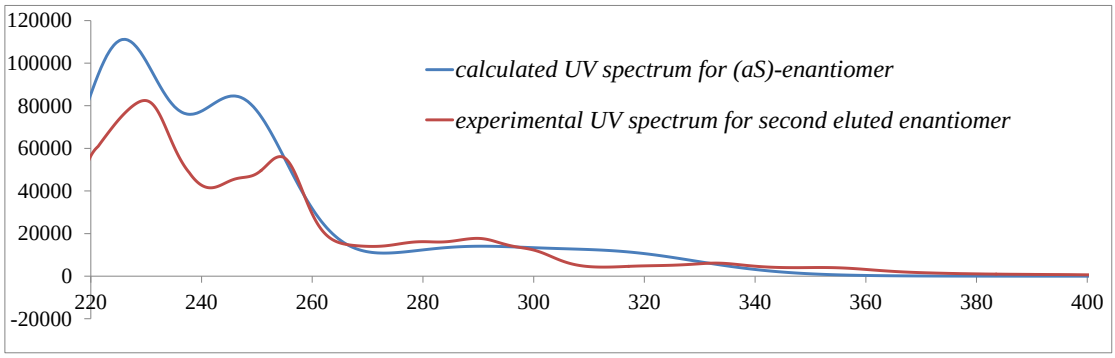

Figure S6. Calculated UV spectrum for *S*-enantiomer and experimental UV spectrum for second eluted enantiomer of **122**.

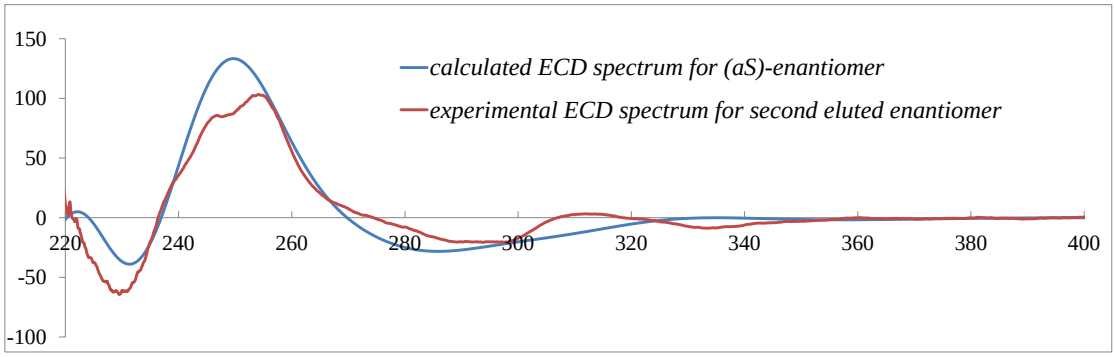

Figure S7. Calculated ECD spectrum for *S*-enantiomer and experimental ECD spectrum for second eluted enantiomer of **122**.

Absolute configuration determination for (±)-122 by comparison of calculated and experimental optical rotation

Optical rotation calculations have been carried out at 589.3 nm by DFT at SMD(CH_2Cl_2)/B3LYP/6-311G(d,p) level for the two populated conformers.

$[\alpha]_D^{25}$ calculated for (*aS*)-enantiomer = + 18, to be compared to $[\alpha]_D^{25}$ = + 22 for the second eluted enantiomer on Chiralpak IC.

Therefore, the second eluted enantiomer on Chiralpak IC is *S*-configuration.

Computational methods for determining absolute configuration of (±)-122

Two conformer geometries were found after a systematic conformational study using DFT at the SMD(CH_2Cl_2)/B3LYP/6-311G(d,p) level. UV and ECD spectra were calculated based on the SMD(CH_2Cl_2)/B3LYP/6-311G(d,p) geometry using TD-DFT at the SMD(CH_2Cl_2)/CAM-B3LYP/6-31G++(2d,2p) level. 30 discrete transitions were calculated for each conformation (the lowest calculated wavelength is 193 nm). The simulated spectra resulting from the Boltzmann averaged sum of the conformations are approximated by the Gaussian distribution (half the bandwidth at 1/*e* peak height = 2000 cm^{-1}) and scaled by 1.02 in order to obtain the best match with the experimental UV spectrum.

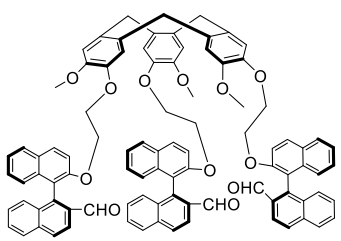

***M*-*R*,*R*,*R*-126**

***M*-*R*,*R*,*R*-126** was prepared as following. To a flame-dried round bottom 100 mL flask was added CTV ***M*-125** (730 mg, 1.0 mmol, 1.0 equiv), ***R*-122** (895 mg, 3.0 mmol, 3.0 equiv), cesium carbonate (1.3 g, 4.0 mmol, 4.0 equiv) and DMF (40 mL), the reaction mixture was stirred for 48 h at room temperature. When reaction completed, the solvent was evaporated, 50 mL of H_2O was added, and the mixture was extracted by EtOAc (3 × 50 mL). Organic phase was collected, dried over anhydrous Na_2SO_4, filtered, and concentrated under vacuum to give crude product, which was purified by recrystallization (EtOAc and petroleum ether) to give the title compound ***M*-*R*,*R*,*R*-126** as a light yellow solid (1.12 g, 81%). **^{1}H NMR** (300 MHz, $CDCl_3$) δ 9.66 (s, 3H), 8.07 (d, *J* = 8.6 Hz, 3H), 7.95 (d, *J* = 9.1 Hz, 3H), 7.89 (d, *J* = 8.6 Hz, 3H), 7.85 – 7.78 (m, 6H), 7.46 – 7.35 (m, 6H), 7.33 – 7.22 (m, 6H), 7.20 – 7.07 (m, 6H), 6.90 (d, *J* = 8.4 Hz, 3H), 6.48 (d, *J* = 24.2 Hz, 6H), 4.53 (d, *J* = 13.7 Hz, 3H), 4.31 – 4.13 (m, 6H), 3.89 – 3.73 (m, 6H), 3.38 (s, 9H), 3.30 (d, *J* = 13.8 Hz, 3H). **^{13}C NMR** (75 MHz, $CDCl_3$) δ 192.73, 154.39, 148.56, 146.47, 141.59, 136.33, 134.57, 133.17, 132.81, 132.27, 131.83, 130.75, 129.12, 128.74, 128.53, 128.22, 128.09, 127.26, 127.20, 126.85, 125.24, 124.27, 122.17, 118.42, 116.82, 114.85, 114.16, 68.12, 67.93, 56.11, 53.42, 36.21, 31.60, 22.66, 14.12. **ESI-HRMS** for ***M*-*R*,*R*,*R*-126** *m*/*z*: found 1404.5024, calcd for $C_{93}H_{72}O_{12}Na$ $[M+Na]^+$ 1404.5021. $[\alpha]_D^{25}$ for ***M*-*R*,*R*,*R*-126**: +47 (CH_2Cl_2, c =0.24).

The procedure for synthesis of ***P*-*S*,*S*,*S*-126** was the same as that of ***M*-*R*,*R*,*R*-126**, as they are enantiomers, the ^{1}H and ^{13}C NMR spectra are exactly the same as that of ***M*-*R*,*R*,*R*-126**. **ESI-HRMS** for ***P*-*S*,*S*,*S*-126** *m*/*z*: found 1404.5027, calcd for $C_{93}H_{72}O_{12}Na$ $[M+Na]^+$ 1404.5021. $[\alpha]_D^{25}$ for ***P*-*S*,*S*,*S*-126**: -46 (CH_2Cl_2, c =0.17).

The procedure for synthesis of ***M*-*S*,*S*,*S*-126**/***P*-*R*,*R*,*R*-126** was similar as that of ***M*-*R*,*R*,*R*-126**. **^{1}H NMR** (300 MHz, $CDCl_3$) δ 9.69 (s, 3H), 8.09 (d, *J* = 8.6 Hz, 3H), 7.99 (d, *J* = 9.1 Hz, 3H), 7.92 (d, *J* = 8.6 Hz, 3H), 7.89 – 7.80 (m, 6H), 7.49 (d, *J* = 9.1 Hz, 3H), 7.40 (d, *J* = 7.0 Hz, 2H), 7.35 (d, *J* = 4.4 Hz, 1H), 7.34 – 7.24 (m, 6H), 7.24 – 7.16 (m, 3H), 7.16 – 7.07 (m, 3H), 6.93 (d, *J* = 8.5 Hz, 3H), 6.49 (d, *J* = 10.3 Hz, 6H), 4.56 (d, *J* = 13.7 Hz, 3H), 4.25 (hept, J = 5.4 Hz, 6H), 3.90 (dt, *J* = 10.6, 5.3 Hz, 3H), 3.80

(dt, J = 10.7, 5.4 Hz, 3H), 3.40 (s, 9H), 3.31 (d, J = 13.6 Hz, 3H). **^{13}C NMR** (75 MHz, $CDCl_3$) δ 192.72, 154.41, 148.53, 146.43, 141.49, 136.29, 134.57, 133.13, 132.82, 132.31, 131.86, 130.71, 129.13, 128.70, 128.49, 128.27, 128.07, 127.24, 127.13, 126.80, 125.29, 124.27, 122.25, 118.41, 116.57, 114.93, 114.10, 68.11, 67.79, 56.10, 36.20, 31.60, 22.67, 14.13. **ESI-HRMS** for ***M*-*S*,*S*,*S*-126** *m*/*z*: found 1404.5022, calcd for $C_{93}H_{72}O_{12}Na$ $[M+Na]^+$ 1404.5021. **ESI-HRMS** for ***P*-*R*,*R*,*R*-126** *m*/*z*: found 1404.5025, calcd for $C_{93}H_{72}O_{12}Na$ $[M+Na]^+$ 1404.5021. $[\alpha]_D^{25}$ for ***M*-*S*,*S*,*S*-126**: +73 (CH_2Cl_2, c =0.22); $[\alpha]_D^{25}$ for ***P*-*R*,*R*,*R*-126**: -73 (CH_2Cl_2, c =0.23).

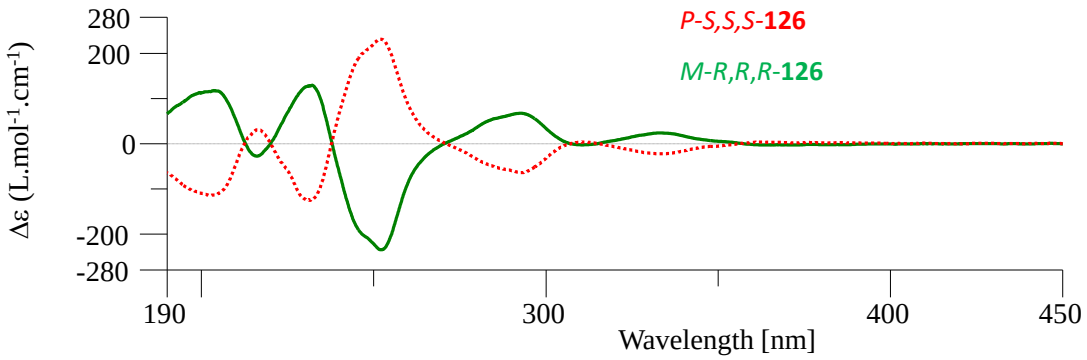

Figure S8. ECD spectra (CH_3CN, 273K) of *M*-*R*,*R*,*R*-**126**/*P*-*S*,*S*,*S*-**126**.

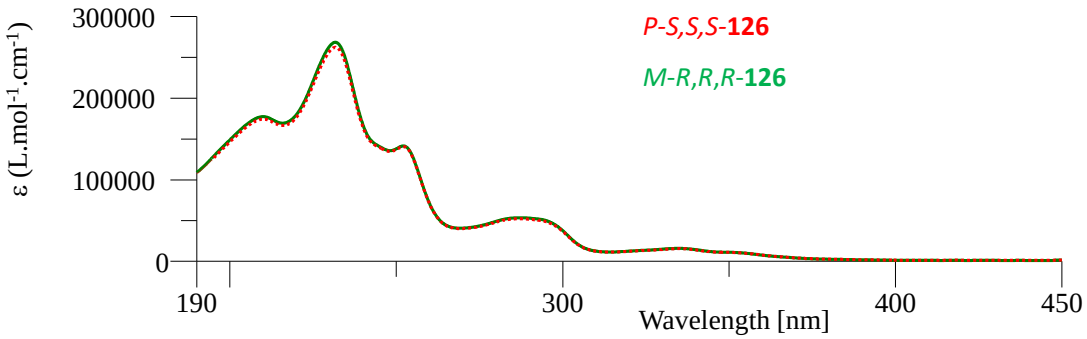

Figure S9. UV spectra (CH_3CN, 273K) of *M*-*R*,*R*,*R*-**126**/*P*-*S*,*S*,*S*-**126**.

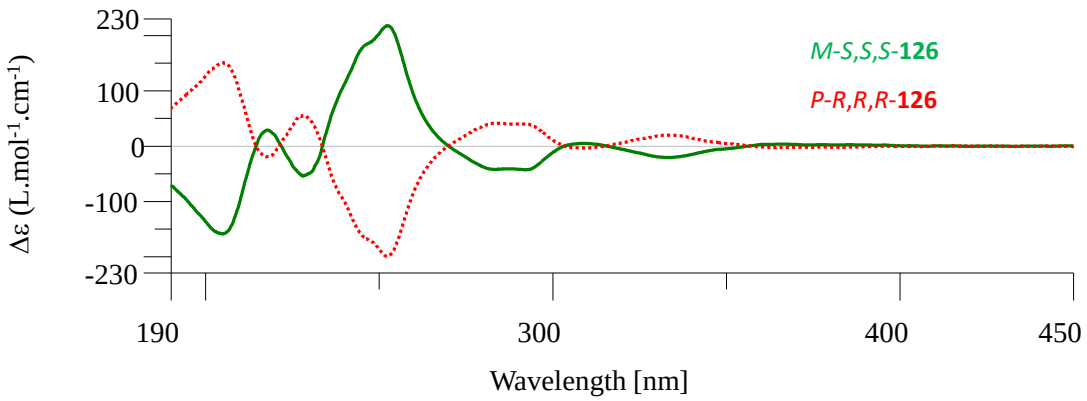

Figure S10. ECD spectra (CH_3CN, 273K) of *P*-*R*,*R*,*R*-**126**/*M*-*S*,*S*,*S*-**126**.

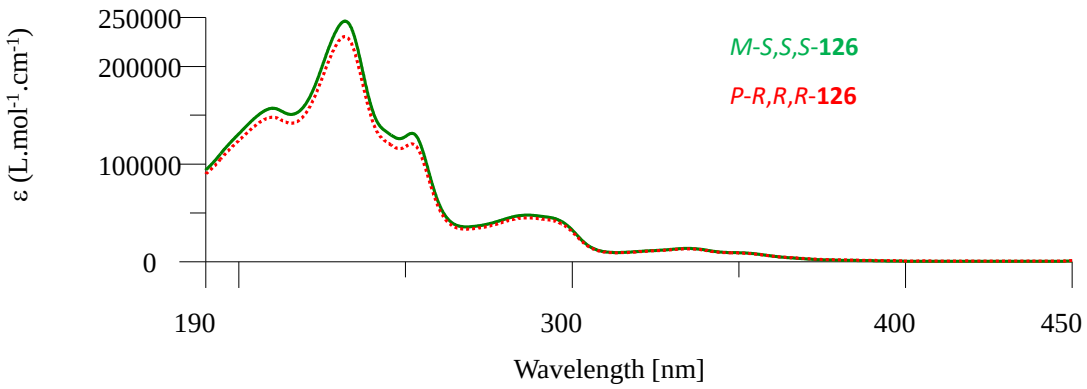

Figure S11. UV spectra (CH_3CN, 273K) of *P*-*R*,*R*,*R*-**126**/*M*-*S*,*S*,*S*-**126**.

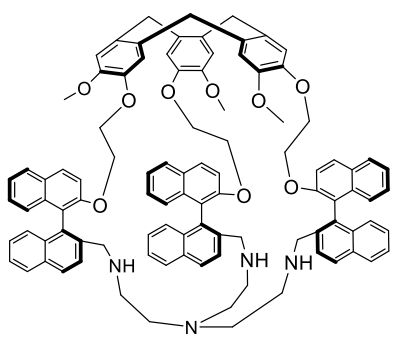

***M*-*R*,*R*,*R*-127**

***M*-*R*,*R*,*R*-127**. To a flame-dried 500 mL round-bottomed flask equipped with a constant pressure funnel was added ***M*-*R*,*R*,*R*-126** (96 mg), MeOH (120 mL) and $CHCl_3$ (120 mL), and a solution of tris(2-aminoethyl)amine (tren) (12 μL) in MeOH (60 mL) $CHCl_3$ (60 mL) was added drop-wise. The reaction was stirred overnight at room temperature, and then was cooled by an ice bath followed by addition of $NaBH_4$ (80 mg). The reaction was stirred for 2 h and then solvent was evaporated. The remaining mixture was added 100 mL of H_2O and extracted by $CHCl_3$ (3 ×50), The combined organic phases were collected, dried over anhydrous Na_2SO_4, filtered, and concentrated under vacuum to give crude product, which was purified on silica gel by flash chromatography (CH_2Cl_2/MeOH/Et_3N; 90/10/2) to give the title compound ***M*-*R*,*R*,*R*-127** as a white solid (49 mg, 47%). **^{1}H NMR** (400 MHz, $CDCl_3$) δ 8.12 (d, *J* = 9.1 Hz, 3H), 7.97 (d, *J* = 8.2 Hz, 3H), 7.90 (d, *J* = 8.1 Hz, 3H), 7.84 (d, *J* = 9.1 Hz, 3H), 7.73 (d, *J* = 8.6 Hz, 3H), 7.67 (d, *J* = 8.5 Hz, 3H), 7.43 (t, 3H), 7.36 (t, *J* = 7.4 Hz, 3H), 7.21 (dd, *J* = 13.8, 6.7 Hz, 6H), 7.14 (dd, *J* = 15.1, 8.0 Hz, 6H), 6.88 (d, *J* = 8.5 Hz, 3H), 6.64 (d, *J* = 21.7 Hz, 6H), 4.78 (t, *J* = 9.3 Hz, 3H), 4.66 (d, *J* = 13.8 Hz, 3H), 4.14 (d, *J* = 11.5 Hz, 3H), 4.03 (d, *J* = 10.0 Hz, 3H), 3.86 (t, *J* = 8.2 Hz, 3H), 3.62 (s, 9H), 3.50 – 3.36 (m, 9H), 3.30 (d, *J* = 11.8 Hz, 3H), 1.88 – 1.67 (m, 6H), 1.24 – 1.13 (m, 3H), 0.72 – 0.55 (m, 3H). **^{13}C NMR** (101 MHz, $CDCl_3$) δ 153.53, 147.77, 147.04, 134.24, 133.06, 132.62, 132.20, 131.96, 129.40, 129.29, 127.85, 127.81, 127.44, 126.58, 126.51, 126.07, 125.64, 125.26, 124.98, 123.93, 121.93, 115.77, 114.01, 113.66, 68.26, 67.85, 56.69, 52.27, 50.87, 45.82, 36.36, 29.72. **ESI-HRMS** for ***M*-*R*,*R*,*R*-127** *m*/*z*: found 740.8444, calcd for $C_{99}H_{92}N_4O_9$ $[M+2H]^{2+}$ 740.8443. $[\alpha]_D^{25}$ for ***M*-*R*,*R*,*R*-127**: -9 (CH_2Cl_2, c =0.70).

The procedure for synthesis of ***P*-*S*,*S*,*S*-127** was the same as that of ***M*-*R*,*R*,*R*-127**, as they are enantiomers, the ^{1}H and ^{13}C NMR spectra are exactly the same as that of ***M*-*R*,*R*,*R*-127**. **ESI-HRMS** for ***P*-*S*,*S*,*S*-127** *m*/*z*: found 740.8445, calcd for $C_{99}H_{92}N_4O_9$ $[M+2H]^{2+}$ 740.8443. $[\alpha]_D^{25}$ for ***P*-*S*,*S*,*S*-127**: +9 (CH_2Cl_2, c =0.90).

The procedure for synthesis of ***M*-(*S*,*S*,*S*)-127**/***P*-(*R*,*R*,*R*)-127** was similar as that of ***M*-*R*,*R*,*R*-127**. **^{1}H NMR** (400 MHz, $CDCl_3$) δ 8.03 (d, *J* = 9.0 Hz, 3H), 7.93 (d, *J* = 8.1 Hz, 3H), 7.84 (d, *J* = 8.1 Hz, 3H), 7.63 (s, 6H), 7.47 (d, *J* = 9.1 Hz, 3H), 7.39 (q, *J* = 7.0 Hz, 6H), 7.25 – 7.21 (m, 3H), 7.21 – 7.17 (m, 3H), 7.10 (d, *J* = 8.4 Hz, 3H), 6.97 (d, *J* = 8.4 Hz, 3H), 6.65 (s, 3H), 6.56 (s, 3H), 4.63 (d, *J* = 13.6 Hz, 3H), 4.56 – 4.45 (m, 3H), 4.19 (dt, *J* = 11.8, 4.3 Hz, 3H), 4.05 (s, 6H), 3.47 – 3.28 (m, 9H), 3.14 (s, 9H), 1.78 – 1.66 (m, 3H), 1.65 – 1.54 (m, 3H), 1.35 – 1.21 (m, 3H), 1.16 – 1.03 (m, 3H). **^{13}C NMR** (101 MHz, $CDCl_3$) δ 153.53, 147.77, 147.04, 134.24, 133.06, 132.62, 132.18, 131.96, 129.40, 129.29, 127.85, 127.81, 127.44, 126.58, 126.51, 126.07, 125.64, 125.26, 124.98, 123.93, 121.93, 115.77, 114.01, 113.66, 77.26, 68.26, 67.85, 56.69, 52.27, 50.87, 45.83, 36.36, 29.72. **ESI-HRMS** for ***M*-(*S*,*S*,*S*)-127** *m*/*z*: found 740.8443, calcd for $C_{99}H_{92}N_4O_9$ $[M+2H]^{2+}$ 740.8443. **ESI-HRMS** for ***P*-(*R*,*R*,*R*)-127** *m*/*z*: found 740.8442, calcd for $C_{99}H_{92}N_4O_9$ $[M+2H]^{2+}$ 740.8443. $[\alpha]_D^{25}$ for ***M*-*S*,*S*,*S*-127**: +19 (CH_2Cl_2, c =1.0); $[\alpha]_D^{25}$ for ***P*-*R*,*R*,*R*-127**: -17 (CH_2Cl_2, c =0.60).

Alternative procedure for synthesizing 111-Cl

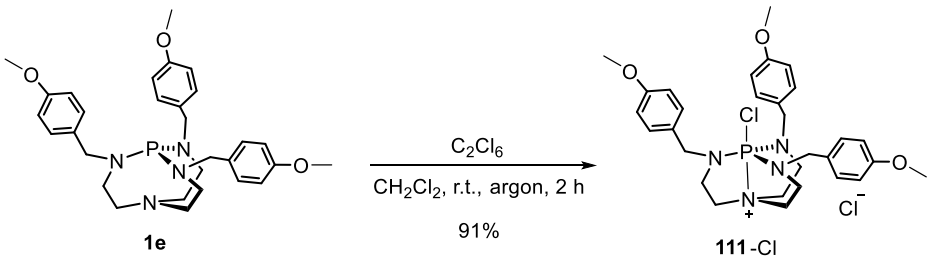

Scheme S13. Synthetic procedure for preparation of **111**-Cl.

In addition to procedure described in Scheme S10, an alternative procedure was used here to synthesize **111**-Cl referring to a reported procedure.[117] To a flame-dried Schlenk tube was added freshly prepared Verkade's superbase **1e** (1 mmol, 535 mg), dried CH_2Cl_2 (3 mL), and hexachloroethane (1 mmol, 237 mg), the mixture was stirred under argon at room temperature for 2 h. When reaction finished, solvent was evaporated under vacuum, the residual was washed by Et_2O (10×3 mL) to give pure **111**-Cl as a white solid (550 mg, 91%). Characterizations are the same as described in Scheme S10.

Procedure for preparing 111-PF_6

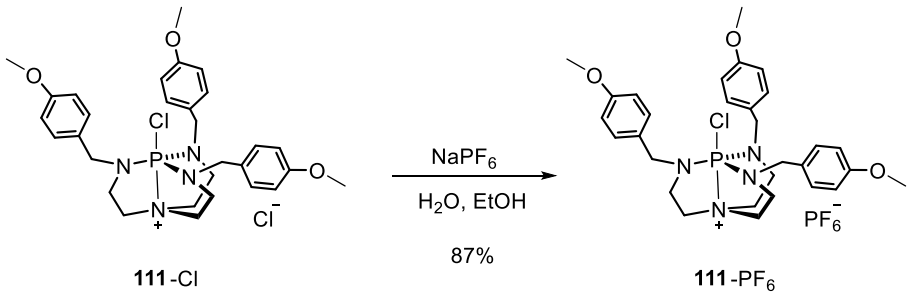

Scheme S14. Synthetic procedure for preparing **111**-PF_6.

In a 10 mL round-bottomed flask was added deionized water (2 mL), ethanol (1 mL) and **111**-Cl (200 mg), the mixture was stirred and a solution of $NaPF_6$ (80 mg) in deionized water (2 mL) was added dropwise, white solid precipitated instantaneously, stirring for another 2 h, which was then filtered and washed (3 mL, H_2O : EtOH, 2:1) to give pure **111**-PF_6 as a white solid (205 mg, 87%). **^{1}H NMR** (400 MHz, $CDCl_3$) δ 7.21 (d, *J* = 8.6 Hz, 6H), 6.86 (d, *J* = 8.6 Hz, 6H), 4.56 (d, *J* = 14.1 Hz, 6H), 3.80 (s, 10H), 3.22 (dt, *J* = 12.9, 6.6 Hz, 6H), 3.08 (td, *J* = 6.5, 3.4 Hz, 6H). **^{13}C NMR** (75 MHz, $CDCl_3$) δ 159.41, 129.10, 128.66, 128.59, 114.28, 55.31, 54.68, 54.63, 45.03, 44.90, 43.77, 43.66. **^{31}P NMR** (162 MHz, $CDCl_3$) δ -18.76, -131.01, -135.41, -139.82, -144.22, -148.63, -153.04, -157.44. **^{19}F NMR** (376 MHz, $CDCl_3$) δ -70.67, -72.56.

Procedure for preparing 2e-PF6

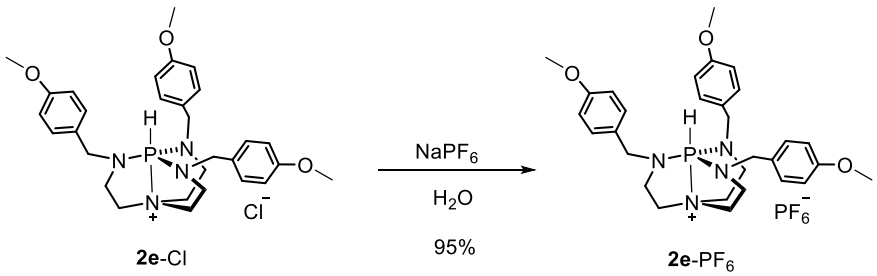

Scheme S15. Synthetic procedure for preparing **2e**-PF_6.

In a 10 mL round-bottomed flask was added deionized water (2 mL), and **2e**-Cl (200 mg), the mixture was stirred and a solution of $NaPF_6$ (80 mg) in deionized water (2 mL)

was added dropwise, white solid precipitated instantaneously, stirring for another 2 h, which was then filtered and washed by water (3 mL) to give pure **2e**-PF_6 as a white solid (226 mg, 95%). **^{1}H NMR** (400 MHz, $CDCl_3$) δ 7.08 (d, J = 8.5 Hz, 6H), 6.87 (d, J = 8.5 Hz, 6H), 5.82 (d, $^1J_{P\text{-}H}$ = 496.2 Hz, 1H), 4.10 (d, $^3J_{P\text{-}H}$ = 17.1 Hz, 6H), 3.81 (s, 9H), 3.27 – 3.16 (m, 6H), 3.10 – 2.99 (m, 6H). **^{13}C NMR** (75 MHz, $CDCl_3$) δ 159.36, 128.99, 128.92, 128.69, 114.42, 55.34, 51.00, 50.79, 46.89, 46.78, 39.00, 38.92. **^{31}P NMR** (162 MHz, $CDCl_3$) δ -11.76, -131.06, -135.46, -139.86, -144.27, -148.67, -153.07, -157.47. **^{19}F NMR** (376 MHz, $CDCl_3$) δ -71.27, -73.17. **ESI-HRMS** *m*/*z* found 535.2842, calcd for $C_{57}H_{63}N_4O_9PCl^+$ $[M]^+$ 535.2838.

Procedure for preparing 133-Cl

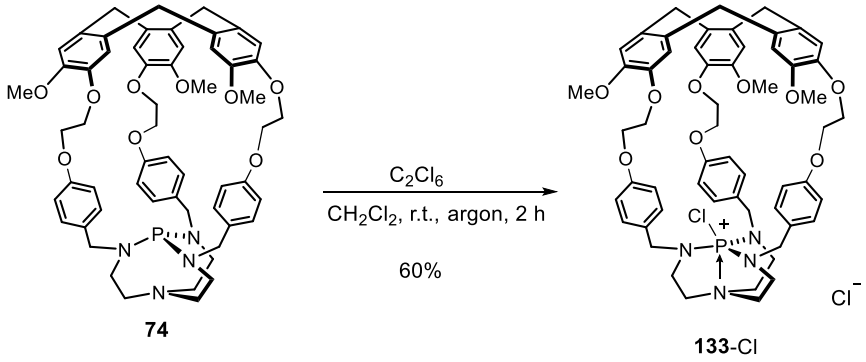

74 **133**-Cl

Scheme S16. Synthetic procedure for preparing **133**-Cl.

The synthesis of **133**-Cl referred to a reported procedure.[117] To a flame-dried Schlenk tube was added freshly prepared encaged Verkade's superbase **74** (0.24 mmol, 235 mg), dried CH_2Cl_2 (3 mL), and hexachloroethane (0.24 mmol, 57 mg), the mixture was stirred under argon at room temperature for 2 h. When reaction finished, solvent was evaporated under vacuum, the residual was washed by Et_2O (5×3 mL) to give pure **133**-Cl as a white solid (150 mg, 60%). **^{1}H NMR** (400 MHz, $CDCl_3$) δ 6.79 (d, J = 8.4 Hz, 6H), 6.73 (d, J = 5.1 Hz, 6H), 6.64 (d, J = 8.4 Hz, 6H), 4.64 (d, J = 13.7 Hz, 3H), 4.44 – 4.29 (m, 8H), 4.29 – 4.19 (m, 4H), 4.18 – 4.05 (m, 6H), 3.98 – 3.87 (m, 3H), 3.75 (s, 9H), 3.69 – 3.57 (m, 3H), 3.50 – 3.39 (m, 9H). **^{13}C NMR** (101 MHz, $CDCl_3$) δ 158.89, 156.63, 148.46, 146.84, 132.67, 132.00, 130.78, 126.74, 123.25, 116.40, 115.54, 115.25, 114.93, 77.26, 67.03, 66.55, 65.81, 56.67, 56.52, 54.16, 54.12, 53.42, 45.23,

45.13, 44.98, 36.24, 15.25. **^{31}P NMR** (162 MHz, $CDCl_3$) δ -24.25. **ESI-HRMS** for **133** *m*/*z*: found 1013.4044, calcd for $C_{57}H_{63}N_4O_9PCl^+$ $[M]^+$ 1013.4016.

Procedure for preparing encaged sulfide proazaphosphatrane 134

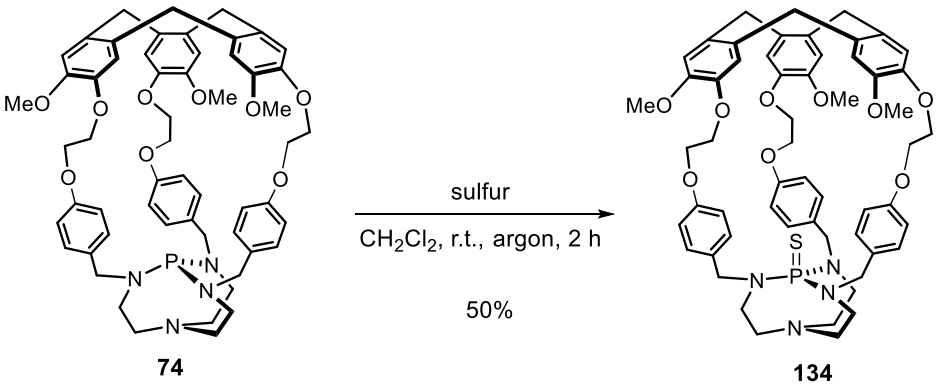

Scheme S17. Synthetic procedure for preparing encaged sulfide proazaphosphatrane **134**.

The synthesis of encaged sulfide proazaphosphatrane **134** referred to a reported procedure.[133] To a flame-dried Schlenk tube was added freshly prepared encaged Verkade's superbase **74** (0.24 mmol, 235 mg), dried CH_2Cl_2 (3 mL), and sulfur (0.24 mmol, 8 mg), the mixture was stirred under argon at room temperature for 2 h. When reaction finished, solvent was evaporated under vacuum, the residual was washed by Et_2O (5×3 mL) to give pure **134** as a white solid (121 mg, 50%). **^{1}H NMR** (400 MHz, $CDCl_3$) δ 7.20 (d, *J* = 8.5 Hz, 6H), 6.85 (d, *J* = 8.5 Hz, 6H), 6.72 (d, *J* = 3.9 Hz, 6H), 4.61 (d, *J* = 13.7 Hz, 3H), 4.51 – 4.32 (m, 9H), 4.21 – 4.01 (m, 9H), 3.71 (s, 9H), 3.40 (d, *J* = 13.8 Hz, 3H), 3.18 (s, 3H), 2.99 (d, *J* = 18.4 Hz, 3H), 2.93 – 2.79 (m, 6H). **^{13}C NMR** (75 MHz, $CDCl_3$) δ 156.72, 149.07, 147.11, 133.47, 132.11, 132.07, 128.16, 118.77, 116.20, 115.91, 68.79, 67.34, 57.22, 50.81, 49.49, 36.47. **^{31}P NMR** (121 MHz, $CDCl_3$) δ 73.22. **ESI-HRMS** for **134** *m*/*z*: found 1011.4128, calcd for $C_{57}H_{64}N_4O_9PS^+$ $[M+H]^+$ 1011.4126.

Procedure for preparing encaged selenide proazaphosphatrane 135

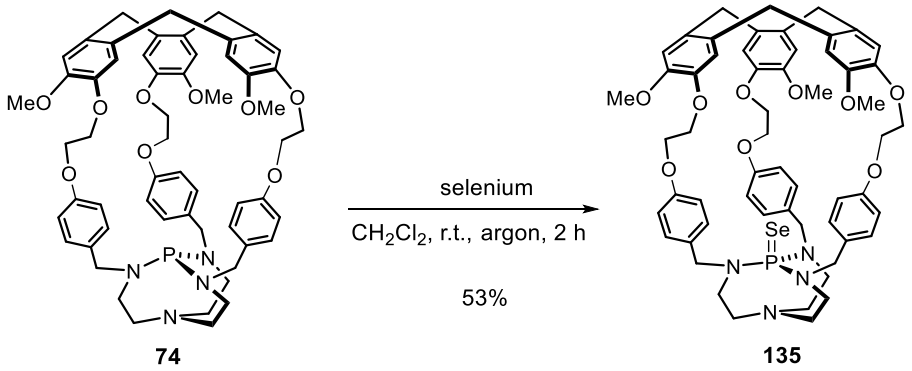

Scheme S18. Synthetic procedure for preparing encaged selenide proazaphosphatrane **135**.

The synthesis of encaged sulfide proazaphosphatrane **135** referred to a reported procedure.[133] To a flame-dried Schlenk tube was added freshly prepared encaged Verkade's superbase **74** (0.24 mmol, 235 mg), dried CH_2Cl_2 (3 mL), and selenium (0.24 mmol, 19 mg), the mixture was stirred under argon at room temperature for 2 h. When reaction finished, solvent was evaporated under vacuum, the residual was purified on silica gel by flash column chromatography ($CHCl_3$/MeOH 15:0.5) to give pure **135** as a white solid (134 mg, 53%). **^{1}H NMR** (400 MHz, $CDCl_3$) δ 7.21 (d, *J* = 8.4 Hz, 6H), 6.87 (d, *J* = 8.2 Hz, 6H), 6.69 (d, *J* = 4.4 Hz, 6H), 4.59 (d, *J* = 13.7 Hz, 3H), 4.55 – 4.34 (m, 9H), 4.19 – 3.97 (m, 9H), 3.72 (s, 9H), 3.38 (d, *J* = 13.8 Hz, 3H), 3.17 (s, 3H), 3.02 – 2.71 (m, 9H). **^{13}C NMR** (75 MHz, $CDCl_3$) δ 156.70, 149.00, 146.97, 133.39, 132.79, 131.95, 131.45, 130.87, 128.54, 128.35, 118.57, 116.43, 116.04, 115.61, 68.86, 67.64, 66.45, 57.15, 56.36, 50.87, 48.80, 36.46. **^{31}P NMR** (121 MHz, $CDCl_3$) δ 71.13. **ESI-HRMS** for **135** *m*/*z*: found 1081.3403, calcd for $C_{57}H_{63}N_4O_9PSeNa^+$ $[M+Na]^+$ 1081.3398.

^{1}H NMR Titrations

A solution of host **111**-PF_6 or **2e**-PF_6 (5.0 mM in CD_3CN, 500 µL) was titrated in NMR tubes with aliquots of a concentrated solution (20 mM in CD_3CN) of halide anions. The shifts of the $N_{eq}CH_2$ protons of the hosts signals were measured after each addition and plotted as a function of the guest/host ratio ([G]/[H]). The association constant K_a was obtained by nonlinear least-squares fitting of these plots using the Bindfit program. K_a, covariance, and RMS are given below for each halide anion.

Guest	Host	K_a [M^{-1}]	Covariance	RMS (ppm)
Cl^-	**111**-PF_6	66	5.34×10^{-4}	3.87×10^{-4}
	2e-PF_6	-	-	-
Br^-	**111**-PF_6	23	4.85×10^{-4}	3.46×10^{-4}
	2e-PF_6	-	-	-
I^-	**111**-PF_6	15	1.36×10^{-4}	1.46×10^{-4}
	2e-PF_6	-	-	-

Proposed mechanism for the formation of 111

We proposed the mechanism below for the formation of compound **2** obtained when mixing **1b** and $TiCl_4$ in DCM**.** The first step -the Lewis acid/base interaction- is represented by a red dashed line on scheme S6, and appears precluded with the encaged superbase **1a**. This mechanism is based on that proposed by J.G. Verkade for the formation of a similar compound by mixing the oxidized superbase and $O{=}PCl_3$.[117]

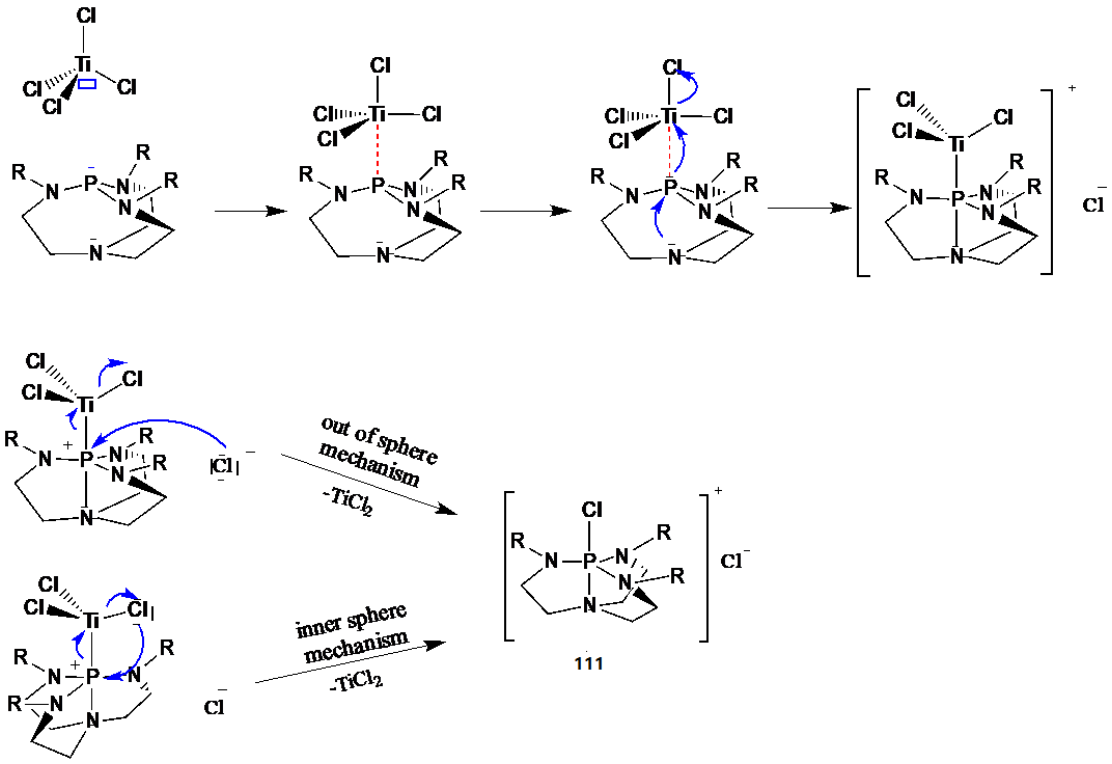

Scheme S19. Proposed mechanism for the formation of **111**. - - - Lewis acid/ base interaction.

Computational method

All electronic structure calculations were carried out within density functional theory (DFT) framework. Since the inspected systems are particularly flexible, intramolecular interactions are likely to dictate their shape. Therefore, weak interactions corrections were included by means of a nowadays current procedure. The energy contributions

arising from atoms polarizabilities are added on top of the DFT electronic energy.[147] Full geometry opimizations were performed using the B3LYP functional and 6-31G* a basis set in the Gaussian G09 suite of programs.[148]

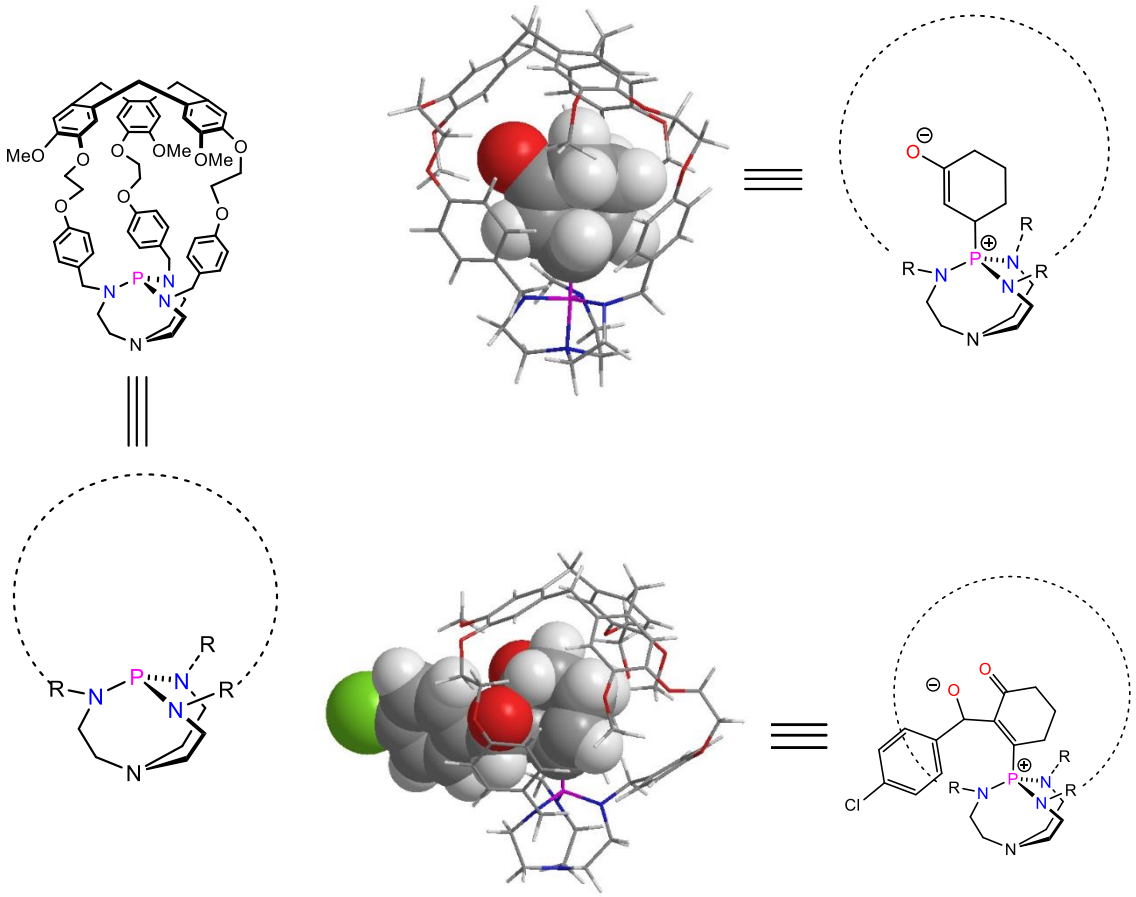

Scheme S20. Simplified representation of the structure of **74** (left), and DFT optimized intermediate structures of the substrate@encaged-superbase (right).

[147] Grimme, S.; Antony, J.; Ehrlich, S.; Krieg, S. *J. Chem. Phys*. **2010**, *132*, 154104.
[148] Gaussian 09, Revision D.01, M. J. Frisch, G. W. Trucks, H. B. Schlegel, G. E. Scuseria, M. A. Robb, J. R. Cheeseman, G. Scalmani, V. Barone, B. Mennucci, G. A. Petersson, H. Nakatsuji, M. Caricato, X. Li, H. P. Hratchian, A. F. Izmaylov, J. Bloino, G. Zheng, J. L. Sonnenberg, M. Hada, M. Ehara, K. Toyota, R. Fukuda, J. Hasegawa, M. Ishida, T. Nakajima, Y. Honda, O. Kitao, H. Nakai, T. Vreven, J. A. Montgomery, Jr., J. E. Peralta, F. Ogliaro, M. Bearpark, J. J. Heyd, E. Brothers, K. N. Kudin, V. N. Staroverov, R. Kobayashi, J. Normand, K. Raghavachari, A. Rendell, J. C. Burant, S. S. Iyengar, J. Tomasi, M. Cossi, N. Rega, J. M. Millam, M. Klene, J. E. Knox, J. B. Cross, V. Bakken, C. Adamo, J. Jaramillo, R. Gomperts, R. E. Stratmann, O. Yazyev, A. J. Austin, R. Cammi, C. Pomelli, J. W. Ochterski, R. L. Martin, K. Morokuma, V. G. Zakrzewski, G. A. Voth, P. Salvador, J. J. Dannenberg, S. Dapprich, A. D. Daniels, Ö. Farkas, J. B. Foresman, J. V. Ortiz, J. Cioslowski, and D. J. Fox, Gaussian, Inc., Wallingford CT, 2009.

Energy of the first intermediate (right, upper part) when compared to the initial state: -89.56 kJ.mol^{-1}; Energy of the second intermediate (right, lower part) when compared to the initial state: -18.21 kJ.mol^{-1}.

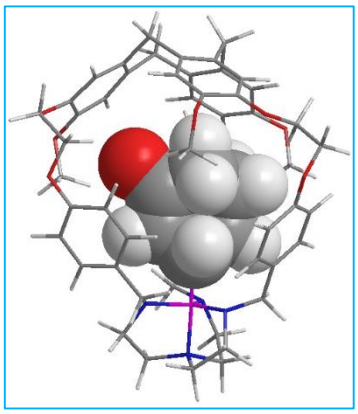

First calculated intermediate:

Cartesian coordinates

149

E(RB3LYP) = -3756.02644981

C	-2.316146	-2.550223	-3.723869
C	2.584840	-2.623277	-2.882013
C	3.493891	-1.571404	-2.959748
C	4.379769	-1.269916	-1.914106
C	4.380206	-2.080228	-0.769412
C	3.420427	-3.098837	-0.675374
C	2.503593	-3.367868	-1.686127
C	-1.214611	-0.478163	1.312792
C	-1.818260	-0.170956	-0.031286
C	-0.898135	0.788718	-0.821778
C	0.505831	0.166104	-0.893361
C	1.130837	0.020098	0.495165
C	0.160557	-0.544930	1.536826
C	5.351070	-1.890606	0.389537
C	4.733219	-1.164093	1.571679
C	4.744845	0.228323	1.731414
C	-1.403928	-2.101830	-4.686641
C	4.054557	0.770124	2.826801
C	3.363223	-0.004689	3.755190
C	3.389731	-1.410736	3.610346
C	4.070880	-1.951212	2.524622
C	2.584388	-3.552595	4.329532
C	1.603633	-3.861380	3.194523
C	-0.784715	-3.827928	3.002149
C	-1.998380	-3.664810	3.690208

C	-1.322984	-0.732231	-4.971006
C	-3.149552	-3.312317	2.999811
C	-3.125538	-3.103785	1.611485
C	-1.940815	-3.400379	0.930898
C	-0.781046	-3.783472	1.601811
C	-4.247362	-2.369042	0.917225
C	-4.981038	-0.469179	2.428365
C	-6.433599	0.018649	2.117569
C	-6.763524	-0.335780	-0.300918
C	-2.113393	0.168307	-4.255908
C	-5.852935	-0.106098	-1.511782
C	1.479692	0.227149	5.255874
C	5.479221	1.176542	0.787879
C	4.631954	1.781891	-0.326494
C	3.942517	2.974306	-0.039838
C	3.148085	3.620332	-0.985919
C	2.994982	3.033848	-2.259167
C	3.693602	1.870881	-2.547744
C	-2.996790	-0.263853	-3.263507
C	4.529480	1.234859	-1.616007
C	2.587272	5.414049	0.489806
C	1.782849	6.710600	0.457226
C	-0.360893	5.615977	0.505659
C	-1.330579	5.074760	-0.344613
C	-2.135367	4.026009	0.092783
C	-1.996981	3.502625	1.382985
C	-1.083480	4.110882	2.250653
C	-3.100116	-1.638724	-3.026249
C	-0.274749	5.163641	1.828390
C	0.831284	3.658729	-2.978149
C	5.249400	-0.031355	-2.064930
C	0.252467	-4.176340	-1.862798
C	-2.666439	2.226152	1.831323
C	-5.019886	2.503022	1.225847

C	-6.302027	1.988363	0.560881
C	-3.763657	0.761939	-2.443766
C	0.563032	-2.730364	-5.936627
C	1.601875	-2.120847	-5.002961
H	-7.117192	2.630920	0.937962
H	-0.643681	-0.357912	-5.728213
H	-2.011220	1.232443	-4.460228
H	-3.777550	-2.002358	-2.261626
H	-2.376292	-3.615029	-3.523843
H	-5.914581	-0.991618	-2.159386
H	-6.611159	-1.346164	0.083176
H	-7.796102	-0.311793	-0.695931
H	-4.069835	-3.160855	3.559615
H	-1.995996	-3.769873	4.770395
H	0.131389	-3.953699	1.041885
H	-1.901565	-3.273232	-0.147835
H	1.901659	-4.781278	2.669279
H	1.570927	-3.015676	2.501465
H	3.555655	-4.031846	4.142922
H	2.188037	-3.951685	5.266312
H	4.033513	1.845739	2.981954
H	4.061008	3.404591	0.948212
H	3.580452	1.464912	-3.548994
H	0.420030	2.642393	-2.893501
H	0.610731	4.214190	-2.062916
H	0.373805	4.165772	-3.832458
H	6.353464	0.676780	0.361780
H	5.880409	2.001621	1.388905
H	-4.866472	3.549076	0.932492
H	0.100258	-4.352435	-2.930169
H	-0.063660	-3.153042	-1.624958
H	-0.338016	-4.881785	-1.272408
H	-1.905236	1.422175	1.883018
H	-3.056573	2.340157	2.854431

H	-4.530582	1.240702	-3.066637
H	-3.090957	1.572246	-2.145116
H	-5.229373	-2.766062	1.207450
H	-4.168198	-2.488737	-0.168047
H	-5.173045	2.508818	2.315453
H	1.492769	0.994896	0.852354
H	2.011354	-0.629576	0.464779
H	1.147228	0.775725	-1.541493
H	0.427568	-0.818873	-1.377149
H	-1.820788	-0.991394	2.046714
H	-0.840709	1.756947	-0.316562
H	-1.251212	0.960577	-1.838842
H	-1.968056	-1.067834	-0.668036
H	-4.405789	0.317891	2.921093
H	-5.001525	-1.303602	3.131473
H	4.094718	-3.026664	2.393452
H	6.256988	-1.385217	0.047243
H	5.676636	-2.883531	0.722905
H	6.194125	-0.146922	-1.530061
H	5.518303	0.084276	-3.121908
H	3.357620	-3.711227	0.218960
H	3.539909	-0.969469	-3.860486
H	1.291819	-1.136329	-4.630292
H	2.534515	-1.990571	-5.574015
H	1.795857	7.158883	1.462065
H	2.251462	7.414310	-0.234980
H	-6.745768	0.748436	2.875206
H	-7.130801	-0.823193	2.205598
H	0.889108	-0.188733	4.434329
H	1.584897	-0.518016	6.050789
H	1.007820	1.128952	5.661402
H	0.935029	-3.681864	-6.323254
H	0.393303	-2.055915	-6.788285
H	3.625172	5.665982	0.758155

H	2.203477	4.715717	1.242539
H	-1.406839	5.463555	-1.355068
H	0.433714	5.606823	2.520050
H	-2.847953	3.572963	-0.590931
H	-0.971053	3.729683	3.263226
H	-6.265145	0.724931	-2.100185
H	-6.253929	2.160711	-0.517272
N	-4.281213	-0.903800	1.216884
N	-6.569814	0.586656	0.795573
N	-3.768368	1.767901	0.959450
N	-4.438580	0.219593	-1.252797
O	1.775446	-3.014471	-3.920919
O	0.662672	-1.058397	2.581985
O	2.762567	-2.159085	4.568992
O	0.305974	-4.049608	3.775214
O	2.775119	0.656442	4.792213
O	2.520787	4.823730	-0.795640
O	0.450997	6.577246	-0.034541
O	2.235346	3.619427	-3.245762
O	1.614642	-4.391027	-1.478024
O	-0.661116	-3.073500	-5.292641
P	-3.619282	0.269142	0.222688

Second calculated intermediate:

Cartesian coordinates

163

E(RB3LYP) = -4561.22228662

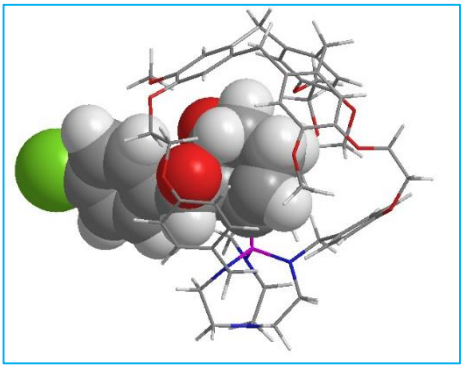

C	2.213263	-0.950161	4.611249
C	-0.091894	-4.920574	0.148629
C	4.714488	-3.948589	0.431489
C	3.618579	-3.128693	0.706525
C	3.721289	-1.738829	0.635201
C	4.960415	-1.182782	0.294875

C	1.997964	-0.187872	-0.419798
C	1.200153	1.144880	-0.284479
C	-0.073697	0.879394	0.553243
C	-0.984520	-0.070110	-0.237322
C	-0.261321	-1.386499	-0.563514
C	-0.600832	-4.819392	1.462683
C	1.122443	-1.206847	-1.124403
C	-3.196513	-4.301109	-1.989757
C	-3.219255	-2.885646	-2.555501
C	-4.226295	-1.944479	-2.267459
C	0.856485	-1.276178	4.689682
C	-4.113441	-0.650750	-2.798028
C	-3.050689	-0.270959	-3.607336
C	-2.072824	-1.225178	-3.938466
C	-2.168829	-2.505503	-3.406290
C	-1.340975	-0.576129	-6.100561
C	-1.950386	-4.540181	1.634667
C	-0.111713	0.002549	-6.775308
C	1.130312	1.368223	-5.196336
C	1.365008	2.675741	-4.742301
C	-0.111421	-0.334344	4.336122
C	2.241815	2.907065	-3.689737
C	2.929359	1.849376	-3.070168
C	2.697211	0.556233	-3.547314
C	1.794060	0.302749	-4.580931
C	3.876319	2.083219	-1.904933
C	3.632956	4.443061	-1.129494
C	-2.832476	-4.340372	0.562521
C	4.436286	5.177017	-0.031010
C	4.702440	4.038794	2.172832
C	0.294407	0.897734	3.826567
C	4.303565	2.566530	1.926396
C	-1.972679	1.829964	-3.552332
C	-5.415924	-2.226228	-1.355384

C	-5.156020	-1.732856	0.059920
C	-5.469139	-0.395647	0.347910
C	-5.165064	0.192860	1.573317
C	-4.463392	-0.565959	2.535888
C	-2.331782	-4.461536	-0.742479
C	-4.202332	-1.905222	2.263628
C	1.649192	1.210271	3.674223
C	-4.558090	-2.520459	1.054683
C	-6.059874	2.306533	0.909201
C	-6.253013	3.698572	1.498473
C	-3.910124	4.260605	1.438373
C	-2.749226	4.119131	2.203854
C	-1.506108	4.078083	1.584689
C	-1.382763	4.199645	0.196292
C	-2.544898	4.406438	-0.553387
C	-0.970950	-4.755968	-0.924461
C	2.603042	0.289704	4.125330
C	-3.802260	4.436358	0.052305
C	-3.438952	1.189838	3.795324
C	-4.277977	-4.008773	0.890877
C	1.786662	-5.205299	-1.289187
C	-0.052599	4.032733	-0.521680
C	1.476498	5.301293	0.883208
C	2.725144	5.511060	1.766052
C	2.050014	2.522829	3.043823
C	-0.175460	-3.385510	4.245263
C	2.505647	-0.854600	0.995993
C	0.801964	-3.990197	3.232023
C	6.069879	-1.978752	0.007889
C	5.930173	-3.364859	0.078181
Cl	7.326317	-4.393537	-0.269902
H	-0.098523	3.138693	-1.146102
H	0.102379	4.868657	-1.221723
H	2.655307	3.108107	3.746867

H	1.154643	3.114964	2.843962
H	4.817344	2.526163	-2.251796
H	4.160828	1.135568	-1.447941
H	1.559949	5.960754	0.008187
H	-0.849370	-2.029671	-1.214923
H	-1.323099	0.414541	-1.163006
H	-1.885729	-0.286574	0.349270
H	-0.051762	-1.898327	0.391116
H	4.630663	-5.028879	0.500440
H	7.028502	-1.540476	-0.252286
H	5.073415	-0.098085	0.275970
H	2.665080	-3.562212	0.980217
H	2.964339	0.025767	1.512467
H	-0.612630	1.793897	0.805749
H	0.230805	0.371435	1.469797
H	2.871268	-0.053958	-1.042218
H	0.910372	1.442670	-1.304242
H	2.697901	4.970781	-1.335969
H	4.209398	4.493737	-2.056685
H	-1.380285	-3.209544	-3.654614
H	-4.213172	-4.649506	-1.792802
H	-2.801042	-4.968505	-2.764381
H	-4.952908	-4.438852	0.146888
H	-4.534356	-4.501036	1.836528
H	-0.593886	-4.845720	-1.936383
H	-2.326026	-4.512633	2.653289
H	1.651191	-4.414538	3.776344
H	1.159472	-3.216711	2.540611
H	-6.625899	4.371688	0.712536
H	-6.995705	3.663418	2.298709
H	4.423484	6.251499	-0.283000
H	5.481149	4.852280	-0.088954
H	-2.245589	2.142779	-2.534070
H	-1.011382	1.308692	-3.530853

H	-1.884872	2.708438	-4.196660
H	-0.621009	-4.174123	4.859268
H	-0.978239	-2.841632	3.732066
H	-7.038970	1.945788	0.557232
H	-5.378610	2.328023	0.049208
H	-2.845816	4.007306	3.278131
H	-4.687635	4.586370	-0.556277
H	-0.623183	3.906837	2.188760
H	-2.477035	4.523833	-1.632992
H	4.633775	1.917919	2.742519
H	2.530151	5.125370	2.767538
H	2.784894	6.610895	1.867004
H	-1.165797	-0.581112	4.421153
H	-0.459476	1.617120	3.514903
H	3.663091	0.515338	4.049079
H	2.943459	-1.696666	4.904732
H	4.780053	2.196719	1.017163
H	5.784697	4.152786	2.027201
H	4.507596	4.307588	3.217567
H	2.384206	3.929913	-3.357149
H	0.840751	3.492942	-5.228226
H	1.573191	-0.725857	-4.830413
H	3.167331	-0.300688	-3.077338
H	-0.347299	0.194324	-7.827384
H	0.730320	-0.696756	-6.738112
H	-1.666690	-1.478499	-6.640697
H	-2.147466	0.163394	-6.121267
H	-4.866182	0.100553	-2.577233
H	-5.985145	0.182956	-0.409584
H	-3.698354	-2.474519	3.039140
H	-2.755671	1.303303	2.944747
H	-4.165065	2.005949	3.774855
H	-2.865328	1.214863	4.725749
H	-5.670372	-3.287469	-1.363974

H	-6.292028	-1.704682	-1.758795
H	0.624018	5.680647	1.458706
H	1.642073	-4.233740	-1.774552
H	1.355575	-6.008970	-1.902701
H	2.853686	-5.384883	-1.157239
N	3.364838	3.012398	-0.859510
N	3.990475	4.969421	1.322230
N	1.109284	3.947998	0.383052
N	2.850082	2.452589	1.782704
O	0.198754	-5.104737	2.540234
O	1.582725	-1.916942	-2.015123
O	1.550237	-1.450034	1.689184
O	-1.002910	-0.910706	-4.750497
O	0.238910	1.272815	-6.226788
O	-3.004191	1.012513	-4.114593
O	-5.535770	1.469251	1.922613
O	-5.088568	4.230198	2.129354
O	-4.083269	-0.086351	3.761807
O	1.229207	-5.210523	0.023925
O	0.516523	-2.520539	5.161374
P	2.164265	2.632709	0.273577

NMR spectra

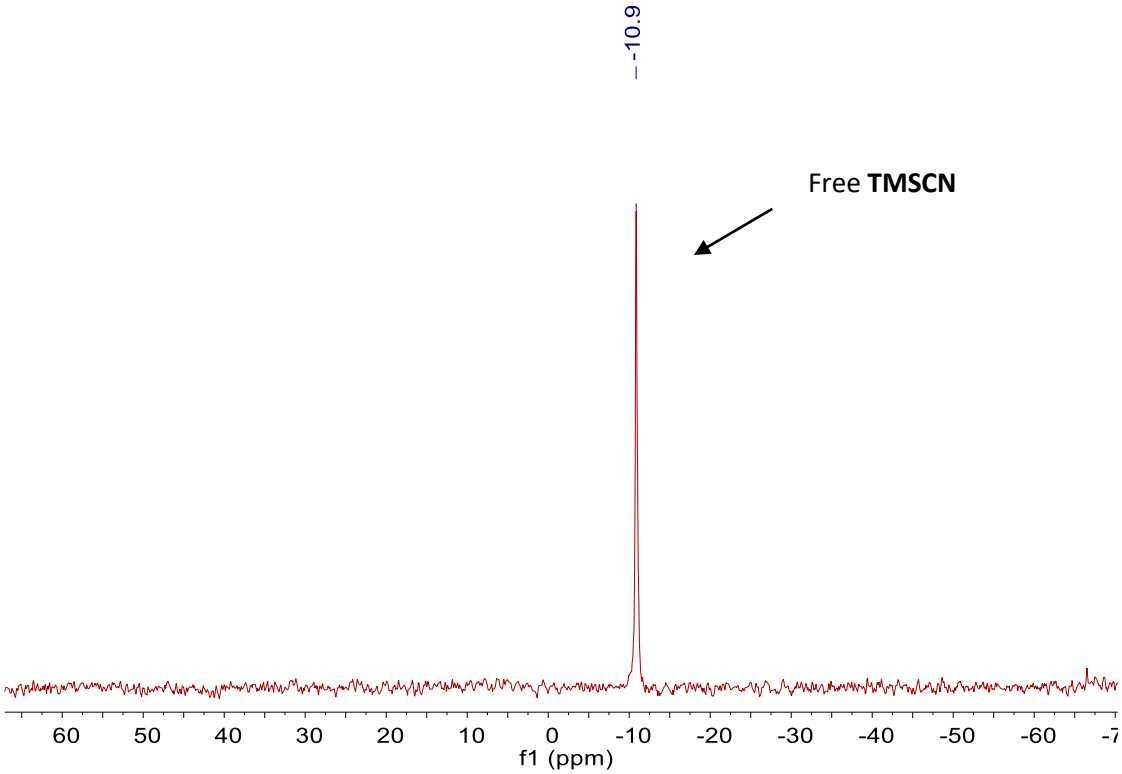

Figure S12. ^{29}Si (298K, 79.5 MHz) spectrum of TMSCN.

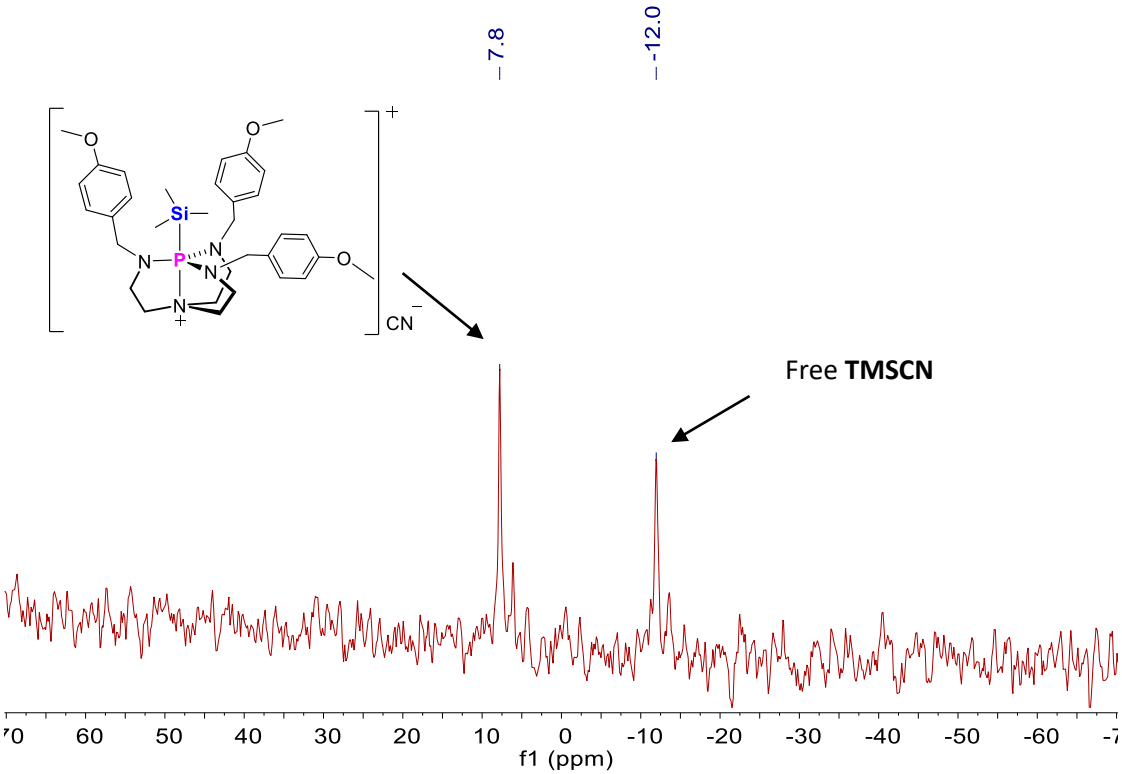

Figure S13. ^{29}Si (298K, 79.5 MHz) spectrum of equimolar **1e** with TMSCN.

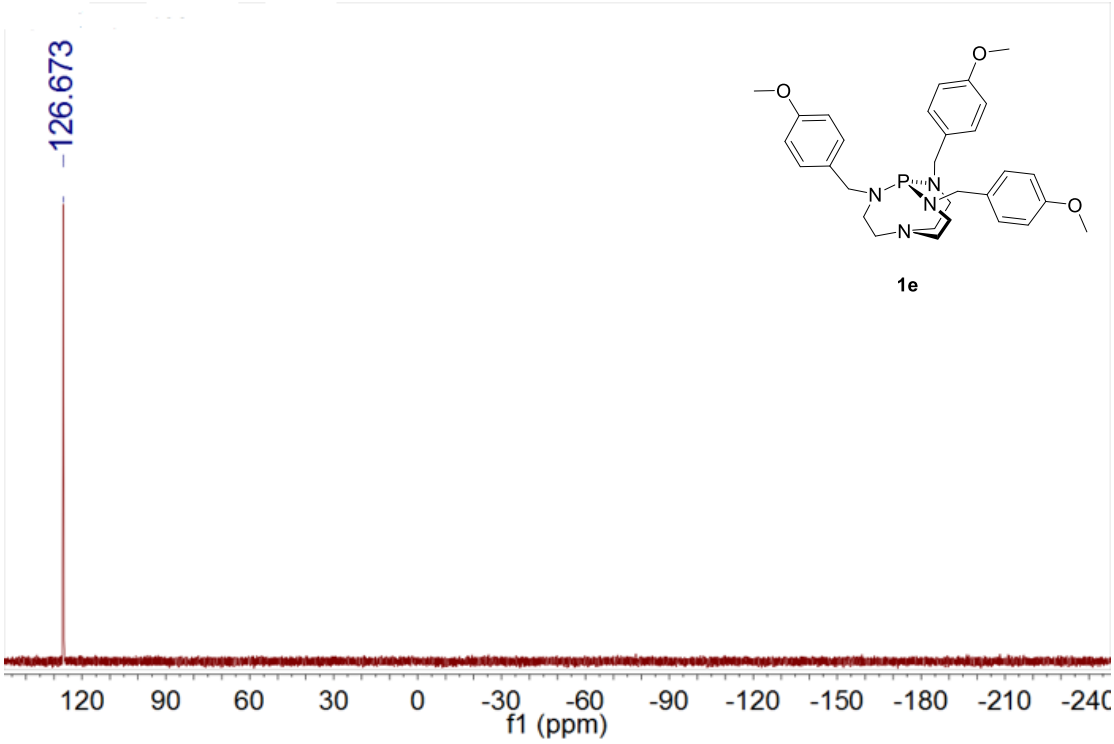

Figure S14. ^{31}P NMR (298K, CD_2Cl_2, 162 MHz) spectrum of **1e**.

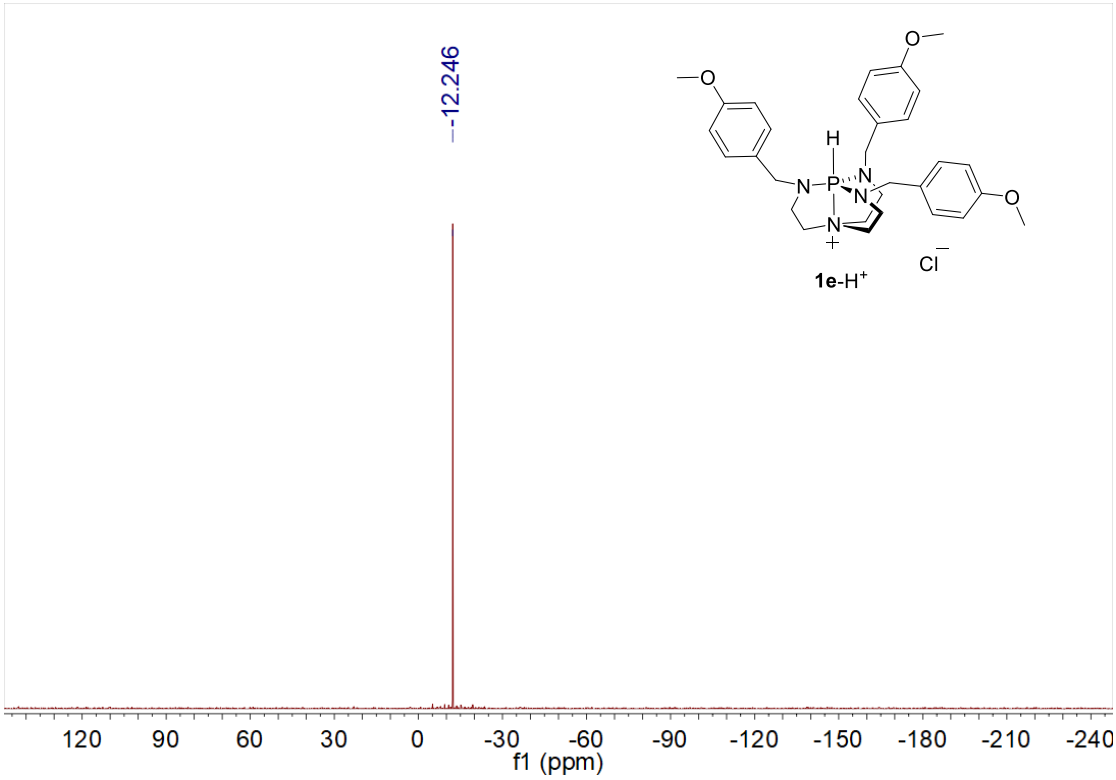

Figure S15. $^{31}P\{^1H\}$ NMR (298K, CD_2Cl_2, 162 MHz) spectrum of **1e**-H^+.

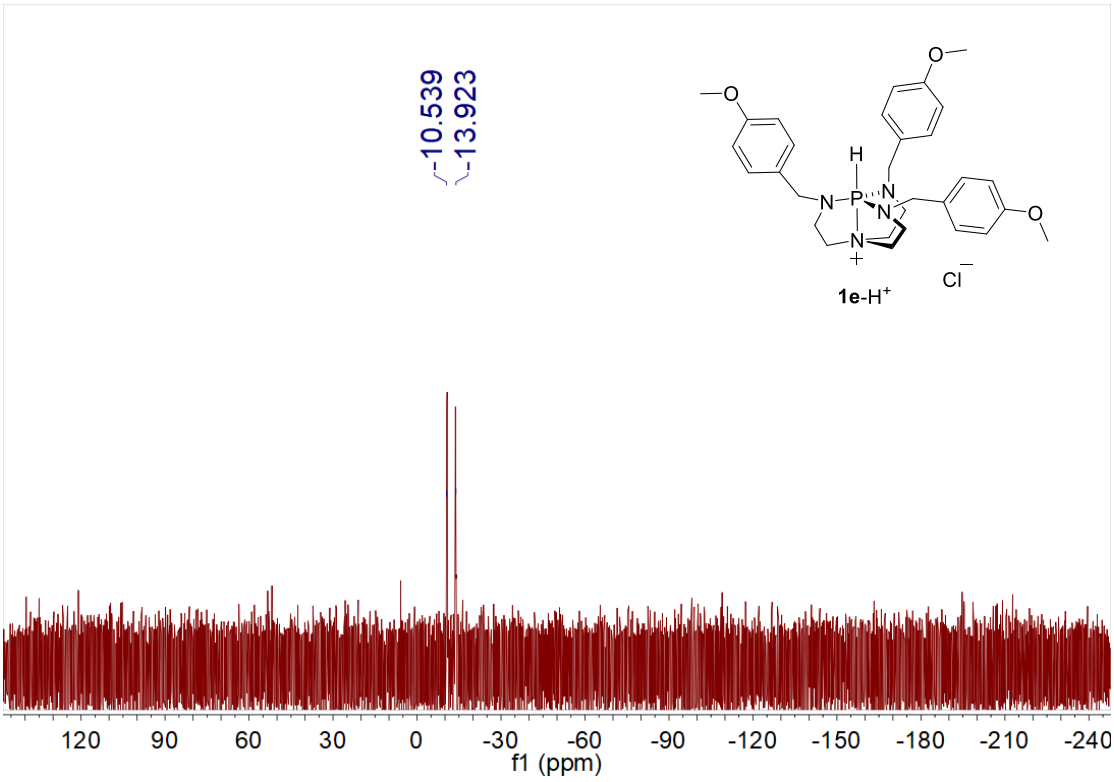

Figure S16. ^{31}P NMR (298K, CD_2Cl_2, 162 MHz) spectrum of **1e**-H^+.

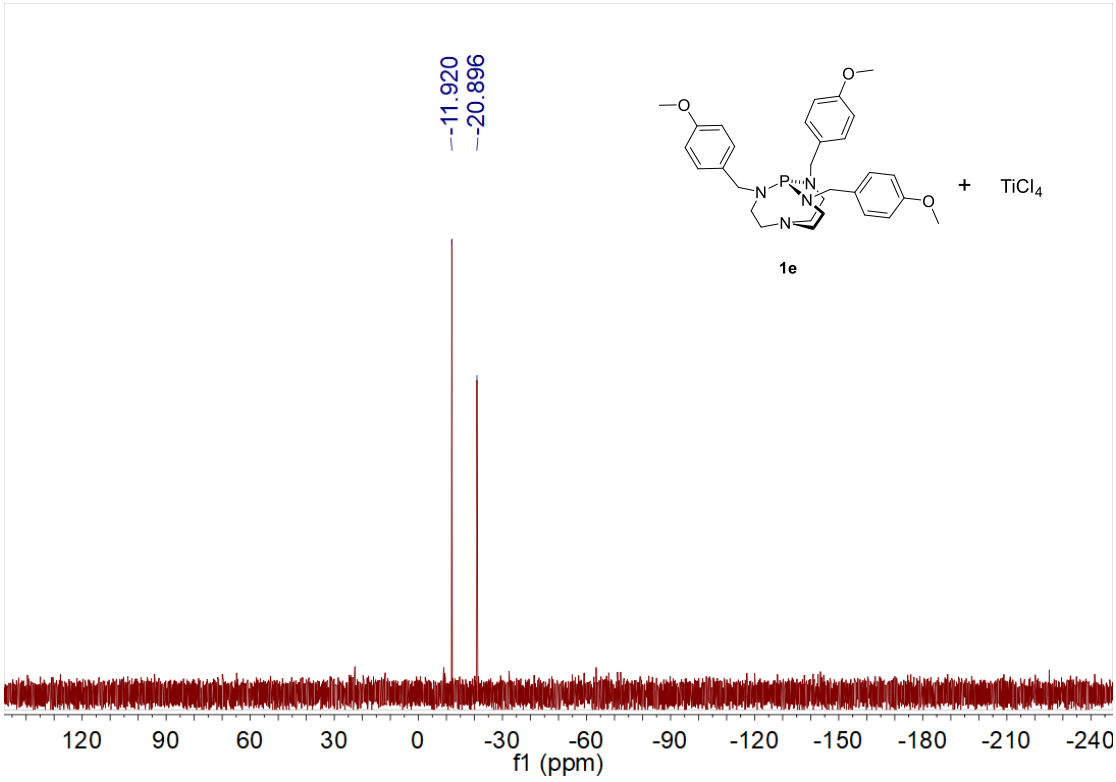

Figure S17. $^{31}P\{^1H\}$ NMR (298K, CD_2Cl_2, 162 MHz) spectrum of the reaction of **1e** with $TiCl_4$.

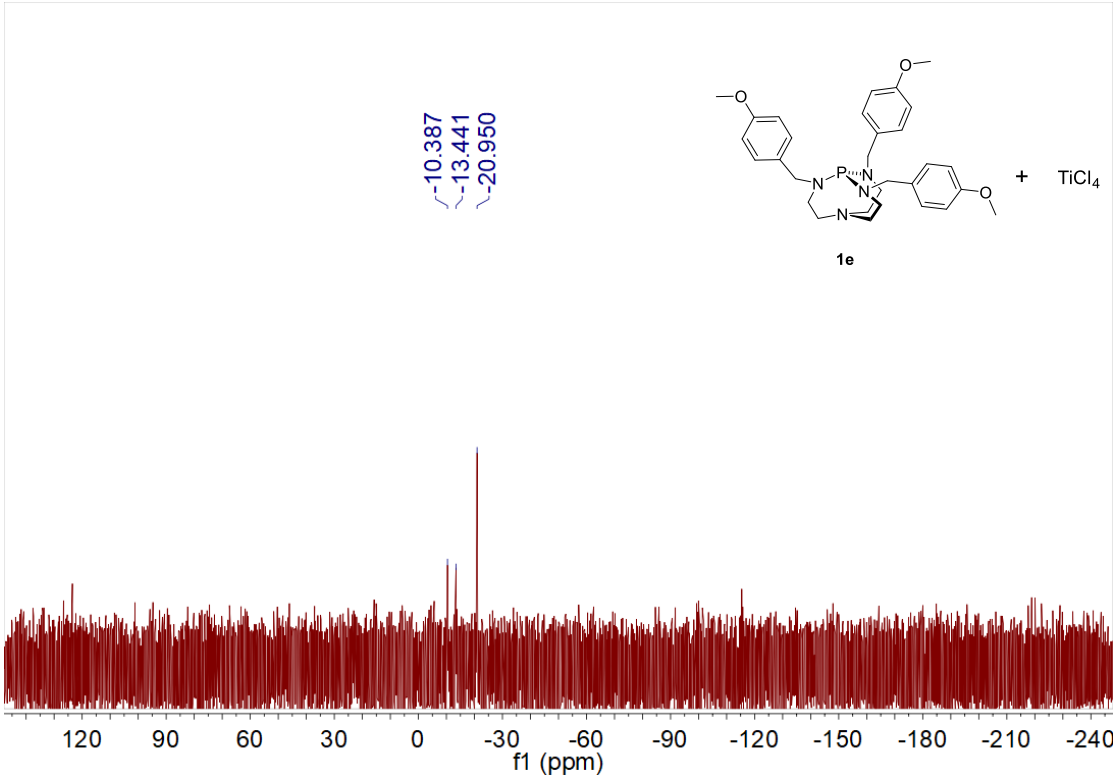

Figure S18. ^{31}P NMR (298K, CD_2Cl_2, 162 MHz) spectrum of the reaction of **1e** with $TiCl_4$.

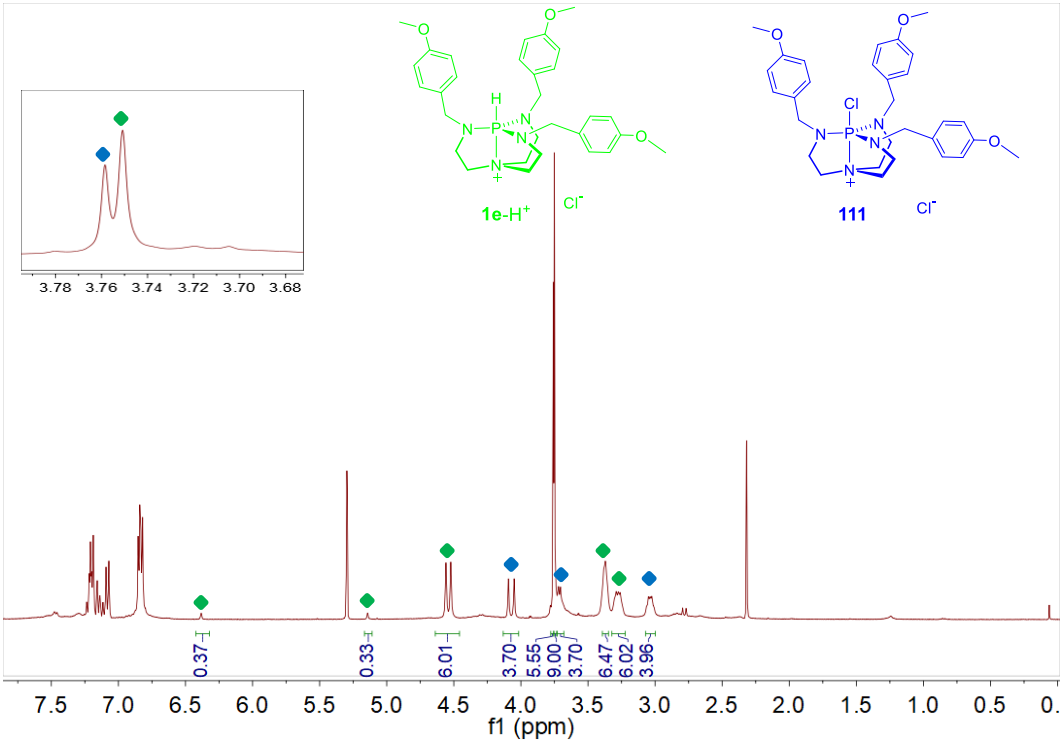

Figure S19. ^{1}H NMR (298K, CD_2Cl_2, 400 MHz) spectrum of the reaction of **1e** with $TiCl_4$. Green color represents signals from **1e**-H^+, and blue color for **111**.

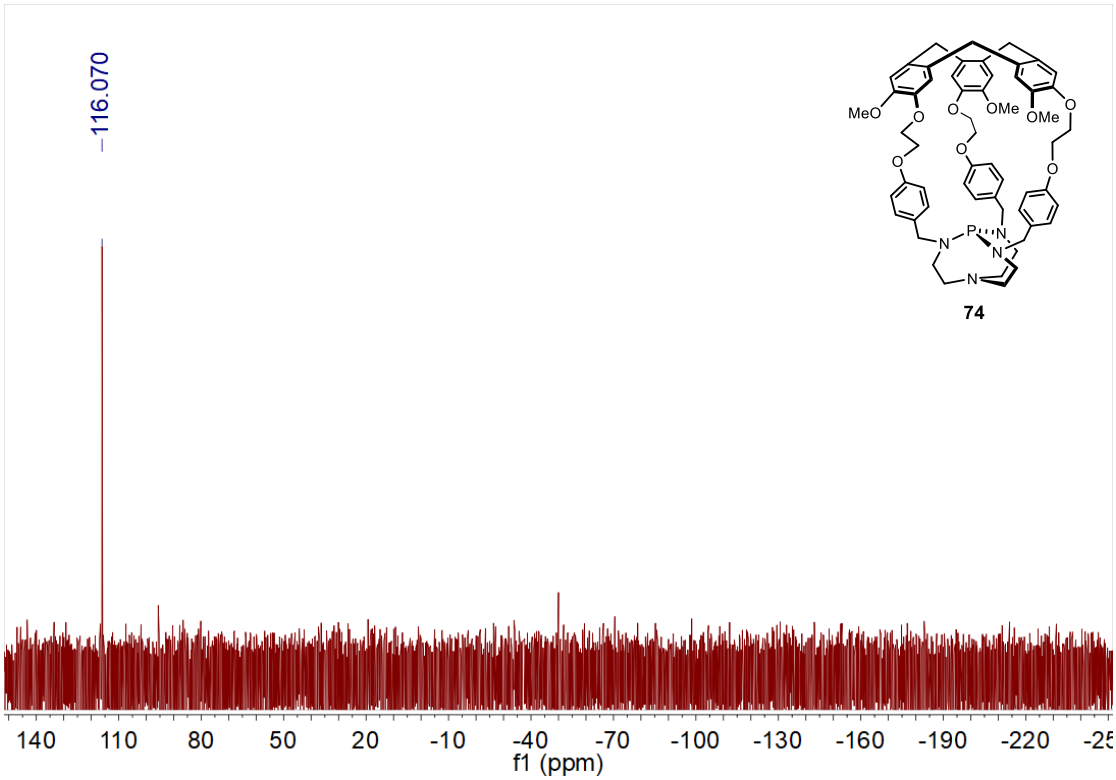

Figure S20. ^{31}P NMR (298K, CD_2Cl_2, 162 MHz) spectrum of **74**.

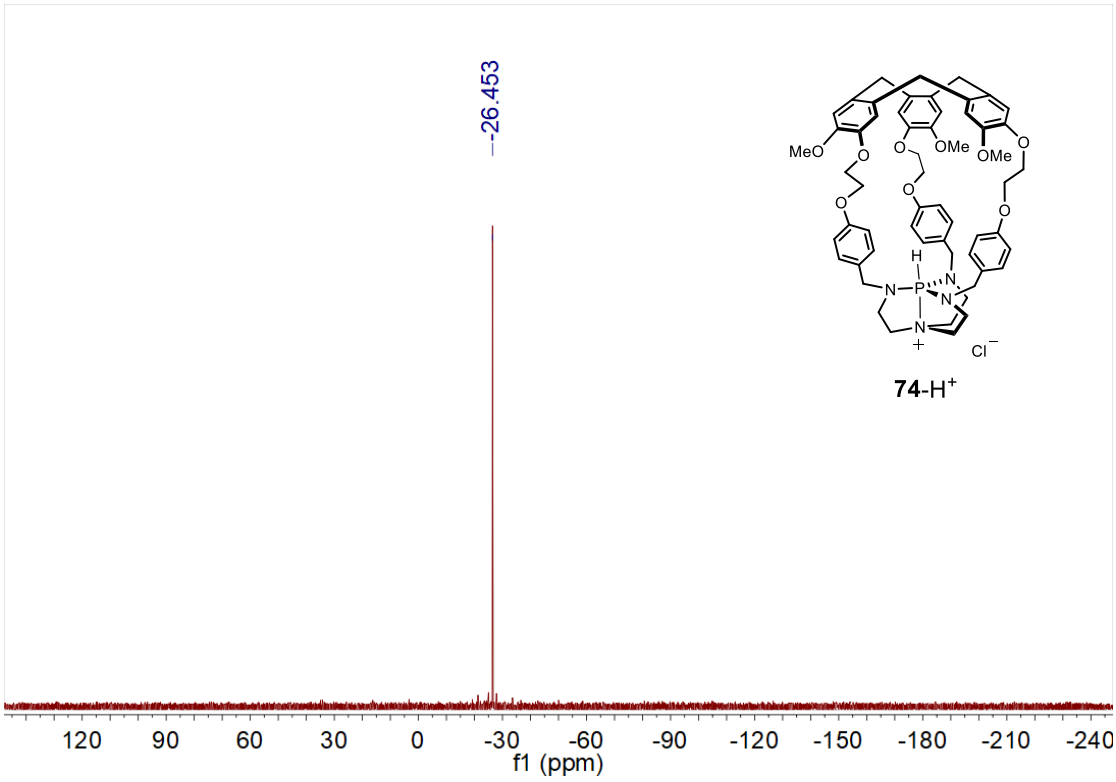

Figure S21. $^{31}P\{^1H\}$ NMR (298K, CD_2Cl_2, 162 MHz) spectrum of **74**-H^+.

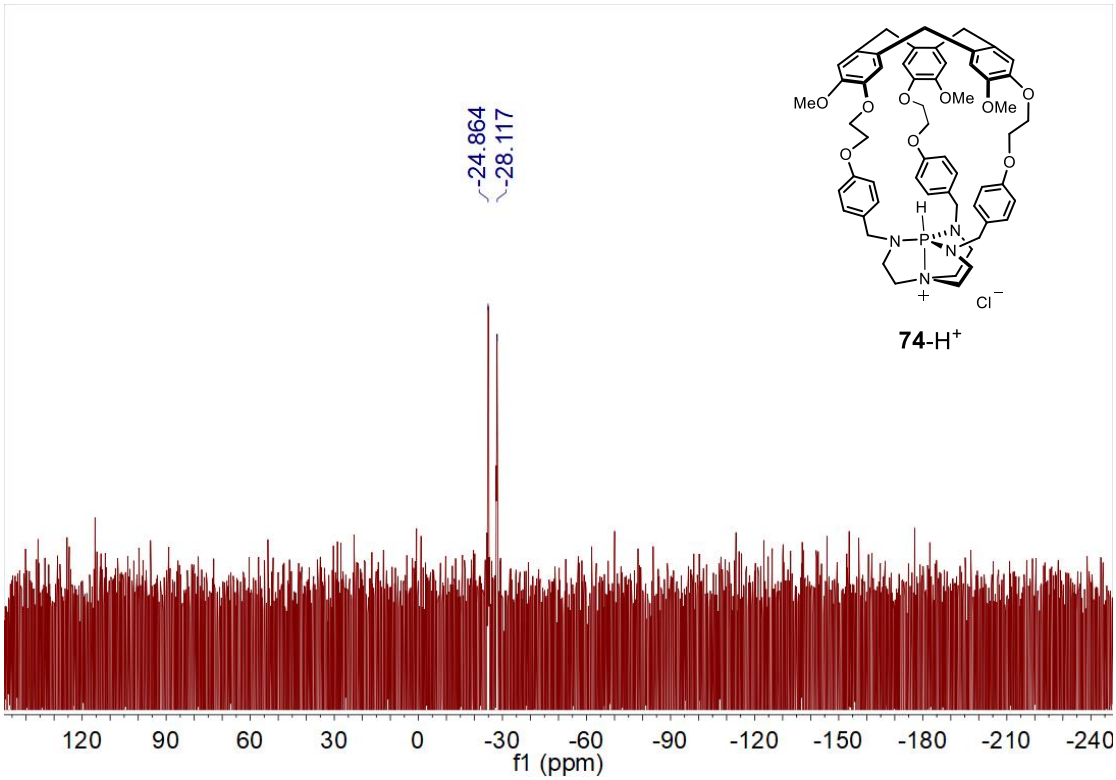

Figure S22. ^{31}P NMR (298K, CD_2Cl_2, 162 MHz) spectrum of **74**-H^+.

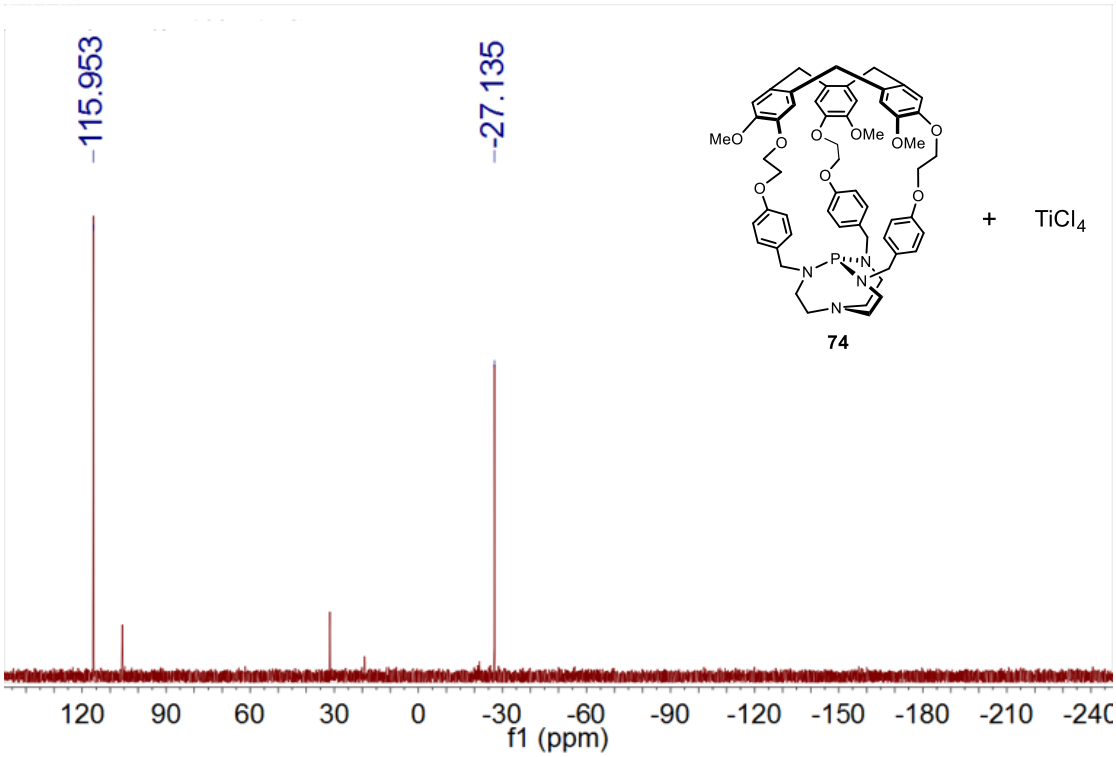

Figure S23. $^{31}P\{^1H\}$ NMR (298K, CD_2Cl_2, 162 MHz) spectrum of **74** with $TiCl_4$.

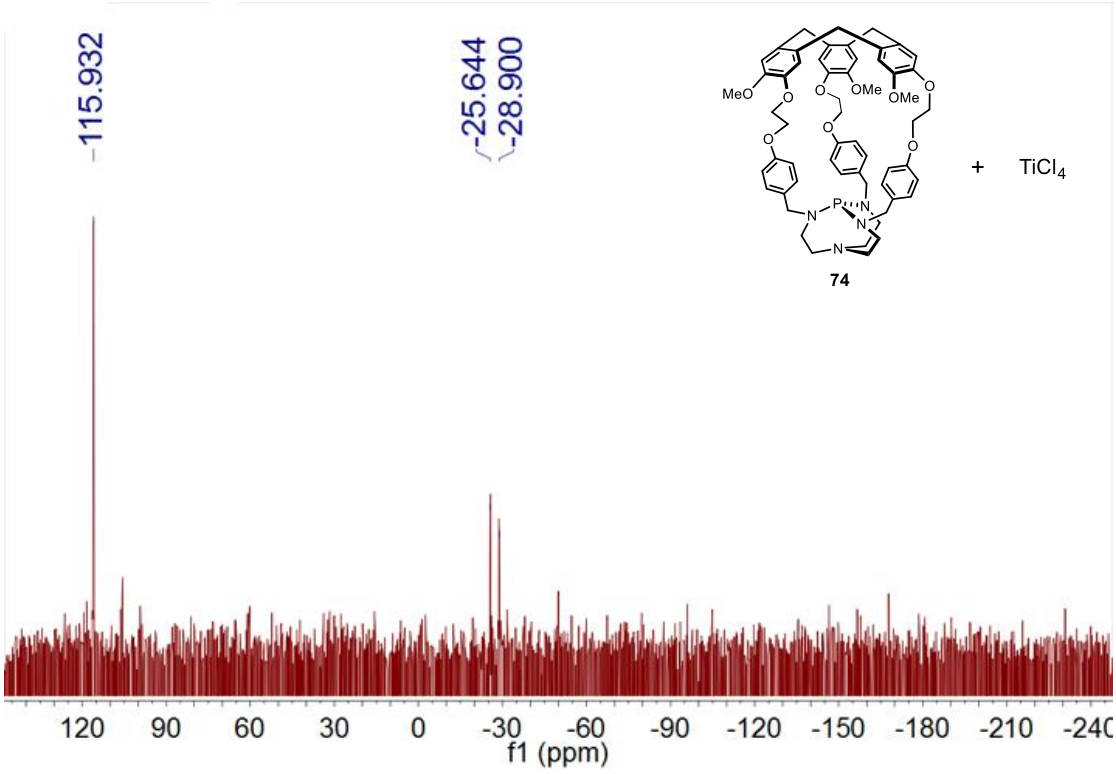

Figure S24. ^{31}P NMR (298K, CD_2Cl_2, 162 MHz) spectrum of **74** with $TiCl_4$.

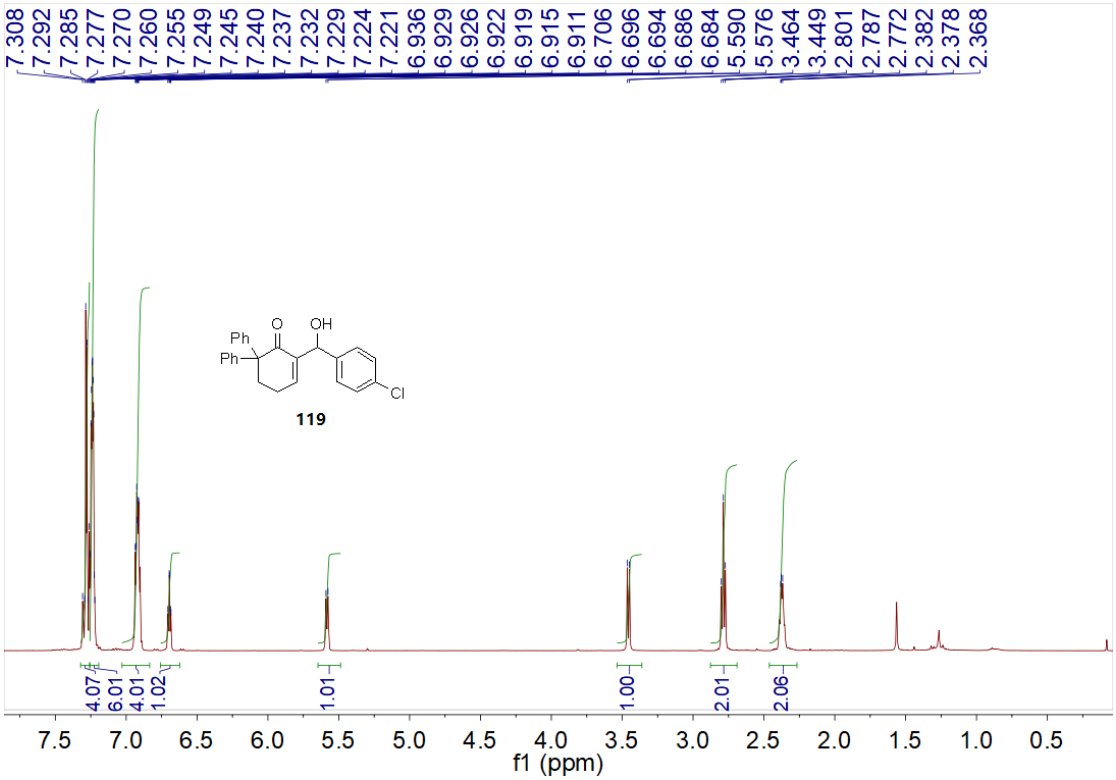

Figure S25. ^{1}H NMR (298K, $CDCl_3$, 400 MHz) spectrum of **119**.

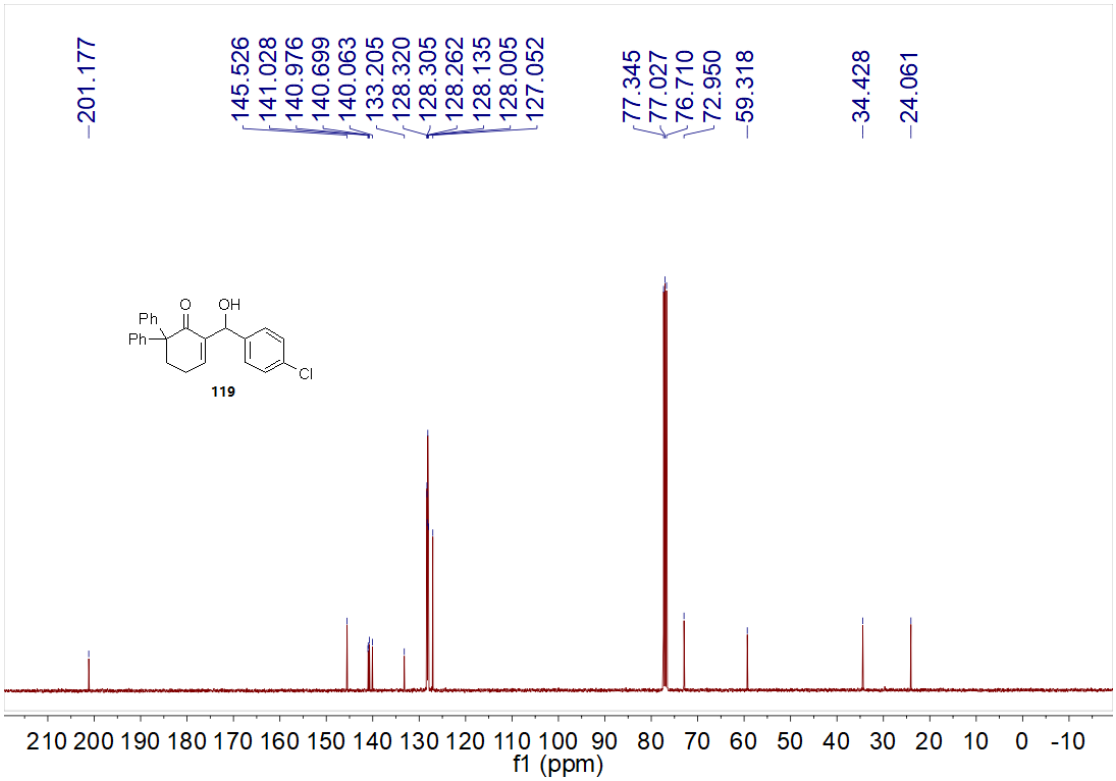

Figure S26. ^{13}C NMR (298K, $CDCl_3$, 101 MHz) spectrum of **119**.

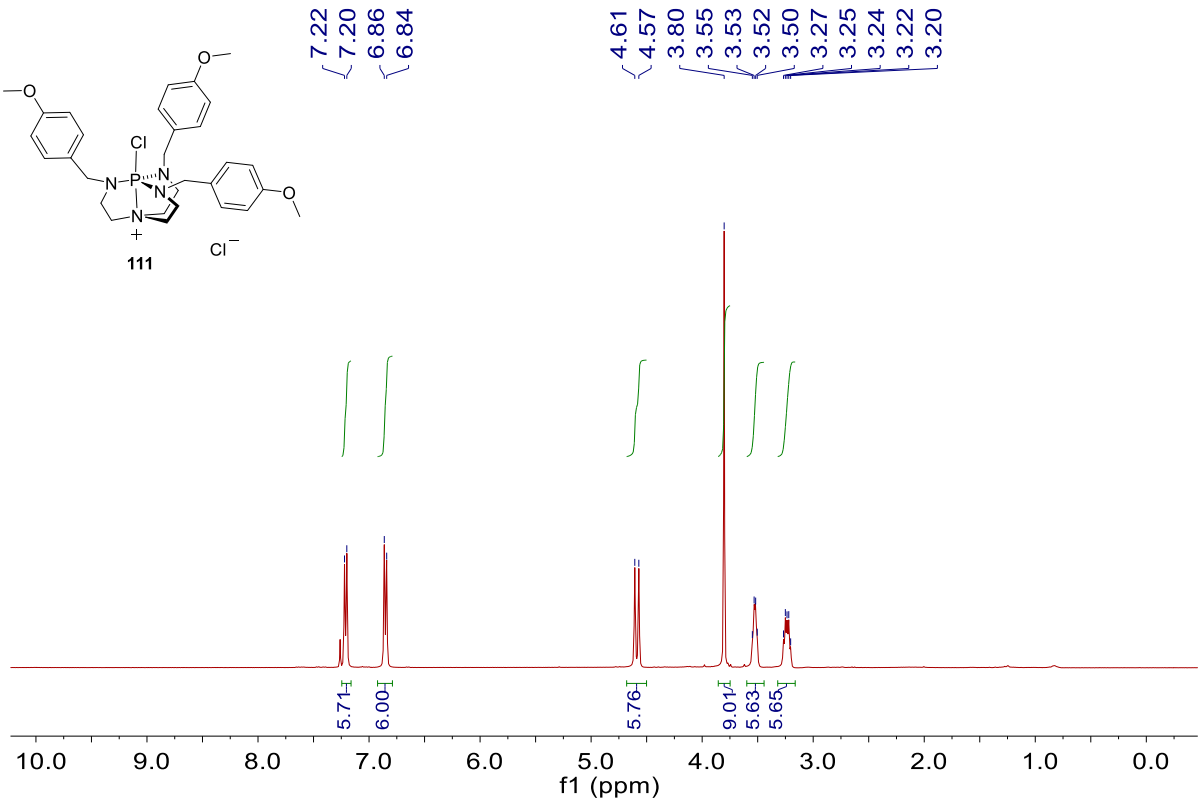

Figure S27. ^{1}H NMR (298K, $CDCl_3$, 400 MHz) spectrum of **111**.

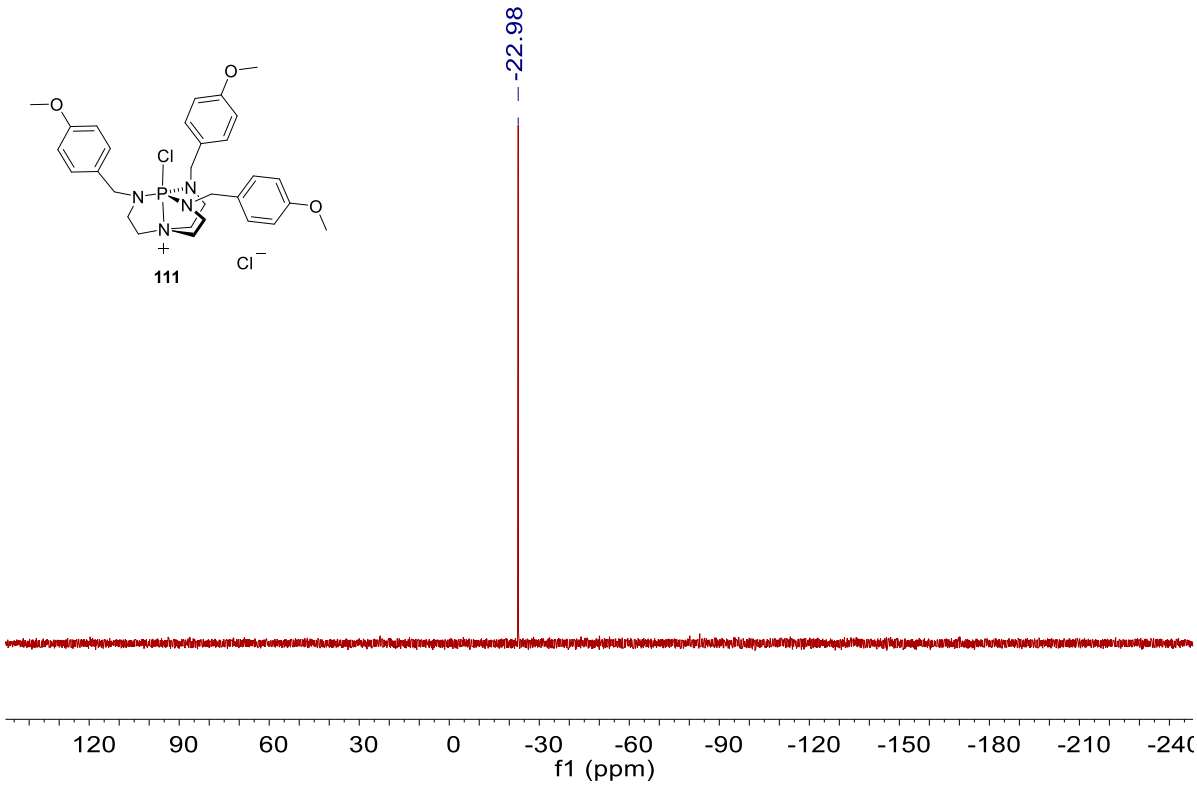

Figure S28. ^{31}P NMR (298K, $CDCl_3$, 162 MHz) spectrum of **111**.

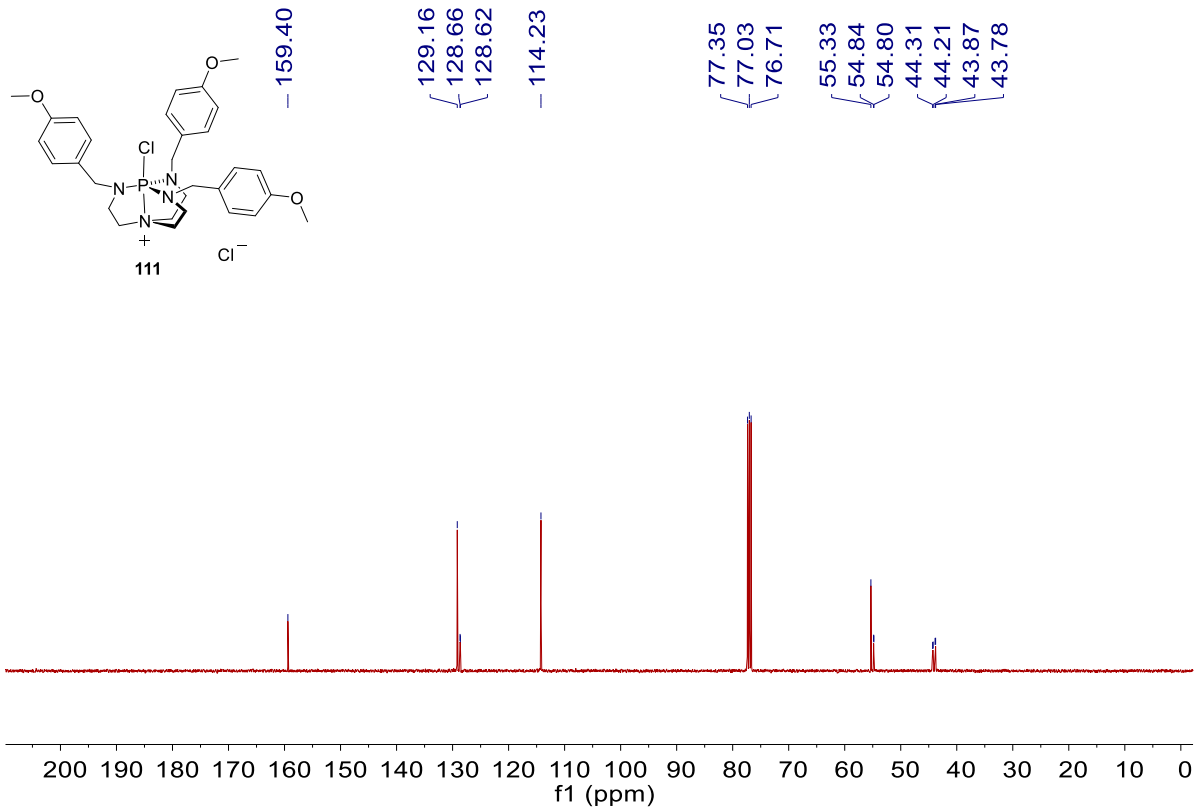

Figure S29. ^{13}C NMR (298K, $CDCl_3$, 101 MHz) spectrum of **111**.

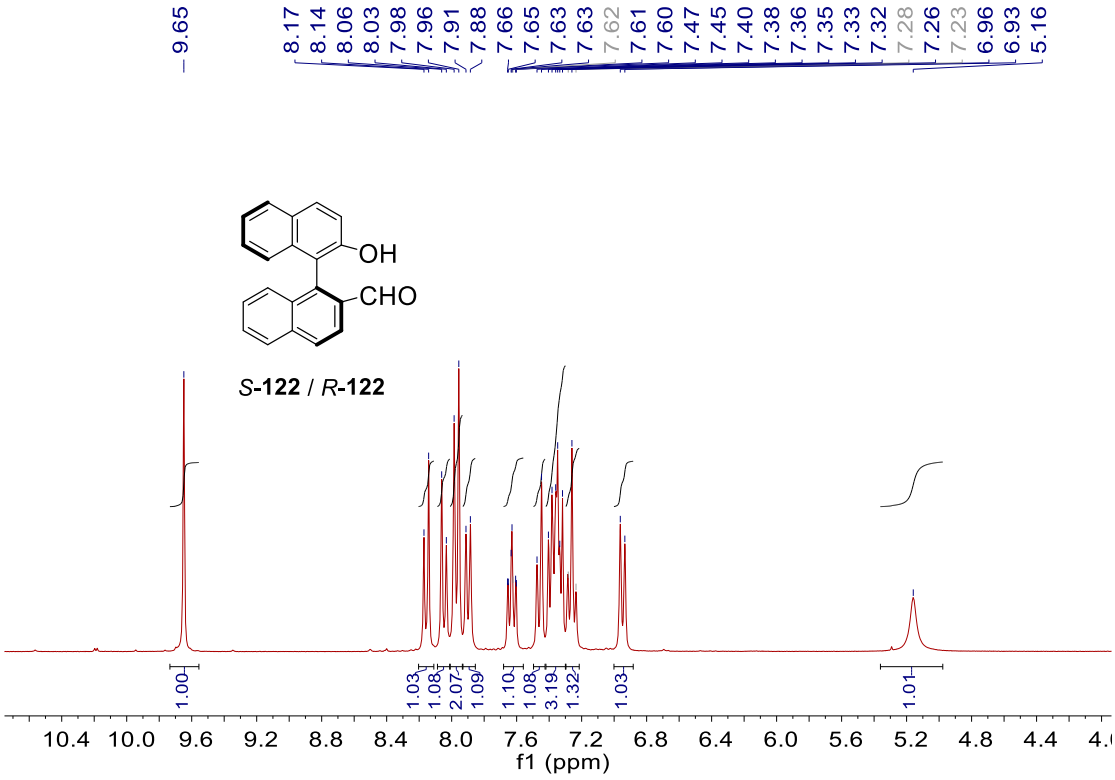

Figure S30. ^{1}H NMR (298K, $CDCl_3$, 300 MHz) spectrum of *S*-122/*R*-122.

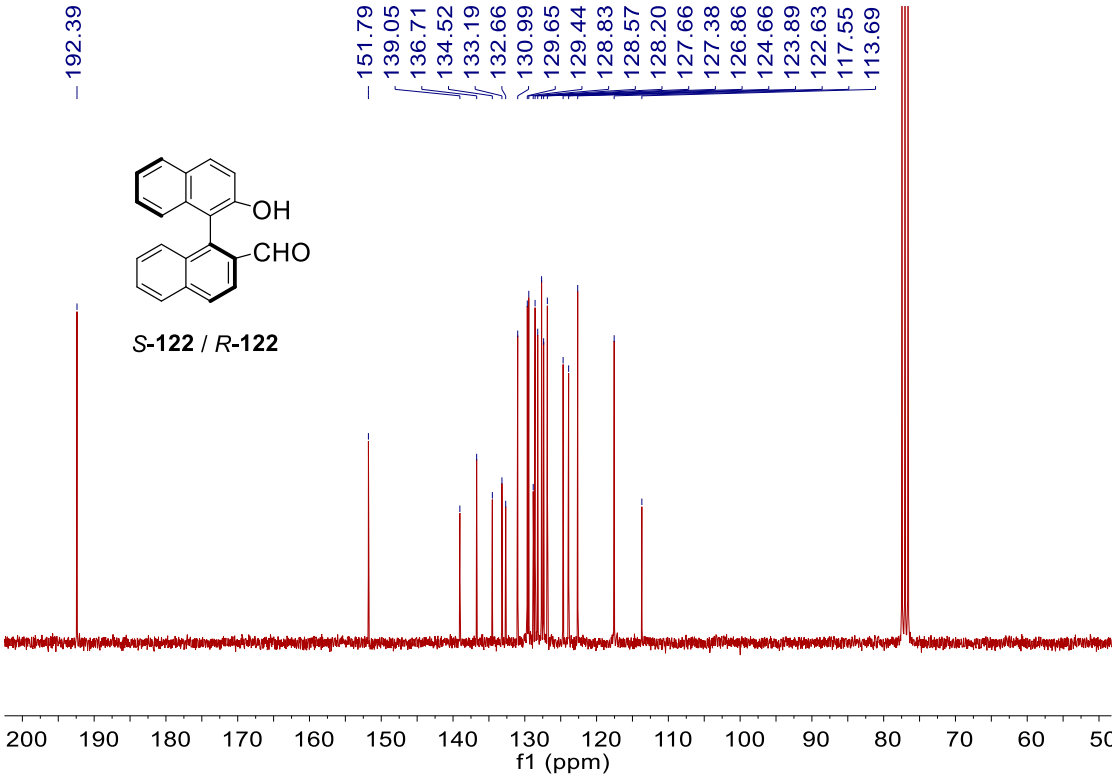

Figure S31. ^{13}C NMR (298K, $CDCl_3$, 75 MHz) spectrum of *S*-**122**/*R*-**122**.

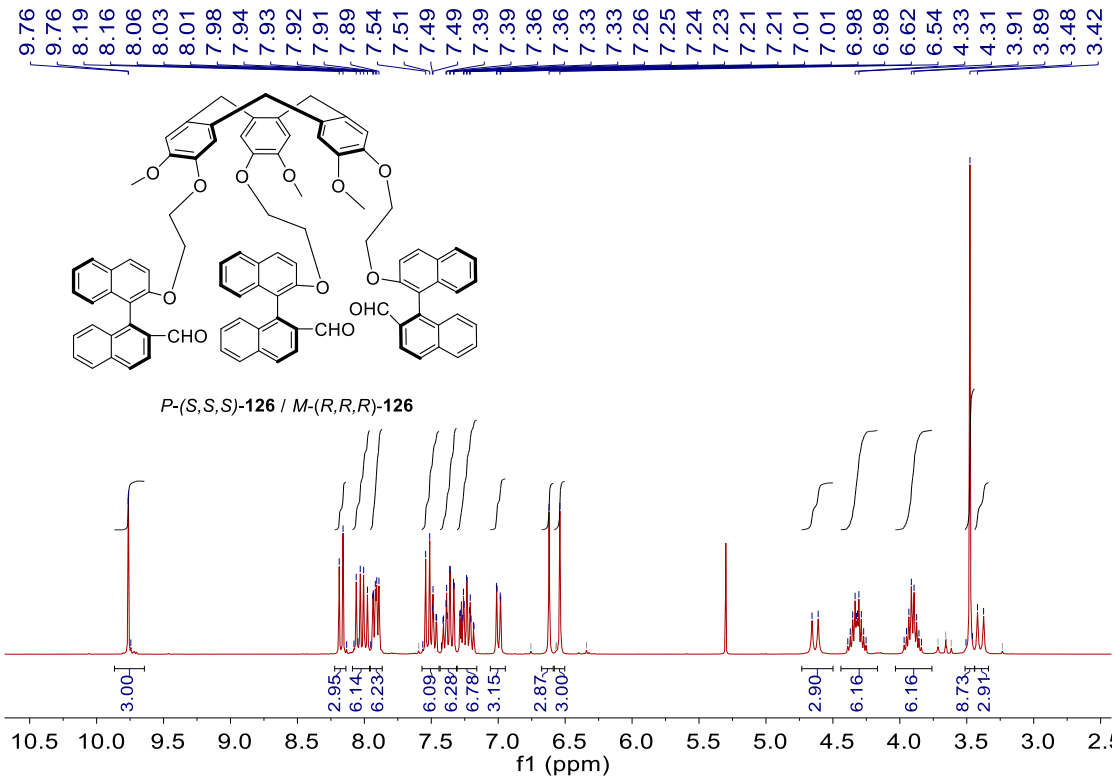

Figure S32. ^{1}H NMR (298K, $CDCl_3$, 300 MHz) spectrum of *P*-*S*,*S*,*S*-**126**.

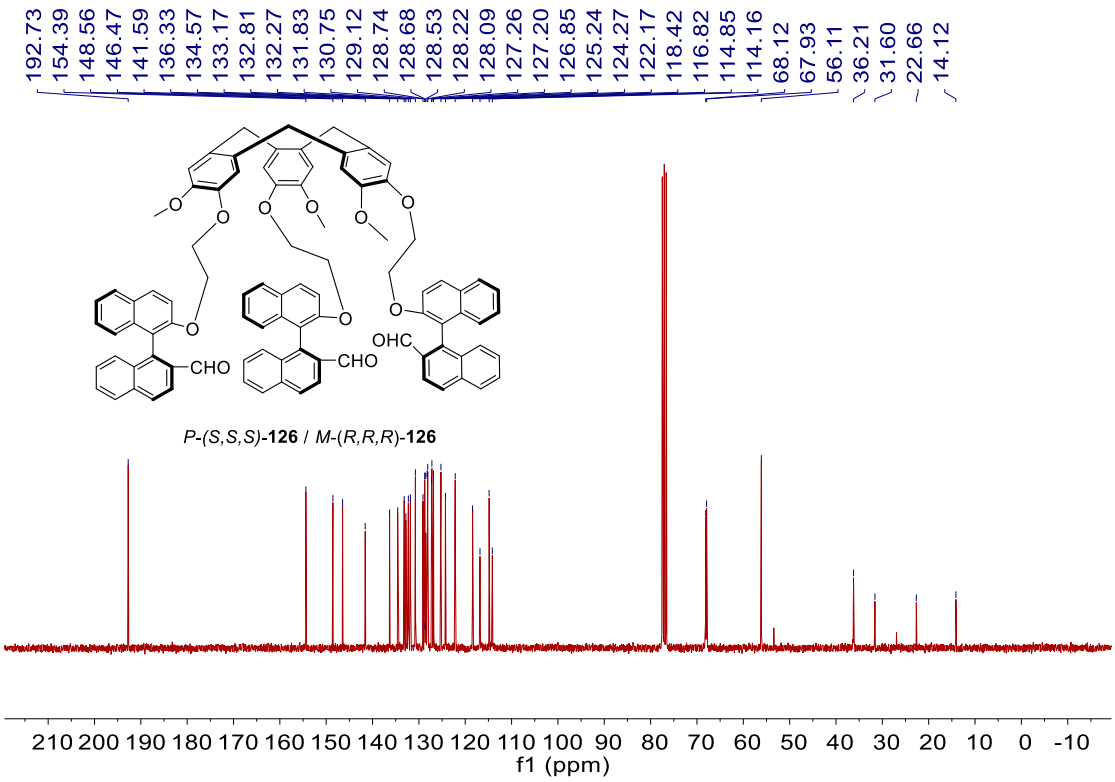

Figure S33. ^{13}C NMR (298K, $CDCl_3$, 75 MHz) spectrum of *P*-*S*,*S*,*S*-**126**.

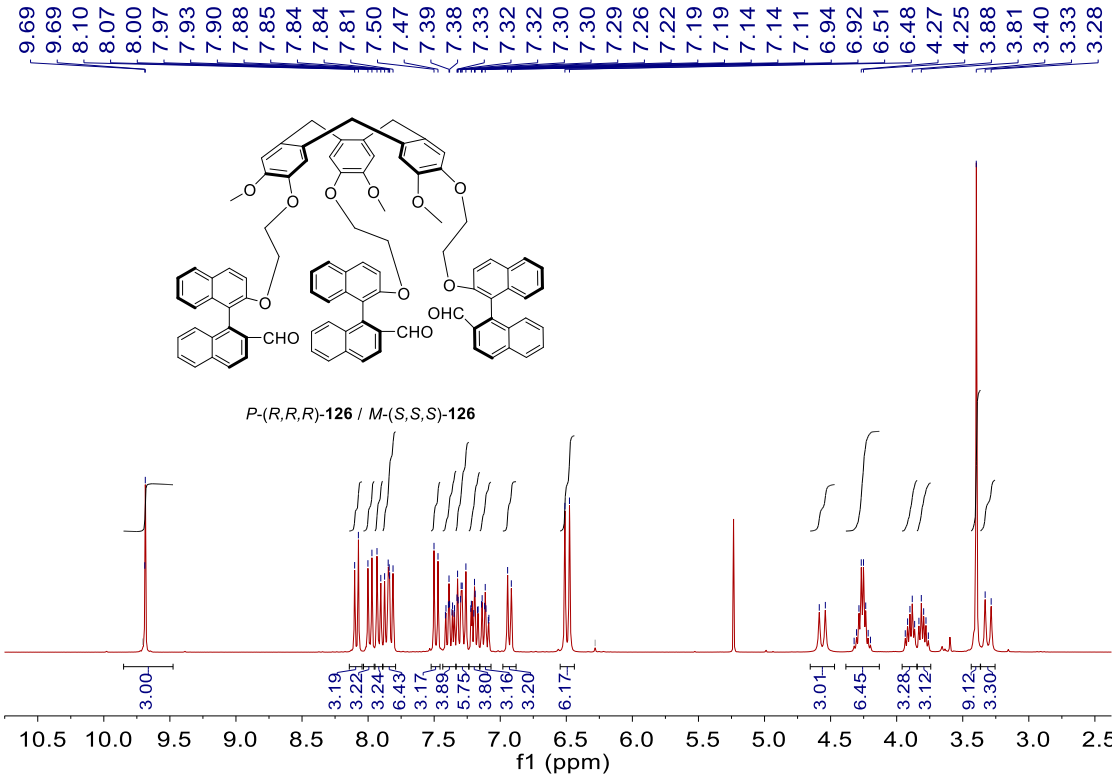

Figure S34. ^{1}H NMR (298K, $CDCl_3$, 300 MHz) spectrum of *P*-*R*,*R*,*R*-**126**.

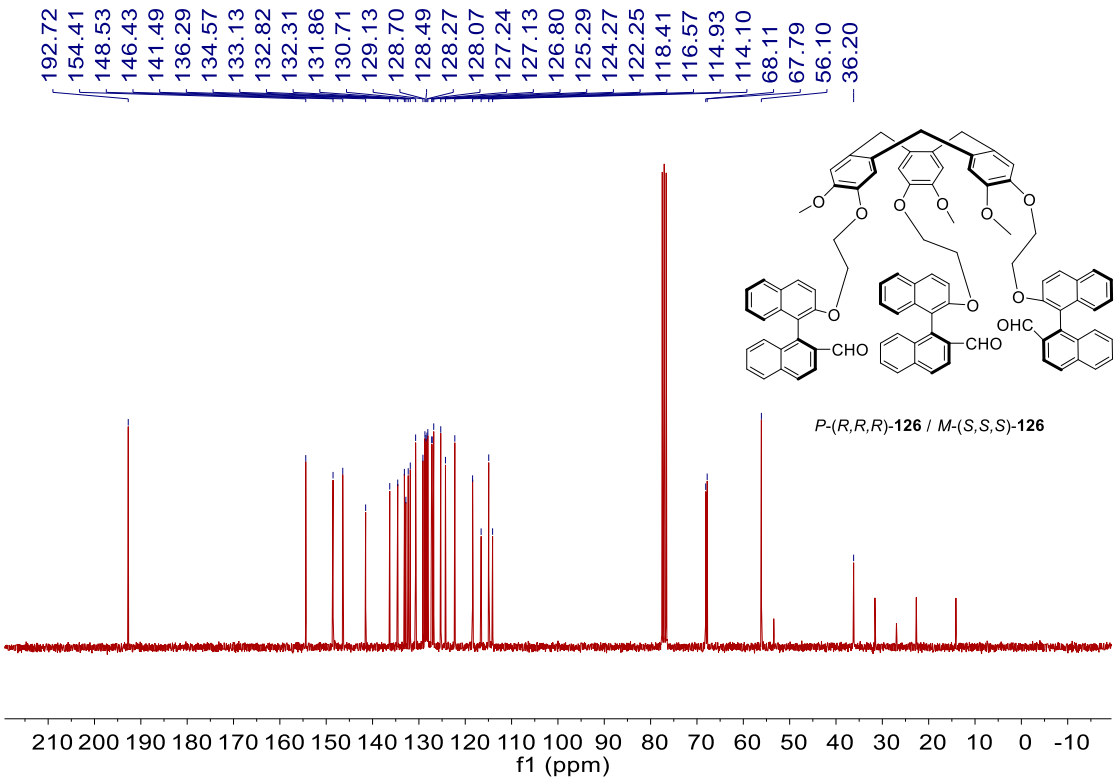

Figure S35. ^{13}C NMR (298K, $CDCl_3$, 75 MHz) spectrum of *P*-*R*,*R*,*R*-**126**.

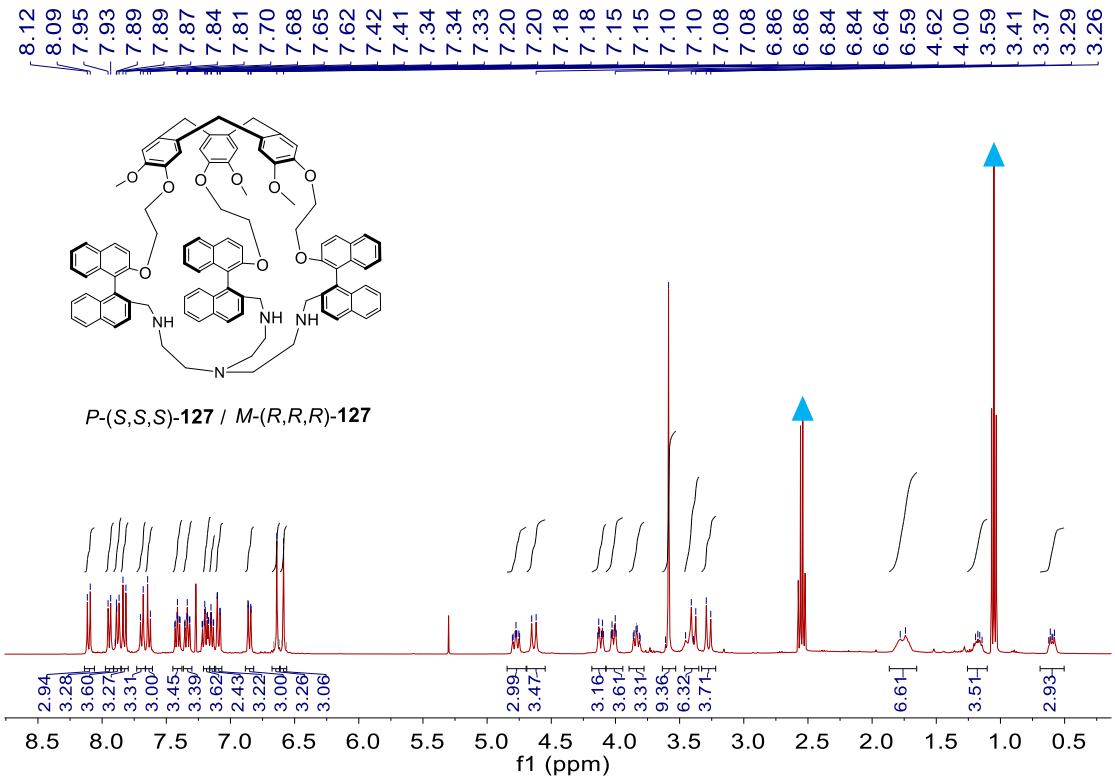

Figure S36. ^{1}H NMR (298K, $CDCl_3$, 400 MHz) spectrum of *P*-*S*,*S*,*S*-**127**. ▲ : Et_3N.

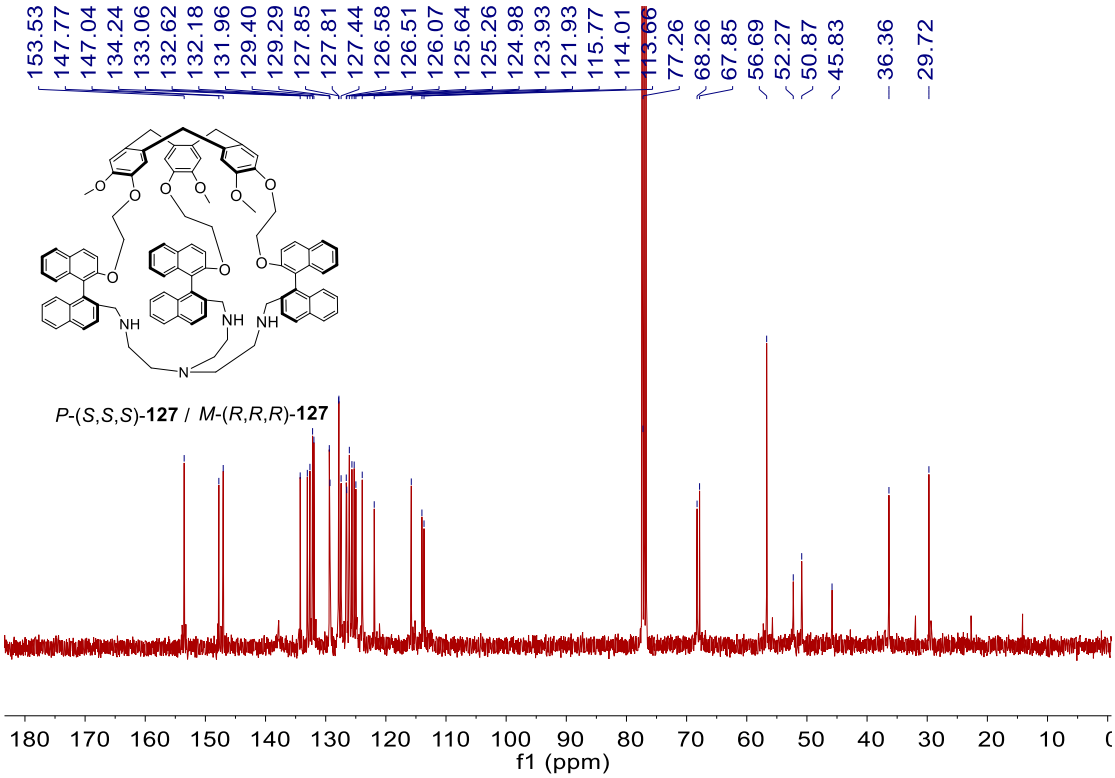

Figure S37. ^{13}C NMR (298K, $CDCl_3$, 101 MHz) spectrum of *M*-*R*,*R*,*R*-**127**.

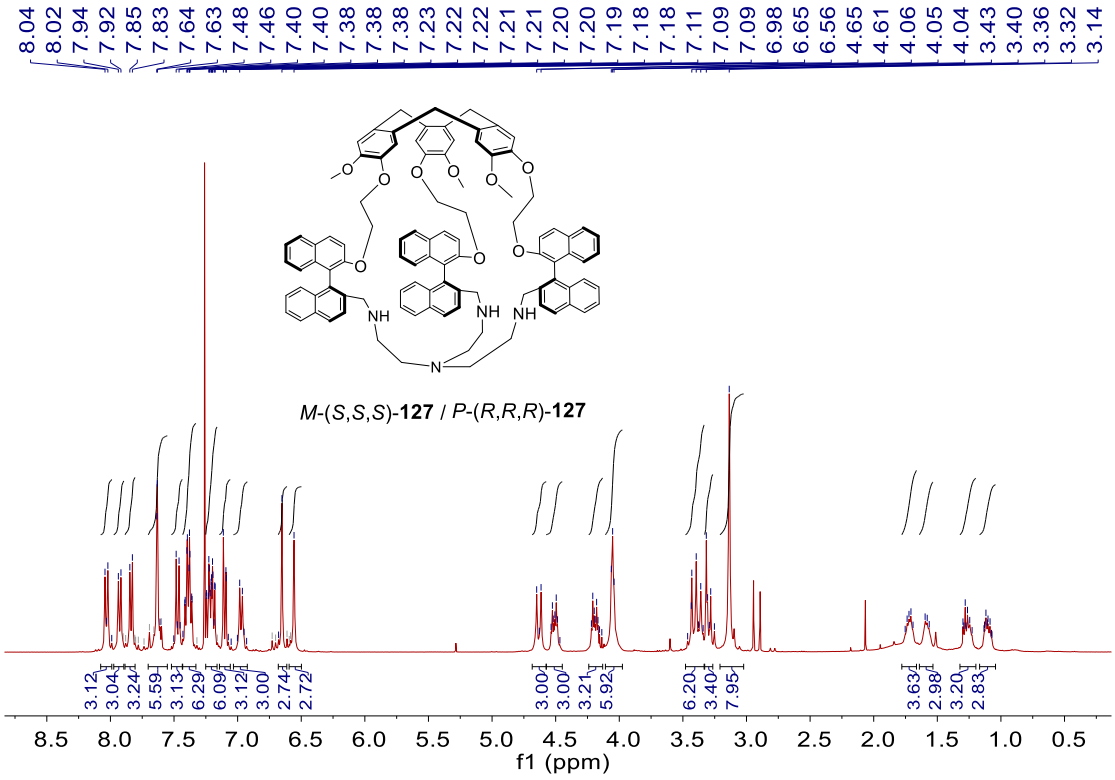

Figure S38. ^{1}H NMR (298K, $CDCl_3$, 400 MHz) spectrum of *M*-*S*,*S*,*S*-**127**.

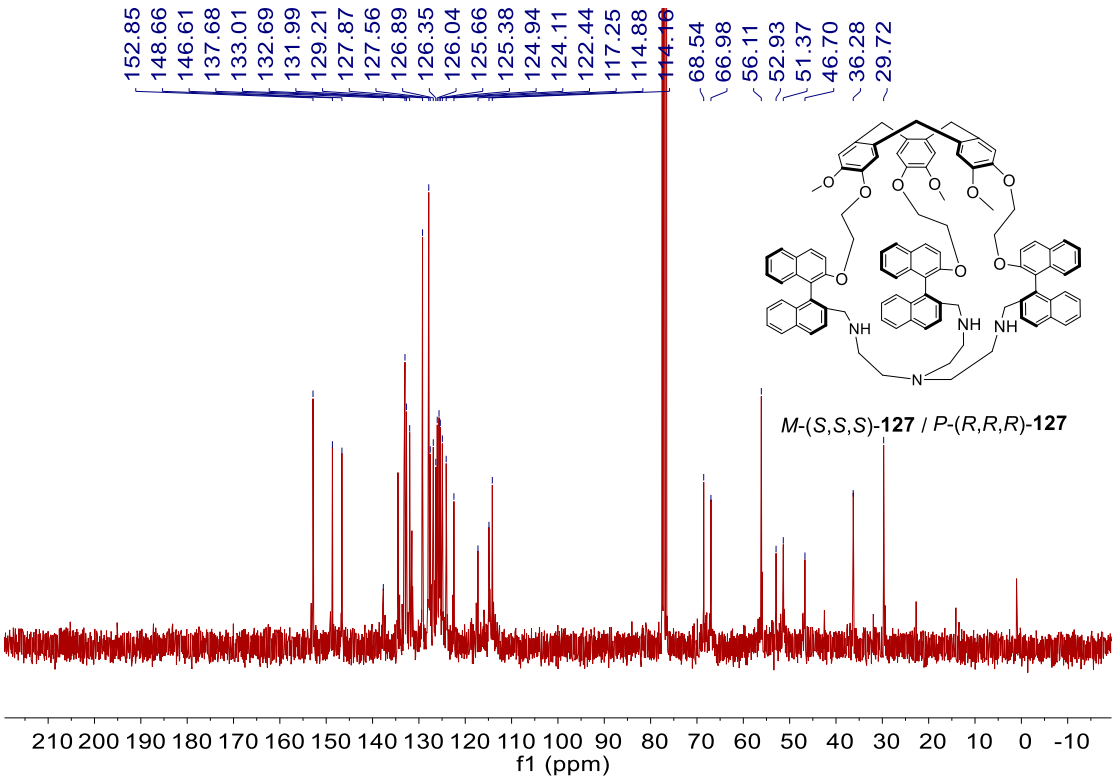

Figure S39. ^{13}C NMR (298K, $CDCl_3$, 75 MHz) spectrum of *P*-*R*,*R*,*R*-**127**.

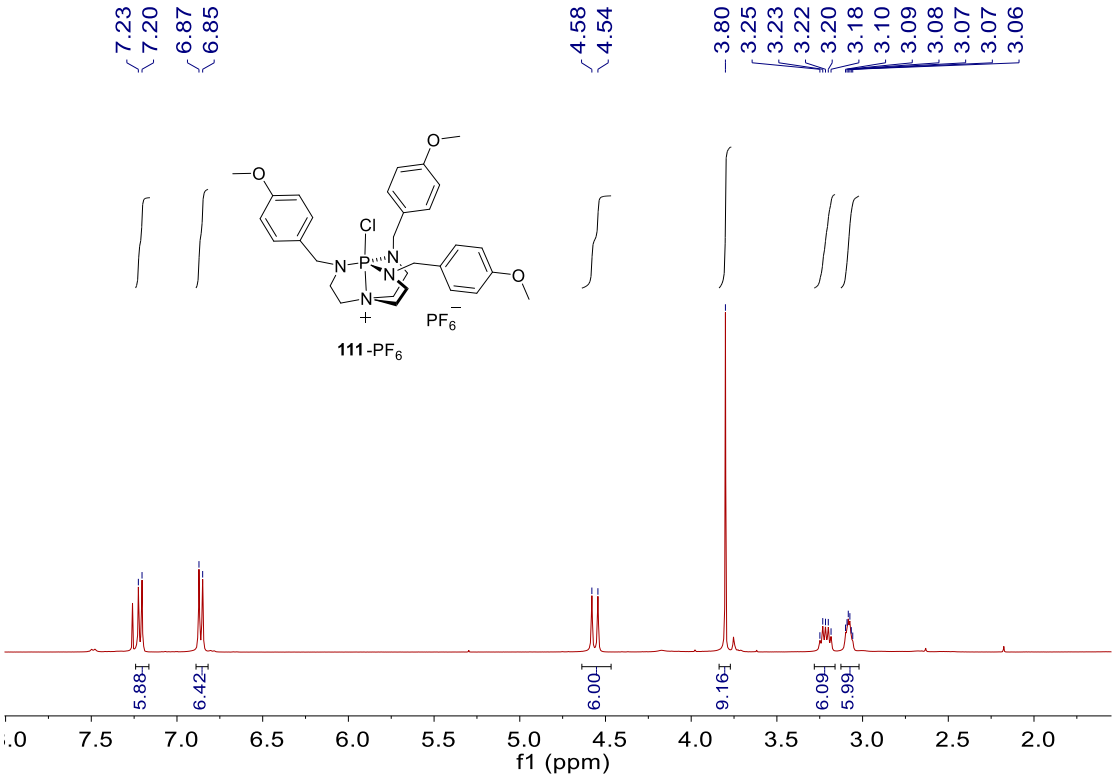

Figure S40. ^{1}H NMR (298K, $CDCl_3$, 400 MHz) spectrum of **111**·PF6.

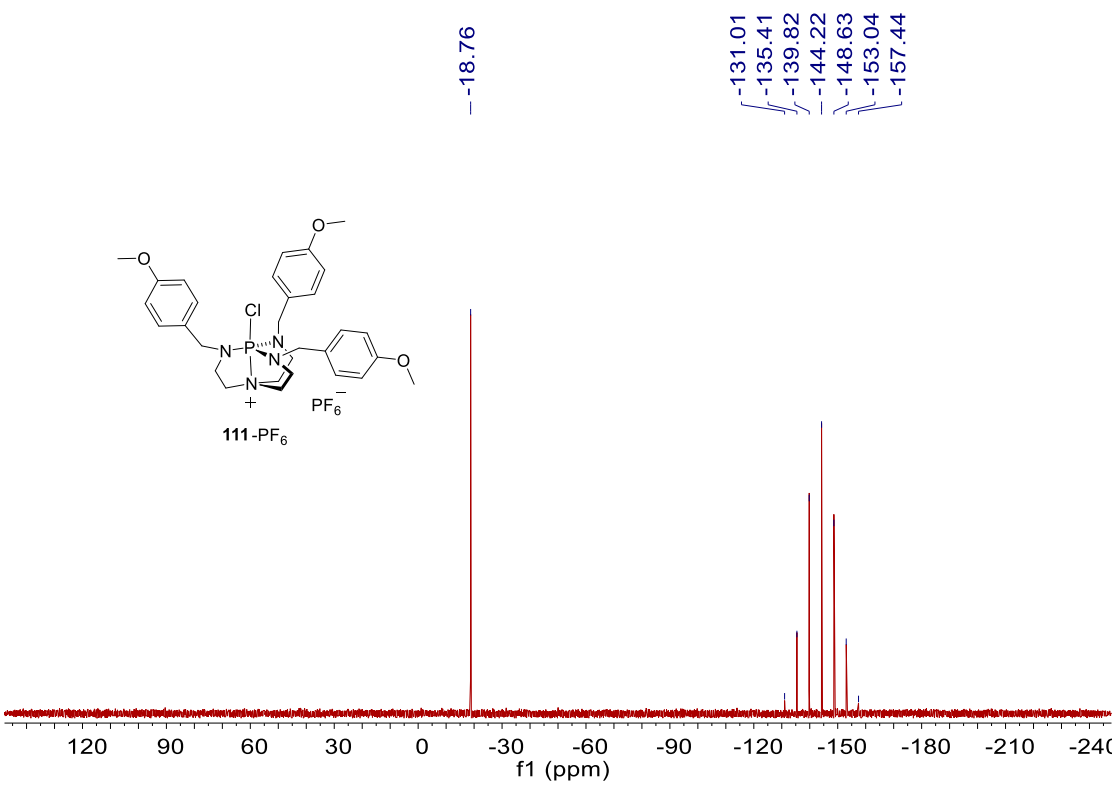

Figure S41. ^{31}P NMR (298K, $CDCl_3$, 162 MHz) spectrum of **111**·PF6.

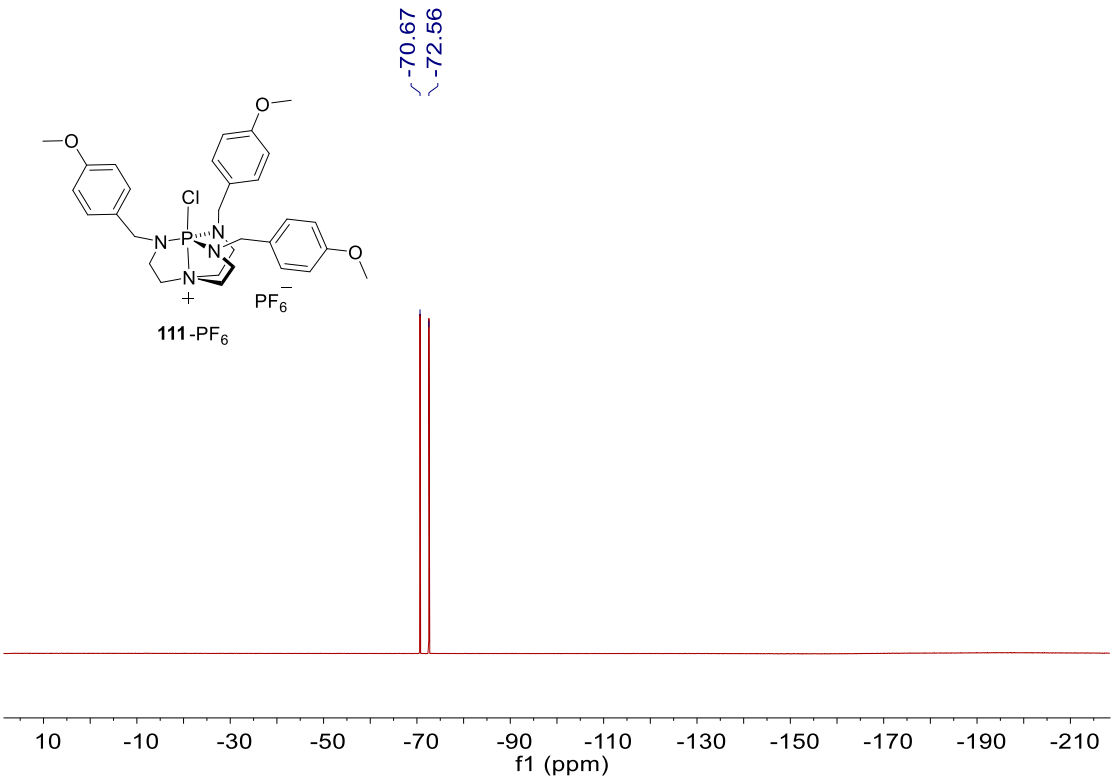

Figure S42. ^{19}F NMR (298K, $CDCl_3$, 376 MHz) spectrum of **111**·PF6.

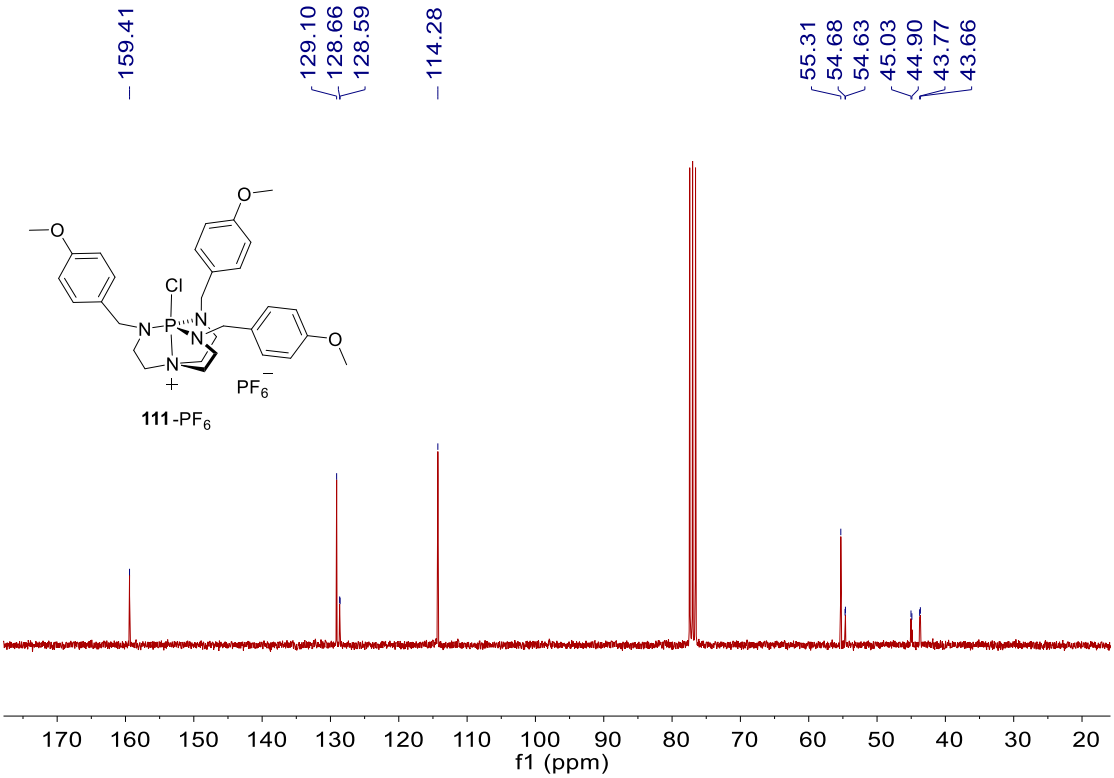

Figure S43. ^{13}C NMR (298K, $CDCl_3$, 75 MHz) spectrum of **111**·PF6.

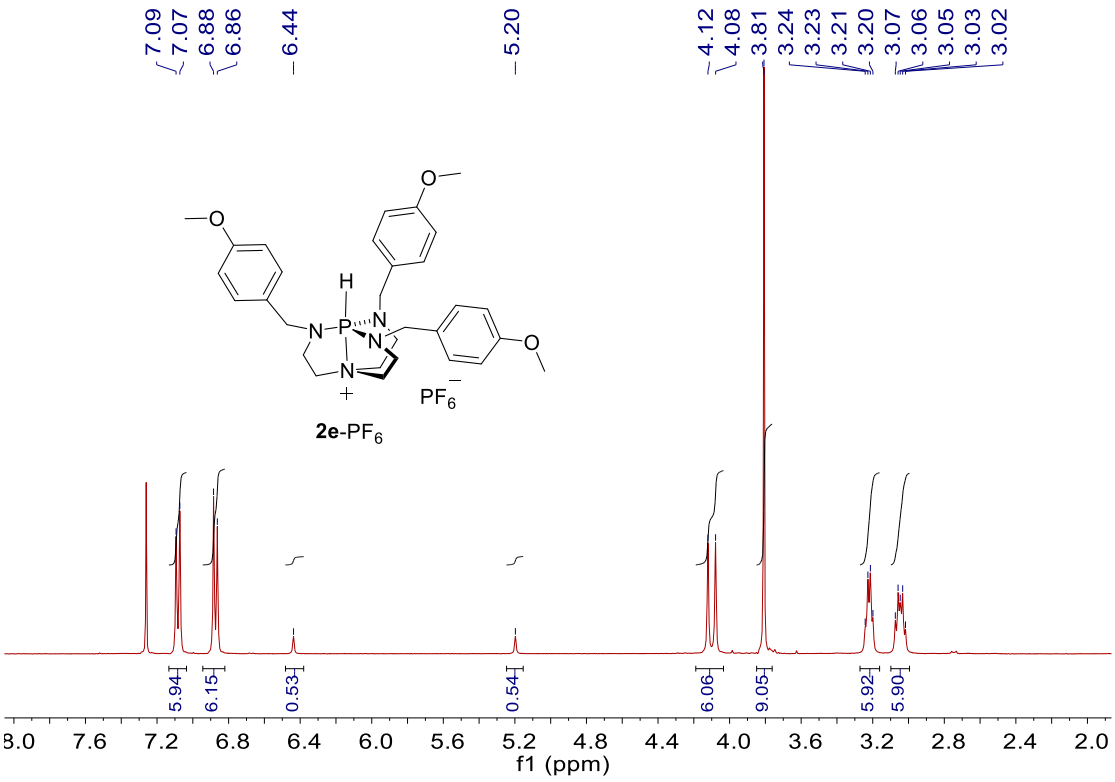

Figure S44. ^{1}H NMR (298K, $CDCl_3$, 400 MHz) spectrum of **2e**·PF6.

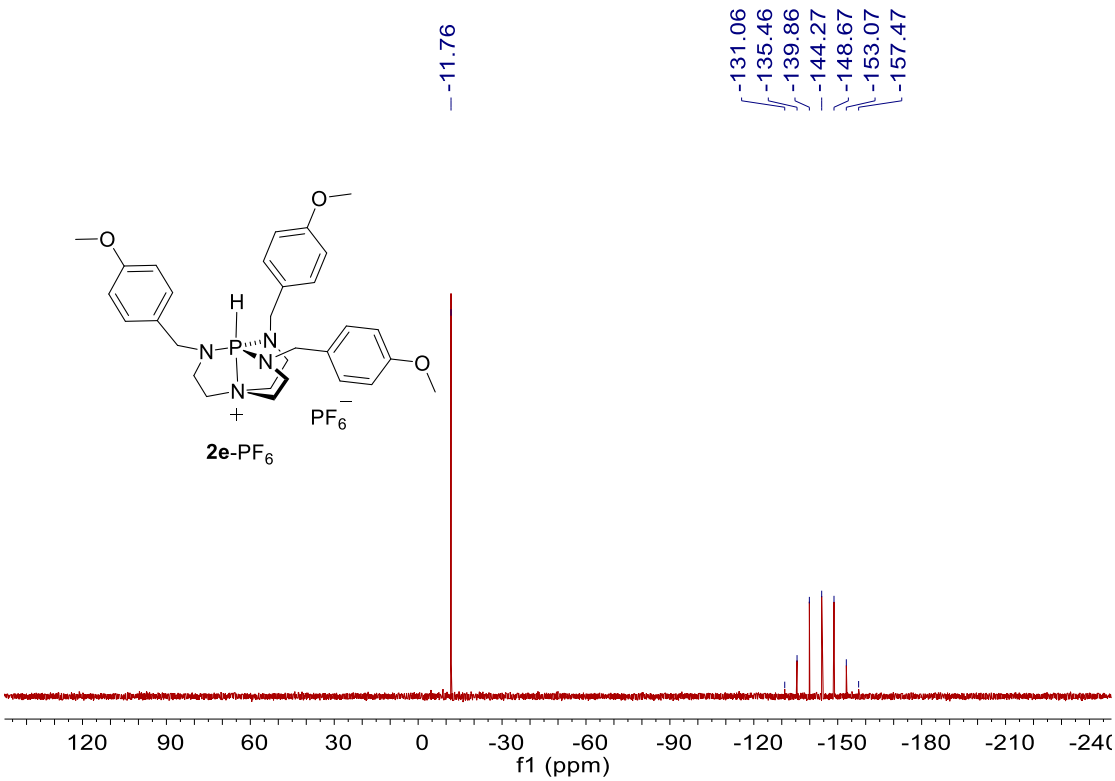

Figure S45. ^{31}P NMR (298K, $CDCl_3$, 162 MHz) spectrum of **2e**·PF6.

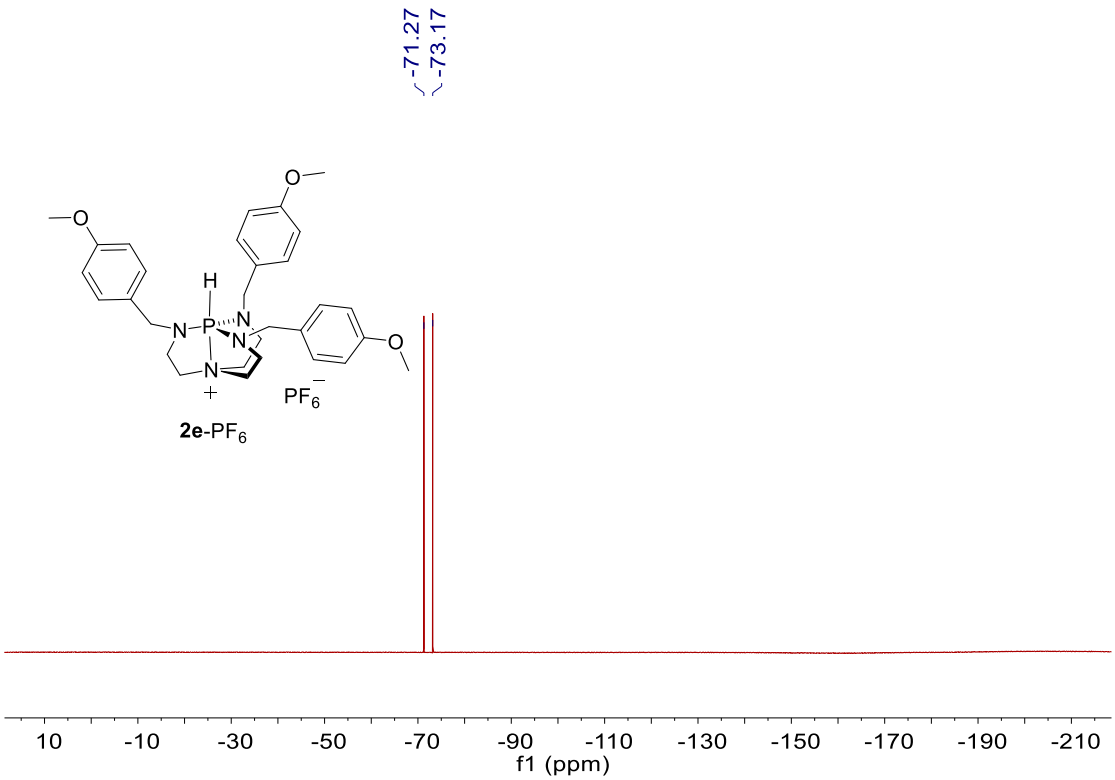

Figure S46. ^{19}F NMR (298K, $CDCl_3$, 376 MHz) spectrum of **2e**·PF6.

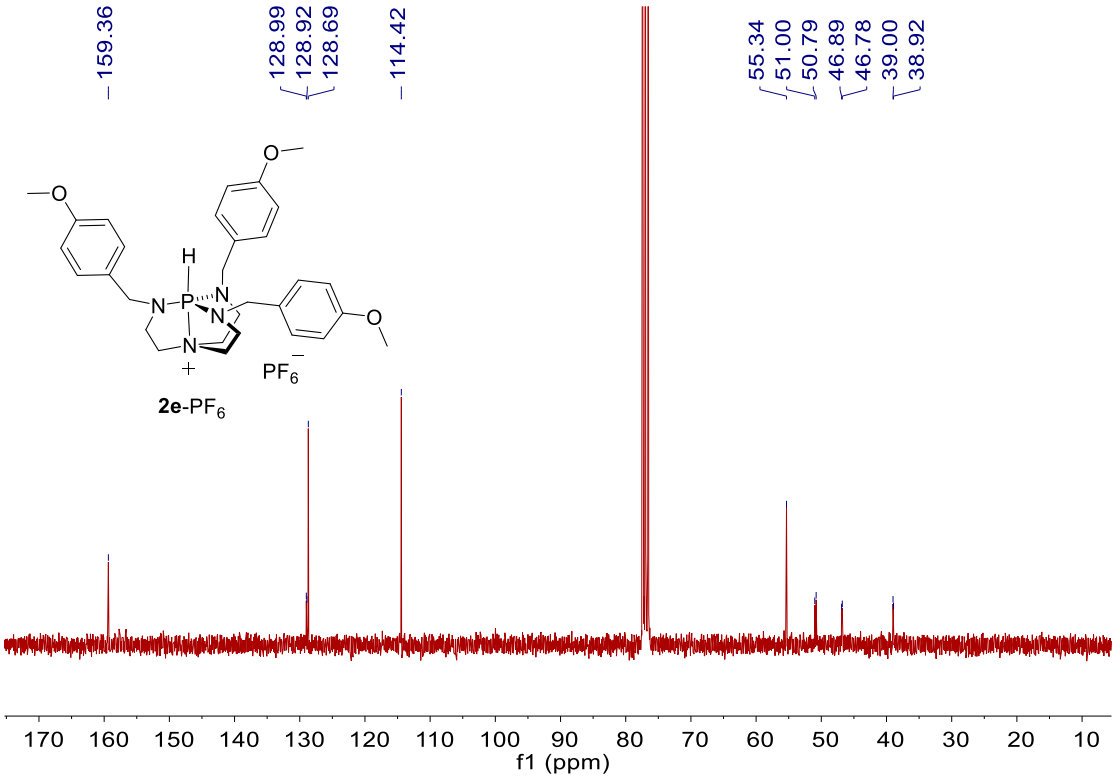

Figure S47. ^{31}C NMR (298K, $CDCl_3$, 75 MHz) spectrum of **2e**·PF6.

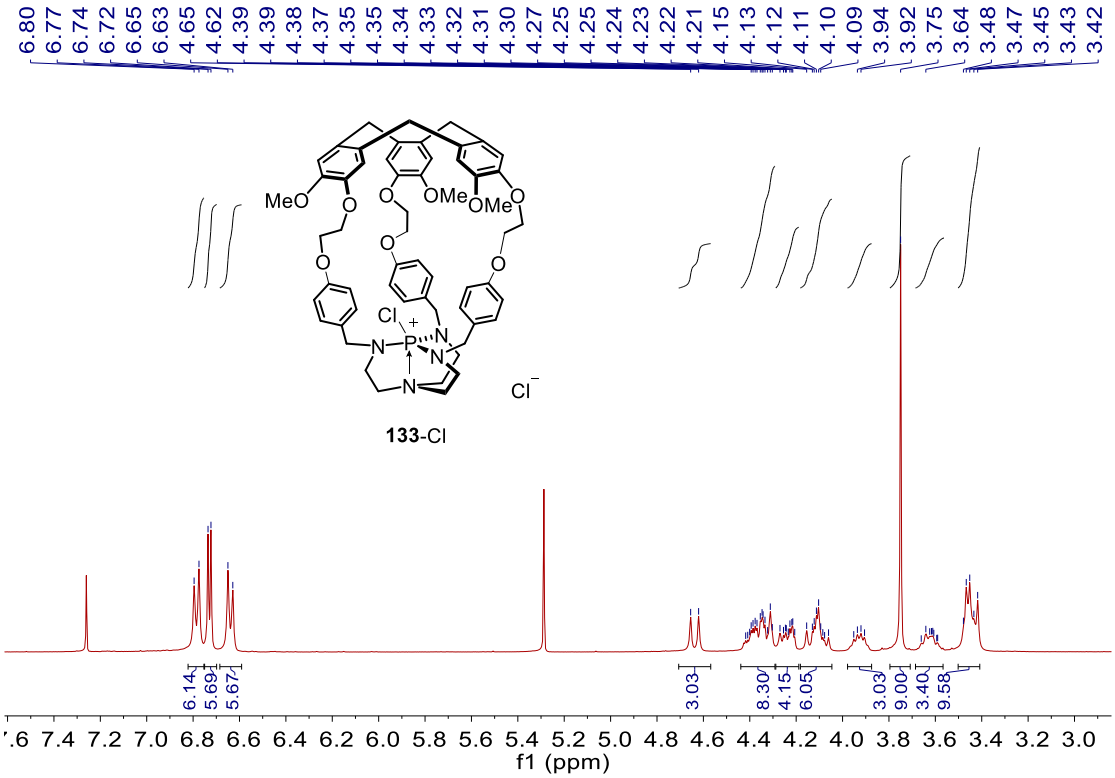

Figure S48. ^{1}H NMR (298K, $CDCl_3$, 400 MHz) spectrum of **133**·Cl.

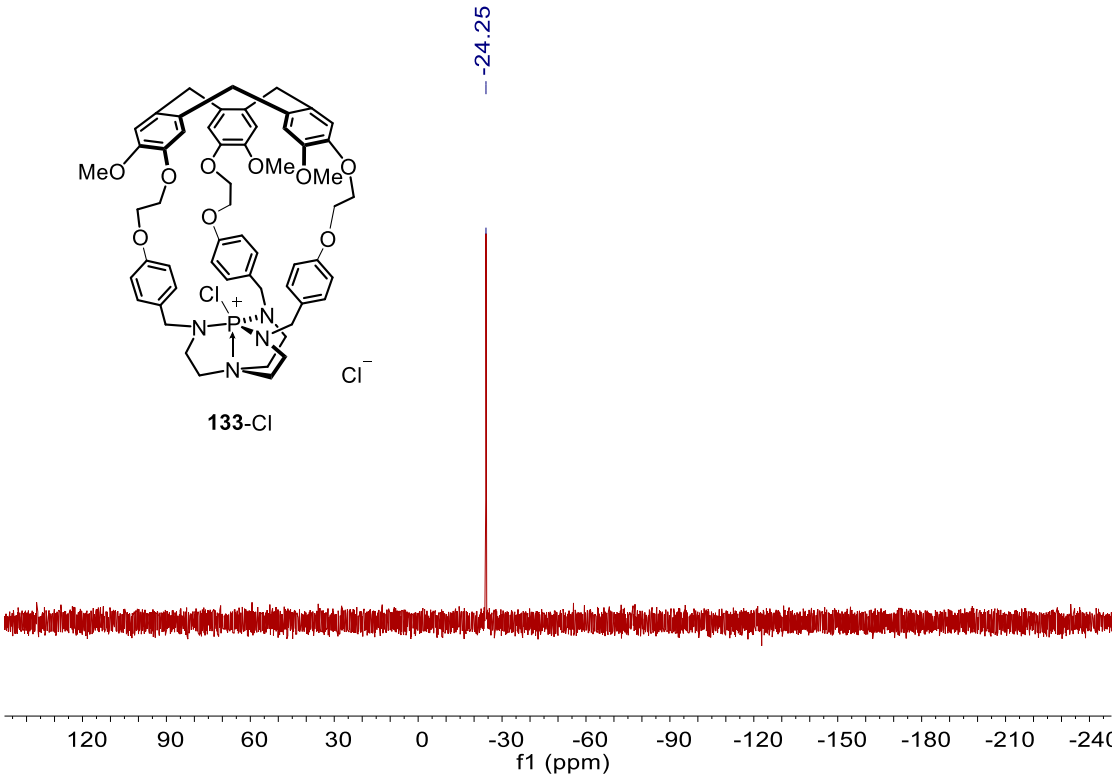

Figure S49. ^{31}P NMR (298K, $CDCl_3$, 162 MHz) spectrum of **133**·Cl.

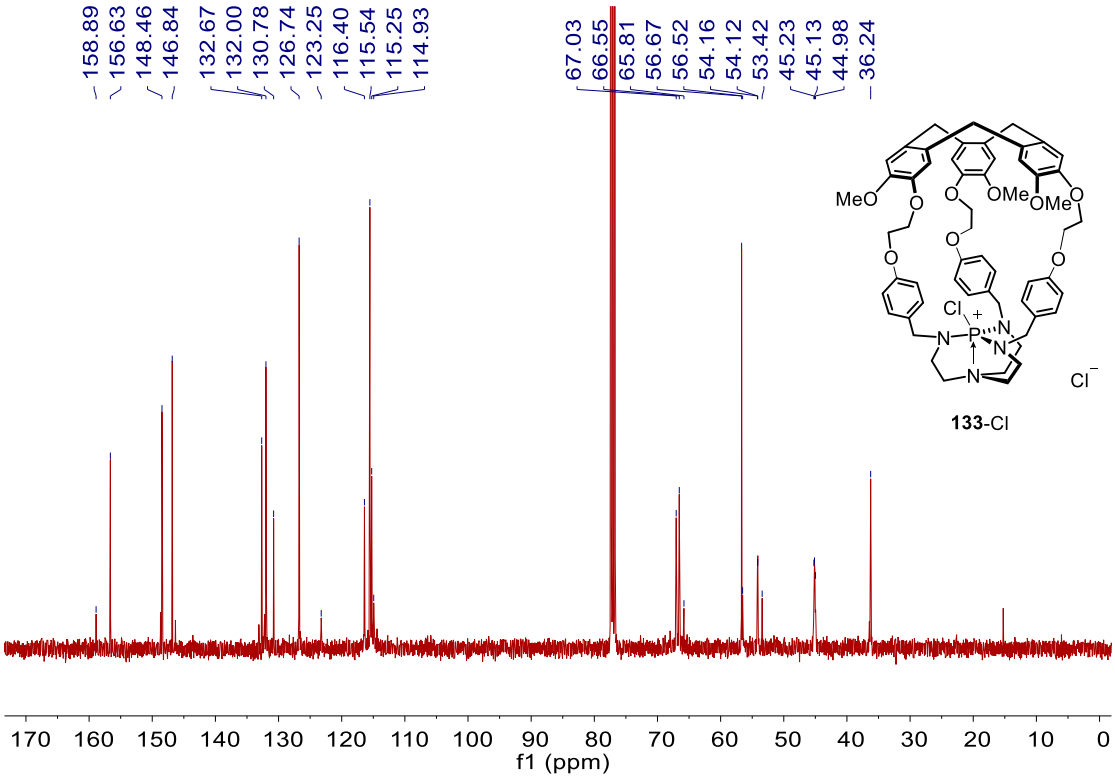

Figure S50. ^{13}C NMR (298K, $CDCl_3$, 101 MHz) spectrum of **133**·Cl.

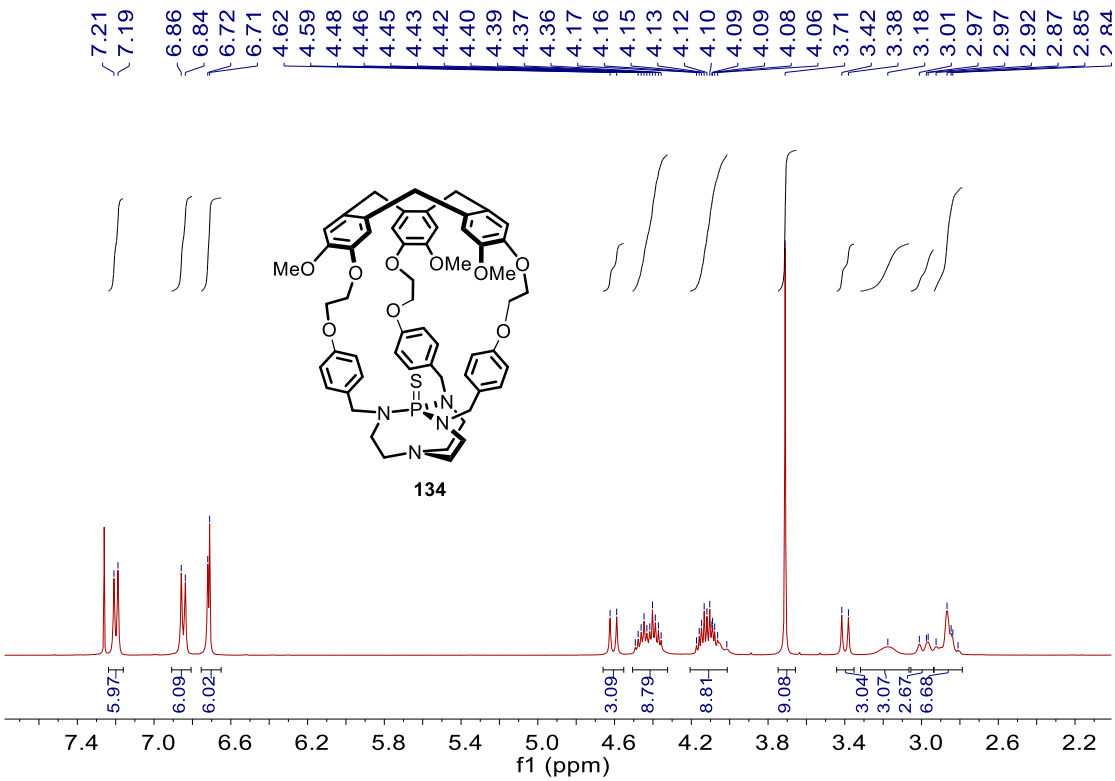

Figure S51. ^{1}H NMR (298K, $CDCl_3$, 400 MHz) spectrum of **134**.

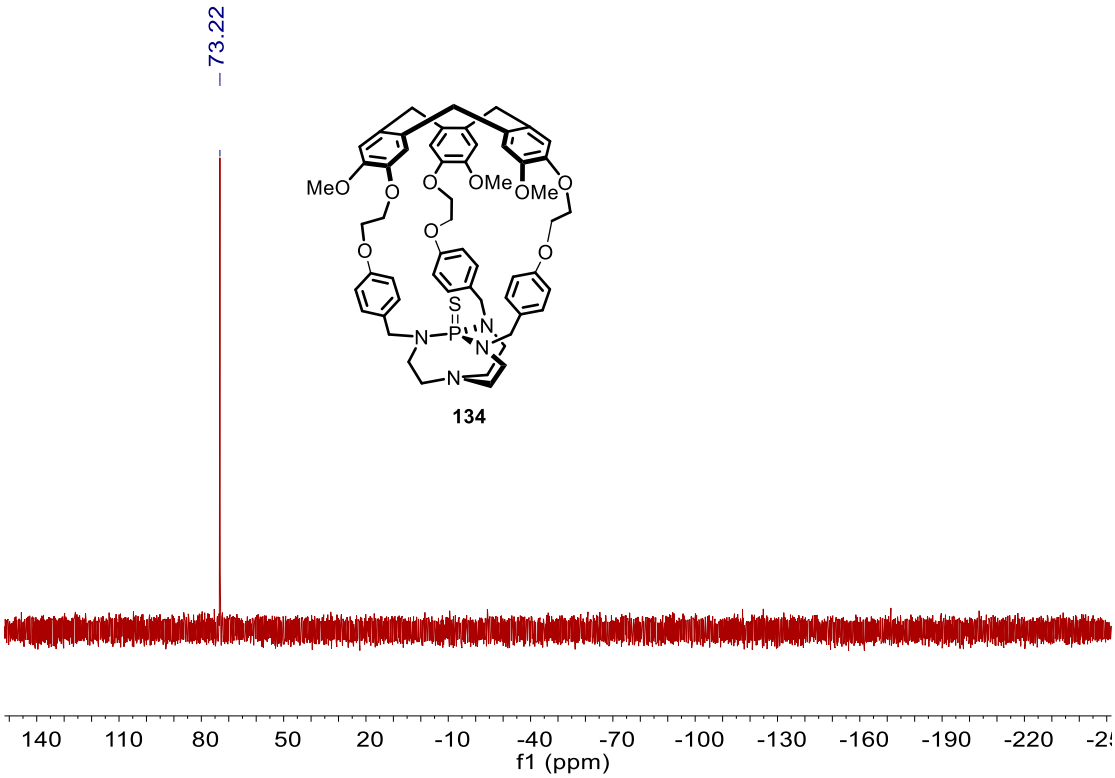

Figure S52. ^{31}P NMR (298K, $CDCl_3$, 121 MHz) spectrum of **134**.

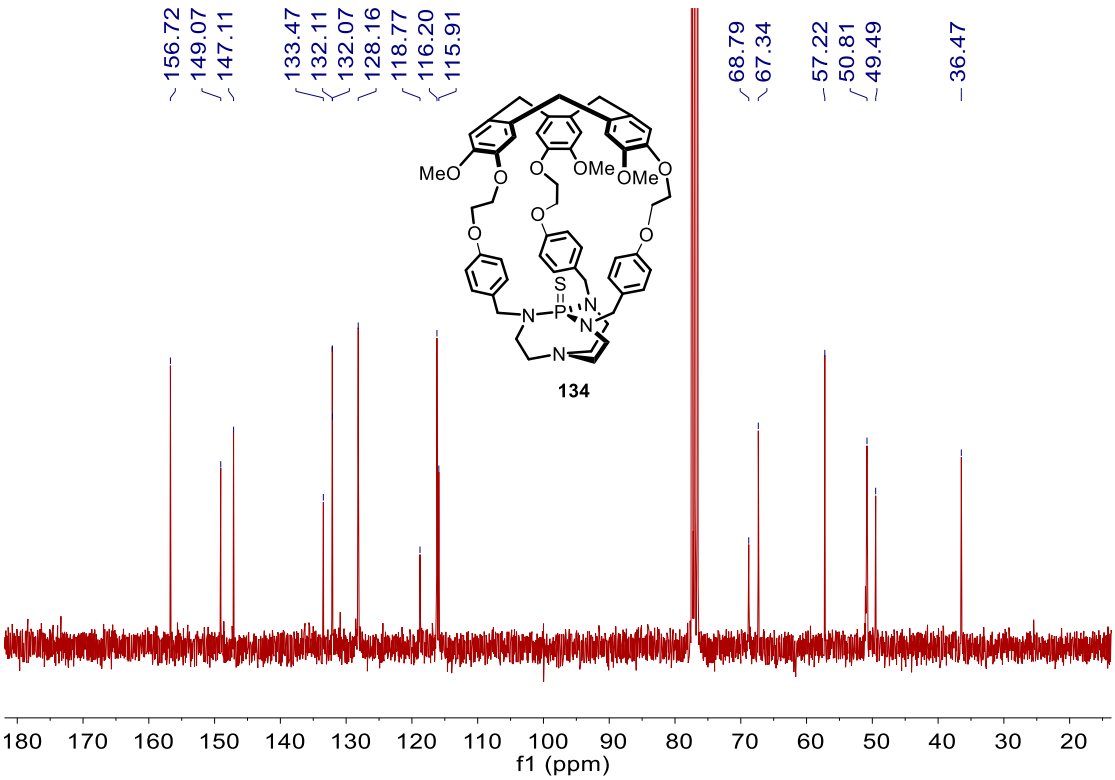

Figure S53. ^{13}C NMR (298K, $CDCl_3$, 75 MHz) spectrum of **134**.

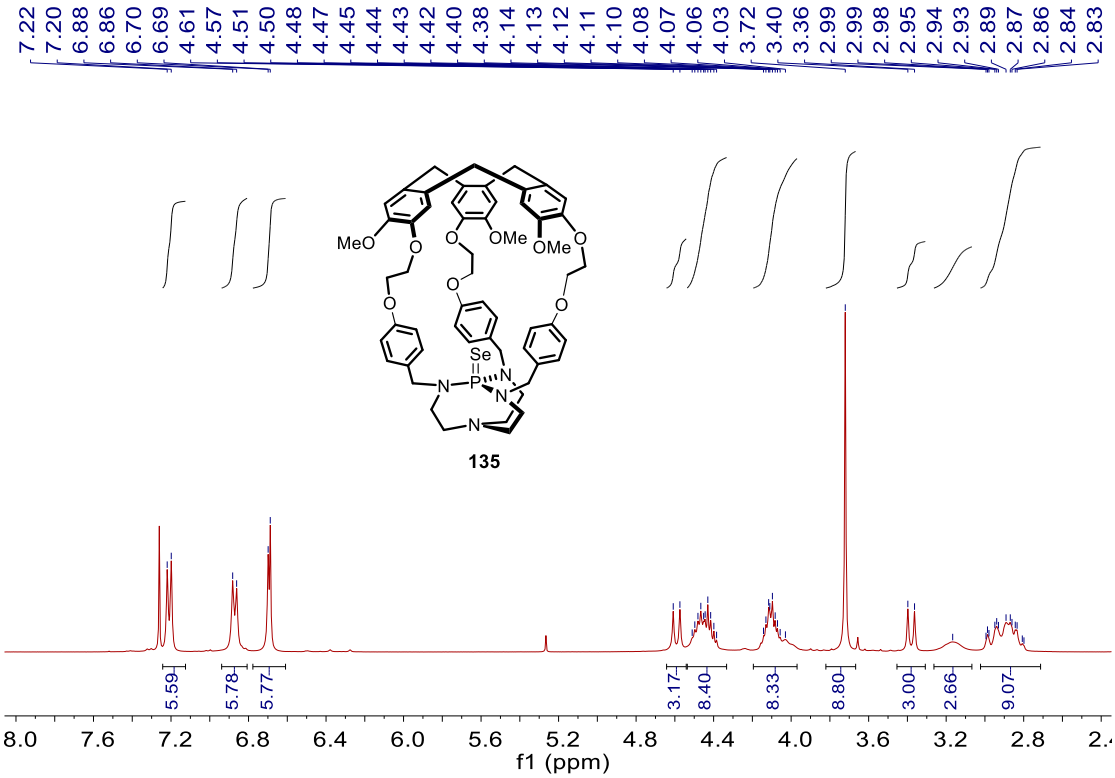

Figure S54. ^{1}H NMR (298K, $CDCl_3$, 400 MHz) spectrum of **135**.

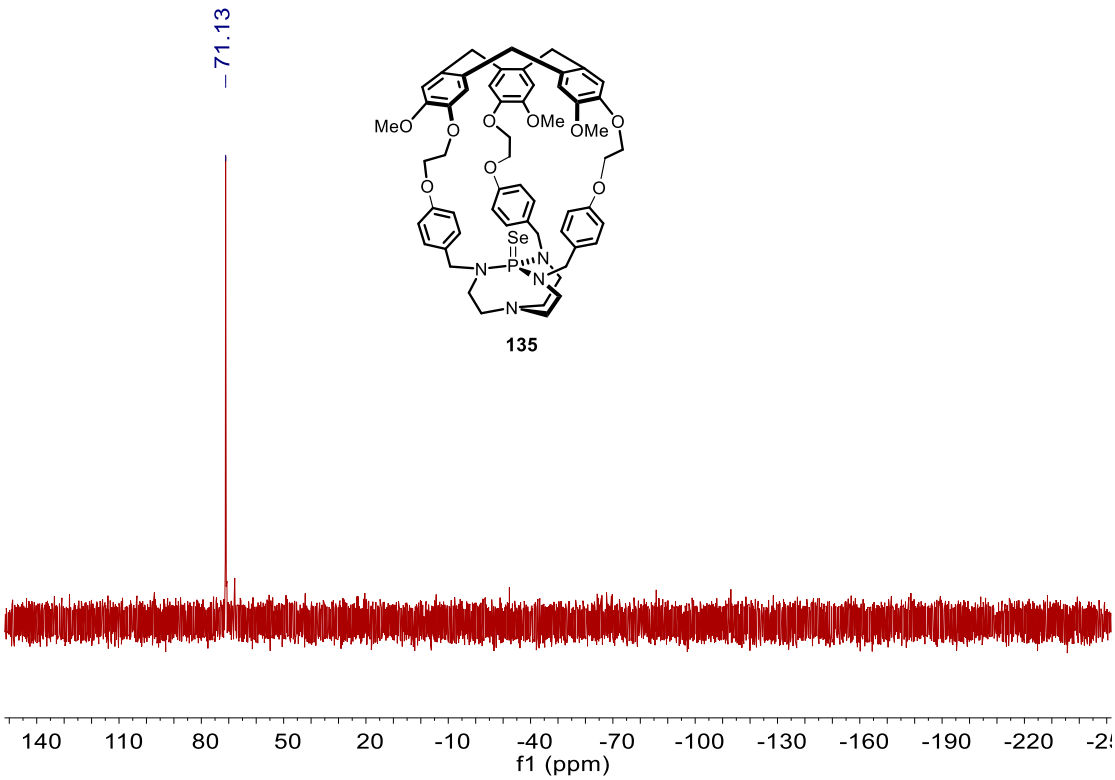

Figure S55. ^{31}P NMR (298K, $CDCl_3$, 121 MHz) spectrum of **135**.

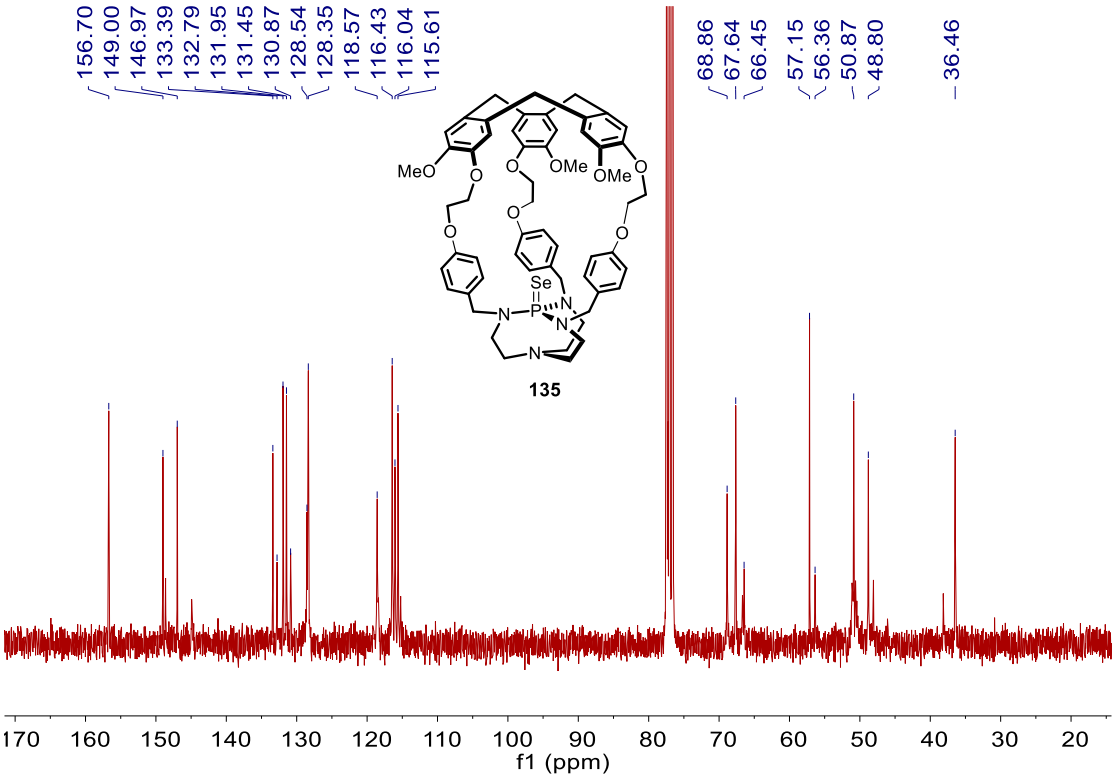

Figure S56. ^{13}C NMR (298K, $CDCl_3$, 75 MHz) spectrum of **135**.

Mass spectra

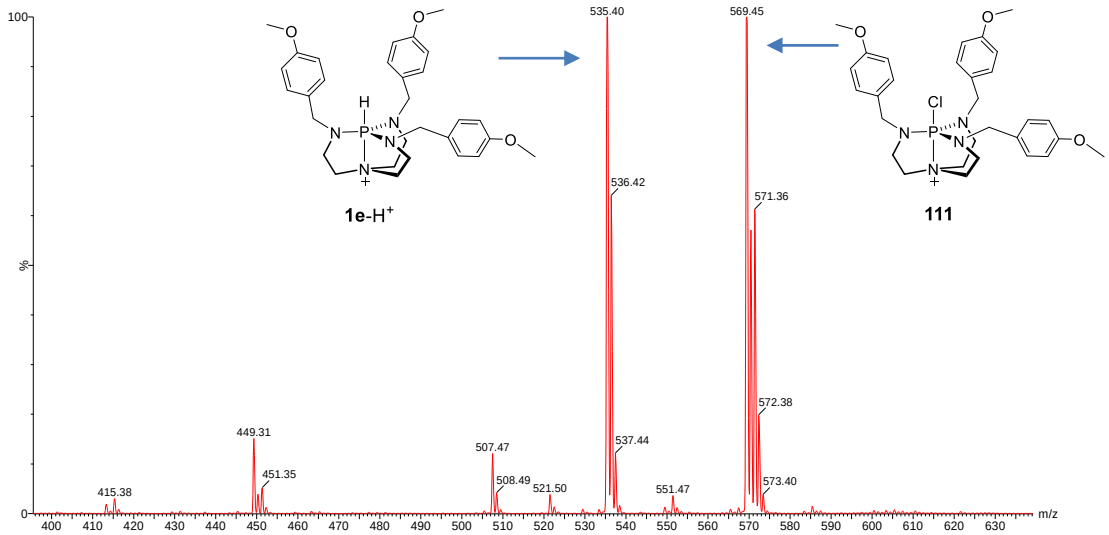

Figure S57. Mass spectrum for the reaction of **1e** and $TiCl_4$.

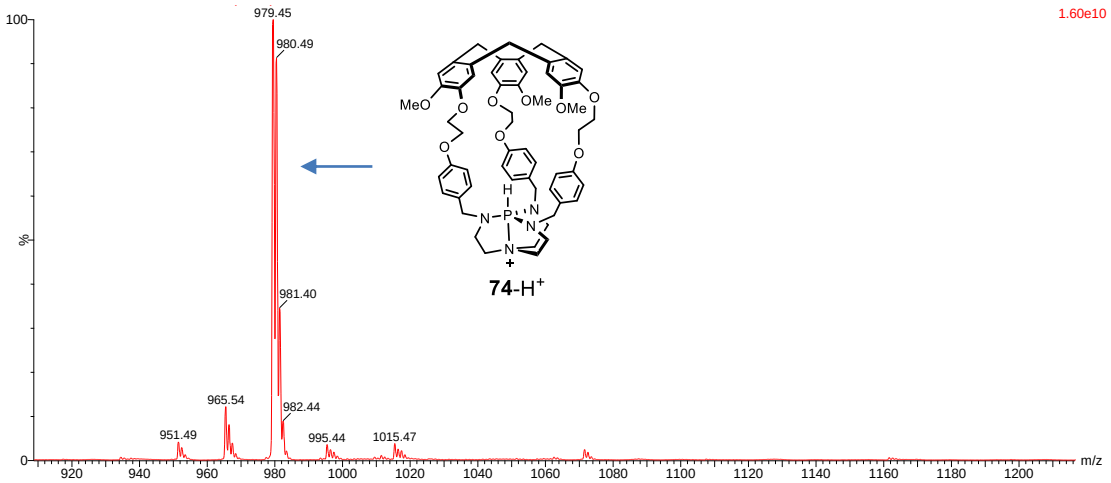

Figure S58. Mass spectrum for the reaction of **74** and $TiCl_4$.

RESUME

Au cours de ces travaux de thèse, nous avons exploré de nouvelles applications des proazaphosphatranes et de leurs dérivés, en particulier leur confinement dans une cage moléculaire. Dans la première partie, une bibliographie présente la littérature concernant (i) la découverte et les applications de proazaphosphatranes, (ii) les catalyseurs confinés dans des cages covalentes et (iii) la liaison halogène - une interaction non covalente émergente-. Par la suite, l'utilisation de proazaphosphatranes comme organocatalyseur très efficace pour la réaction de Strecker est décrit. Ensuite, un système FLP (paire de Lewis frustrée) comprenant un proazaphosphatrane encagé comme base de Lewis et du $TiCl_4$ comme acide de Lewis a été utilisé pour catalyser la réaction de MBH (Morita-Baylis-Hillman). Finalement, un azaphosphatrane chloré a été synthétisé, et ses propriétés de reconnaissance vis à vis de différents anions halogénures, par liaison halogène, a été étudié.

MOTS-CLES:

Chimie supramoléculaire, Proazaphosphatrane, Superbases, Catalyse, Strecker reaction, Chiralité, Hémicryptophane, Liaison halogène, reconnaissance

ABSTRACT

In this dissertation, our goal is to explore new applications of proazaphosphatranes and their derivatives, especially in a confined space. In the first part, a comprehensive literature review regarding 1) discovery and application of proazaphosphatranes, 2) confined covalent cages based organo- and metal-catalysts, and 3) halogen bonding – an emergent noncovalent interaction has been demonstrated. Subsequently, proazaphosphatrane as highly efficient organocatalyst for the Strecker reaction is discussed. And a FLP (frustrated Lewis pair) system comprising an encaged proazaphosphatrane as Lewis base and $TiCl_4$ as Lewis acid for MBH (Morita–Baylis–Hillman) reaction is reported. In the end, chlorinated azaphosphatrane is synthesized and studied in the recognition of different halide anions by halogen bonding, exhibiting a preferable affinity for chloride over bromide and iodide.

KEYWORDS:

Supramolecular chemistry, Proazaphosphatrane, Superbase, Catalysis, Strecker reaction, Chirality, Hemicryptophane, Halogen bonding, Recognition